Exploring the Role of Prostaglandin G/H Synthase Signalling in Chemoresistance in Acute Myeloid Leukaemia

Thesis submitted in accordance with the requirements of the University of Liverpool for the degree of

Doctor in Philosophy

By

Abdullah Mohammad Alshammari

August 2023

Dedication

I dedicate this thesis to my father Mohammad Alshammari, who passed away in 2014 during my master's studies, my mother, my brothers, my sisters, my wife, my son Mohammad and to the rest of my family.

Declaration

The work presented in this thesis has not been previously submitted in support of an application for any other degree or qualification, either from this university or any other institute of learning.

Declaration of Originality

This thesis represents the culmination of my independent research conducted during my PhD studies in the Department of Pharmacology and Therapeutics, Institute of Systems, Molecular and Integrative Biology (ISMIB), University of Liverpool, Liverpool, United Kingdom. The experiments presented in the results chapter were performed under the guidance and supervision of Dr John Woolley while all data analysis, interpretation, and conclusions drawn from the findings are solely my own.

Abdullah Alshammari

August 2023

Abstract

Antioxidant signalling is demonstrated to be important for leukemic stem cell (LSC) and haematopoietic stem cell (HSC) function. HSCs, which are found in the bone marrow, are found to be more quiescent under hypoxic conditions. Reduced cell division creates problems for these cells, with the majority of cells using this process to address oxidative damaged DNA and proteins. In this situation, HSCs must approach oxidative damage management in other ways. Prostaglandins improve mechanisms to protect from oxidative stresses through causing reductions in reactive oxygen species (ROS). Prostaglandin G/H synthases (PTGS1/2) play the main role in catalysing synthesis of prostaglandins. Research has demonstrated that PGE2, produced through PTGS1/2 activity, assists HSCs in surviving, proliferating and homing within their niche. Similarly, the data provided in this study points to a protective function of PTGS1/2 signal pathways for acute myeloid leukaemia.

PTGS genes were investigated for their association with outcomes in AML, in an approach combining biochemistry, bioinformatics, molecular biology and cellular biology. Analysis of bioinformatics databases aimed to assess how PTGS1/2 was expressed in AML and the effects of this expression on outcomes including overall survival. An efficacy assessment was made for PTGS1 inhibitors (SC560, Tenidap) for AML cell lines. Flow cytometry was used to evaluate the cell cycle and apoptosis. Lentiviral PTGS1/2 over-expression was used for U937 and HL-60 in order to assess how these genes act in cell survival, proliferative activity and resistance to drugs. Finally, PTGS1/2 was analysed in terms of promotion of immunosuppression in acute myeloid leukaemia.

Investigation of freely accessible bioinformatics databases demonstrated increased PTGS1 expression in the HSC, which reduced in cells committed to a lineage for myeloid progenitor cells. This was not found for PTGS2. There is a notable association between increased expression of PTGS1 and lower overall survival in data on AML (TCGA, Verhaak), with none seen for PTGS2. Findings in vitro show that inhibiting PTGS1 (SC560, Tenidap) leads to decreased growth of cells, arrests the cell cycle and elevates apoptosis. Overexpressed PTGS1 leads to higher WNT signalling for AML cell lines, as well as raising PGE2 secretions and reversing PTGS1 inhibitor impacts. Other effects of increased PTGS1 expression include resistance to cytarabine, as linked with lower generation of ROS. It is notable that overexpression of PTGS1 and PTGS2 lead to significant differences in transcriptome alterations in AML, which could explain the varied patient outcomes with PTGS1/2 overexpression.

Acknowledgements

Looking back at this PhD journey, I could not feel more grateful and humbled for what I have been given by so many people. I would like to express my gratitude and admiration for everyone who was part of this incredible experience.

I want to start by expressing my sincere gratitude and appreciation to my advisors, Dr. John Woolley and Prof. Dave MacEwan for their advice, insights and assistance that made this effort feasible. John, I want to express my gratitude for the opportunity to work in your group. Your contagious joy and optimism always kept me going! We both know how my experience in the lab, but you have never let me fall. You have trusted in my decisions, guided me, supported me and were always available. Thank you!

Also, I would like to thank my “lab mates” - Fiona Healy, Abdullah Alsufyani and James Griffin, I am very happy of being part of such group of people, who were always willing to assist in any possible way. Thank you all! I’m also very grateful to my dearest friends, Abdullah, Saad, Humood, Ahmed, Ammar, and Taha for their support and precious suggestions. Thank you all!

Table of Contents

List of Figures

Chapter I:

Chapter III:

Chapter IV :

Chapter V:

Chapter VI:

List of Tables

Chapter I:

Chapter II:

Chapter III:

Chapter V:

Chapter VI:

Abbreviations

Acute myeloid leukaemia	AML
Additional sex comb-like 1	ASXL1
Adenosine triphosphate	ATP
Age-related clonal haematopoiesis	ARCH
Ammonium persulfate	APS
Analysis of Variance	ANOVA
Annexin V-Propidium Iodide	AV/PI
Arachidonic acid	AA
B cell lymphoma 2	Bcl2
B-cell lymphoma-extra large	Bcl-xL
BCL-2 associated X	BAX
BCL-2 homology	BH
BCL-2-associated death promoter	BAD
BCL-2-homologous antagonist killer	BAK
BH3 interacting-domain death agonist	BID
Bone marrow	BM
Bovine serum albumin	BSA
CCAAT enhancer binding protein α	CEBPA
Chimeric antigen receptor modified T cells	CAR-T
Clonal haematopoiesis of indeterminate potential	CHIP
Colony-Forming Cells	CFCs
Copy number variations	CNVs
Cyclooxygenase	COX
Cytogenetically normal acute myeloid leukaemia	CN-AML
Deoxyribonucleic acid	DNA
Deoxyribonucleotide triphosphate	dNTP
Differentially expressed genes	DEGs

Dimethyl sulfoxide	DMSO
Double distilled water	ddH20
Dulbecco Modified Eagle Medium	DMEM
Enhanced chemiluminescence	ECL
Enhanced green fluorescent protein	EGFP
Ethidium bromide	EtBr
Ethylenediaminetetraacetic acid	EDTA
Fetal Bovine Serum	FBS
Fluorescence-activated cell sorting	FACS
Fms-like tyrosine kinase 3	FLT3
French-American-British	FAB
Haematopoietic Cell Transplantation Comorbidity Index	HCT-CI
Haematopoietic growth factor	GM-CSF
Haematopoietic stem cell transplantation	HSCT
Haematopoietic stem cells	HSCs
Half maximal inhibitory concentration	IC_{50}
Horseradish peroxidase	HRP
Immunoglobulin	Ig
Interleukin-3	IL-3
Internal tandem duplication	ITD
Isocitrate dehydrogenase	IDH
Leukemic stem cells	LSCs
Long-Term Culture-Initiating Cells	LTC-Ics
Long-term reconstituting haematopoietic stem cells	LT-HSCs
MAPK/ERK Kinase	MEK
Minimal residual disease	MRD
Mixed lineage leukaemia	MLL
monoclonal antibody	mAb
Multipotent progenitors	MPPs
Myeloid cell leukemia 1	Mcl-1

Natural killer cells	NK
Next Generation Sequencing	NGS
Nucleophosphin 1	NPM1
p53 upregulated modulator of apoptosis	PUMA
Phosphate-buffered saline	PBS
Phosphoinositide-3-kinase	PI3K
Polyacrylamide gel electrophoresis	PAGE
Poly-ADP ribose polymerase	PARP
Polyethylenimine	PEI
Polymerase Chain Reaction	PCR
Principal Component Analysis	PCA
Prostaglandin-endoperoxide synthase	PTGS
Prostaglandins	PG
Protein Tyrosine kinases	PTKs
Reactive oxygen species	ROS
Red blood cells	RBCs
Reverse Transcriptase	RT
Roswell Park Memorial Institute	RPMI
Runt-related transcription factor	RUNX1
Short-term reconstituting haematopoietic stem cells	ST-HSCs
Signal transducer and activator of transcription 5	STAT5
Sodium dodecyl sulfate	SDS
Sodium dodecyl sulfate-polyacrylamide gel electrophoresis	SDS-PAGE
Spleen focus-forming virus	SFFV
T cell receptors	TCRs
Ten–eleven translocation oncogene family member 2	TET2
Tetramethylethylenediamine	TEMED
Thrombopoietin	TPO
Thromboxane	TX
Transcription Activator Like Effector Nuclease	TALEN

Tris-acetate-EDTA	TAE
Tris-buffered saline and Tween 20	TBST
Truncated BID	tBID
Tumour protein 53	p53
Tumour protein p53	TP53
Tyrosine kinase domain	TKD
White blood cells	WBCs
World Health Organisation	WHO

Chapter I

Introduction

1.1 Acute myeloid leukaemia

A haematological malignancy is a blood cancer which develops from cells which arise from the bone marrow (BM). These cancers are categorised into several groups, including multiple myeloma, leukaemia, Hodgkin and non-Hodgkin lymphoma. Acute myeloid leukaemia (AML) is an aggressive malignant disease arising in cells from myeloid progenitors in which haematopoietic stem and progenitor cells over-proliferate with reduced differentiation, leading myeloblast cells (immature myeloid progenitor cells) to accumulate within bone marrow and peripheral blood. While the cells from which chronic myeloid leukaemia originates have been identified as haematopoietic stem cells (HSCs), the cells from which AML originates have yet to be identified. As immature leukemic cells are produced in larger numbers, this reduces the numbers of other differentiated blood cells, lowering white blood cell (WBC), red blood cell (RBC) and platelet numbers (Khwaja et al. 2016). This can reduce the blood's ability to clot, increase frequency of infection and make patients anaemic.

Between 30% and 70% of patients with AML survive at five years' post-diagnosis, a rate which varies by risk factor and sub-type (Liersch et al. 2014). AML occurs more frequently in males, and in older age groups (Juliusson et al. 2009). Frequently reported symptoms of the disease include bleeding, loss of appetite, weight loss, fatigue and raised temperature brought on by lowered red blood cell levels. Without treatment, death may occur in a matter of weeks.

1.1.1 Haematopoiesis

Blood cells are produced through haematopoiesis, initiated within the embryo and continuing throughout life. Common pluripotent haematopoietic stem cells (HSCs) are the progenitors of the whole range of cells of haematopoietic lineage (Baum et al., 1992). HSCs demonstrate the ability to renew themselves long term, to sustain proliferative activity and to differentiate into multiple lineages (McCulloch, 1983), and make up just 0.01% of nucleated cell numbers in bone marrow (Rossi et al. 2011). HSCs produce both myeloid and lymphoid haematopoietic lineages, which each show restricted differentiation capacity (Zhang et al., 2018). The long-term reconstituting haematopoietic stem cell (LT-HSC) differentiates to form short-term reconstituting HSCs (ST-HSCs) within the normal haematopoietic cell hierarchy. Multipotent progenitors (MPPs) arise from ST-HSCs having lower capacity for self-renewal and a capacity for reconstitution of less than one month. In contrast, the reconstitution ability of LT-HSCs is long term, measured at over 34 months, maintaining the capacity to self-renew and differentiate into multiple lineages across the lifespan (Orkin and Zon, 2008; Yang et al., 2005). Thus, both myeloid and lymphoid progenitor cells arise from MPPs which are classified accordingly as lymphoid-primed or myeloid-primed. Haematopoietic cell types with terminal differentiation, including platelet, erythrocyte, dendritic, granulocyte and macrophage cell types, derive from common myeloid progenitor cells. The multipotent lymphoid progenitor cell can give rise to immune mediator cells including T- and B-cells, natural killer cells and dendritic cells (**Figure 1. 1**).

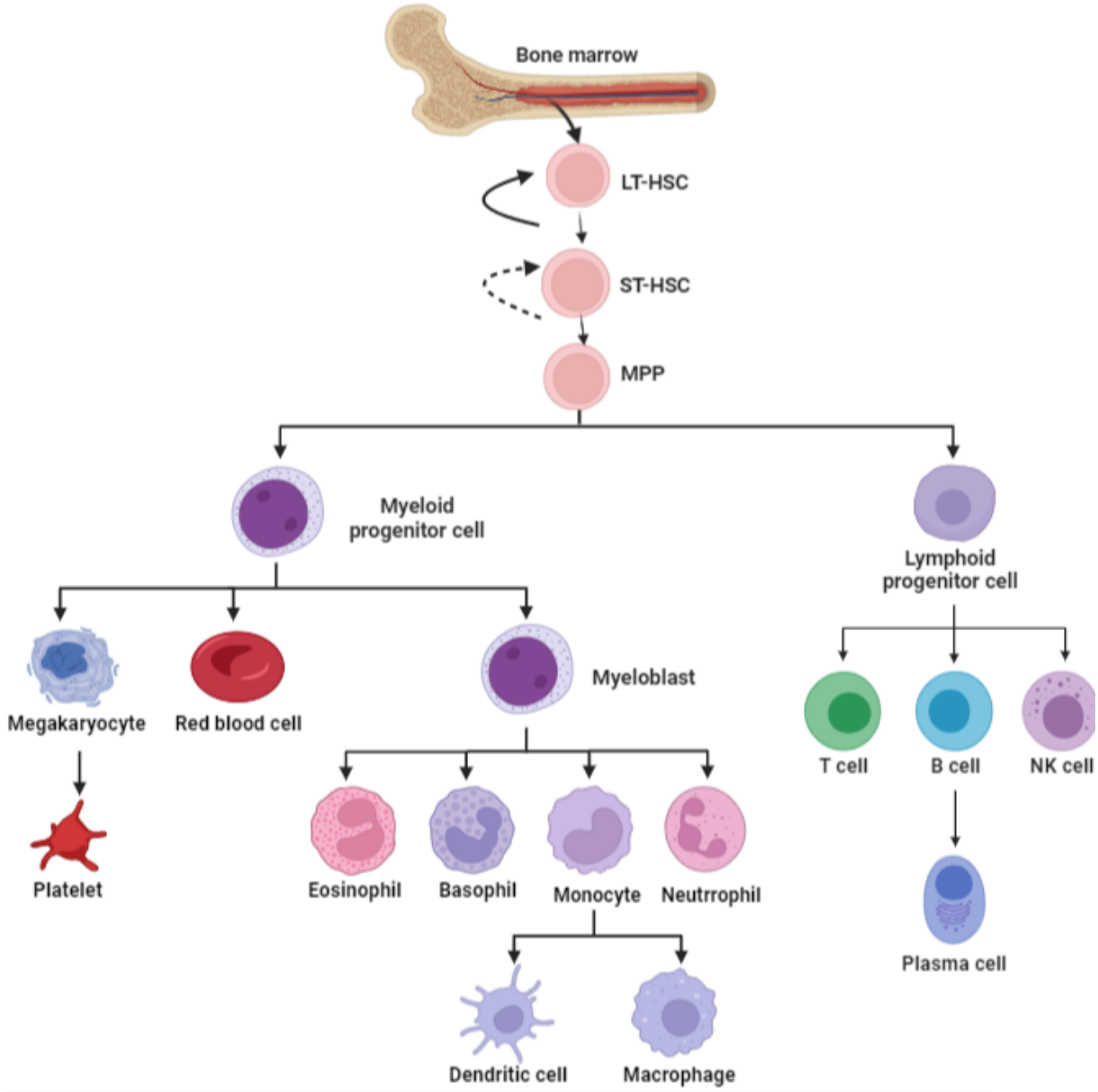

Figure 1. 1 Normal haematopoiesis.

Normal Process of haematopoiesis. Stem cells differentiate to form myeloid progenitors and lymphoid progenitors, which go on to form various lineages.

Haematopoiesis is classically described as a 2-wave process. This uses a primitive and a definitive wave. The primitive wave or primitive erythropoiesis occurs within the yolk sac and enables macrophage and red blood (erythrocyte) cells to be produced (Palis and Yoder, 2001; Galloway and Zon, 2003). Palis (2014) reports that this primitive erythropoiesis solely arises at this early phase of development within the mesoderm layer and allows oxygenation of the newly-forming tissue (Palis, 2014). The primitive wave is temporary, yet erythroid cell progenitors are not self-renewing or pluripotent.

While the definitive wave in haematopoiesis is initiated again within the yolk sac, it differs in that it later transitions to form the liver, before moving to the thymus, bone marrow and spleen (Jagannathan-Bogdan and Zon 2013). Every haematopoietic cell lineage derives from HSCs and the definitive wave phase. Kondo et al. (2003) reports that HSCs show long-term self-renewal and are able to produce both lineage-restricted ad multi-potent cells (Weissman 2000; Kondo et al. 2003).

1.1.2 Haematopoiesis regulation

Regulation of haematopoiesis occurs through intrinsically and extrinsically occurring factors balancing pluripotent stem cells against differentiation to form different cell lineages. Factors within the haematopoietic stem cell comprise expression of genes, the regulated cell cycle, modified chromatin, damaged DNA and the molecular environment of the bone marrow (Trowbridge 2019; Mann et al. 2022). Among factors acting on regulation extrinsically are haemopoietic cytokines, hypoxia, growth factors, and bone marrow regulation (Zon 2008; Trowbridge 2019; Koranteng et al. 2022). The above factors are

important to stability in mature cell levels within the circulatory blood, as well as for haematopoietic process tp function normally.

To take one of these factors, the haematopoietic growth factor GM-CSF is a promoter of myeloid cell activation, proliferative growth and differentiation, to include dendritic, macrophage and granulocyte cell types (Däbritz 2014; Bhattacharya et al. 2015). In homeostatic processes GM-CSF acts to promote development for eosinophils in circulation, as well as dendritic cells and tissue-resident macrophages (Duncker 2018). In addition, this growth factor contributes to regulating how dendritic cells form in lesions (Shaposhnik et al. 2007). Another haematopoietic growth factor, regulating formation of platelets, is thrombopoietin (TPO) (Kaushansky 1995). It is responsible for stimulating megakaryocyte production, as precursors to platelets, thereby increasing platelet count (Broudy et al. 1995; Kaushansky 1995). The pleiotropic haematopoietic cytokine interleukin-3 (IL-3) is involved with the ability to differentiate and proliferate for committed and primitive multipotent progenitor cells (Arai et al. 1990; Hara and Miyajima 1996). While haematopoiesis does not depend on IL-3, this cytokine is significant in extrinsic regulation of the process, and is a vital contributor to immune response (Ihle 1992).

When cytokines and other extrinsic contributors are dysregulated, cancers of the blood such as leukaemia may develop (Keller 1993; Trowbridge 2019). This points to the importance of balancing extrinsic and intrinsic factors for normal haematopoietic processes and in prevention of haematological disease.

1.1.3 HSCs regulation in the bone marrow niche

Bone marrow forms the main location where haematopoiesis occurs in the adult, and haematopoietic stem cells live in this medium, differentiating and self-renewing dynamically subject to strict regulation (Sánchez-Aguilera and Méndez-Ferrer 2017). Within the bone marrow are the vascular niche and endosteal niche, high-complexity micro-environments which have different cells, growth factors, cytokines, osteoblasts, molecular components of the extracellular matrix, and a vascular network (Wei and Frenette 2018). In this environment, regulation of adhesive, survival, self-renewal and differentiative activities takes place for progenitor cells and HSCs (Tamma and Ribatti 2017). Osteoblasts or CXCL12-abundant reticular cells are important contributors to the regulatory processes as they produce CXCL12, a chemokine involved in promoting proliferative activity and differentiation in short-term haematopoietic stem cells (Konopleva and Jordan 2011).

Where pathologies exist, the BM microenvironment is shown to be a mediator of resistance to chemotherapies via multiple processes. For haematopoietic malignancy, changes occur in the way in which the leukaemia cells interact with the haematopoietic niche, thus impeding haematopoiesis (Chagastelles and Nardi 2011, Desitter et al. 2011). This can be seen in studies of FLT3-ITD-transgenic mice for instance, where lower levels of normal HSCs and induced endothelial cell TNF expression are associated with myeloid proliferation induced by FLT3-ITD (Mead et al. 2017). Other work has pointed to osteoblast protection of CXCR4-expressing AML cells in the BM against induction of death by CXCL12 (Kremer et al. 2014). CXCL12 protein is bound to CXCR4 to initiate

several survival pathways, among which are MAPK/ERK, JAK/STAT and PI3K/AKT. Leukemic cell CXCR4 signalling can be enhanced through FLT3-ITD signalling: this activates Pim1 kinase and this goes on to phosphorylate The CXCR4 intracellular domain, thus increasing receptor signalling and recruiting larger numbers of FLT3-ITD-expressing cells to the perivascular niche (Grundler et al. 2009). GM-CSF and IL-3 cytokine expression by BM-resident stromal cells can protect FLT3-ITD cells from tyrosine kinase inhibitors (TKIs) through upregulation of their Axl receptor (Dumas et al. 2019). This points to the capacity for interaction between haematopoietic cells and BM niche cells in normal as well as malignant haematopoiesis.

1.1.4 Clonal evolution of AML

While profiling of AML cells documents multiple thousands of unique somatic mutations, the mean number of gene mutations in an AML clone is just 13 gene: a low number when compared with some different types of malignancy (Ley, 2013). Moreover, single-cell studies show that various unique clones which differ in their evolutionary path may be found within one individual. Some mutations within those clones demonstrate functional redundancy, pointing to shared signal pathway faults as possibly causing AML transformations (Morita et al., 2020). AML mutations probably originate within progenitor cells or HSCs, which may then gain the ability to self-renew. Research on HSCs and leukaemia cells obtained from individuals with AML reveals that a proportion of the HSCs are pre-leukemic, having certain mutations which the AML clones have without showing a full leukemic phenotype and growth advantage (Jan et al., 2012). It is possible that later clone cells mutate in ways which give benefits

in terms of selection: e.g. blocking differentiation, and this may lead to the development of AML, which would align with established theories in which malignancies progress from a single cell (Nowell 1976). In addition, certain AML cell mutations could arise as passenger mutations, which give no advantages to the cell but are simply random mutations which arise in pre-leukemic clones (Welch et al. 2012).

Clonal haematopoiesis of indeterminate potential (CHIP) describes any somatic mutation of the BM or blood without cytopenia or further features of malignancy (Heuser et al. 2016). Age-related clonal haematopoiesis (ARCH) occurs with substantially greater frequency in elderly people, and neoplastic transformation is therefore more likely to emerge in this group (Jaiswal et al. 2014). In ARCH, haematopoietic clone cells with certain mutations expand preferentially and gin selective advantage (Shlush 2018).

1.1.5 Leukemic stem cells

A significant proportion of AML relapses are due to minimal residual disease (MRD), in which a small malignant cell population survives following chemotherapeutic intervention. Such cells, termed leukemic stem cells (LSCs) frequently show chemotherapeutic resistance. LSCs are blood stem cells with mutations which are capable of producing clonal AML cells which also have those mutations. These cells are frequently not active, and targeting them with established chemotherapeutic approaches is challenging (Jordan 2007). LSCs inhabit the bone marrow niche as part of a cell population with specific surface markers, among which are CD34+ CD38- and CD123+: these are protective against chemotherapy. In light of this, researchers have put forward a number

of potential therapeutic approaches, the targets of which include relevant metabolic pathways, components within the BM environment, surface antigens, and specific epigenetic characteristics (Ishikawa et al. 2007; Pollyea and Jordan 2017). Despite this, the number of effective agents to target LSCs remains limited. Further, an AML patient could have a heterogenous range of LSC subclones, which increases the challenge involved in developing effective treatments (Vetrie et al. 2020) due to the potential for relapse from clones which resist treatment.

There is a current research focus on further exploring LSCs' bio-characteristics in comparison with normal progenitor and cells and HSCs, and differences in LSCs in different patients (Thomas and Majeti 2017). This should provide an essential knowledge base from which to develop therapeutic strategies which target LSCs in AML. Initial work in this area has shown the presence of not only quiescent progenitor cells, usually refractory to conventional chemotherapeutic approaches, in the majority of AML cases sampled, but also clonogenic Colony-Forming Cells (CFCs) as well as Long-Term Culture-Initiating Cells (LTC-ICs). A large proportion of these showed active division and response to a range of cytokines and growth factors (Guan et al. 2003). The reactiveness of LSCs to haematopoietic growth factors and cytokines including G-CSF and IL-3 can trigger cell cycle progression and increase their vulnerability to chemotherapeutic agents (Pollyea and Jordan 2017), leading to the current research attention on understanding the biological basis for regulation LSC cell cycle initiation.

In metabolic terms, quiescent LSCs show reduced oxidative phosphorylation levels and depend more upon fatty acid oxidation than normal HSCs (Thomas

and Majeti 2017; Mistry et al. 2021). Epigenetically, LSC and non-LSC offspring vary, with both alterations in histone and DNA methylation being major contributors. A further current topic of research is the relationship between genetically heterogenous AML LSCs and outcomes clinically, pointing to the importance of understanding the impact of sub-clonal variations for the functioning of LSCs and response to treatment (Thomas and Majeti 2017).

Clinical outcomes for AML are negatively associated with LSCs, which are linked to greater incidence of MRD, as well as lower overall survival. Moreover, both epigenetic signature and gene expression in LSCs are independently associated with AML survival, underscoring LSCs' significance. Moreover, research demonstrates the survival of LSCs through AML treatment, providing an explanatory factor in therapeutic resistance and relapse (Thomas and Majeti 2017).

1.1.6 AML classifications

The two major systems which are applied to classify AML are the French-American-British (FAB) and World Health Organization (WHO) systems.

1.1.1.1 FAB classification

The French-American British classification system launched in 1976, with a heavy focus on morphological features of the cell and cytogenetics. FAB sets a minimum threshold of 20-30% blast cells within bone marrow and peripheral blood to identify AML (Bennett et al. 1976). Classification of AMLs depends on the cell types involved and their stage of maturity in order to distinguish 8 subtypes, labelled M0-M7. Assessments are made via light microscopy. Further, certain AML subtypes have associations with cytogenetic abnormality. The categories within this classification system are described in **Table 1. 1** (Kumar 2011).

However, some research suggests that FAB classifications do not effectively inform prognosis, with variations in immunophenotype and cytogenetic features within each category which should be added to morphological assessments to achieve accurate prognoses (Keating et al. 1996; Tallman et al. 2004). Despite this, in the patient who has undergone bone marrow transplant, categories the M6 and M7 in combination with NPM1 and/or FLT3ITD status, might have value for prognosis (Canaani et al. 2017).

Table 1. 1 FAB classification of AML

FAB Subtype	Description
M0	Undifferentiated AML
M1	AML with minimal maturation
M2	AML with maturation
M3	Acute promyelocytic leukaemia
M4	Acute myelomonocytic leukaemia
M4 eso	Acute myelomonocytic leukaemia with eosinophilia
M5	Acute monocytic leukaemia
M6	Acute erythroid leukaemia
M7	Acute megakaryoblastic leukaemia

1.1.1.2 WHO classification

The WHO's classification system was first made available in 2001, and connects data on molecular genetics, cytogenetics and clinical findings. Here, AML is divided into 6 major classes: AML not otherwise specified, myeloid sarcoma, AML with myelodysplasia-related changes, AML with recurrent genetic abnormalities, therapy-related AML, and myeloid proliferation related to Down syndrome (Arber et al. 2016). The criteria used in this system to classify AML were produced in a consensus-based process involving professionals in haematopathology and clinical oncology. Under these criteria, AML is determined where there is a minimum of 20% blasts within the bone marrow. However, if a patient has certain translocations, such as t(8;21) (q22;q22), inv(16)(p13q22), t(16;16)(p13;q22), and t(15;17)(q22;q12), they are identified as having AML whether or not they reach 20% blasts. **Table 1.2** provides for a more detailed description of the categories and genetic abnormalities.

Table 1. 2 WHO classification of AML

AML with recurrent genetic abnormalities
AML with t (8;21) (q22; q22.1); RUNX1-RUNX1T1
AML with inv (16) (p13.1q22) or t (16;16) (p13.1; q22); CBFB-MYH11
APL with PML-RARA
AML with t (9;11) (p21.3; q23.3); MLLT3-KMT2A
AML with t (6;9) (p23; q34.1); DEK-NUP214
AML with inv (3) (q21.3q26.2) or t (3;3) (q21.3; q26.2); GATA2, MECOM
AML (megakaryoblastic) with t (1;22) (p13.3; q13.3); RBM15-MKL1
Provisional entity: AML with BCR-ABL1
AML with mutated NPM1
AML with biallelic mutations of CEBPA
Provisional entity: AML with mutated RUNX1
AML with myelodysplasia-related changes
Therapy-related myeloid neoplasms
AML, NOS
AML with minimal differentiation
AML without maturation
AML with maturation
Acute myelomonocytic leukaemia
Acute monoblastic/monocytic leukaemia
Pure erythroid leukaemia
Acute megakaryoblastic leukaemia
Acute basophilic leukaemia
Acute panmyelosis with myelofibrosis
Myeloid sarcoma
Myeloid proliferations related to Down syndrome
Transient abnormal myelopoiesis (TAM)
Myeloid leukaemia associated with Down syndrome

1.1.7 The epidemiology of AML

Acute myeloid leukaemia is reported to be the commonest acute leukaemia diagnosis for adults, and for young people has a 15-20% prevalence rate among other types of cancer (O'Donnell et al., 2012). In 2018, approximately 19,520 diagnoses were made in the United States: however, the disease remains relatively uncommon. The National Cancer Institute's review of SEER data covering the period 2011 to 2015 found that AML occurred at a rate of 4.3 cases per 100,000 population, with mortality standing at 2.8 per 100,000 (Cancer Research UK, 2011-2015). The likelihood of AML increases after 60 years of age, with incidence rising from 1.3-12.2 cases per 100,000 at an age of >65 (De Kouchkovsky and Abdul-Hay 2016). AML occurs at a greater incidence in the male population than the female, and ethnic group has an additional influence on incidence. Cancer Research UK reports that total relative survival at five years was 14 % for UK males and 16% for UK females. This drops to approximately 5% fife-year survival in the >65 age group, while below 65, the rate is 40-65%. Despite being less frequent than some other forms of leukaemia, AML's lower survival rate mean that it has the highest mortality. This points to the need to significantly improve clinical treatment options, as proper treatment provision is currently challenging, with the older demographic for this disease.

1.1.8 Cytogenetics

Cytogenetics is central to understandings of the genetic cause of a range of disorders, among which is AML. Based on examining abnormal areas in the chromosomes, including translocations and deletions, non-random genetic events are implicated in causing AML initiation and progression for around 52% of patients (Byrd et al., 2002). Associations are identified between certain cytogenetic alterations, such as t(8;21)(q22;q22), t(15;17)(q22;q12), and inv(16)(p13.1;q22), and greater AML survival and extended remission periods. Conversely, abnormalities on chromosomes 5 and 7, complex karyotypes as characterised by 3 alterations in chromosomes, 11q23 region alterations are associated with poor response to treatment, with reduced total survival (Dohner et al., 2015). Despite this, cytogenetically normal acute myeloid leukaemia (CN-AML) is found in between 40% and 50% of cases under conventional banding analysis (Gaidzik and Döhner 2008). These cases form an intermediate-risk group for relapse, but outcome is widely variable across the group. Molecular screening is thus essential in order to classify and determine prognoses for CN-AML with accuracy in order to develop optimised therapeutic interventions.

1.1.9 Mutations in AML

Identifying molecular alterations is critical to classifying, prognosticating and treating AML (Marcucci et al. 2011; Network 2013; Lindsley et al. 2015), and developments in sequencing technologies have allowed extensive characterisation of genetic components within AML, with a special focus on core-binding factor AML (Network 2013). Determination of particular mutations in genes as well as altered expression of genes have increased understanding

of the mechanisms involved in leukemogenesis, as well as informing clinical strategies.

A frequently-occurring type of AML mutation affects Nucleophosmin 1 (NPM1), which is mutated in between 25% and 30% of cases (Schnittger et al. 2005; Falini et al. 2007). NPM1 mutation leads the NPM1 protein to be abnormally expressed within cytoplasm rather than nucleus and causes myeloid cells to proliferate and leukaemia to develop (Falini et al. 2007; Cheng et al. 2010). Mutation in NPM1 is linked to higher overall survival rate as well as greater sensitivity to intensive chemotherapeutic treatment (Döhner et al. 2005).

In between 18% and 22% of AML patients, DNA Methyltransferase 3A (DNMT3A) is mutated, found in cytogenetically normal CN-AML (34%) (Ley et al. 2010). DNMT3A mutations disrupt methylation normal haematopoietic processes, and there is no consensus on their importance for prognosis (Marcucci et al. 2012). Recently published work suggests that such mutations are in fact negative for prognosis, in particular when found in the older patient (Marcucci et al. 2012).

Further, Fms-like tyrosine kinase 3 (FLT3) mutations are identified in 20% of AML patients overall, and in between 30% and 45% of CN-AML cases, including internal tandem duplication (ITD) and tyrosine kinase domain (TKD) mutation (Kelly et al. 2002; Dohner et al. 2015). Constitutive activation of the FLT3 signalling pathway is promoted by these mutations (Kelly et al. 2002; Kayser et al. 2009). Although agreement has not yet been reached regarding the significance of FLT3-TKD mutations to prognosis, they are associated with poorer outcome and greater probability that disease will recur (Gale et al. 2008).

Between 15% and 20% of AML cases present mutations in isocitrate dehydrogenase (IDH), rising to between 25% and 30% in CN-AML patients. These mutations include IDH1 and IDH2 mutation in particular, which are gain-of-function mutations, disrupting the enzyme's normal functioning and promoting leukemogenesis (Marcucci et al. 2010; Marcucci et al. 2011; Patel et al. 2012). For CN-AML presenting wild-type FLT3 and NPM1 mutation, mutated IDH is associated with both lower overall survival and survival without disease (Marcucci et al. 2010; Paschka et al. 2010). Clinical trials to assess selective inhibitors targeting mutant IDH show potential for this therapeutic approach (Fathi et al. 2015).

Further mutations have been identified as contributors to the development of AML. These include ten–eleven translocation oncogene family member 2 (TET2), runt-related transcription factor (RUNX1), CCAAT enhancer binding protein α (CEBPA), additional sex comb-like 1 (ASXL1), mixed lineage leukaemia (MLL), tumour protein p53 (TP53), c-KIT, splicing factor gene mutations, cohesion complex member mutations. These vary in their meaning for prognosis, and each is a useful source for understanding the biological features of AML, stratified risk, and promising targets for therapies (Meyers et al. 1993; Sattler and Salgia 2004; Mrózek et al. 2007; Chou et al. 2011; Metzeler et al. 2011). Overall, research to identify and explain abnormalities present at molecular level have transformed understanding of AML and this is informing radical developments in clinical approaches. Through extending this research and continuing clinical trials, the possible benefits of targeting such abnormalities can be more fully achieved and clinical outcomes improved.

1.1.10 AML prognosis and treatment

AML survival at five years has improved, reaching about 30%, while for the older age group, prognoses are poor, with challenges from co-morbidities, toxicity from treatment, and poorer therapeutic response (Döhner et al. 2010). Determining the best treatment for individual patients involves stratifying risk using prognostic characteristics, in which cytogenetic factors are the strongest predictors of remission and overall survival rate (De Kouchkovsky and Abdul-Hay, 2016). While clinical components are needed to indicate therapeutic approach, cytogenetic variants enable patients to be divided into favourable, intermediate and adverse prognosis groups (Mrózek et al. 2012).

Induction therapy

Induction therapy forms the basis of treatments for AML, and includes chemotherapeutic treatments designed to achieve complete remission (CR). Within this, a regimen of "7+3" is standard, and uses an anthracycline (e.g. idarubicin or daunorubicin) in combination with a high dosage of cytarabine, which is an analogue for deoxycytidine (O'Donnell et al. 2017). For the first three days of the treatment cycle, it is usual to give the patient 60 / 90 mg/m^2 daunorubicin or 10-12 mg/m^2 idarubicin at the same time, 100 mg/m^2 cytarabine is provided through continuous infusion from day 1-7. This regimen aims to induce CR, as determined by: aspirate sampling of BM with lower than 5% blasts (immature blood cells); >200 nucleated cells; signs of marrow spicules; without blasts which show Auer rods / features of extramedullary disease; more than 1000/µL neutrophils at absolute count; and a platelet count of or over 10^5/µL (Cheson et al. 2003). Daunorubicin is most often used of the

anthracyclines, at 45-60 mg/m^2 per day, with a response of 60-80% in patients under 50 (De Kouchkovsky and Abdul-Hay 2016). Various trials show that increasing this dose to 90 mg/m^2 for younger adults and those between 60 and 65 raises the CR rate and extends overall survival (Fernandez et al. 2009; Löwenberg et al. 2009). The UK's National Cancer Research Council's (NCRI) prospective randomised trial compared 60 mg/m^2 and 90 mg/m^2 daunorubicin for induction therapy in 1206 patients with AML, based on concern about toxicity at the higher dose, and frequent selection of the lower dose. None of the trial's subgroups showed benefits when given the higher over the lower dose (Burnett et al. 2015).

As older AML patients have an adverse prognosis with little increase seen in survival rate, novel therapies are urgently needed. A possible approach is to target genetic abnormalities identified in the disease. As part of this, research is ongoing on use of FLT3 inhibitors, used alone or with lower intensity courses of chemotherapy. Targeted therapeutics are used for initial treatment, maintenance treatment after transplant, and where patients relapse or show refractory illness. Targeted therapies have transformed clinical outcomes in chronic myeloid leukaemia (CML) through the application of TKIs including Imatinib in targeting the Bcr-Abl fusion protein. Before treatment with Imatinib was started, in the period from 1989 to 2001, CML survival at 5 years was around 4 in 10, while from 2001-2013, with Imatinib being used, 9 in 10 patients survived at 5 years (Brunner et al. 2013; Beinortas et al. 2016). In AML, chemotherapeutic regimens are adapted considering the aggression of the disease, access to compatible stem cells, and the fitness of patients.

Consolidation therapy

The aim of consolidation or post-induction therapy, is relapse prevention and elimination of MRD within the BM to either resolve the disease completely or allow for later transplant. Next-generation sequencing and real-time PCR to assess MRD are now significant tools used to monitor responses to treatment and show greater reliability than simply morphology for prediction of relapse (Grimwade and Freeman 2014; Kohlmann et al. 2014). However, the heterogeneity of acute myeloid leukaemia (AML) poses challenges in determining the absolute risk of leukaemia development by following mutational clones. Specific clones including DNMT3A gene mutations could continue to be present in post-treatment long-term remission periods (Shlush et al. 2014). Two major approaches to consolidation exist: chemotherapeutic interventions, which can include targeted drugs; and transplant of HSCs (Estey and Döhner 2006). The approaches may be combined or applied singly, in line with the specific leukaemia present, how fit the patient is, and access to compatible donated cells. For adults under 60 with a favourable risk profile, remission is shown to be effectively lengthened and survival increased via post-induction chemotherapeutic treatment using an intermediate dosage of cytarabine (1.5 g/m^2) across 3-4 cycles twice per day on days one, three, and five (Byrd et al. 2002). This group is generally treated only with chemotherapy, with transplant only used if the patient relapses (Estey and Döhner 2006). When research testing a 3-course regime of high and low doses (3 g/m^2 versus 1.5 g/m^2) of cytarabine for a sample aged under 60 found no difference in outcome between the two groups (Burnett et al. 2013), the lower dose was later adopted as standard-of-care treatment, with the exception of specific subgroups of AML,

including CBF AML [such as t(8:21) and inv(16)] and NPM1 mutated AML, which remained at 3 g/m^2 (Byrd et al. 2002; Burnett et al. 2013). In patients over 60, no benefits were found for higher-dose cytarabine, which was linked to greater neurotoxic effects, at times not reversible (Schiffer 2014). Based on this, the elderly age group receives 5000-1000 mg/m^2 as standard (Dohner et al. 2015).

For intermediate- and high-risk AML patients in complete remission, the greatest effectiveness in the long term is seen for allogeneic HSC transplant, potentially curing between 50% and 60% of cases during their first complete remission (Appelbaum 2003; Popat et al. 2012). Despite this, some patients are never offered a transplant, based on having co-morbid conditions, not achieving CR or no compatible donor being found (Appelbaum 2003). Therefore, the treatment strategy is post-induction chemotherapy for maintenance of CR and to prevent the leukaemia load from rising whilst patients wait for transplant. The decision of whether to pursue consolidation or move immediately to transplantation must be based on the individual case: consolidation has risks in terms of mortality and morbidity and can hinder transplantation and cure. Research this century points to a need to broaden the criteria to qualify for transplant to include more than solely age (Appelbaum 2003; Sorror et al. 2005). Rather, comorbidity, remission status at the time of the decision, and performance prior to transplant should also be considered. The Haematopoietic Cell Transplantation Comorbidity Index (HCT-CI) has broad acceptance and is validated for use to assess co-morbidity, in which increased scores are associated with a poorer clinical outcome (Sorror et al. 2005). Improved supportive care, a greater range of donation possibilities, including cord graft,

and haplo-identical donation, and lower intensity preparative regimes (Popat et al. 2012).

Alternative strategies for AML therapy

Azacitidine, decitabine and other hypomethylating agents, are promising as alternative induction approaches in elderly people with AML for whom intensive chemotherapeutic approaches are not suitable (Fenaux et al. 2009), potentially enabling essential genes in differentiation and proliferative activity to function normally. Hypomethylating agents can also bind irreversibly to DNA methyltransferases and inhibit these, depressing tumour suppressor genes (Liu et al. 2022). Further work is needed however to fully elucidate the potential contribution of such agents in treating refractory AML in older patients, and phase II and III clinical trials are still underway.

Novel targeted therapies for improved AML management

Recently, frequently occurring gene mutations and various profiles based on different gene expression patterns have been identified for AML, which enables new inhibitor drugs and targeted therapeutic approaches to be developed. Various novel therapeutic candidates have so far been tested at the clinical trial stage and have shown potential to increase survival, whether as a single therapy or an addition to existing chemotherapeutic strategies. The major targeted drug groups used presently to treat AML are briefly described below.

FLT3 inhibitors

Drugs in the FLT3 inhibitor group are targeted at the FLT3 gene mutation which frequently occurs in acute myeloid leukaemia. The various FLT3 kinase

inhibitors include sorafenib, quizartinib (AC220), midostaurin, gilteritinib, crenolanib, and lestaurtinib (Salman et al. 2021; Wang et al. 2021; Capelli et al. 2022), and can be classified in two main ways: as 1st and 2nd generation members of the FLT3 inhibitor group; or as types I and II. Among members of type I include midostaurin, gilteritinib, lestaurtinib, and crenolanib, and these function by binding the receptor at the active conformation to inhibit receptors with FLT3-TKD and FLT3-ITD mutations. The second type of FLT3 inhibitor includes quizartinib and sorafenib, and works by binding to a pocket which neighbours the ATP-binding site, selectively inhibiting receptors with FLT3-ITD mutations (Kennedy and Smith 2020). The FLT3 inhibitor drug class has been shown to be significantly clinically effective in for relapsed or refractory AML, with possibilities for combined therapy alongside different antileukemic drugs (Daver et al. 2019; Smith 2019). Despite this promise, challenges are present, with patients becoming resistant to these agents via secondary FLT3 mutation, parallel pathway upregulation and extracellular signal molecules (Kennedy and Smith 2020).

IDH2 inhibitors

Isocitrate dehydrogenase (IDH) inhibitors have been developed based on the fact that in about 1 in 5 new diagnoses of AML, the genes IDH1 and IDH2 have gain of function mutations. They target IDH in order to improve differentiation and maturation of malignant clones (Stein 2015). Enasidenib binds to the allosteric site of IDH2 R140Q and IDH2 R172K mutants only, resulting in clinical response, with decreased β hydroxyglutarate and myeloid differentiation (Stein 2023). Among further IDH1 inhibitors currently or previously under research are

ivosidenib, olutasidenib, IDH305, and BAY1436032 (Wouters 2021). AGI-6780 is an agent which has not yet reached clinical trial, which inhibits the IDH2/R140Q enzyme, potentially lowering concentrations of D-2-HG concentration and inducing differentiation of cells (Chen et al. 2020). The findings from phase 1 and 2 trials suggest that IDH2 inhibitors may be safe, well-tolerated and effective (Stein 2015; Cerchione et al. 2021), but it is also considered that cells may become resistant to this group of inhibitors through a multi-mechanism evolutionary process or selective process (Cerchione et al. 2021).

PRMT inhibitors

Promising findings are reported for use of PRMT inhibitors to treat AML. When PRMT5 has been chemically inhibited, defective AML cell growth has been shown (Radzisheuskaya et al. 2019). MS023 hydrochloride has been shown to have good selectivity, potency and activity in the cell in inhibiting human type I PRMTs (He et al. 2019). High-throughput screening led to the discovery of AMI-1 and then other pan-inhibitors of PRMTs, which are selective for PRMT as compared to proteins (Wang et al. 2022). Inhibiting PRMT5 is known to improve the ability to eliminate FLT3-ITD AML stem cells when therapy also includes tyrosine kinase inhibitor (TKI) (Kumar et al. 2022). Moreover, this approach allows selective targeting of AML stem cells, via a mechanism involving p53 (Toulmin et al. 2018). In general, the PRMT inhibitor group has potential in efforts to eliminate LSCs when treating AML.

DOT1L inhibitors

The DOT1L inhibitor drug class targets a mutation in the DOT1L gene which frequently arises in AML. Among this group is Pinometostat (EPZ-5676), which has undergone phase 1 clinical trials in an adult cohort suffering from refractory/relapsed leukaemia, with AML included (Stein et al. 2015). Research shows that DOT1L inhibitors are responsible for blocking self-renewal abnormality caused by losing cohesin (Heimbruch et al. 2021). When investigated preclinically, this group has demonstrated potential assessments of efficacy for treating AML have not yet been completed.

Immune therapy

The cytotoxicity of monoclonal antibodies (mAbs) may have direct applications or indirect ones through combination with radiation or chemotherapy. In particular, researchers have assessed gemtuzumab ozogamicin for use in treating AML (Castaigne et al. 2012), which is a monoclonal antibody binding to the transmembrane protein CD33, whose expression occurs in cell types with myeloid lineages. When used in combination with calicheamicin, which has high potency cytotoxicity, gemtuzumab ozogamicin binds to CD33 and therefore allows the drug complex to enter the cell. Gemtuzumab ozogamicin has been FDA-approved since 2017 in treating patients of 2 or older for relapse or refractory CD33-postive AML.

A further immune therapeutic approach involves genetic modification of T cells to form chimeric antigen receptor modified T cells (CAR-T), allowing expression of specific vectors for antigen recognition on the cell's surface. When the CAR-T cell's antigen binding domain binds to those antigens, T cell receptors (TCRs)

are activated, with cytotoxic consequences for the leukemic cell (Gill et al. 2014). Among potential antigens, CD33 and CD123 have drawn attention for AML treatment, as they are significantly over-expressed by AML blasts (Mardiros et al. 2013). There are 13 trials in process presently aiming to establish safety and effectiveness for this therapy for AML.

1.2 Reactive Oxygen Species

Reactive oxygen species (ROS) are originally supposed to be a harmful by-product that is formed in the mitochondria through aerobic metabolism (Qi, Fang *et al*. 2015, Cieślar-Pobuda, Yue *et al*. 2017). However, recent research has indicated that ROS regulate physiological and biological roles in cellular processes (Reczek and Chandel 2015). Under typical physiological conditions, both antioxidant enzymes and modulators tightly control ROS. It can be challenging to detoxify beyond the scope of the antioxidant cellular defence system when there is excessive ROS accumulation (Mohyeldin, Garzón-Muvdi *et al*. 2010, Bigarella, Liang *et al*. 2014). Proliferation, differentiation, genomic mutations, ageing, and stem cell death can all be impacted by oxidative stress, which results from excessive ROS generation and compromised antioxidant systems (Balaban, Nemoto *et al*. 2005, Hernández-García, Wood *et al*. 2010, Reczek and Chandel 2015, Luo, Chiang *et al*. 2017). Recent reports on embryonic and adult stem cells have demonstrated that ROS regulate this balance between stem cell self-renewal and differentiation, which is essential for tissue homeostasis throughout an organism's lifespan (Cieślar-Pobuda, Yue *et al*. 2017). Thus, the modulation of the redox state is vital for sustaining the activity of stem cells and is critical for the fate determination of stem cells.

The negative effect of ROS is attributed to the oxygen free radicals they carry which, in turn, lead to affected cells experiencing changes that drive cancer initiation especially if these cells are impacted over an extended period (Schieber and Chandel 2014) The O_2-free radicals contain unpaired valence shell electrons, thereby making them extremely reactive. These reactive molecules can damage DNA and protein within the cell (Ray, Huang *et al*.

2012). Though ROS are distributed all over the body under normal conditions, their presence is decreased through physiological procedures. Maintaining low levels of ROS is crucial for HSC processes owing to the lack of cell division regulation in HSCs. Consequently, under high conditions of ROS exposure, damage to DNA or proteins that cannot be managed by repair mechanisms can lead to differentiation and production of cells containing mutations or that are damaged, ultimately leading to disease progression (Ludin, Gur-Cohen *et al*. 2014). Given the evidence implicating ROS species in AML by way of HSC processes and the significance of keeping ROS species to low levels in HSC processes, the following stages of research will involve examination of means of controlling ROS species as a possible treatment pathway.

1.3 Prostaglandin-Endoperoxide Synthase

Oxygenases in mammals have been researched with prostaglandin-endoperoxide synthase (PTGS) which known as the cyclooxygenase isoforms (COX-1 and COX-2) being the most favoured and recognised. Prostanoids are metabolites that originate from arachidonic acid (AA) and through the sequential reaction of phospholipases, PTGS1 or PTGS2, and terminal prostaglandin (PG) synthases, giving rise to the prostanoids; PGE2, PGF2α, PGD2, PGI2 or thromboxane (TX) A2 (**Figure 1. 2** shows the role of PTGS in AA conversion). These prostanoids are active (biologically) metabolites. Both PTGS1 and PTGS2 are translated from different genes but still have similar homology of structure and function. Nevertheless, their functions remain distinct with PTGS1 acting as the constitutive isoform, and for the most part PTGS2 is inducible (Smith and Langenbach 2001). This model is not definite as numerous exceptions exist. For instance, throughout maturation of lymphoid cells, PTGS1 is regulated (Rocca and FitzGerald 2002, Rocca, Maggiano *et al*. 2002). PTGS2 expression occurs stably in the kidney, thymus, brain and also tissues involved in reproduction (Smith and Langenbach 2001). *COX* isoforms are observed to be expressed differently; for example, the upregulation of PTGS2 by monocytes and granulocytes following their activation leading to production of TXA2 and PGE2 (Rocca and FitzGerald 2002). There has been an increase in literature currently reporting the involvement of prostanoids and PTGS in the haematopoietic process with CD34 stem cells expressing PTGS1 and producing PGE2 (Rocca, Secchiero *et al*. 2002).

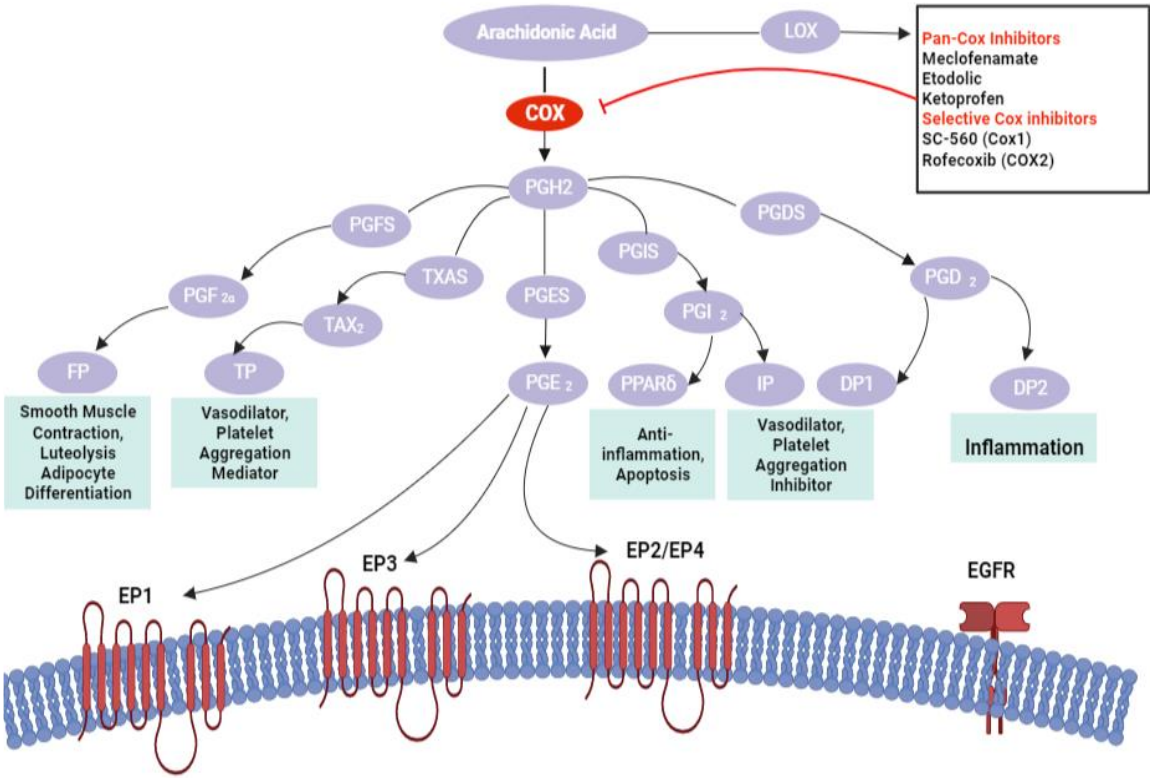

Figure 1. 2 The PTGS role in Prostaglandin synthases. PTGS catalyses alteration of arachidonic acid (AA) to PGH2, which can then be converted to various prostanoids.

1.4 Cancer and The Action of Prostaglandins

Human oesophageal carcinomas were the first cancers exemplifying the action of prostaglandins (PG) in tumours where they illustrated how they can impact cancerous cells leading to invasion and metastasis. These finding were observed in a study on nude mice and their action was identified as associated with the generation of PGE2 and PGF2a (Botha, Robinson *et al*. 1986). Many cancers show evidence of a rise in PGE2 levels and also its impact on numerous cells signalling pathways which contribute to propagation of cancerous phenotypes and their subsequent progression (Wang and DuBois 2010, Sha, Brüne *et al*. 2012, Nakanishi and Rosenberg 2013).

The two isoforms; PTGS1 and PTGS2 are known to be involved in the biosynthesis of PG; specifically, in the committed step. As note previously, PTGS1 and -2 have structural and functional similarities, thus resulting in both producing PGH2. Nevertheless, both isoforms differ in where and when they are expressed as they differ in their distribution in tissues and the synthetic processes that are therefore associated. Thus, their target biological functions vary. The majority of organs express PTGS1 constitutively including the brain, lungs, kidneys, spleen, prostate, gastrointestinal tract, platelets and the liver. The prostanoids resulting from PTGS1 catalytic action contribute to maintenance of homeostasis. Overall, research has indicated that the prostanoid basal rate is preserved through the catalytic action of PTGS1. Re-modelling of cell membranes leads to the generation of free AA which, in turn, leads to a fast rise in prostanoid levels. Contrastingly, alterations in conditions brought about by inflammatory and pathological (including cancerous) changes through release of growth factors and inflammatory instigators leads to the activation of PTGS2 (Smith, DeWitt *et al*. 2000, RICCIOTTI and FITZGERALD 2011). Thus, this results in prostanoid levels being elevated as a response to changes and through the induction of PTGS2. Further research, however, has indicated that pathological changes can lead to the elevation in the expression of both *PTGS1* and *PTGS2* which are both found in normal cells, hence challenging the ideas of “inducible” and “constitutive” actions (Zidar, Odar *et al*. 2009). Research into the isoforms are extensive regarding their expression and regulatory processes. These studies have lately reported on the processes involved in the regulation of the transcription of their genes, as well as the

expression of such genes in both co-transcriptional and post-transcriptional processes (Kang, Mbonye *et al*. 2007, Lutz and Cornett 2013).

There has also been significant research into cancer-associated inflammation and the involvement of PTGS (more specifically PTGS-2) as well as prostaglandins, with a specific interest in PGE2. These association have been studied in many tumour-associated conditions and include haematological tumours (Ramon, F Woeller *et al*. 2013). Aberrant expression of PTGS-2 can result from mutations affecting transcription or post-transcriptional processes and it is such irregular PTGS-2 expression that is reported as a characteristic of tumour cells (Harris 2007, Greenhough, Smartt *et al*. 2009).

PTGS-1 has not been as extensively studied in cancer as PTGS-2, primarily because of its presence as the constitutive isoform which controls the cells' homeostasis and the functioning of tissues. Accordingly, PTGS-1 was not believe to have a role in cancer development and progression. Nevertheless, certain studies have indicated higher levels of expression of PTGS-1 in various cancers (Rouzer and Marnett 2009). Overall, these findings indicated a role for both isoforms of PTGS in tumour carcinogenesis pathways.

Chapter II

Materials and Methods

2.1 Materials

2.1.1 Reagents and kits

In Appendix (**Table A1**), all reagents and kits used in this project are listed.

2.1.2 Buffers

Table 2. 1 shows a list of common buffers used in this research**.**

Table 2. 1 List of buffers

Name	Constituents
10 x Running buffer	1% (w/v) SDS, 1.92 M glycine, 0.25 M Tris
10 x TBS	10 mM Tris-HCl. 150 mM NaCl, pH 7.6
10 x Transfer buffer	0.25 M Tris, 1.92 M glycine
Resolving buffer	1.5 M Tris-HCl. 0.45 (w/v) SDS, pH 8.8
Stacking gel buffer	0.5 M Tris-HCl. 0.45 (w/v) SDS, pH 6.8
TBS-T	1 x TBS, 0.1% tween 20
5% BSA Blocking buffer	1 g BSA in 20 ml TBS-T
1 x Annexin V binding buffer	10 mM HEPES/NaOH (pH 7.4), 140 mM NaCl, 2.5 mM CaCl2

2.1.3 Antibodies

All antibodies were purchased from Cell Signalling Technology (CST) through New England Biotech (NEB, Hitchin, UK). A list of the common antibodies used in this research is found in **Table 2. 2**.

Table 2. 2 Primary and secondary antibodies

Antibody	Source	Cat. No.	Dilution	MW (kDa)	Species
Anti-Mouse IgG	CST	7076	1:3000	n/a	Horse
Anti-Rabbit IgG	CST	7074	1:3000	n/a	Goat
β-Actin	CST	3700	1:5000	45	Mouse
COX2	CST	12282	1:1000	74	Rabbit
COX1	CST	9896	1:500	70	Rabbit
AKT	CST	2920	1:2000	60	Mouse
P-AKT	CST	4060	1:2000	60	Rabbit
p44/42 MAPK	CST	9102	1:1000	42,44	Rabbit
P-p44/42 MAPK	CST	4370	1:2000	42,44	Rabbit
MPO	CST	14569	1:1000	60,80-90	Rabbit
C-MYC	CST	13987S	1:1000	57-65	Rabbit
P-CREP	CST	9198S	1:1000	43	Rabbit
CREP	CST	9197	1:1000	43	Rabbit
P-STAT-5	CST	9351	1:1000	90	Rabbit
STAT-5	CST	25656	1:1000	90	Rabbit
P-GSK-3-β	CST	9336	1:1000	46	Rabbit
GSK-3-β	CST	9832	1:1000	46	Mouse
P-β-Catenin	CST	9561	1:1000	92	Rabbit
β-Catenin	CST	8480	1:1000	92	Rabbit
P-NPM	CST	3520S	1:1000	38	Rabbit
NPM	CST	3542S	1:1000	38	Rabbit
PARP	CST	9532	1:1000	116,90	Rabbit
BCL-2	CST	4223	1:2000	26	Rabbit
BCL-XL	CST	7262	1:2000	30	Rabbit
MCL-1	Abcam	Ab32087	1:1000	35,40	Rabbit
BIM	CST	2933	1:2000	12.15	Rabbit

2.1.4 Cell lines

The AML cell lines OCI-AML-3, U937, Hl-60 and MOLM-13 were purchased from the Deutsche Sammlung von Mikroorganismen und Zellkulturen GmbH (DSMZ) (Braunschweig, DE). AML cell line characteristics are shown in **Table 2. 3**

Table 2. 3 Characteristics of AML cell lines

Cell line	Cell type	Patient age/sex	Leukaemia subtype	Doubling time (h)
OCI-AML-3	Acute myeloid leukaemia	57/male	AML FAB M4	35-40
U937	Histiocytic lymphoma	31/ Female	AML FAB M5	30-40
HL-60	Acute promyelocytic Leukaemia	36/Female	AML FAB M2	36-48
MOLM-13	Acute monocytic leukaemia	70/male	AML FAB M5a	50

2.2 Cell lines maintenance

2.2.1 Cell culture

Roswell Park Memorial Institute (RPMI) Medium 1640 (1X) supplemented with 10% foetal bovine serum (FBS) and 1% penicillin/streptomycin was used to maintain AML cell lines. All cell lines were cultured in a humidified atmosphere at 37°C with 5% carbon dioxide (CO_2). All cell lines were passaged every 2-3 days at a ratio (**Table 2. 4**). Passage number of cells was kept as low as possible.

Table 2. 4 Cell medium and splitting ratio		
Cell line	**Culture medium**	**Splitting ratio**
OCI-AML-3	RPMI	1:9
U937	RPMI	1:9
MOLM-13	RPMI	1:4
HL-60	RPMI	1:9

2.2.2 Cell counting

The trypan blue exclusion methodology was utilised to routinely count cells and determine viability. Briefly, trypan blue stains non-viable cells dark blue due to its ability to pass through ruptured cell membranes in these cells. In contrast, live cells have impermeable membranes, so they appear as a shiny bright halo under the microscope. Cells were counted using a haemocytometer after being diluted 1:1 in PBS with trypan blue (0.1% (w/v)).

2.2.3 Cell lines cryopreservation

Each cell line stock at low passage number (<10) was prepared for use during this study. For preservation, cell pellets were extracted by centrifugation at 300 g for 5 minutes, culture medium was replaced with freezing media (10% DMSO in FBS) and transferred to cryovials (Corning, UK). A ‘Mr. Frosty’ freezing container (Thermo-Fisher) was used to keep the cryovials at -80ºC for 24 hours, in order to slowly reduce the temperature preventing ice-crystal formation, before being placed in liquid nitrogen for long-term storage.

2.2.4 Cryopreserved cell lines thawing

Cryovials were warmed in a water bath at 37°C to recover cells from liquid nitrogen. Then they were transferred to a fresh tube containing 10ml of fresh medium to dilute out the DMSO in the freezing medium. Subsequently the DMSO and dead cells were removed by using centrifuge at 300g for 5 minutes. The cell pellets were then resuspended in appropriate volume of fresh media and incubated in a humidified incubator at 37°C with 5% CO_2.

2.2.5 Selective Cox-1 inhibitor SC-560 and Tenidap treatment of AML cells

Each cell line was seeded in 6 well plates at density of $1x10^6$ cells per ml in 2ml RPMI and incubated overnight at 37°C with 5% CO_2. After 24 hours the cells were treated with varying concentrations of SC-560 and Tenidap for indicated times and incubated at 37°C. After treatment medium was removed by centrifugation (300 g for 5 minutes) at 4°C and cell pellets were kept in ice for processing in downstream assays.

2.3 Protein analysis

2.3.1 Cell lysate preparation

Cells were harvested in 15 ml tubes on ice to prepare protein lysates. Followed by centrifugation at 300 g for 5 minutes (at 4^{o}C), pellets were washed with 1ml ice-cold PBS and transferred to 1.5ml Eppendorf tubes, then these pellets were lysed with Radio-Immunoprecipitation Assay buffer (RIPA buffer). These samples were incubated in ice for 20 minutes. They then were sonicated on ice and cleared by centrifugation at 21000 g for 5 minutes. The supernatants were placed in new Eppendorf tubes, which were subsequently used for protein determination.

2.3.2 Protein quantification by Bradford assay

a Bio-Rad DC protein assay kit (Bio-Rad laboratories Ltd, UK) was used to measure total protein concentration according to the manufacturer's instructions. briefly, different concentrations of Bovine Serum Albumin (BSA) protein standards were prepared. First, 5 µL of both standers and samples (in triplicate) were placed in a 96-well plate. Then, at a 1:50 dilution, reagent A and reagent S were mixed, and 25µL of this mixture was added with 200µL of reagent B to each well. Then the plate was incubated in the dark for 20 minutes at room temperature. A plate reader (Bio-Tek, UK) was used at 650nm to measure the absorbance of the samples.

2.3.3 Sample preparation

Lysate samples were diluted with RIPA buffer to obtain the appropriate concentration of total protein (30µg in 20µL with 4x Laemmli buffer). These samples were placed on a heating block at 95°C for 5 minutes to denature proteins. Following this, proteins were analysed by A Sodium Dodecyl Sulphate Polyacrylamide Gel Electrophoresis (SDS-PAGE) and western blotting.

2.3.4 Protein separation by SDS-PAGE

Separation of proteins' size ranges using SDS-PAGE according to molecular weight was applied. Both 10% and 12% of polyacrylamide gels were used according to target protein's size (**Table 2. 5**).

Table 2. 5 Resolving and Stacking gel recipes for 4 gels

	Resolving Gel		Stacking Gel
	10%	12%	5%
ddH2O	16.6 ml	14 ml	5.8 ml
Resolving	10 ml	10 ml	-
Acrylamide (30%)	13.4 ml	16 ml	1.7 ml
Stacking buffer	-	-	2.5 ml
10% APS	400 µl	40 µl	60 µl
TEMED	40 µl	40 µl	20 µl

Assembled gels in the Mini-PROTEAN® Tetra Vertical Electrophoresis Cell (Bio-Rad) were placed into a tank filled with pre-made SDS running buffer (192 mM glycine, 25 mM Tris and 0.1% (w/v) SDS). Then in the first line of each gel were filled with 10 µl of Page Ruler PlusTM protein ladder (Thermo Fisher). The next wells of the gel were filled with equal amounts of diluted protein (calculated as described previously). An equal amount of 1X loading dye was added to empty wells. lastly, the equipment was connected to a power supply to run the gels at a constant voltage of 130 V for 90 minutes.

2.3.5 Western blotting

Once the separation was completely done, the gels were washed by transfer buffer (192 mM glycine and 25 mM Tris) (Geneflow, UK) for 5 minutes prior to transfer. Separated proteins by SDS-PAGE were then transferred to Hybond-ECL nitrocellulose (Amersham) at 100 V for 1 hour. Following transfer, the membranes were washed with 1 x TBS-T (Tris-buffered saline containing 0.1% Tween 20). These membranes were incubated with blocking buffer (TBS-T containing 5% (w/v) non-fat milk or 5% (w/v) BSA) on shaker for 1 hour at room temperature. Following this step membranes were incubated overnight at 4ºC with the suitable primary antibody. The membranes were then washed three times with TBS-T to gain a good result, which then were incubated with an appropriate secondary antibody for 1hour at room temperature. Following this, membranes were washed three times with TBS-T followed by a wash with TBS prior to be developed with enhanced chemiluminescence (ECL) (Millipore). The ChemiDoc imaging system (Bio-Rad) was used to visualise membranes.

2.3.6 Quantification of protein expression

Quantification of the immune reactive bands found on ChemiDoc was used to assess the relative abundance of particular proteins. ImageJ (National Institution of Health (NIH), Version 1.48n) was used for densitometric analysis. Next, by dividing each phospho-protein by its own total protein, the ratio of each condition was calculated. After that, bar graphs were created using GraphPad Prism 8.

2.4 Functional assays

2.4.1 Annexin V and Propidium Iodide staining

Flow cytometry analysis was performed using the Thermo Fisher Attune NxT Flow Cytometer to measure cell apoptosis using Annexin V/ PI staining. Cells were prepared by centrifugation at 300 g for 5 min. After being washed twice with PBS, the pellets were resuspended in 100 µl Annexin V binding buffer (140 mM NaCl, 10 mM HEPES, and 2.5 mM CaCl2). The tubes were then incubated for 10 minutes with 2 µl of FITC Annexin V (Biolegend, UK). 10 µl of propidium iodide solution was added, and cells were then incubated for 15 minutes at room temperature (25^{o}C) in the dark. Flow cytometry was used to analyse these cells with proper machine settings. Data analysis was conducted with FlowJo™ v10 Software.

2.4.2 Cell cycle

Flow cytometry (Thermo Fisher Attune NxT Flow Cytometer) and propidium iodide (PI) stain were utilised to conduct cell cycle analysis. Cell pellets were washed with ice cold phosphate buffered saline (PBS) and fixed in 70% ethanol on ice for 30 minutes. These pellets were then washed twice in PBS before being incubated with RNase (5µl of (1 mg/ml stock) for 30 minutes at 37˚C. After incubation, cells were stained at room temperature with 5 µL of PI (1mg/ml stock) for 5 minutes in the dark and analysed by flow cytometry. Data analysis was conducted with FlowJo™ v10 Software.

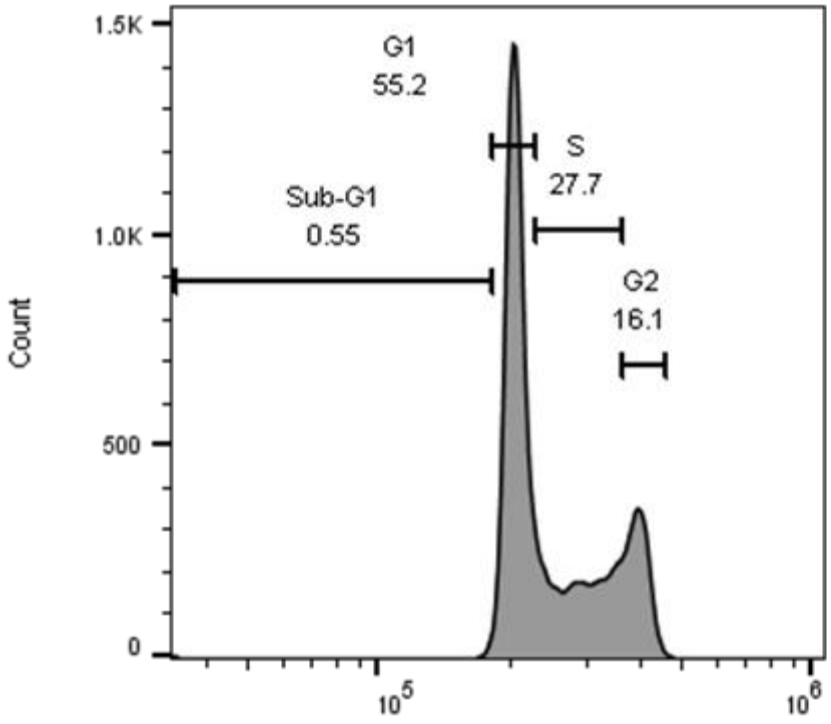

Figure 2. 1 the cell cycle analysis was performed on cells stained with Propidium Iodide (PI) and gated based on their fluorescence intensity.

The gates were applied to the PE histogram, which was obtained from single cells while excluding debris to ensure accurate analysis. The data obtained from the gating were presented as fractions of "live" cells. In order to visualize the prominent G0/G1 peak and smaller G2 peak, the voltages were adjusted accordingly. The region between these two peaks was denoted as the cells in the S-phase.

2.4.3 Measurement of ROS levels

1.4.3.1 CellROX

Cells were grown in a 6-well plate at a density of $5x10^5$ cells per ml in 2ml RPMI and incubated overnight at 37°C with 5% CO_2. The cells were treated with 300nM ara-C and 1µM SC-560 and then incubated for 24 hours. After the recommended time, the cells were stained with CellROX green (Thermo Fisher Scientific, C10444: reactive oxygen species five green colours) at a final concentration of 5 µM for 30 minutes at 37ºC to detect ROS. ROS level in cells was determined by flow cytometry. Data analysis was conducted with FlowJo™ v10 Software.

1.4.3.2 MitoSOX

5µM MitoSOX™ working solution was prepared by diluting the 5mM MitoSOX™ reagent stock solution (Thermo Fisher Scientific, M36008: Red Mitochondrial Superoxide Indicator) in HBSS/Ca/Mg. Cells were grown in a 6-well plate at a density of $5x10^5$ cells per ml in 2 ml RPMI and incubated overnight at 37°C with 5% CO_2. The cells were treated with 300nM ara-C and 1µM SC-560 and then incubated for 24 hours. After a recommended time, the cells were stained with MitoSOX™ working solution at a final concentration of 5 µM. The cells were incubated in the dark for 10 minutes at 37ºC. These cells were washed gently three times with warm PBS. Flow cytometry was used to analyse these cells with proper machine settings. Data was analysed using FlowJo™ v10 Software.

2.4.4 Cell surface expression by flow cytometry

Cells were pelleted at 500 g for 5 min and re-suspended in 100 µL of PBS. To assess cell surface, cells were stained with 1 µg of CD marker antibody or 2.5 µg of an isotype control antibody for 20 min before being washed once with PBS. Pellets were re-suspended in PBS, and cells were analysed by flow cytometry using FlowJo™ v10 Software.

Antibodies:

- Alexa Fluor® 488 antibody (HLA-A,B,C), isotype Mouse IgG2a (Cat: 311415)
- FITC anti-human CD33, isotype Mouse IgGI, k (Cat: 303303)
- FITC anti-human CD86, isotype Mouse IgGI, k (Cat: 374203)
- FITC anti-human CD52, isotype Mouse IgG2a, k (Cat: 316003)

2.5 Molecular biology techniques

2.5.1 Virus production in HEK-293T cells

Packaging plasmid psPAX2, an envelope plasmid encoding VSV-G (pMD2.G) and a lentiviral transfer plasmid are necessary for virus production. Dulbecco's Modified Eagle Medium supplemented with 10% FBS, antibiotic-free, was used to maintain HEK-293T cells. 9 x 10^6 HEK-293T cells were seeded in a T75 flask and adhered overnight. All reagents were brought to room temperature. For the transfection mixture, 150 µL of 150 mM NaCl and 20 µL of 1 mg/mL Polyethylenimine (PEI) were combined in one tube, and 150µL of 150 mM NaCl with 4µg of transfer plasmid (Lentiviral plasmid containing gene of interest) and 2µg of each of the packaging and envelope plasmids were combined in a separate tube. These mixtures were then mixed by vortexing and left for 15 minutes at room temperature before being added dropwise to the HEK-293T cells. Virus-rich media was collected after 72 hours post-transfection, and the media (containing the viral particles) was removed by Ultracentrifugation at 4°C for 2 h at 24000 rpm using a P32ST rotor in a Beckman Ultracentrifuge. The supernatant was removed, the pellet air dried, and then resuspended in 300µl PBS. Aliquot virus was stored at -80^{o}C long term to avoid repetitive freeze-thawing that may decrease the infectivity of the virus..

2.5.2 Transfection of DNA into AML cell

PTGS1 and PTGS2 cDNA clones were transduced into HL-60 and U937 using Polybrene (Sigma). 5 ×10^5 cells were plated into 6-well plates in 2 ml antibiotic-free RPMI 24h before transfection. The following day 8µg/ml of Polybrene was

mixed with 5-20 µg of plasmid DNA. This mixture was then added to the cells dropwise, and the plates were returned to the incubator. The virus was removed after 72 hours by spinning cells down and resuspending in fresh media. An enhanced green fluorescent protein (EGFP) was routinely used to ensure transfection worked as cells could be visualized by fluorescence microscope.

2.5.3 Puromycin selection of transduced cells

$\times 10^5$ transfected and non-transfected (control) cells were plated into 12-well plates in 1 ml RPMI media. The following day, puromycin was added at different concentrations (0.1-0.5 mg/ml). The cells were counted daily using a haemocytometer after diluting 1:1 in PBS with trypan blue. The death cells were compared to the control cells (non-transfected). Puromycin was removed when there was approximately 80% death in the control cells by centrifugation at 2000 rpm for 5 minutes, and the cells were resuspended in fresh media.

2.5.4 RNA extraction

1×10^6 cells were plated into 6-well plates in 2 ml RPMI media. The following day, 300 nM of ara-C was added to the cells and incubated for 24h. After the recommended time, cells were collected into 2 ml Eppendorf tubes. Total RNA was obtained using the Monarch Total RNA Miniprep Kit (New England BioLabs). In brief, the cell pellets were collected by centrifugation (500 g) for 1 min, and the pellets were then resuspended in 300 µM RNA lysis buffer and mixed thoroughly before they were transferred to a gDNA removal column fitted with a collection tube. Most of the gDNA was removed by centrifugation at 16000 g for 30 seconds, and the gDNA removal column was discarded. An equal volume of ≥95% ethanol was added to the lysate, which was then applied

to an RNA purification column. The column was washed with the RNA wash buffer and RPE. Afterwards, the empty spin column was centrifuged to remove any traces of ethanol before being eluted using 30 µl DNase/RNase-free water. The extracted RNA was then placed on ice to assess purity and quantity by nanodrop. The remaining RNA was then stored at -80^{o}C.

2.5.5 Measuring purity and quantity of RNA

The determination of extracted RNA quality and quantity were done by using a nanodrop 2000 spectrophotometer (Thermo Fisher Scientific, UK). Specifically, RNAse-free water was used as a control and 1ul of each RNA sample was used to determine the purity of the RNA extracted using the Nanodrop machine, which measures the absorbance ratio at OD260/280 and OD260/230.

Table 2. 6 purity and quantity of RNA

Sample	ID	ara-C (nM)	RNA (ng/µl)	Purity (Nanodrop) 260/280	Volume (µl)	Total (ng)
U937 wild-type	U1	0	145.4	2.1	30	4362
U937 wild-type	U2	0	174.1	2.07	30	5223
U937 wild-type	U3	0	181.9	2.09	30	5457
U937 wild-type+C	U4	300	141.2	2.09	30	4236
U937 wild-type+C	U5	300	171.4	2.07	30	5142
U937 wild-type+C	U6	300	180.9	2.09	30	5427
U937 PTGS1	U7	0	162.6	2.08	30	4878
U937 PTGS1	U8	0	134.2	2.05	30	4026
U937 PTGS1	U9	0	121.7	2.1	30	3651
U937 PTGS1+C	U10	300	185.5	2.07	30	5565
U937 PTGS1+C	U11	300	79.7	2.09	30	2391
U937 PTGS1+C	U12	300	168.8	2.08	30	5064
U937 PTGS2	U13	0	164.3	2.06	30	4929
U937 PTGS2	U14	0	185.7	2.07	30	5571
U937 PTGS2	U15	0	252	2.09	30	7560
U937 PTGS2+C	U16	300	164.3	2.08	30	4929
U937 PTGS2+C	U17	300	153.3	2.07	30	4599
U937 PTGS2+C	U18	300	104.2	2.06	30	3126
Hl-60 wild-type	H1	0	585.9	2.06	30	17577
Hl-60 wild-type	H2	0	619.3	2.07	30	18579
Hl-60 wild-type	H3	0	756.5	2.08	30	22695
Hl-60 wild-type+C	H4	300	563.2	2.08	30	16896
Hl-60 wild-type+C	H5	300	510.5	2.1	30	15315
Hl-60 wild-type+C	H6	300	522.9	2.08	30	15687
Hl-60 PTGS1	H7	0	564.8	2.06	30	16944
Hl-60 PTGS1	H8	0	654.3	2.05	30	19629
Hl-60 PTGS1	H9	0	529.9	2.09	30	15897
Hl-60 PTGS1+C	H10	300	403.3	2.07	30	12099
Hl-60 PTGS1+C	H11	300	430.8	2.09	30	12924
Hl-60 PTGS1 +C	H12	300	367.2	2.11	30	11016
Hl-60 PTGS2	H13	0	740.6	2.1	30	22218
Hl-60 PTGS2	H14	0	653.4	2.09	30	19602
Hl-60 PTGS2	H15	0	512.9	2.05	30	15387
Hl-60 PTGS2+C	H16	300	470	2.14	30	14100
Hl-60 PTGS2+C	H17	300	430.3	2.07	30	12909
Hl-60 PTGS2+C	H18	300	419	2.07	30	12570

2.5.6 Gel electrophoresis

Agarose gel electrophoresis was performed to determine RNA quality. 1 g of agarose gel was dissolved in 100ml of TAE (40 mM TRIS, 20 mM acetic acid and 1 mM EDTA) with 8% bleach using microwave. 3 µl of ethidium bromide was added to the solution before pouring it. RNA samples were de-natured by heating at 65ºC for 5 minutes in a heat block. RNA samples and an appropriate DNA “ladder” were mixed with a 6x loading dye (NEB), and the gel ran at 100 V for 30 minutes or until sufficient separation was seen. Gels were then visualized ethidium bromide setting on a ChemiDoc imager (Bio-Rad).

2.5.7 RNA sequencing

The samples were sent for sequencing by RNA-seq technology at Glasgow Polyomics (Wolfson Wohl Cancer Res Centre, Glasgow, UK). The raw data was returned electronically and analysed by using different bioinformatics tools. The population of RNA was transformed into a library of cDNA fragments with adaptors linked to one or both ends of up to several base pairs due to the technological requirements for sequencing, and these fragments will travel through short reads.

2.5.8 Quality control

FastQ and bam files are the formats used for RNA-seq data. For each nucleotide, FastQ files provide sequences and quality ratings. The data was uploaded into the FASTQC tool to evaluate the FastQ files' quality. For each sample, FASTQC creates an HTML file. This information is supplied into

MultiQC, which summarises the quality control of all models in a single html file as a report.

2.5.9 RNA-Seq data analysis

The basic analysis was performed under the supervision of Dr Graham Hamilton (the University of Glasgow). Subsequently, a diversity of bioinformatics software, such as Cystoscope V3.9.1, ShinyGO 0.80, iDEP.96, GSEA 4.2.3, Perseus 1.6.8.0 and g:Profiler, was utilised to analyse this data.

g:Profiler.

g:Profiler tool was used to convert the Ensembl Gene ID to gene name. Also, this tool provides comprehensive information, such as functional enrichment analysis results.

Perseus analysis.

The data was visualised using Perseus software (Version 1.6.8.0, Max Planck Institute) (e.g., scatter plots and numeric Venn diagram). The normalised file was loaded to Perseus by clicking the “Genetic matrix upload” button. 2 of 3 biological replicates in at least one group then was applied to filter the data. The ratio of the data to control was taken using RAW gene expressions to visualise the Pearson correlation, scatter plots and numeric Venn diagram.

iDEP.96.

iDEP.96 platform was used for the comprehensive analysis of RNA-seq data. It provides a suite of tools for pre-processing, differential gene expression analysis, clustering, and pathway analysis. The interactive visualizations, such

as heatmaps, correlation matrix, and Principal Component Analysis (PCA), were generated using iDEP.96.

ShinyGO 0.80

A list of differentially expressed genes was prepared from RNA-seq data using iDEP.96. The list was then pasted into the input box on the ShinyGO 0.80 website. This tool allows us to customize various parameters, such as multiple testing correction, the statistical method for enrichment analysis, and visualization options. Then, the "Submit" button was clicked to initiate the analysis. Once the analysis was completed, the data was presented with interactive visualizations, including bar charts and hierarchical clustering trees, representing enriched GO terms or pathways.

2.6 The Enzyme-Linked Immunosorbent Assay

The monoclonal prostaglandin E2 (PGE2) ELISA kit (CAY514010-96) was utilised to quantitatively assess PGE2 levels. The 96 solid wells are used to conduct the experiment. Prepare the samples and standards first, ensuring they have been properly diluted in line with the kit's instructions. The prepared standards and samples should then be added 50µl into the appropriate wells at a time. Then, add 50µl of the PGE2 AChE tracer to each well except the total activity and the blank wells. Then, except total activity, the blank and the non-specific binding wells, add 50µl of the PGE2 conjugate solution to each well (**Table 2. 7**).

The plate should be incubated for the allotted time at the suggested temperature. Discard the contents and thoroughly wash the wells five times with wash buffer after incubation. Subsequently, add 200 µL of the Ellman's reagent to all wells. An ELISA plate reader is used to measure the absorbance at a wavelength between 405 and 420nm. Quantitative analysis is made possible by determining the target antigen concentration in the samples by comparing their absorbance to a standard curve created from known concentrations. To get precise and repeatable results from an ELISA, it is crucial to adhere to the manufacturer's recommendations and optimise the settings.

Table 2. 7 Pipetting summary

Well	ELISA Buffer	Tracer	Standard/Sample	Antibody
Blk	-	-	-	-
TA	-	5 µl	-	-
NSB	100 µl	50 µl	-	-
Std/Sample	-	50 µl	50 µl	50 µl

2.7 Real-time PCR

2.7.1 RNA extractions.

The RNA from the cell pellets under investigation was isolated and extracted using the Monarch Total RNA Miniprep Kit. Cell pellets were reconstituted in 1ml of 1x PBS and spun down at 500 g for 1 minute by the manufacturer's instructions. The supernatant was then discarded. Cells were gently mixed with RNA lysis buffer after being used to lyse them, and the mixture was then pipetted onto a collection tube with a gDNA removal column. The entire centrifugation operation was placed on the column at 16000 g for 30 seconds. The lysis buffer was previously added to the flow through, and absolute ethanol (95%) was mixed by pipetting and then passed to the purification column of the RNA attached to the collecting tube. 500 µl of RNA wash buffer was added to the RNA purification column before centrifugation, discarding the flow through, and centrifuging again. A second washing procedure was carried out with a 2-minute centrifugation period. The RNA purification column was then put into an Eppendorf tube following centrifugation. After adding 50µl of nuclease-free water, the RNA was centrifuged from the purification column's membrane. The Nano-drop was used to gauge the isolated RNA's concentration.

Table 2. 8 RNA Extraction Kit description

Product Name	Supplier	Catalog #	size
Monarch Total RNA Mininprep Kit	New England BioLabs	T2010S	50 preps

2.7.2 cDNA synthesis (Reverse Transcription).

The LunaScript™ RT SuperMix Kit from New England BioLab was used to transcribe and synthesise the cDNA using 1µg of RNA, as the manufacturer's handbook directed. Before commencing and setting up the cDNA synthesis procedure, the tubes containing the RNA sample tubes and the kit's parts were briefly spun down. The cDNA synthesis reaction's setup step is shown in **Table 2. 9**.

Table 2. 9 Preparation of cDNA synthesis Reaction

Component/Reagent	**Volume in 20 ul RXN**	**Final conc.**
LunaScript RT SuperMix (5x)	4 µl	1x
RNA Sample	variable	1 µg
Nuclease-free Water	To 20 µl	

Samples were put in the conventional PCR machine (thermal cycler) after the cDNA synthesis reaction was prepared, and the reactions were then incubated in three stages of thermal cycles (**Table 2. 10**).

Table 2. 10 Thermal Cycling Temperature of cDNA synthesis.

Cycle Stage	**Temperatures**	**No. of Cycles**
Primer Annealing	25 ^{0}C	
cDNA Synthesis	55 ^{0}C	**1x**
Heat Inactivation	95 ^{0}C	

2.7.3 Quantitative/Real Time-Polymerase Chain Reaction (qPCR)

Luna® Universal qPCR Master Mix kit purchased from New England BioLab was used to detect the generated amplicons of the genes of interest and the housekeeping gene based on SYBR green fluorescence detection. The premieres used in this experiment are shown in **Table 2. 11**.

Table 2. 11 RT² qPCR Primer Assay.

Primer Assay	Cat No./ID	Supplier
RT² qPCR Primer Assay for Human PTGS1	PPH01306F-200	**Qiagen**
RT² qPCR Primer Assay for Human PTGS2	PPH01136F-200	
RT² qPCR Primer Assay for Human ACTB	PPH00073G-200	

As shown in **Table 2. 11**, the following reagents were initially combined in a 0.5 ml tube to prepare the qPCR reaction. In order to make the total volume of the qPCR reaction 20 µl in each well, 18 µl of the master mix was put in each well of a 96-well qPCR plate (PrimerDesign) along with 2 µl of the produced cDNA (conc. of the cDNA in this reaction 5 ng/µl).

Table 2. 12 Typical qPCR protocol

Component	**20µl Reaction**	**Final conc.**
Luna Universal qPCR Mix	10 µl	1x
Primers (5µM)	2 µl	-
Nuclease-Free Water	To 18 µl	-

After that, the plate was spun at 500 g for 2 minutes to verify that the qPCR reaction was assembled in the bottom of each well. The plate was then put into the AriaMix qPCR machine, and the reaction's thermal cycling was set up as shown in **Table 2. 12**. The result was normalised using the expression of beta-actin, and the fold change in the gene's expression was measured using the delta-delta Ct technique.

Table 2. 13 qPCR Reaction Thermal Cycling.

Step	Cycles	Temperature	time
Initial Denaturation	1	95°C	1 min
Denaturation	40-45	95°C	15 seconds
Extension		60°C	30 seconds
Melt Curve	1	60-95°C	1min:30sec

2.8 Co-Culture and Immune Assays.

2.8.1 PBMCs extraction and Isolation from Whole Blood by Lymphoprep.

To isolate the PBMCs from 10ml heparinized whole blood collected from a health donor, 10 ml of the whole blood was added into a 50ml falcon tube prefilled with 10 ml 1x PBS to achieve 1:1 dilution. Then, the diluted blood was decanted into another 50ml falcon tube containing 20 ml of Lymphoprep medium. The mixture (Lymphoprep and diluted blood) was centrifuged at 500 g for 25 min at 21^{o}C with no brake and acceleration adjusted at 3. The centrifugation process resulted in a lower layer of erythrocyte separated by a lymphoprep layer that served as a barrier between the erythrocyte and the buffy coat that contains the PBMCs and a third upper layer of plasma on the top of the PBMCs.

Post-centrifugation, the turbid band of PBMCs was carefully collected using a sterilized transfer pipette and placed into a 15 mL conical tube filled with 10mL of 1x PBS using a sterilized transfer pipette. Following an upside-down shake to combine the contents, the capped tube was centrifuged at 300 g for 15 minutes at 4^{o}C. The supernatant from the centrifugation process was removed again with extra caution to avoid disrupting the cell pellets. PBMCs were then resuspended in FBS to a total volume of 3ml. Six 3ml FBS suspended cell aliquots were distributed into 2ml cryovials (6 cryovials/500µl for each). Each cryovial was prefilled with freezing media 500 µl, made of FBS and DMSO 20%, and the final concentration of the DMSO was 10%. The cryovials were placed

in Mr Frosty's container, stored at -80^{o}C for 24h, and then transferred to the liquid nitrogen tank for long-term storage.

2.8.2 CD8 T-cells Suppression/Proliferation Assay

Isolation of CD3 T-cells from PBMCs:

Frozen peripheral blood mononuclear cells (PBMCs) from the blood of a healthy donor were used to isolate human $CD3^{+}$ T-cells using a positive selection kit (EasySep^{TM} Release Human CD3 Positive Selection Kit II). Dr. Lekh's team kindly gave the PBMCs, and I appreciate their collaboration. The PBMCs were defrosted in a water bath before being put into a 50 ml falcon tube that had already been pre-filled with 1x PBS and at least thrice cleaned. $CD3^{+}$ T-cells were isolated using the procedures in the isolation kit. A 5 mL (12 x 75mm) polystyrene round-bottom tub was used because the kit requires $10x10^{8}$ cells/ml, and the PBMCs were resuspended in 1.25 ml of 1xPBS before being transferred. 125 µl of the EasySep^{TM} Human CD3 Positive Selection Cocktail was incubated with PBMCs for 3 minutes at room temperature.

PBMCs were incubated with 125 µl of the EasySep^{TM} Human CD3 Positive Selection Cocktail for 3 minutes at room temperature. 75 µl of EasySepTM Dextran RapidSpheres (beads) were added after the incubation period and incubated once more. After incubation, the tube was topped off with the appropriate medium, made up of 1xPBS with 2% FBS, and then incubated for 3 minutes at room temperature. After incubation, the supernatant was removed, and the isolated $CD3^{+}$ T-cells were adhered to the tube wall. $CD3^{+}$ T-cells were

washed again with the appropriate medium, put in the magnet, and then collected in a 50 ml falcon tube.

T- cells Staining with CFSE (CarboxyFluorescein Succinimidyl Ester)

After $CD3^+$ T-cells were first stained with the cell tracking and proliferation dye CFSE, CD8 T-cells were activated and stimulated to study CD8 T-cell suppression/proliferation in a co-culture system. A 30ml universal tube containing $5x10^6$ $CD3^+$ T-cells was stained by adding 1µl of CFSE before being incubated at room temperature for 5 minutes in the dark. After that, the medium was added to the universal and centrifuged at 350g for 5 min. In RPMI medium enriched with 10% FBS and 1% P/S and adjusted to achieve at $1x10^6$ cells/ml, $CD3^+$ T-cells were counted and resuspended.

CD3+ T-cells Stimulation with Purified anti-human CD3/CD28 Antibodies.

Purified anti-human CD3/CD28 antibodies were used to encourage CD8 T-cell proliferation and activation from $CD3^+$ T-cells to monitor CD8 T-cell suppression/proliferation in a co-culture system with effector cells.

Plate Pre-coating with Purified anti-human CD3.

By pouring 100µl of the working solution into the required wells, 5µg of pure anti-human CD3 was pre-coated onto half of a 96-well U-shaped bottom plate. A purified anti-human CD3 working solution is made by mixing 1ml of 1xPBS with 2.5 µl of anti-human CD3 stock (2mg/ml). The plate was placed in the

incubator for two hours at 37°C with 5% CO_2. After the incubation period, the plate was twice rinsed with 1xPBS to eliminate any extra anti-human CD3 antibody.

$CD3^+$ T-Cell Stimulation with Purified anti-human CD28.

The number of T-cells was adjusted at $5x10^6$ cells/5 ml. 2.5 ml of the cells were stimulated with Purified anti-human CD28, and the other half was left as a negative control. 25 µl of Purified anti-human CD28 were added into 2.5 ml of T- cells to achieve the concentration 10µg/ml (stock conc. of Purified anti-human CD28 was 1mg/ml).

T-Cells and AML Cells Plating:

CD28-stimulated T-cells were added into the wells previously coated with anti-human CD3. The cells were pipetted into the plate wells in 100 µl/well. The number of cells was previously adjusted at $2.5x10^6$ cells/2.5 ml, so each well contains $1x10^5$ cells/100 µl. Un-stimulated T-cells (-ve control) were added into uncoated wells with the same cell density/volume as stimulated T-cells. Effectors cells (AML cell lines) were added to the Stimulated T-cells at ratio (Target: Effector) 1:0.1, 1:1 and 1:10. The number of T-cells the Target cells (T) was consistent in the co-culture system, while the numbers of Effector cells (E) AML cell lines were $1x10^4$, $1x10^5$ and $1x10^6$ cells per 100 µl, AML cells were adjusted at density $10x10^6$ cells/ml in RPMI supplemented with 10 FBS and 1% P/S. The positive and negative controls of stimulated/unstimulated T-cells were cultured alone (with no Effector cells added) in 6 wells each. The plate was then incubated at 37^0C in 5% CO_2 for 4 days.

CD8 T-Cells proliferation Monitoring by Flow Cytometry:

On Day 4, the positive control was checked to monitor the proliferation of CD8 T-cells. The proliferation percentage was >60% compared to the negative control (unstimulated) ~0% proliferation; the experiment was ready to be examined by flow cytometry. APC anti-human CD8 Antibody was added to each well in 2 µl/well to stain proliferating CD8+ T-cells. The plate was then incubated on ice in the dark for 30 mins and then centrifuged at 400g for 5 mins. The supernatant was removed, and 200 µl of 1xPBS was added into each tube and centrifuged as previously. After removing the supernatant, another 200 µl of 1xPBS was pipetted into each well, and the content of the wells was distributed into several Eppendorf tubes according to the number of the tested wells. Finally, samples were assessed by flow cytometry.

2.9 Database analysis

The following platforms were used in this study for data acquired and analysis:

- The Cbioportal (TCGA)
- NCBI GEO (Verhaak project and Metzeler II project)
- DepMap (*PTGS1/2* expression in various human primary diseases)
- Bloodspot (Transcript expression of PTGS1/2 in HSCs and leukaemia classifications)

Data gained were subjected to data filtering process using Microsoft Excel. This process involved the exclusion of samples with missing or incomplete information, ensuring the integrity and reliability of the subsequent analyses. Then, GraphPad Prism 8 software was employed to generate the results presented.

2.10 Statistics

GraphPad Prism 8 was used to analyse the data for this thesis. The relevant results section includes details of the analyses.

Chapter III

3.1 Introduction

Changes in arachidonic acid metabolism significantly affects the way cancer develops and progresses. Within this, previous research points to upregulation of PTGS2 in a range of cancer types, such as colorectal cancer, breast, liver, stomach, bladder and long cancer, for which worse patient outcomes are seen with increased expression of PTGS2. Prostaglandin E2 (PGE2) is the product of PTGS2 which is most notable in cancers, associated with poorer outcomes and contributing significantly to promotion of growth of tumours (Wang and DuBois 2010). Additionally, reports link PTGS1 to maintaining capacity for anchorage-independent growth in colorectal cancer cells, as well as to prostaglandin production at more advanced stages in the developing tumour (Li et al. 2014; Pannunzio and Coluccia 2018). Ding et al. (2019) further suggest that when PTGS1 is downregulated apoptosis may be stimulated in colon cancer cells in humans.

PGE2 is generally accepted as a significant contributor to managing haematopoiesis, been shown in vitro and in vivo to limit myelopoiesis, as well as promoting the formation of colonies of multi-lineage and erythroid cells (Lu et al. 1984; Lu et al. 1987). Moreover, HSC survival is promoted by PGE2, regulatory hematopoietic stem cells and progenitors are encouraged to grow, and hematopoietic recovery after damage from radiation is more rapid (Porter et al. 2013; Ben Nasr et al. 2018).

Researchers have assessed enzyme PTGS1's association with ovarian cancer, and found aspirin to act effectively as a powerful PTGS1/COX-1 inhibitor. Impacts on gastro-intestinal cancers from the PTGS2 and prostaglandin E2

pathway have been investigated. Certain non-steroidal anti-inflammatory drugs (NSAIDs) such as aspirin are reported to lead to decreased occurrence and mortality for several types of cancer when used on a long-term basis. PTGS2 is frequently seen in a range of cancers and linked to poor outcomes. COX-dependent growth of tumours is enhanced through support of death evasion as well as survival, growth, migratory and invasive activity in cancer cells.

3.2 Aims

1. Examine *PTGS1/2* transcript levels in various primary cancer patient datasets, including leukaemia.
2. Utilising online bioinformatics resources to determine whether there is a correlation between the expression of the *PTGS1/2* transcript and the subtype of AML or patient survival outcome.
3. Evaluate expression of *PTGS1* and *PTGS2* in AML cell line models, including transcript variations.
4. Assess the efficacy of the *PTGS1* inhibitors including SC-560 and Tenidap in AML cell lines.

3.3 Results

3.3.1 *PTGS1/2* expression in various human primary diseases

To obtain an overview of *PTGS1/2* expression profiles in haematological and solid cancers, data mining of publicly available patient cohorts was undertaken to determine levels of *PTGS1/2* expression, which were then processed and plotted over a number of tissue samples. Among the 15 human cancers, head and neck cancer and leukaemia had the highest *PTGS1* expression levels (mean expression level: 3.22; 2.821, respectively), while myeloma, bone, eye, lymphoma, breast, brain, bladder, liver, lung, skin, gastric and colorectal cancer had statistical lower significant *PTGS1* expression levels comparing to leukaemia ($P < 0.0001$) (**Figure 3. 1A**). On the other hand, *PTGS2* was highly expressed in head & neck, bladder and pancreatic cancer, while myeloma, lymphoma, leukaemia, breast, eye and liver cancer had the lowest level of *PTGS2* expression.

PTGS2 displayed medium expression in the brain, skin, lung, colorectal and gastric cancer (**Figure 3. 1B**). These results suggest that *PTGS1/2* is expressed in various cancers. Then, further comparison analysis of *PTGS1* and *PTGS2* levels in these cancers was plotted. Although there were no statistically significant differences between *PTGS1* and *PTGS2* expressions in most of the analysed cancers (including head and neck, lymphoma, myeloma, bone, brain, breast, eye, gastric, and liver cancers), patients with leukaemia had an increased expression of *PTGS1* transcripts compared to *PTGS2* levels ($P < 0.0001$). In contrast, *PTGS1* level remained significantly lower in the bladder ($P < 0.0001$), colorectal ($P < 0.05$), lung ($P < 0.0001$), pancreatic ($P < 0.0001$), and

skin ($P < 0.01$) cancers compared to *PTGS2* level (**Figure 3. 1C**), suggesting that these solid tumours and leukaemias may regulate and signal through *PTGS1/2* differentially.

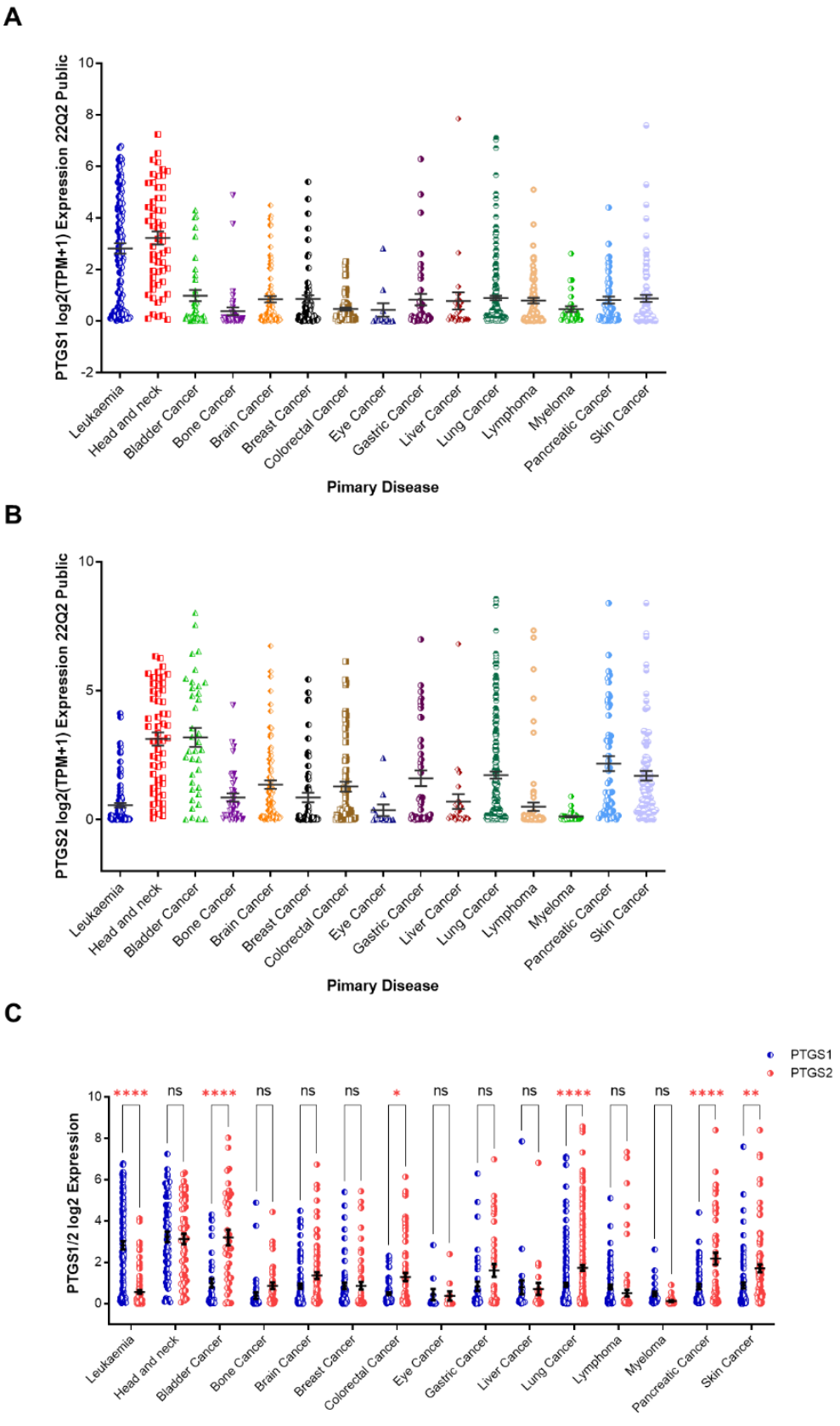

Figure 3. 1 PTGS expression across a wide range of primary diseases.

*(**A**) PTGS1 and (**B**) PTGS2 expression in different human cancers. One-way ANOVA significance testing was conducted using Dunnett's multiple comparisons test. (**C**) Comparison between PTGS1 and PTGS2 expression levels in these cancers. Values are displayed as the log_2 transformed mean value. Legend is as follows: ^{ns} p: non-significant, * p < 0.05, ** p < 0.01, ***p < 0.001 and ****p < 0.0001. Data were acquired from DepMap (https://depmap.org/portal/depmap, accessed on 1 March). GraphPad Prism 8 software was employed to generate the results presented.*

3.3.2 Transcript expression of *PTGS1/2* in HSCs and leukaemia classifications

All mature blood cells originate from haematopoietic stem cells (HSCs), which undergo a hierarchy of lineage decisions via several progenitor cells. Thus, the HSC hierarchy was examined for *PTGS1/2* expression to determine if there was any correlation between *PTGS1/2* expression and HSC lineages. So, human normal haematopoiesis cells (with data taken from GSE42519) were plotted as a hierarchical tree using the Bloodspot tool. This interactive hierarchical tree displays that the most primitive cells in the hierarchy, the HSC, multipotent progenitors (MPP) and common myeloid progenitors (CMP), had the highest expression of *PTGS1*. In contrast, the expression declined greatly in more mature progenitors such as granulocyte-macrophage progenitors (GMP), early promyelocytes (PM), late PM and myelocytes (MY) (**Figure 3. 2A**). In contrast, *PTGS2* was more highly expressed in monocytes (Mono), band cells (BC) and bone marrow polymorphonuclear neutrophil granulocytes (BM_PMNs). However, GMP, early PM, late PM and MY had the lowest *PTGS2* expression (**Figure 3. 2B**).

Next, a comparison analysis of the levels of *PTGS1* and *PTGS2* in various stages of haematopoiesis was plotted (Figure 3. 2 C), revealing a significant

expression difference of *PTGS1* in HSC ($P < 0.0001$), MPP ($P < 0.0001$), CMP ($P < 0.0001$) and MEP ($P < 0.0001$). Similarly, despite lower RNA expression of both *PTGS1* and *PTGS2*, *PTGS1* levels are significantly higher in early-PM ($P < 0.0001$), late-¬PM ($P < 0.0001$), MY ($P = 0.004$) GMP and ($P = 0.0483$). Furthermore, there was no statistically significant difference in expression level in MM ($P = 0.0842$) and Mono ($P = 0.9611$). On the other hand, the level of *PTGS2* transcript was statistically significantly higher than the *PTGS1* level in PMN cells ($P = 0.0290$) and PC ($P = 0.038$) (**Figure 3. 2C**).

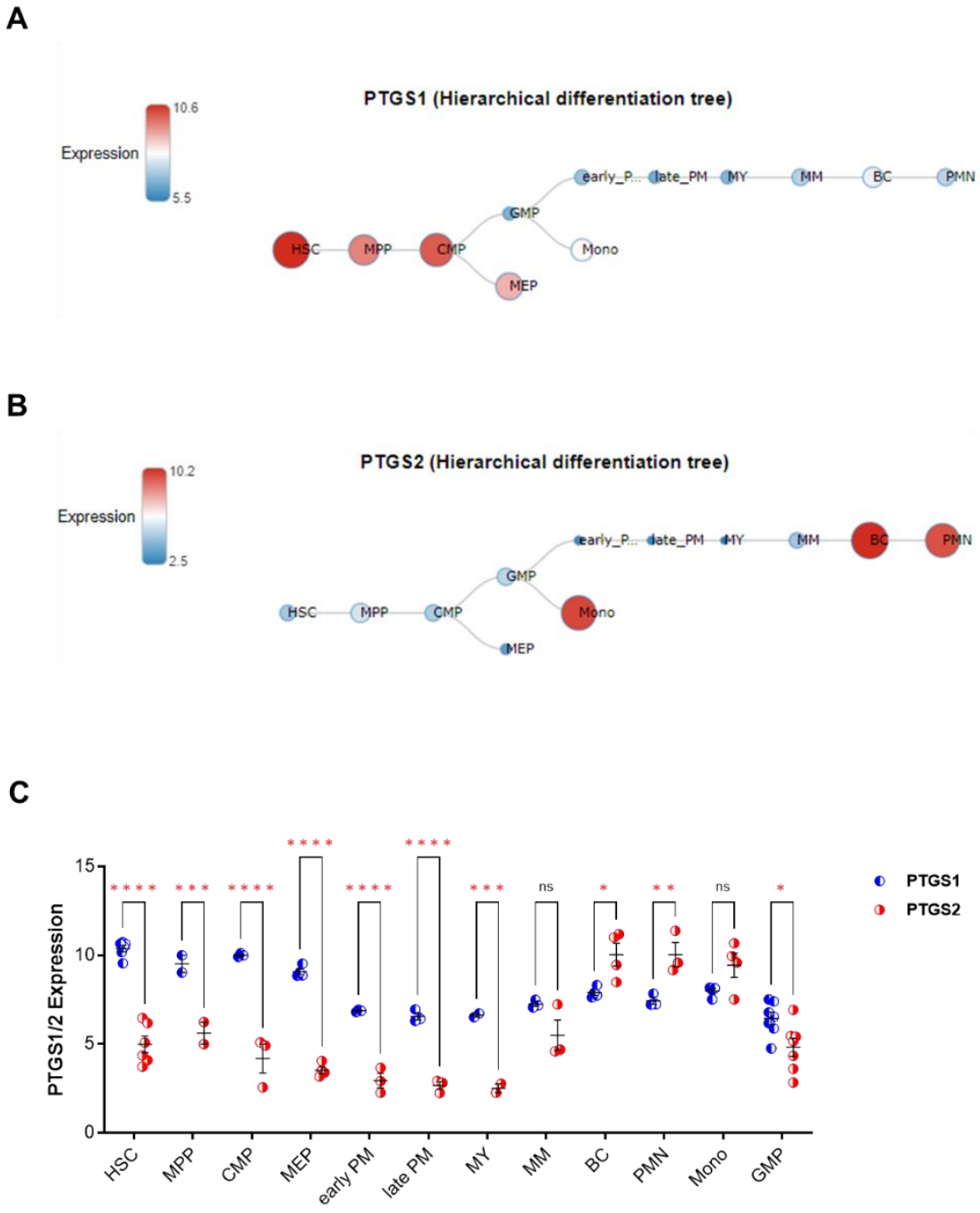

Figure 3. 2 PTGS1/2 expression across stages of HSC hierarchy on curated microarray data.

*An interactive hierarchical tree shows the expression of (**A**) PTGS1 and (**B**) PTGS2 in haematopoietic cells at different maturation stages. The lineages are coloured red for cells that are highly PTGS expressed or blue for cells that have lower genes expressed at the extremes of these thresholds. The bloodspot platform was used to generate the interactive hierarchical tree. (**C**) Comparison analysis of PTGS1/2 expression across blood cell production. The mean +/- SEM value after the log_2 transformation is displayed. Dunnett's multiple comparisons test was used for a one-way ANOVA*

*significance test. The following are legends: ns p: non-significant, * p < 0.05, ** p < 0.01, ***p < 0.001 and ****p < 0.0001. GraphPad Prism 8 software was employed to generate the results presented. The data was acquired from GSE42519 using the Bloodspot server (BloodSpot (ku.dk), accessed on 15 April 2020).*

As the *PTGS1/2* displayed differential expression levels in leukaemia, 101 patient samples were subdivided by the leukaemia classification recorded for each patient, including CLL, CML, AML and ALL, as shown in part **A** and **B** of **Figure 3. 3**. Both *PTGS1* and *PTGS2* had the highest level of expression in AML among the rest of leukaemia types. One-way ANOVA using Dunnett's multiple comparisons test was applied to compare the means of leukaemia types in a single analysis. The results based on the *PTGS1* expression levels show that the mean difference between AML and CML is not considered significant, as the p-value is 0.1714. Similarly, the difference between AML and CLL is insignificant (p= 0.05912). However, the mean difference between AML and ALL is highly significant (p <0.0001). Also, the mean difference between the CML and ALL groups is statistically significant (p <0.001, **Figure 3. 3A**).

Based on the *PTGS2* mRNA level, it appears that the means of the "AML" and "CML" groups are not significantly different, as the p-value of 0.7969 is greater than 0.05. Similarly, the means of the "AML" and "CLL" groups, "CML" and "CLL" groups, and "CML" and "ALL" groups are not significantly different, as the p-values of 0.1695, 0.6142, and 0.0569 respectively. However, the means of the "AML" and "ALL" groups are significantly different (P <0.0001, **Figure 3. 3B**).

Two-way ANOVA significance testing was conducted to compare the transcript expression of *PTGS1* with *PTGS2* in patients with these leukaemia types using Dunnett's multiple comparisons test. Although both *PTGS1* and *PTGS2* had high transcript levels in AML patients, *PTGS2* expression is statistically lower. Remarkably, all patients with leukaemia showed a higher expression of PTGS1, in comparison to *PTGS2* level (**Figure 3. 3C**). Notably, the CML and AML groups showed significantly highest expression of the *PTGS1* transcript in comparison with *PTGS2* level (both $p < 0.0001$).

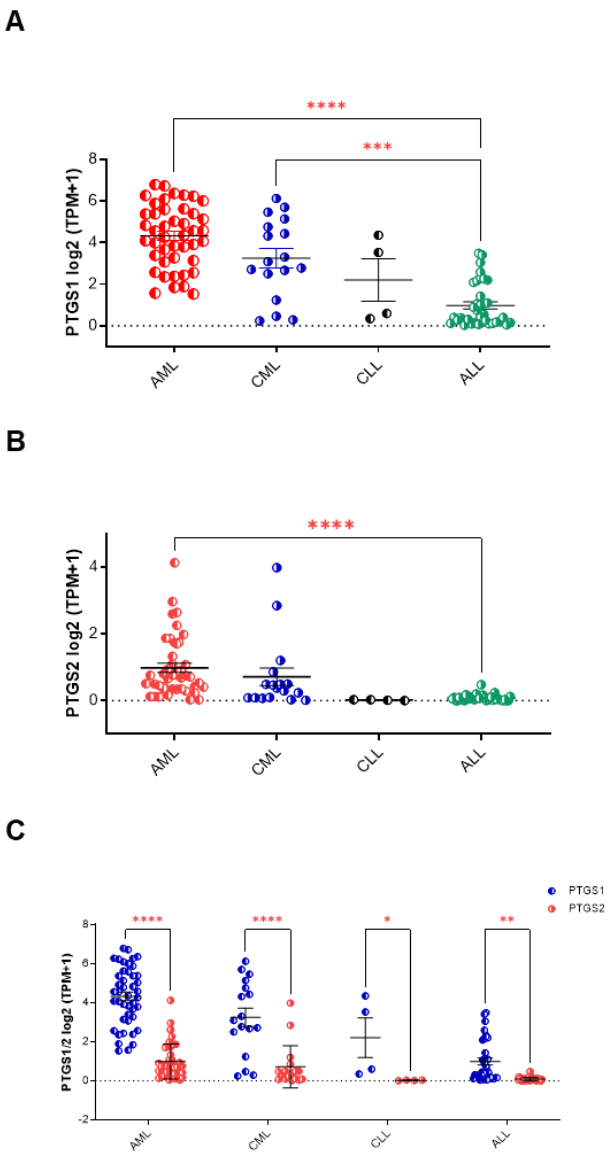

Figure 3. 3 PTGS1/2 expression across leukaemia classifications and AML subtypes.

(A) *PTGS1/2 expression comparison analysis expression in leukaemia classifications. Data was acquired from Expression 22Q2 Public using DepMap (https://depmap.org/portal/depmap, accessed on 1 March 2020).* ***(B)*** *The transcriptional expression of PTGS1/2 across AML subtypes according to FAB subtypes. (**C**) Clinical data was obtained from (GSE6891) Verhaak project using NCBI GEO (http://www.ncbi.nlm.nih.gov/geo/, accessed on 4 March 2020). The values are shown as the mean +/- SEM log_2-transformed. One-way ANOVA significance testing was conducted using Dunnett's multiple comparisons test. Legend is as following: ns: non-significant; * p < 0.05; ** p < 0.01; *** p < 0.001; **** p < 0.0001. GraphPad Prism 8 software was used to generate and analyse the results presented.*

3.3.3 Association of *PTGS1/2* expression with survival outcomes in AML patients

The clinical data and survival fractions were obtained from 3 independent AML patient datasets to include a variety of disease phenotypes. The *PTGS1/2* transcript levels were assessed by analysing the survival data in 169 patients from the TCGA database, 456 patients from GSE6891 (referred to herein as the "Verhaak" dataset) and 79 patients from GSE12417 (referred to herein as the "Metzeler II" dataset). These data are described in **Figure 3. 4**, **Figure 3. 5** and **Figure 3. 6**, respectively. Patients were divided into upper-quartile and lower-quartile groups according to the value of *PTGS1/2* transcript expression. These figures show flow diagrams for the included data in part **A**. Clinical characteristics of the included patients' age, gender, FAB subtype, cytogenetic and survival state are listed in **Table 3. 1.**

The FAB classification documented for each sample was used to subdivide *PTGS1*, as indicated in Appendices (**Figure A. 1**). In each database, a statistical test for an overall difference in mean +/- SEM was determined to be significantly different in *PTGS1* expression, across all FAB groups. In both TCGA (**Figure A. 1A**) and Verhaak datasets (**Figure A. 1B**), the M3 subgroup expressed the lowest *PTGS1* of all groups, whereas M1 had the lowest *PTGS1* expression in Metzeler II dataset (**Figure A. 1C**). The most significant differences in the TCGA dataset were between M3 and M2, M4, and M5 ($P<0.0001$ for all). Similarly, the differences between M3 and either M2 or M5 were statistically considered the most significant differences ($p <0.0001$ or $p=0.0006$, respectively). Metzeler II data shows the most significant differences between M1 and M2 or M4 ($p < 0.0001$ for both).

Table 3. 1 Clinical characteristics and survival outcomes

Characteristic		TCGA dataset (n = 197)				P-value*
		PTGS1^{Low} (n=37)		*PTGS1*^{High} (n=38)		
		No.	%	No.	%	
Sex						
	Male	18	49	18	47.4	1
	Female	19	51	20	52.6	
Age, years						
	Median, range	51 (21-76)		51 (23-76)		1
WBC, x10⁹/l						
	Median, range	12 (1-172)		26 (1-203)		0.324
Platelets, x10⁹/l						
	Median, range	45 (12-351)		44 (9-215)		0.9
	Missing			1		
Bone marrow blast, %						
	Median, range	72 (0-92)		62 (0-100)		0.1
	Missing					
FAB classification						
	M0	4	10.8	1	2.6	0.0143
	M1	9	24.3	10	26.3	<0.0001
	M2	6	16.2	13	34.2	<0.0001
	M3	12	32.4	0	0	-
	M4	5	13.5	7	18.4	<0.0001
	M5	1	2.7	5	13.1	0.0077
	M6	0	0	1	2.6	-
	M7	0	0	1	2.6	-
Cytogenetics						
	Normal	16	43.2	21	55	1
	Abnormal	18	48.6	12	31.5	
	Unknown	3	8.1	5	13	
Cytogenetic risk						
	Favorable	15	40	3	7.8	0.014
	Intermediate	14	37.8	23	60.5	
	Adverse	7	18.9	11	28.9	
	Unknown	1	2.7	1	2.6	
Median survival, months		46.73		16.3		0.0213
Hazard ratio (95% CI)		2.01(1.08-3.73)				

Then, we evaluated the differences between *PTGS1* and *PTGS2* expression in the M0 to M6 FAB subtypes of selected patients. In TCGA data (**Figure 3. 4B**), the most significant difference between *PTGS1* and *PTGS2* levels was in M1

subtype group (p = 0.0199), but there were no significant differences seen between *PTGS1* and *PTGS2* expression in the other subtypes. While in Verhaak data (**Figure 3. 5B**) *PTGS2* transcripts were significantly higher than *PTGS1* transcripts in the AML-M4 subtype (p = 0.0079). *PTGS1* showed the highest expression differences in AML-M0 and AML-M1 subtypes (p = 0.0189 and 0.0311, respectively). Furthermore, no statistically significant difference was found between the expressions of *PTGS1* and *PTGS2* among AML-M3, AML-M5 and AML-M6 subtypes. In contrast, data from the Metzeler II dataset (**Figure 3. 6B**) showed no significant differences between *PTGS1* and *PTGS2* levels in any FAB subtypes.

Next, survival data were compared between the top quartile (*PTGS1/2* ^{High}) and bottom quartile (*PTGS1/2* ^{low}) groups of patients with differing either *PTGS1* as in part **C** or *PTGS2* expression as in part **D** of each figure. Using Kaplan-Meier survival analysis, these subdivided groups were compared for overall survival (OS).

This analysis revealed that the *PTGS1* ^{High} patients had significantly shorter OS than that of the *PTGS1-Low* patients in TCGA (p = 0.0213; **Figure 3. 4C**), and *PTGS1-High* was correlated with an almost two-fold increased probability of death (hazard ratio (HR) = 2.017, as determined by a log-rank test). The median survival time was estimated to be 16.3 months in the *PTGS1-High* cohort and 46.73 months in the *PTGS1-low* cohort. Similar OS was significantly shorter in the Verhaak clinical dataset (p = 0.0132; **Figure 3. 5C**). The median survival time of the *PTGS1-Low* vs *PTGS1-High* AML patient groups were 34.92 and 14 months, respectively. The HR for high to low expressing AML patients was 1.538 using a log-rank test. On the other hand, no difference in OS rates of the

PTGS2 ^{High} vs *PTGS2* ^{Low} AML patient groups were observed for either the TCGA (p=0.934, **Figure 3. 4D**) or Verhaak (p=0.815, **Figure 3. 5D**) datasets. In the relatively smaller Metzeler II patient dataset, although there were no statistically significant differences in OS found between either *PTGS1* ^{High} and *PTGS1* ^{Low} (**Figure 3. 6C**) or *PTGS2* High and *PTGS2* Low (**Figure 3. 6D**), both *PTGS1* ^{High} and *PTGS2* ^{High} were associated with increased risk of death in AML patients (HR 1.57 and 1.8, respectively).

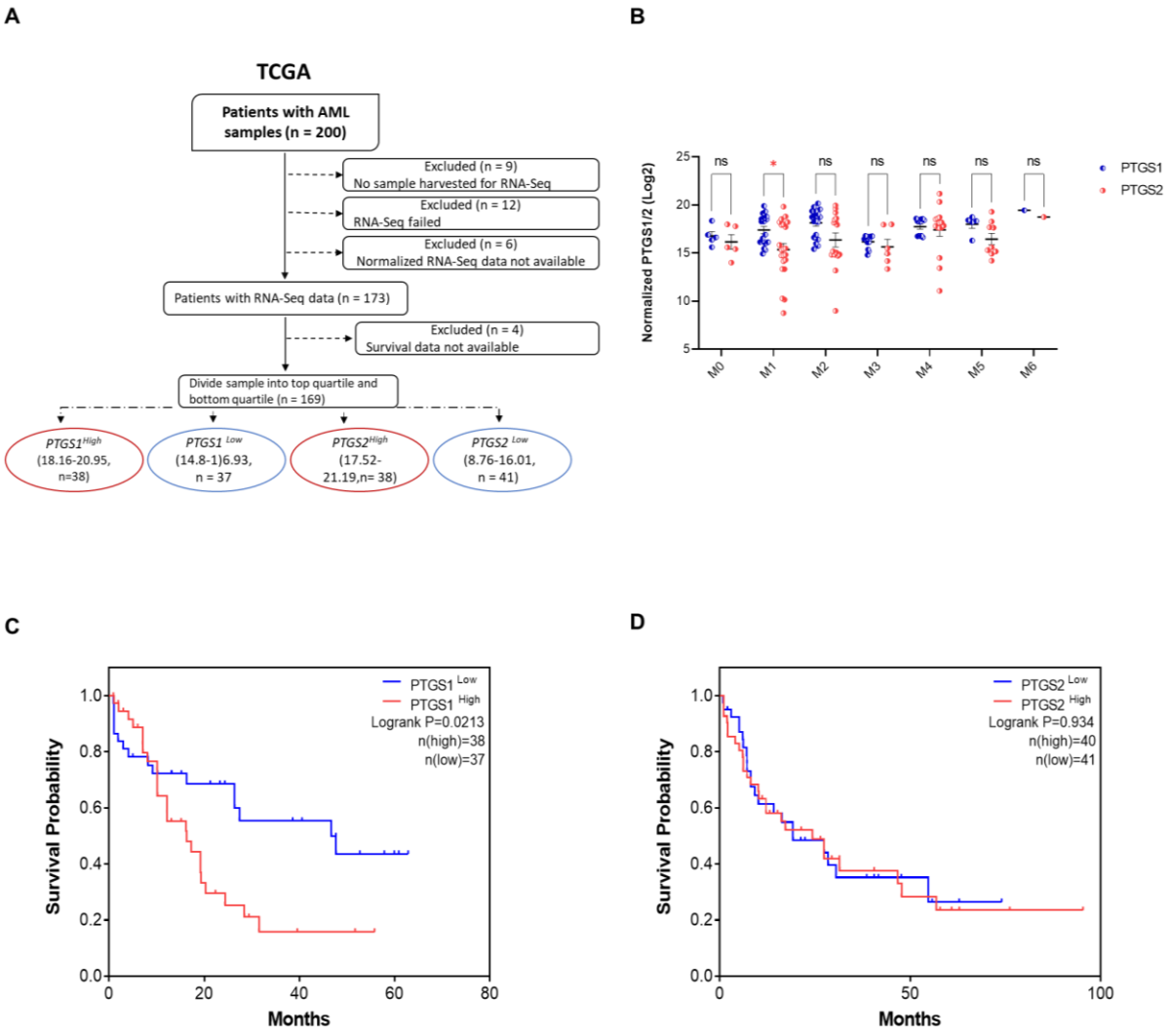

Figure 3. 4 Patients with AML in the PTGS1^{High} cohort from TCGA dataset correlated with poor survival probability.

RNA-seq and survival probability were acquired from TCGA using Cbioportal (cBioPortal for Cancer Genomics, accessed on 1 March 2020). **(A)** Flow diagram shown the number of samples excluded (right) and the number of samples included (left) at each stage. **(B)** Comparative analysis of the transcriptional expression of *PTGS1* and *PTGS2* across AML subtypes according to FAB subtypes. Values are presented as the mean +/- SEM log_2-transformed. One-way ANOVA significance testing was conducted using Dunnett's multiple comparisons test. The p values for the difference in means +/- SEM are as following: ^{ns} p: non-significant and * $p < 0.05$. **(C)** Survival curve was gained using the Kaplan Meier analysis and were compared using Logrank (Mantel-Cox test). Patients were divided according to PTGS1/2 expression into top quartile (*PTGS1/2 ^{high}*) and bottom quartile (*PTGS1/2 ^{low}*). All p values < 0.05 were considered statistically significant. GraphPad Prism 8 software was used to generate and analyse the results presented

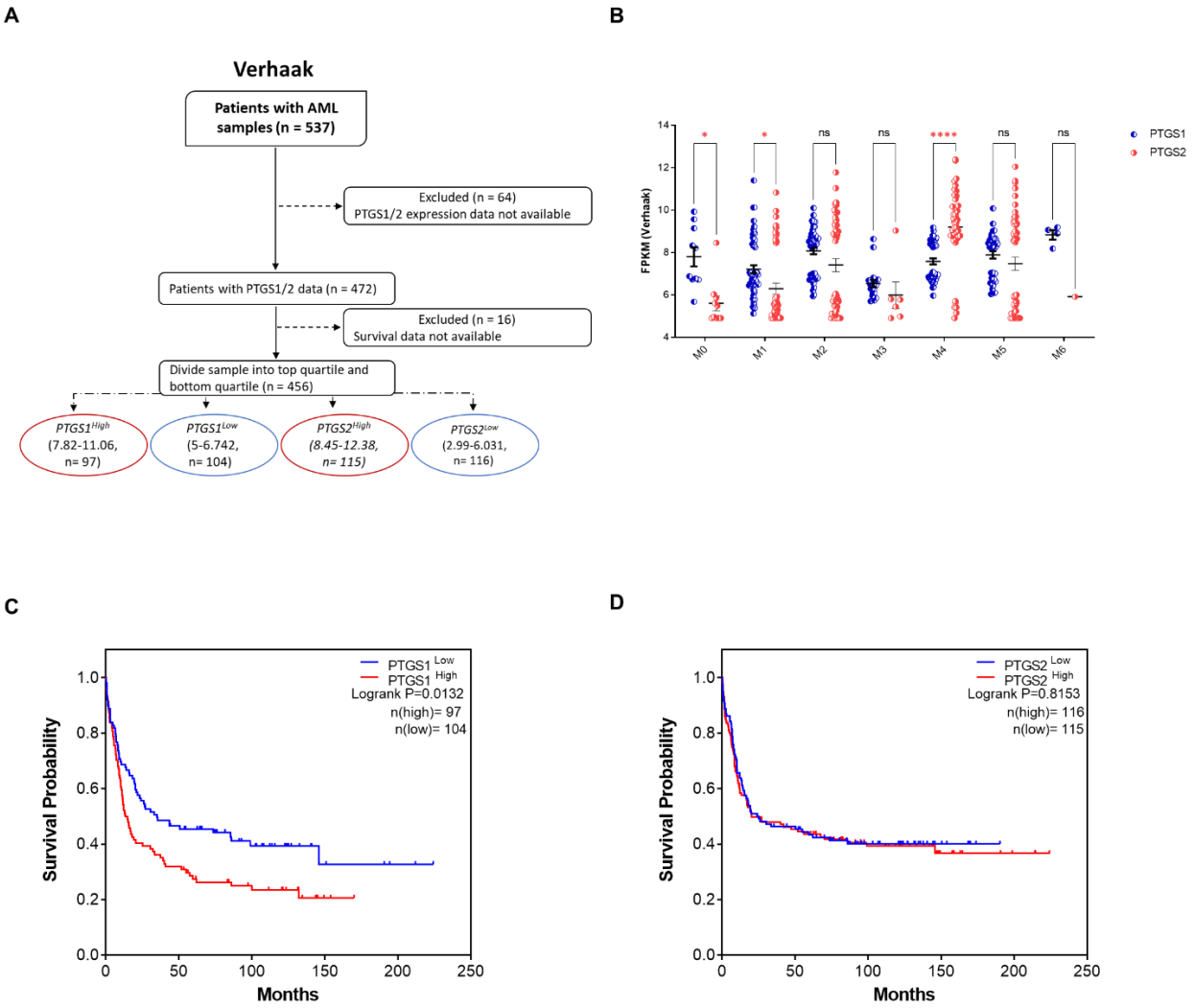

Figure 3. 5 Patients with AML in the PTGS1 ^{High} cohort from Verhaak dataset correlated with poor survival probability.

*Clinical data were obtained from (GSE6891) Verhaak project using NCBI GEO (http://www.ncbi.nlm.nih.gov/geo/, accessed on 4 March 2020). **(A)** Flow chart displayed as seen in **figure 3.4 A**. **(B)** Scatter dot plot presented the comparison between PTGS1 and PTGS2 transcription level across AML subtypes according to FAB subtypes. Values are represented as the mean +/- SEM log_2-transformed. One-way ANOVA significance testing was conducted using Dunnett's multiple comparisons test. The p values for the difference in means +/- SEM are as following: ^{ns} p: non-significant, * p < 0.05 and **** p < 0.0001. **(C)** Survival curve was done by the Kaplan Meier analysis and were compared using Logrank (Mantel-Cox test). According to PTGS1/2 expression, patients were divided into top quartile (PTGS1/2 ^{high}) and bottom quartile (PTGS1/2 ^{low}). All p values <0.05 were considered statistically significant. GraphPad Prism 8 software was used to generate and analyse the results presented.*

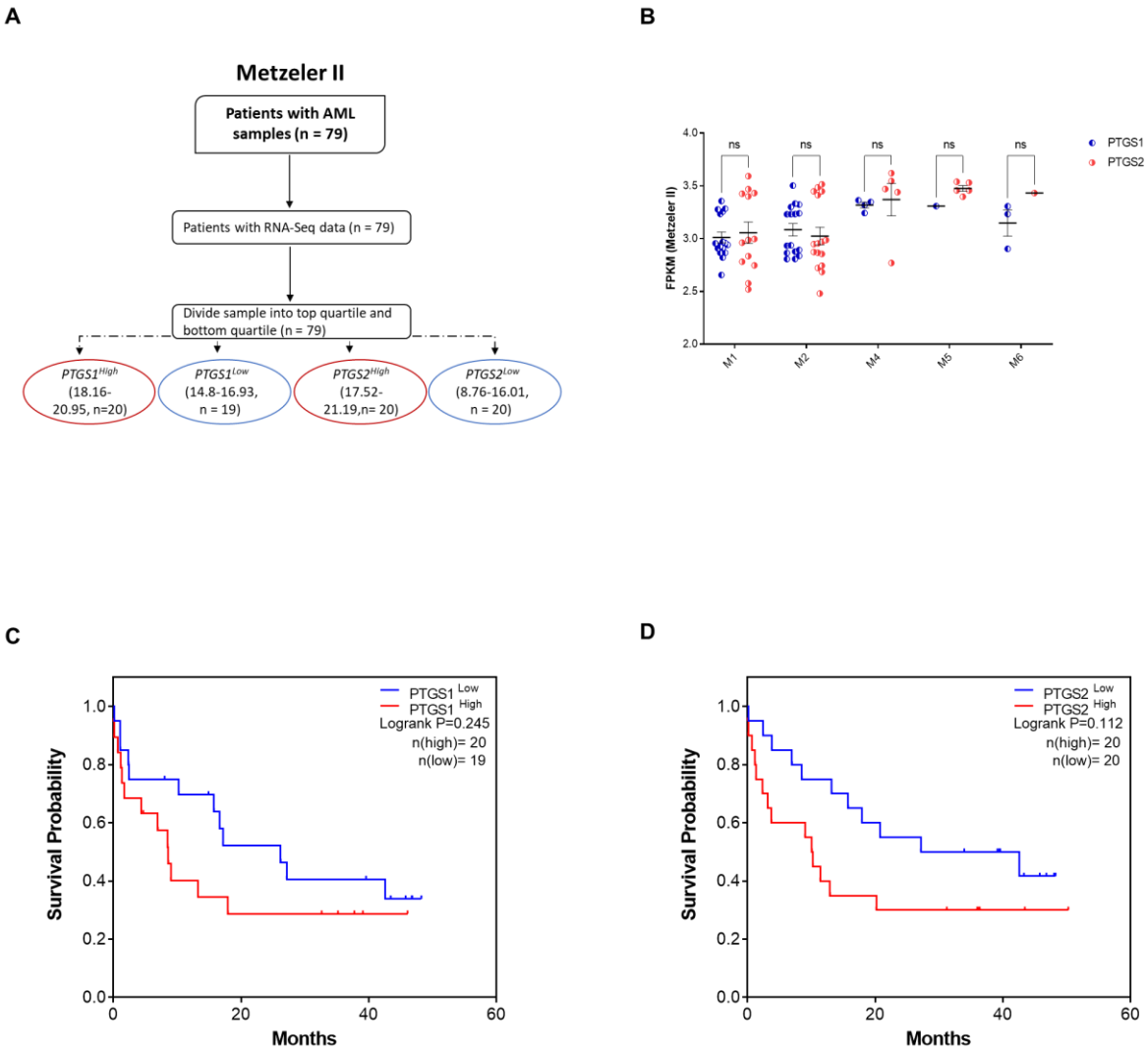

Figure 3. 6 Patients with AML in both PTGS1^{High} and PTGS2^{High} cohort from Metzeler II dataset correlated with poor survival probability.

*Data were extracted from (GSE12417) Metzeler II set using NCBI GEO (http://www.ncbi.nlm.nih.gov/geo/, accessed on 4 March 2020). **(A)** Flow diagram exhibited as seen in **figure 3.4 A**. **(B)** The comparison between PTGS1 and PTGS2 expression levels across AML subtypes according to FAB subtypes are shown as scatter dot plot. Values are shown as the mean +/- SEM log_2-transformed. One-way ANOVA significance testing was done by Dunnett's multiple comparisons test. The p values for the difference in means +/- SEM are as following: ^{ns} p: non-significant, * p < 0.05 and **** p < 0.0001. **(C)** Survival curve was conducted using the Kaplan Meier analysis and were compared using Logrank (Mantel-Cox test). Patients were divided according to PTGS1/2 expression into top quartile (PTGS1/2 ^{high}) and bottom quartile (PTGS1/2 ^{low}). All p values <0.05 were considered statistically significant. GraphPad Prism 8 software was used to generate and analyse the results presented*

3.3.4 Association of *PTGS1/2* transcript expression with different cytogenetic risk

Cytogenetic analysis of included AML cases in TCGA clinical dataset showed normal karyotype in 35 (47.9%) cases, abnormal karyotype in 36 (49.3%) cases and unknown karyotype in 2 (2.73%) cases. Cytogenetic findings in AML patients were divided into three groups: good (favourable) risk, intermediate (normal) risk, and poor (unfavourable) risk. There were 18 (24.6%) patients in the good risk group, and cytogenetic abnormality includes patients with the t(15;17), inv(16), del(7q) and the t(8;21). There were 37 (50.68%) patients in the normal risk group, including patients with del(5q) and normal karyotype. The poor group includes 18 (24.6%) patients with trisomy 8, del(7q) and complex karyotypes (**Figure 3. 7A**).

Similarly, in the Verhaak AML cohort (n = 170), patients were divided into good, intermediate and poor risk groups. 52.35% of the patients belonged to the intermediate group, while 23.53% and 24.12% of the AML patients were associated with the good and poor group, respectively (**Figure 3. 7B**).

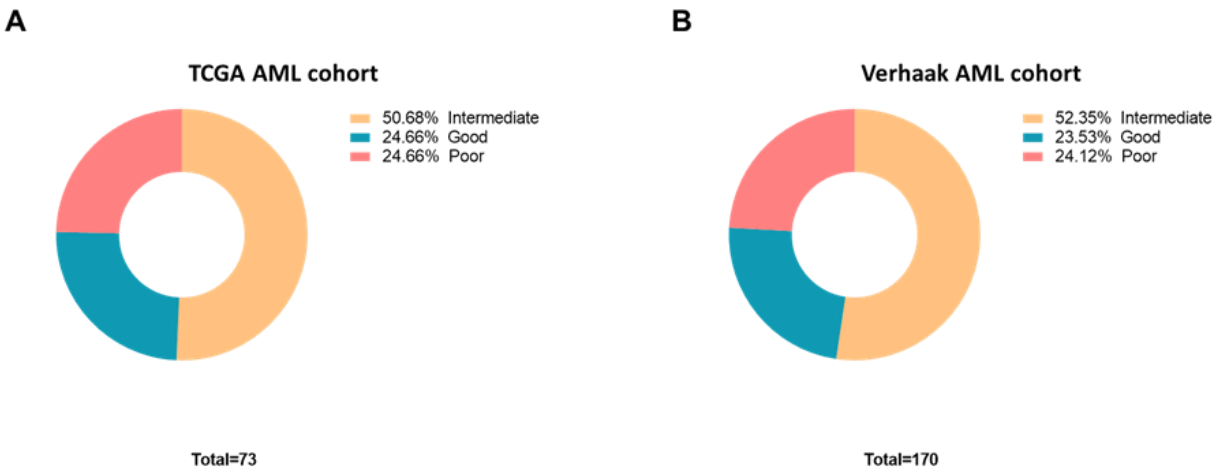

Figure 3. 7 Distribution of cytogenetic risk categories in AML patients.

A) *Cytogenetic data (n = 73) were acquired from the TCGA using Cbioportal (cBioPortal for Cancer Genomics, accessed on 1 March 2020).* ***B)*** *Cytogenetic data (n = 170) were obtained from (GSE6891) Verhaak project using NCBI GEO (http://www.ncbi.nlm.nih.gov/geo/, accessed on 4 March 2020). AML patients were divided into three groups according to their cytogenetic risk categories: good (favourable) risk, intermediate (normal) risk, and poor (unfavourable) risk. GraphPad Prism 8 software was used to generate the results presented*

We then evaluated those groups' *PTGS1* and *PTGS2* expression levels to determine whether *PTGS1* or *PTGS2* correlates with cytogenetic risk. Significance testing was performed by one-way ANOVA with Dunnett's multiple comparisons test ($p < 0.05$). In TCGA AML data, the analysis showed that the good risk group tended to have the lowest mRNA levels of *PTGS1* (**Figure 3. 8A**). In contrast, level of *PTGS2* expression was no significant difference among AML patients stratified by cytogenetic risk groups (**Figure 3. 8B**). In agreement, low expression of *PTGS1*, but not *PTGS2*, was associated with good cytogenetic risk categories of AML patients ($p < 0.05$, Figure 3. 8A and B). Only 8.11% of patients with $PTGS1^{High}$ belonged to the good risk group compared to 41.67% of patients with $PTGS1^{Low}$. The data also shows that among the

patients with high levels of *PTGS1*, 62.16% and 29.73% were classified as intermediate and poor risk categories, respectively. On the other hand, the vast majority of AML patients with low levels of *PTGS1* belonged to (41.67%) good and (38.89%) intermediate risk group (**Figure 3. 8C**).

Moreover, the intermediate risk group had the lowest *PTGS2* expression, and the poor risk group had the highest *PTGS2* expression. Dunnett's multiple comparisons test was applied to compare the means of various groups and identify which groups are significantly different from each other (**Figure 3. 8B**). The analysis indicated that the differences between these risk groups are not statistically significant. Although there was no statistically significant difference between the three groups, the data in **Figure 3. 8D** seems to indicate that the percentage of patients with $PTGS2^{High}$ is higher in the group with intermediate (37.5%) than in the groups with good (30%) and poor (32.5%) risk categories. However, it is worth noting that the percentage differences between groups are small. On the other hand, for the group with low *PTGS2* expression, the percentage of intermediate risk (63.16%) is much higher than the percentage of good (21.05%) or poor (15.79%) outcomes.

Similarly, in Verhaak AML dataset, the data showed that the good risk group tended to have the lowest *PTGS1* mRNA levels (**Figure 3. 8E**), while the mean of *PTGS2* mRNA level was almost the same in all cytogenetic risk groups (**Figure 3. 8F**). Thus, AML patients with favourable cytogenetic risk category showed statically significant decreased expression of *PTGS1*, but not *PTGS2* ($p < 0.001$, **Figure 3. 8E** and **F**). A small percentage of patients with high levels of *PTGS1* were considered to be in the good risk group (10.34%) compared to

a larger percentage of patients with low levels of *PTGS1* (36.84%). Additionally, a significant number of patients with high *PTGS1* levels were classified as intermediate (58.62%) or poor (31.03%) risk. In contrast, the majority of patients with low *PTGS1* levels were considered to be in either the intermediate (45.26%) or the good (36.84%) risk groups (**Figure 3. 8G**).

Furthermore, the intermediate risk group had a slightly higher expression of *PTGS2* among the three groups; the good and poor risk groups had almost the same level of *PTGS2* expression. A statistical test was used to determine if there were significant differences between the means of the groups. The results showed that the differences between the groups were not statistically significant (**Figure 3. 8F**). Also, the data in **Figure 3. 8H** suggests that a higher percentage of patients with high levels of *PTGS2* were present in the intermediate-risk group (55.26%) compared to the good (25.79%) and poor (18.95%) risk groups. On the other hand, for the group with low *PTGS2* expression, the percentage of patients in the intermediate risk group (63.16%) is much higher than the percentage of patients in the good (21.05%) or poor (15.79%) risk groups. It is important to note that the differences in rates of AML patients are stratified by cytogenetic categories between the $PTGS2^{High}$ and $PTGS2^{Low}$.

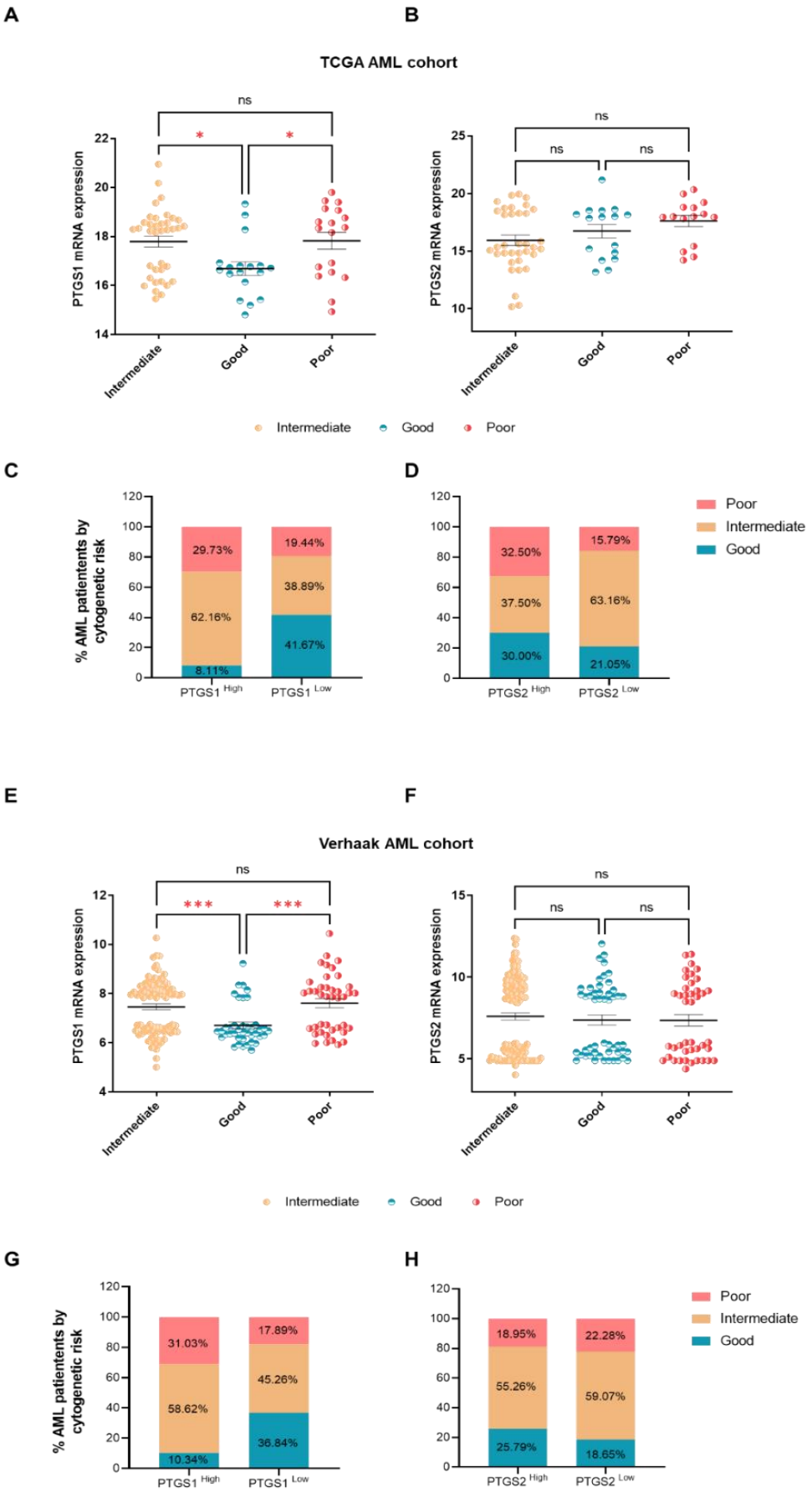
A
B
TCGA AML cohort
ns
*
*
PTGS1 mRNA expression
22
20
18
16
14
Intermediate
Good
Poor
ns
ns
ns
PTGS2 mRNA expression
25
20
15
10
Intermediate
Good
Poor
Intermediate
Good
Poor
C
D
% AML patientents by cytogenetic risk
120
100
80
60
40
20
0
29.73%
62.16%
8.11%
19.44%
38.89%
41.67%
PTGS1 High
PTGS1 Low
32.50%
37.50%
30.00%
15.79%
63.16%
21.05%
PTGS2 High
PTGS2 Low
Poor
Intermediate
Good
E
F
Verhaak AML cohort
ns
***
***
PTGS1 mRNA expression
12
10
8
6
4
Intermediate
Good
Poor
ns
ns
ns
PTGS2 mRNA expression
15
10
5
Intermediate
Good
Poor
Intermediate
Good
Poor
G
H
% AML patientents by cytogenetic risk
120
100
80
60
40
20
0
31.03%
58.62%
10.34%
17.89%
45.26%
36.84%
PTGS1 High
PTGS1 Low
18.95%
55.26%
25.79%
22.28%
59.07%
18.65%
PTGS2 High
PTGS2 Low
Poor
Intermediate
Good

Figure 3. 8 Association of *PTGS1/2* mRNA levels with different cytogenetic Risk.

The cytogenetic data (n = 73) were acquired from the TCGA using Cbioportal. Cytogenetic finding in AML patients was divided into three groups: good (favorable) risk, intermediate (normal) risk, and poor (unfavorable) risk. The comparison analysis between these groups according to (**A**) *PTGS1* expression levels or (**B**) *PTGS2* expression levels was applied. The values are shown as the mean +/- SEM log_2-transformed. The percentage distribution of cytogenetic subgroups was calculated for both (**C**) $PTGS1^{high}$ and $PTGS1^{low}$ cohort or (**D**) $PTGS2^{high}$ and $PTGS2^{low}$ cohorts. The cytogenetic data (n = 170) were obtained from (GSE6891) Verhaak project. The comparison analysis between these groups according to (**E**) *PTGS1* expression levels or (**F**) *PTGS2* expression levels was applied. The values are shown as the mean +/- SEM log_2-transformed. The percentage distribution of cytogenetic subgroups was calculated for both (**G**) $PTGS1^{high}$ and $PTGS1^{low}$ cohort or (**H**) $PTGS2^{high}$ and $PTGS2^{low}$ cohorts. GraphPad Prism 8 software was used to generate and analyse the results presented.

3.3.5 *PTGS1/2* expression in different AML cell lines

Given the association of *PTGS1* with poor outcomes in AML patients, we next set out to develop cell line models of *PTGS1* and *PTGS2* over-expression for *in vitro* studies. First, we optimized primers and cycling conditions for quantitative PCR (qPCR). Utilising the gradient function of the T100^{TM} Thermal Cycler (BIO-RAD), gradient temperatures (58 to 68°C) were set. **Figure 3. 9** reveals an agarose gel with the 6 samples loaded onto the block. The best temperatures for both PTGS1 primers (**Figure 3. 9A**) and PTGS2 primers (**Figure 3. 9B**) and single PCR products were observed from both sets of reactions indicating primer specificity for each target.

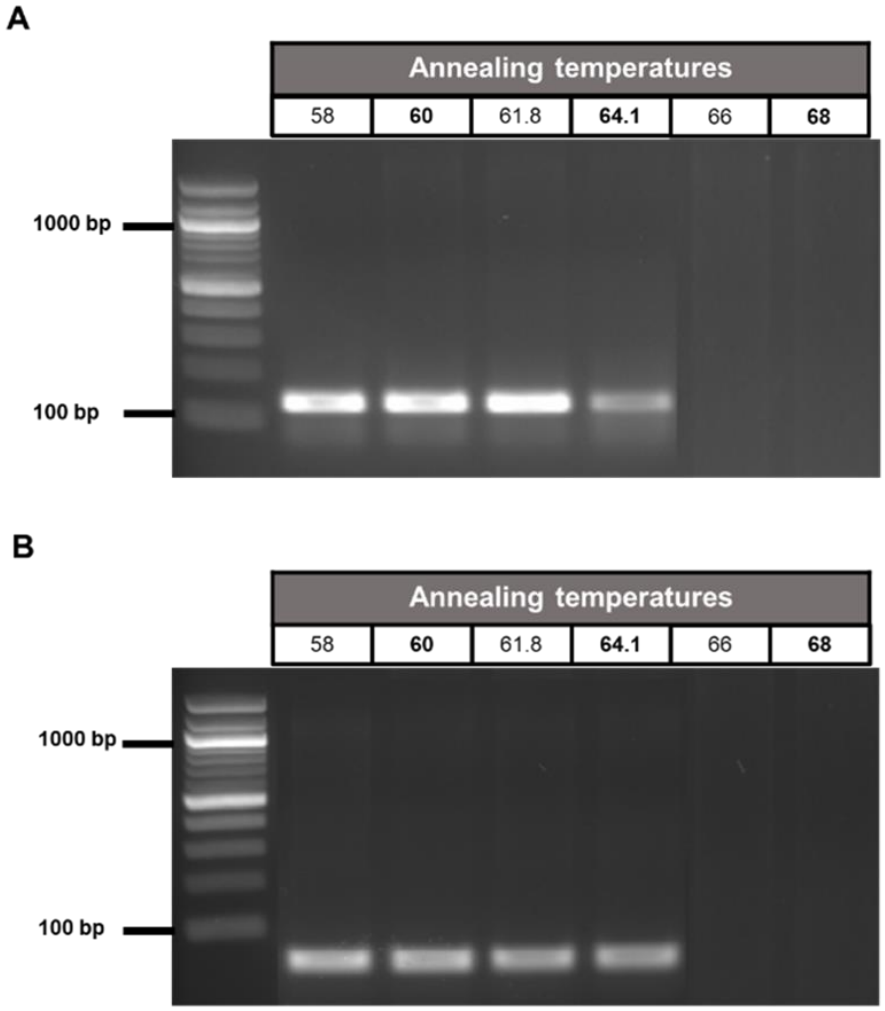

Figure 3. 9 Experimental determination of optimal annealing temperature.
Agarose gel (2%) was used to load 7 µl of 100 bp DNA ladder onto the first lane and 20 µl of gradient PCR products for determination of annealing temperatures for ***(A)*** *PTGS1 and* ***(B)*** *PTGS2 primers onto the next lanes. Agarose gels were visualized on a ChemiDoc (Bio-Rad). The optimal annealing temperature was selected and applied to the qPCR experiment.*

qPCR was performed to quantify the expression levels of either *PTGS1* or *PTGS2* genes in four different AML cell lines. The results showed that all the cell lines expressed both forms of *PTGS*, and the *PTGS1* expression levels were higher in all selected cell lines (**Figure 3. 10A**). Two-way ANOVA significance testing was conducted using Sidak's multiple comparisons test. The results indicate that *PTGS1* was significantly higher than *PTGS2* in all cells ($P < .00001$). Next, the qPCR products were separated using 2% agarose gel to confirm this result. The agarose gels were visualised on a ChemiDoc. **Figure 3. 10B** shows a single band with expected size (106bp for *PTGS1*) and (91bp for *PTGS2*).

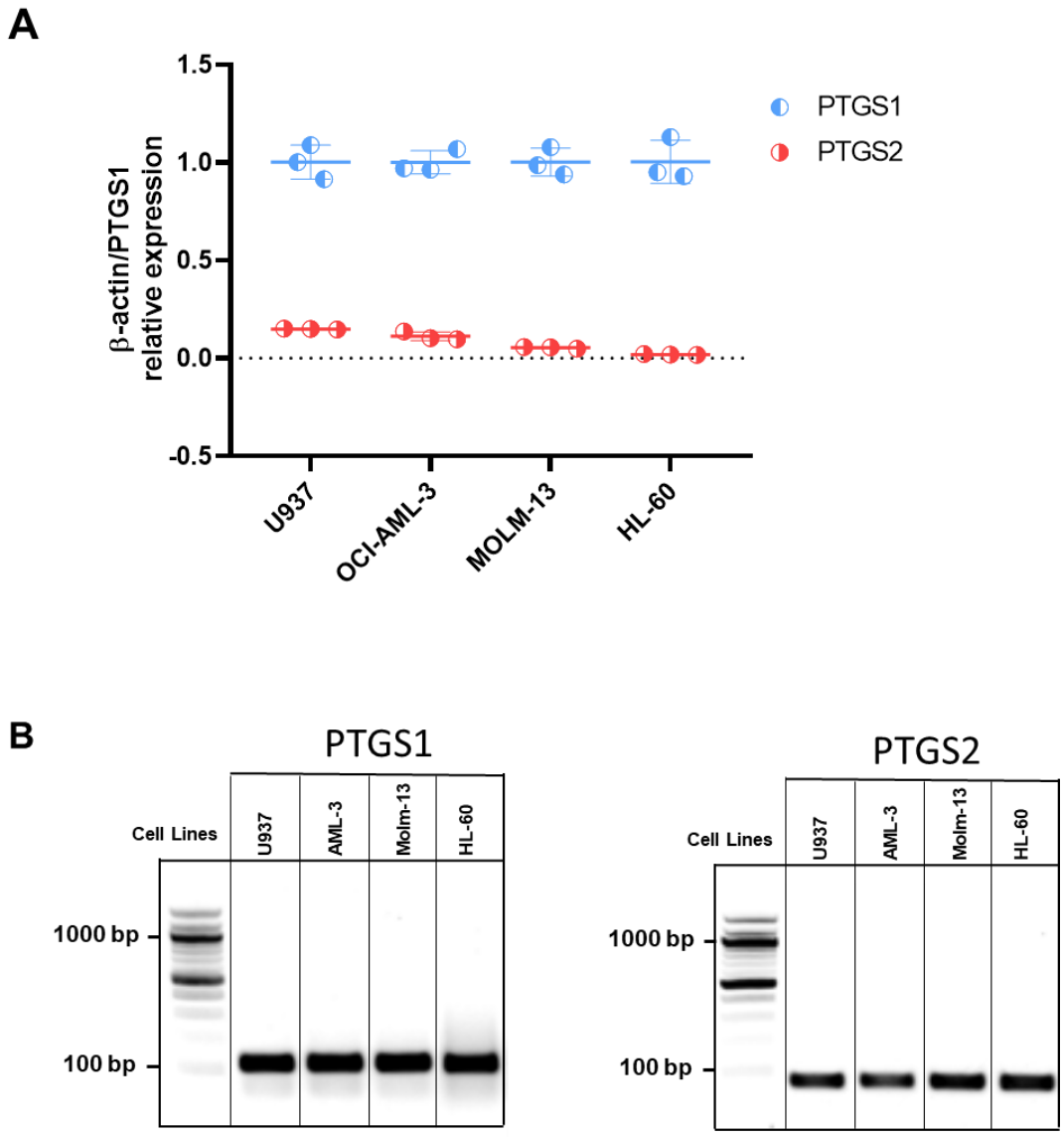

Figure 3. 10 The transcript expression of PTGS1 and PTGS2 in AML cell lines.

mRNA expressions of (A) PTGS1 and PTGS2 genes were analysed by RT-qPCR. Data was normalised to β-actin. Results represent the mean +/- SEM for 3 independent experiments. The qPCR products for (B) PTGS1 and PTGS2 were then loaded onto the wells of 2% agarose gel. The cDNA was obtained from AML cell lines, which include U937, OCI-AML-3, MOLM-13 and HL-60. Agarose gels were visualised on a ChemiDoc (Bio-Rad).

3.3.6 Inhibition of *PTGS1* activity in AML cell lines.

Next, to test the functional importance of *PTGS1/2* expression in AML U937, OCI-AML-3 and MOLM-13 cell lines were treated *in vitro* with increasing concentration of the *PTGS1* selective inhibitors SC-560 (0.01-10 µM) or Tenidap (0.01-100 µM), and cell viability was measured using Trypan blue. The effect of these treatments was assessed after four days. Treatment with SC-560 or Tenidap reduced cell numbers in all examined cell lines (**Figure 3. 11**).

Dose response curves over 96h demonstrate that MOLM-13 cell line is less sensitive to SC-560 (EC_{50} 1.6 µM, **Figure 3. 11C**), while U937 cell line is high sensitive to SC-560 (EC_{50} 0. 25 µM, **Figure 3. 11A**). The EC_{50} value of SC-560 for OCI-AML-3 cell line is 0.53 µM (**Figure 3. 11B**). The dose response curves of Tenidap show that U937 cell line is highly senstive to Tenidap (EC_{50} 0. 68 µM, **Figure 3. 11A**). Whereas both OCI-AML-3 (**Figure 3. 11C**) and MOLM-13 (**Figure 3. 11C**) cell line is less sensitive to Tenidap (EC_{50} 2.9 µM and 2.9 µM, respectively).

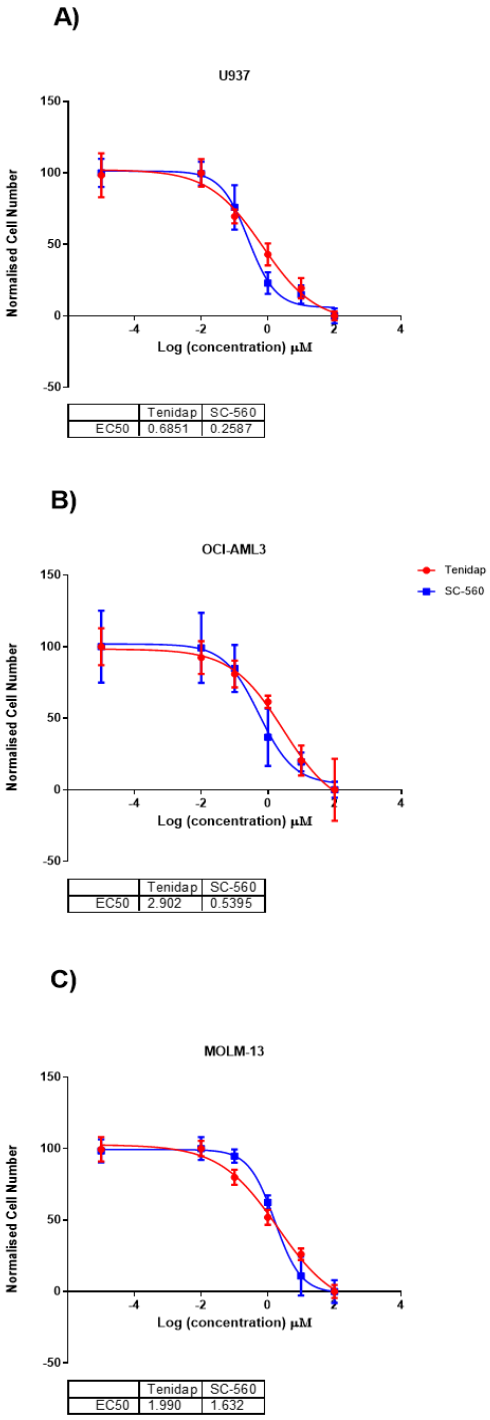

Figure 3. 11 Dose-response curve indicating the effect of PTGS1 inhibitors on AML cell lines.

*Using trypan blue**, (A)** U937 **(B),** OCI-AML-3 and **(C)** MOLM-13 treated with different concentrations (0.001, 0.01, 0.1, 1, 10, 100 µM) of PTGS inhibitors (either SC-560 or Tenidap) for up to 96h were counted and analysed to establish a dose-response and EC_{50} for these cell lines. The dose-response curves were fitted by nonlinear regression using GraphPad Prism 8 program (n = 3).*

3.3.7 PTGS1 inhibitors induced growth inhibition in AML cell lines.

To study the effects of PTGS1 inhibitors on AML cell lines, we examined the in *vitro* growth properties of U937, OCI-AML-3 and MOLM-13 over time using SC-560 and Tenidap. These cells were treated with DMSO as a vehicle control and cells treated with either 1 µM or 10 µM of PTGS1 inhibitors (SC-560 or Tenidap). The data shows the number of cells at different time points (0 to 6 days).

From the data in **Figure 3. 12**, it appears that the growth of the cells was affected by treatment with SC-560. The number of cells in the 10µM SC-560 treatment group is generally reduced compared to the number of cells in the control and 1µM SC-560 treatment groups at each time point. Similarly, the number of cells in the 1µM SC-560 treatment group is generally lower than that in the control group at each time point.

When analysing the data for U937 cell line (**Figure 3. 12A**), by day 1, the group treated with 1µM SC-560 had a slight decrease in the number of cells compared to the vehicle group, and the group treated with 10µM SC-560 showed a greater decline. This trend of cell decrease continues for the group treated with 10µM SC-560, reaching its lowest point on day 6. The cells treated with 1µM SC-560 also showed a decline but at a slower rate on day 6.

Upon analysing the data for the OCI-AML-3 cell line (**Figure 3. 12B**), a slight inhibition in cell numbers for the 1µM SC-560 group compared to the vehicle group at 24h was seen, and the group treated with 10µM SC-560 showed a significant decrease. Cell inhibition continued for the group treated with 10µM

SC-560, reaching its lowest point on day 6. Also, the number of cells treated with 1μM SC-560 decreased but at a slower rate.

From the data for MOLM-13 (**Figure 3. 12C**), it is clear that there is a decline in cell numbers over time for all groups, but the rate of decline is different among the groups. The vehicle group appears to have the highest percentage of cell growth at all time points, followed by the 1μM SC-560 group and then the 10μM SC-560 group. Interestingly, the 1μM SC-560 group has a relatively small decline in cell numbers between days 1 and 2 but then experiences a more significant decline between days 2 and 3. Similarly, the 10μM SC-560 group experiences a relatively small reduction in cell numbers until day 3 but then significantly declines between days 3 and 4. On days 5 and 6, the cell numbers for both 1μM SC-560 and 10μM SC-560 groups appear to stabilise, with the 10μM SC-560 group having a slightly higher percentage of cells on day 6.

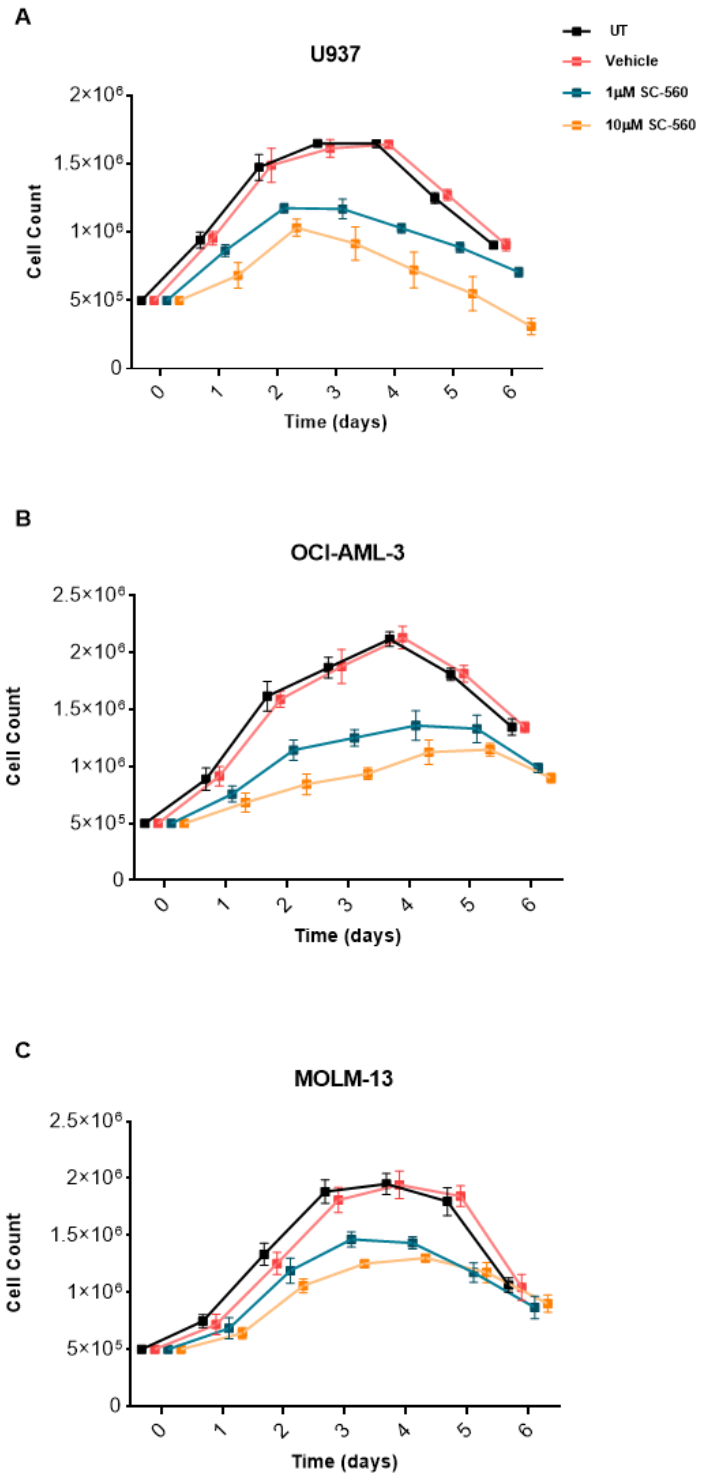

Figure 3. 12 Growth curve indicating the inhibition of AML cell growth.

*5×10^5 cells of **(A) U**937, **(B)** OC-AML-3 and **(C)** MOLM-13 were treated with different concentrations of SC-560 (1 µM and 10 µM) for up to 6 days. As a vehicle control, 1 µl/ml DMOS was added to the cells. The cells were counted daily using Trypan blue cell counts to create a growth curve. The x-axis represents time (days), and the y-axis*

displays the number of cells. The data represents the mean +/- SEM for 3 independent experiments. The results presented were generated using GraphPad Prism 8 software.

Similarly, based on the data in **Figure 3. 13**, it seems that the treatment of Tenidap impacted the growth of cells, where the cell count in the 10μM and 1μM treatment groups were consistently fewer than the control group at each time interval. Additionally, the cell count in the 1μM treatment group was also found to be fewer than the control group during each time point.

U937 treated with 1μM Tenidap group had a relatively small decline in cell numbers between days 1 and 2 but then experienced a more significant decline between days 2 and 3. Similarly, The cell numbers for the 10μM Tenidap group showed a minimal decrease until the third day, but a larger decrease occurred between the third and fourth day. On days 5 and 6, the cell numbers for both 1μM Tenidap and 10μM Tenidap groups continued to decline, with the 10μM Tenidap group having a much lower percentage of cells on day 6 (**Figure 3. 13A**).

From the OCI-AML-3 data (**Figure 3. 13B**), it is clear that there was a decline in cell numbers over time for all groups. The vehicle group appears to have the lowest number of decreasing cells at all time points, followed by the 1μM Tenidap group and then the 10μM Tenidap group. It is also interesting to note that the 1μM Tenidap group appears to have the most stable number of cells over time, with a relatively small decline in cell numbers between days 1 and 2 and a relatively stable number of remaining cells between days 2 and 6. The 10μM Tenidap group faced a relatively small decline in cell numbers until day 3 but then experienced a more significant decline between days 3 and 4. But, the reduction in cell numbers continues on all days, and the number of cells on day

6 is significantly lower than it was on the first day. The 1μM Tenidap group encountered a decline in cell numbers over time, but it is less drastic than the decline in the 10μM Tenidap group, with the number of cells being relatively stable between days 2 and 5.

Based on MOLM-13 data (**Figure 3. 13C**), by day 1, the number of cells decreased slightly in the group treated with 1μM Tenidap and significantly in the group treated with 10μM Tenidap compared to the control group. This downward trend in cells persisted for the group given 10μM Tenidap, reaching its lowest point on day 6. A drop was also seen in the group given 1μM Tenidap, but it happened more gradually.

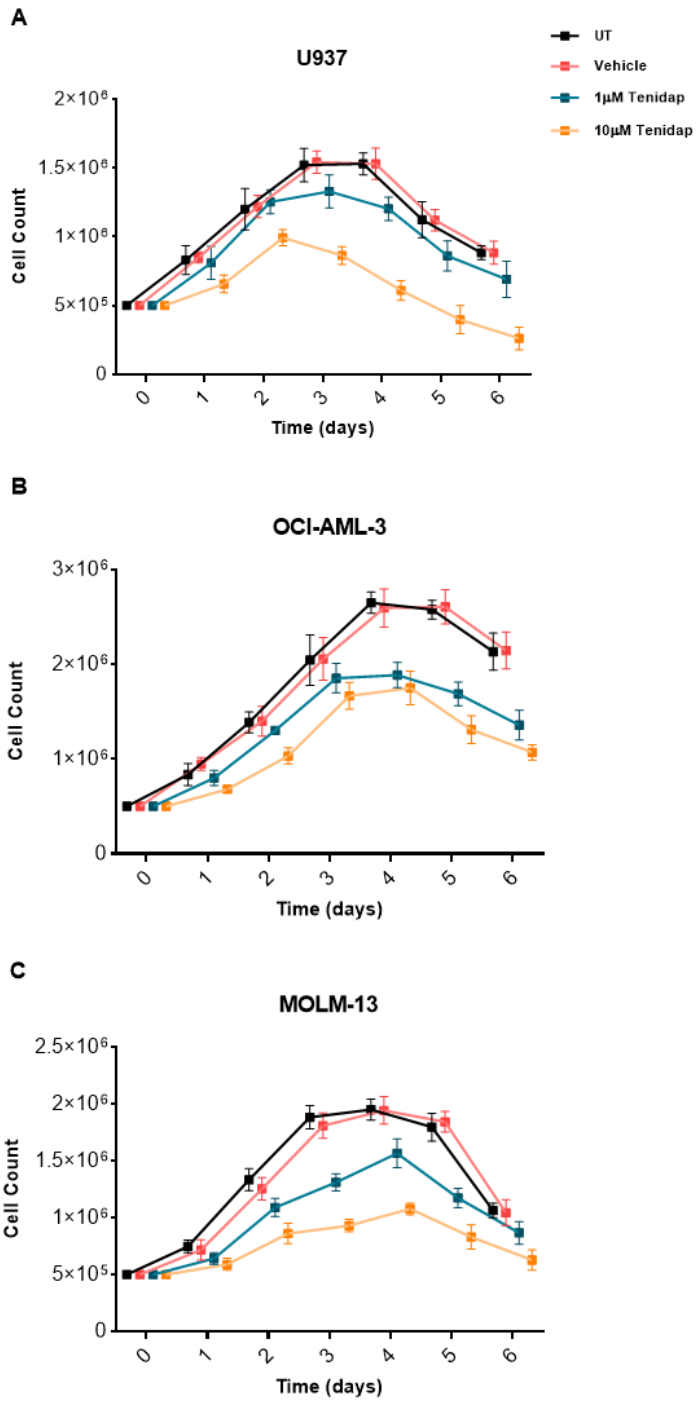

Figure 3. 13 Growth curve indicating the inhibition of AML cell growth.

(A) *U937,* ***(B)*** *OC-AML-3 and* ***(C)*** *MOLM-13 were incubated with different concentrations of Tenidap (1 µM and 10 µM) for up to 6 days. DMSO (1 µl/ml) was used as the control (vehicle). Cells were counted daily using trypan blue to generate a growth curve for these cell lines. The x-axis represents the progression of time, and the y-axis displays the number of cells present at each point in time. Results represent the mean +/- SEM for 3 independent experiments. The results presented were generated using GraphPad Prism 8 software.*

3.3.8 Induction of apoptosis in AML cell lines by *PTGS1* inhibitors.

We investigated whether *PTGS1* inhibition impacts cell death in order to get mechanistic insights into how *PTGS1* inhibitors affect AML cells. In this experiment, we used U937 and OCI-AML-3 that had been treated with either vehicle (DMSO) or *PTGS1* inhibitors (SC-560 or Tenidap) and grown over 96h for analysis. The cell lines' response following treatment was measured by flow cytometry using Annexin-V/ propidium iodide (PI; **Figure 3. 14A**). Generally, treatment with SC-560 or tenidap slightly increased apoptosis and decreased cell viability in both AML cell lines. However, the percentages of Annexin V-positive cells, including apoptotic and necrotic cells, were not statistically significant.

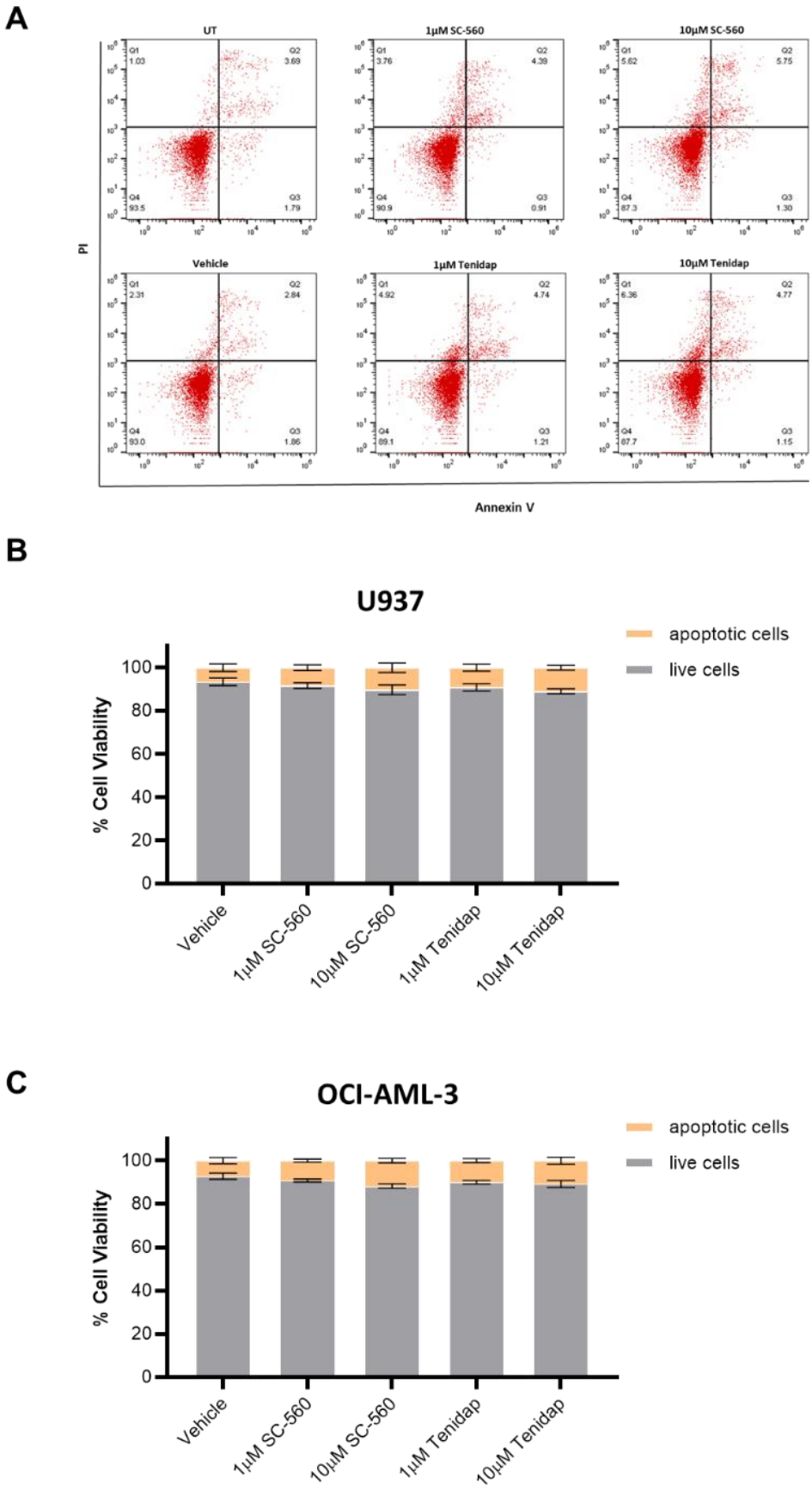

Figure 3. 14 Effect of PTGS1 inhibitors on apoptosis induction in AML cell lines.

The quantification of apoptotic cells using flow cytometric analysis was applied through dual staining with Annexin V/FITC and propidium iodide (PI). ***(A)****The percentages of cells in each quadrant, namely lower left (Annexin* V^-/PI^-*, live cells), lower right (Annexin* V^+/PI^-*, early apoptotic cells), upper left (Annexin* V^-/PI^+*, necrotic cells), and upper right (Annexin* V^+/PI^+*, late apoptotic cells) were determined. The bar chart illustrates the percentage of* ***(B)*** *U937 and* ***(C)*** *OCI-AML-3 viability. These cells were treated with either SC-560 or tenidap (1 and10 μM) for 72h, after which apoptosis was assessed by Annexin V/PI. The vehicle cells were treated with DMSO for 72h. Results represent the mean +/- SEM for 3 independent experiments. One-way ANOVA significance testing was done using Dunnett's multiple comparisons test. The bar charts presented were generated using GraphPad Prism 8 software.*

3.3.9 Effect of SC-560 and Tenidap on cell cycle progression in AML cells.

Given the dramatic effect of *PTGS1* inhibition on cell numbers but not apoptosis, we next examined cell-cycle progression upon *PTGS1* inhibition in AML cell line models. Cell cycle analysis by quantitation of DNA content using flow cytometry was performed to determine the cell cycle phases and the rate of cell proliferation. In this experiment, the analysis was conducted on OCI-AML-3 and U937 cells using propidium iodide. To evaluate the effects of SC-560 and Tenidap on cell cycle progression, these cells were treated with either SC-560 (1μM or 10μM) or Tenidap (1μM or 10μM) for 72 h before the analysis was performed. These cells were then fixed in 70% ethanol, preserving the cellular structure and enabling the dye to penetrate the cells. The analysis results are shown in **Figures 3. 15** and **3. 16**.

Incubation of OCI-AML-3 cells with Tenidap (1μM or 10μM) for 72h resulted in a significant increase in the population of G1-phase cells compared to untreated cells (P=0.0032 and 0.0043, respectively). This increase in the population of G1-

phase cells was accompanied by a decrease in the population of S-phase and G2-phase cells. Although the observed decline in the proportion of cells in the S and G2 phases, the reduction was not statistically significant (p=0.3275 and 0.8390, respectively) when cells were treated with Tenidap (1μM). However, when cells were treated with a higher concentration of Tenidap (10μM), a statistically significant decrease in the percentage of cells in S and G2 phases (p= <0.0001) was observed compared to control cells (**Figure 3. 15C**).

In order to investigate the effect of SC-560 on cell cycle progression in OCI-AML-3 cells, cells were treated with varying concentrations of SC-560 (1μM or 10μM) for 72 hours, followed by analysis of the cell cycle distribution by flow cytometry. The results showed that both concentrations of SC-560 led to a significant increase in the proportion of cells in the G1 phase compared to vehicle cells (P= 0.0398 and 0.0005, respectively). Additionally, there was a non-significant decrease in the number of cells in the S phase due to SC-560 treatment (P= 0.9194 and 0.4331). However, a significant decline in the proportion of cells in the G2 phase was observed when cells were exposed to either 1μM or 10μM of SC-560 compared to control cells (p=0.0037 and 0.0002). These findings are illustrated in **Figure 3. 15D**.

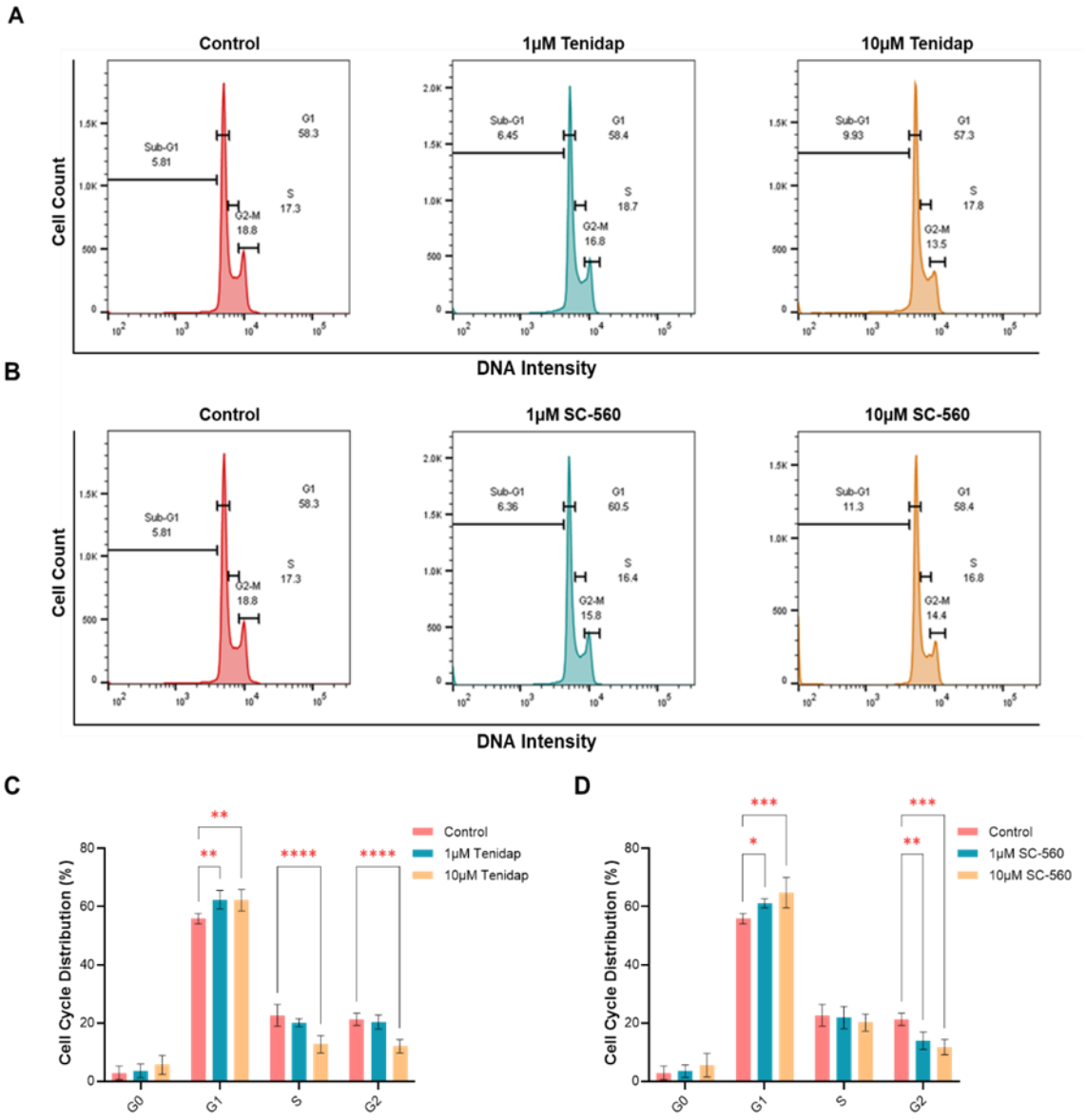

Figure 3. 15 Both SC-560 and Tenidap cause cell cycle arrest in OCI-AML-3 cell line.

(A) *Representative histogram of gated OCI-AML-3 cell line in the G0, G1, S, and G2 phases that were treated with at different concentrations of tenidap (1 μM and 10 μM) for 72h, while* ***(B)*** *SC-560 were added to the cells at two different concentrations (1 μM and 10 μM) for 72h. Control cells were treated with DMSO (vehicle control). The cell cycle analysis was performed on fixed cells stained with PI using flow cytometry.* ***(C)*** *Quantitative analysis of cell distribution was conducted using at least 10000 cells per condition. Each bar shows the mean +/- SEM of the results from three independent experiments. *p < 0.05; **p < 0.01 vs. control. The bar charts presented were generated using GraphPad Prism 8 software.*

Similarly, U937 cells were treated with varying concentrations of Tenidap (1µM or 10µM) for 72 hours to investigate the effect of Tenidap on cell cycle progression. The results revealed that both concentrations of Tenidap showed a significant accumulation of cells in the G1-phase after treatment (P=0.0499 and 0.0265, respectively) with reductions in cells in the S and G2 phases. The differences in cell cycle phase reduction between the control and treated cells were insignificant. However, a statistically significant decrease in the proportion of cells in the G2-phase was observed in cells treated with 10µM of Tenidap compared to vehicle control cells (P= 0.0414, **Figure 3. 16C**).

To accomplish this, cells were treated with either 1µM or 10µM of SC-560 for 72 hours, followed by an analysis of the cell cycle distribution by flow cytometry. The results indicated that both concentrations of SC-560 significantly increased the proportion of cells in the G1 phase compared to vehicle control cells (P= 0.0024 and 0.0034, respectively). There were also non-significant decreases in the number of cells in the S phase due to SC-560 treatment (P= 0.2208 and 0.2027). However, a significant decline in the proportion of cells in the G2 phase was observed when cells were exposed to 10µM of SC-560 compared to control cells (P= 0.0338, respectively). These results are further supported by the data illustrated in **Figure 3. 16D**. Overall, these results suggest that treatment with *PTGS1* inhibitors (SC-560 or Tenidap) led to cell cycle arrest at the G1-phase in AML cell lines, with a stronger effect observed at higher concentrations.

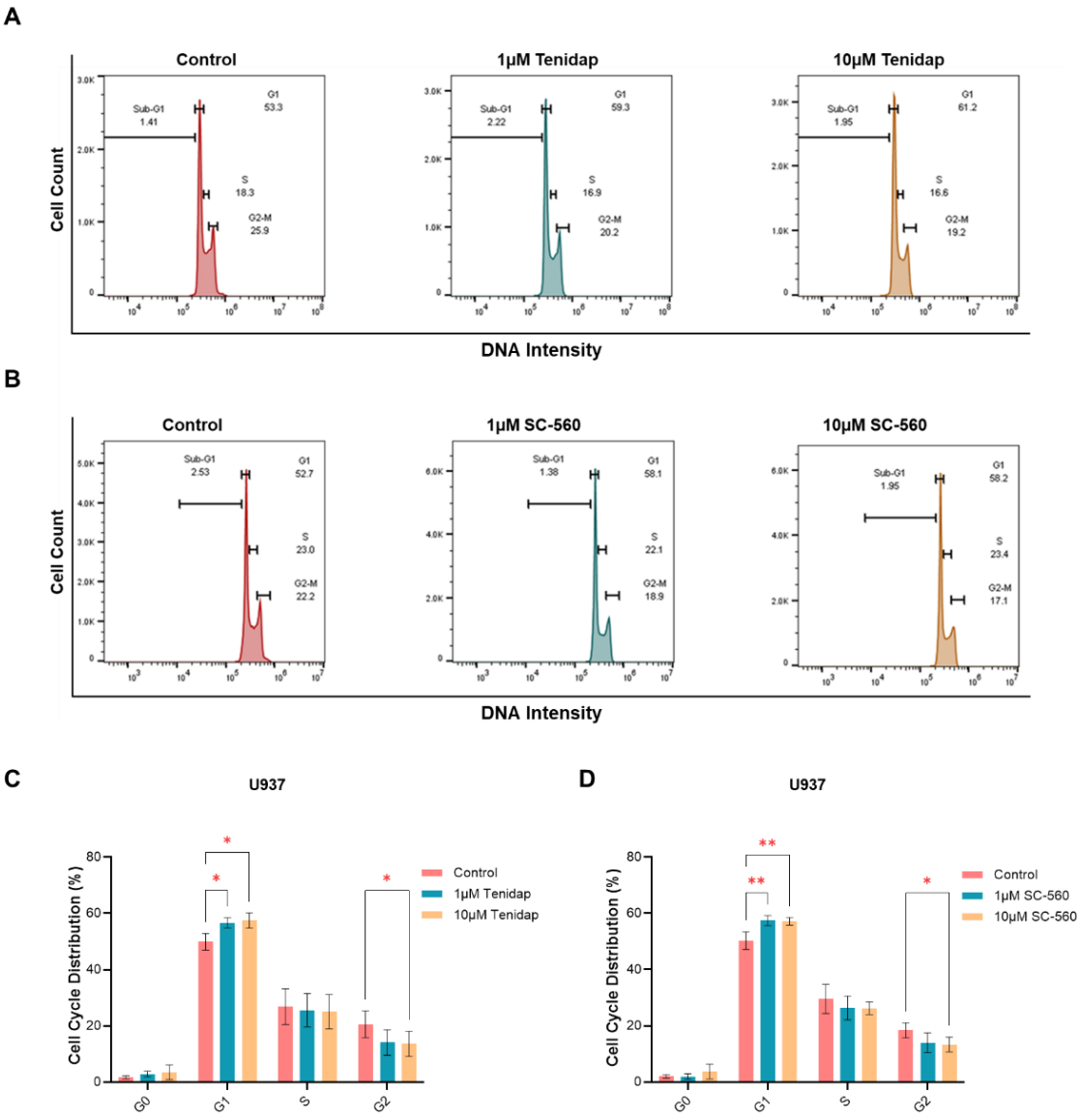

Figure 3. 16 PTGS1 inhibitors induce cell cycle arrest in U937 cell line.

A representative histogram of the gated U937 cell line in the G0, G1, S, and G2 phases following treatment with tenidap at two different concentrations (1 μM and 10 μM) for 72 hours is shown in Figure ***(A)*** *and Figure* ***(B)*** *shows cells incubated with SC-560 at two different concentrations (1 mM and 10 mM) for the same time. Control cells treated with DMSO (vehicle control). The cell cycle study was carried out using flow cytometry on fixed cells labelled with PI.* ***(C)*** *At least 10,000 cells per condition were used to examine cell dispersion quantitatively. Each bar displays the average of the outcomes from three separate experiments. *p 0.05; **p 0.01 in comparison to control. The bar charts presented were generated using GraphPad Prism 8 software.*

3.3.10 Role of PTGS1 inhibition on cell signalling in AML cell lines.

To better understand the effects of *PTGS1* inhibition on cell growth in AML, we next aimed to elucidate the impact of *PTGS1* inhibitors (SC-560 or tenidap) on cell signalling in AML cells. To achieve this, OCI-AML-3 and U937 cells were treated with SC-560 or tenidap at a concentration of 1μM for various time points. Total cellular protein extracts were prepared and subjected to immunoblot analysis using specific antibodies including phospho-AKT and phospho-ERK1/2, and their unphosphorylated forms (**Figure 3. 17** and **Figure 3. 18**).

For the U937 cell line, treatment with SC-560 or tenidap (1μM) increased AKT's phosphorylation at 2 hours post-treatment. This effect was significantly increased after 6 hours of treatment compared to untreated cells. However, after 24 hours, there was a decline in the phosphorylation of AKT, and by 48 hours, there was a significant decline after treatment with SC-560 compared with control cells. Also, the results showed a significant increase in the phosphorylation of ERK1/2 at 6 hours post-treatment with SC-560, while after 48 hours, both SC-560 and tenidap resulted in a significant inhibition in the phosphorylation of ERK1/2 (**Figure 3. 17**).

Similarly, 6 hours after treatment with SC-560 or tenidap(1μM), the phosphorylation of AKT significantly increased in the OCI-AML-3 cell line in response to treatment compared to control cells. This observed increase in the phosphorylation of AKT began to decline at 24 hours post-treatment. Our data also revealed a significant increase in the phosphorylation of ERK1/2 after 6 hours of SC-560 and tenidap treatment, while after 24 hours, the phosphorylation of ERK1/2 decreased to the normal level. Overall, these

findings suggest that treatment with PTGS1 inhibitors significantly affects the activation of phospho-AKT and phospho-ERK1/2 in both U937 and OCI-AML-3 cell lines. However, this effect is time-dependent, with the activation of these pathways peaking at 6 hours post-treatment and declining after 24 hours (**Figure 3. 18**).

A

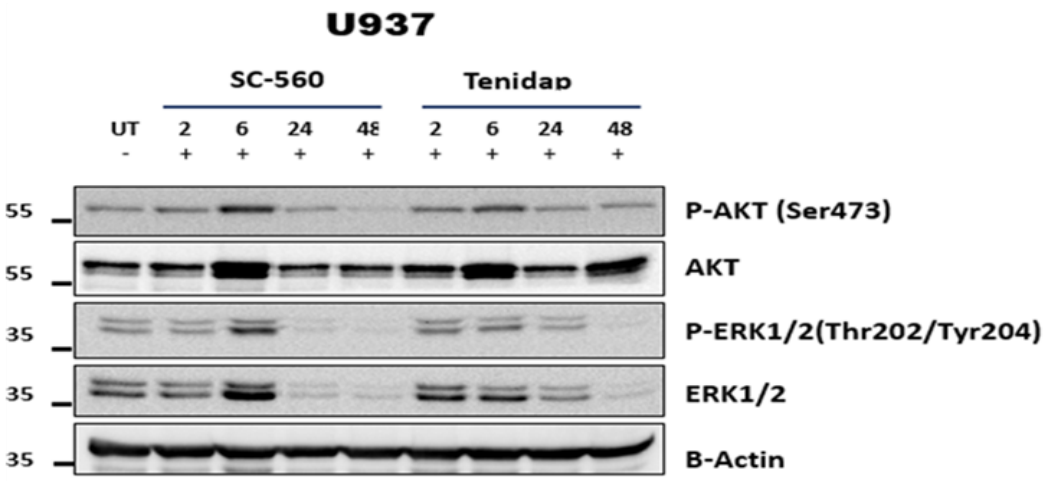
U937
SC-560
Tenidap
UT 2 6 24 48 2 6 24 48
- + + + + + + + +
55
55
35
35
35
P-AKT (Ser473)
AKT
P-ERK1/2(Thr202/Tyr204)
ERK1/2
B-Actin

B

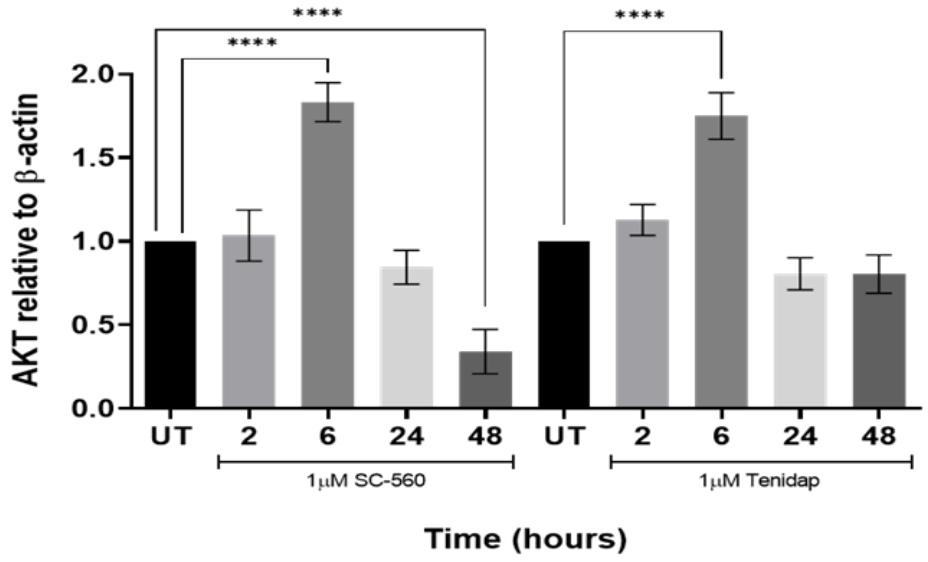
****
****
****
AKT relative to β-actin
2.0
1.5
1.0
0.5
0.0
UT 2 6 24 48 UT 2 6 24 48
1μM SC-560
1μM Tenidap
Time (hours)

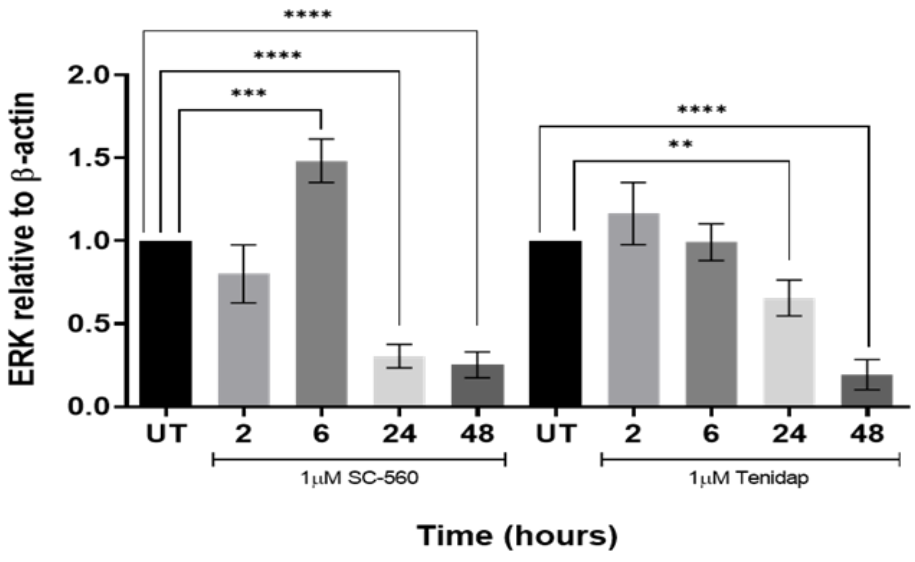
****
****
***
****
**
ERK relative to β-actin
2.0
1.5
1.0
0.5
0.0
UT 2 6 24 48 UT 2 6 24 48
1μM SC-560
1μM Tenidap
Time (hours)

C

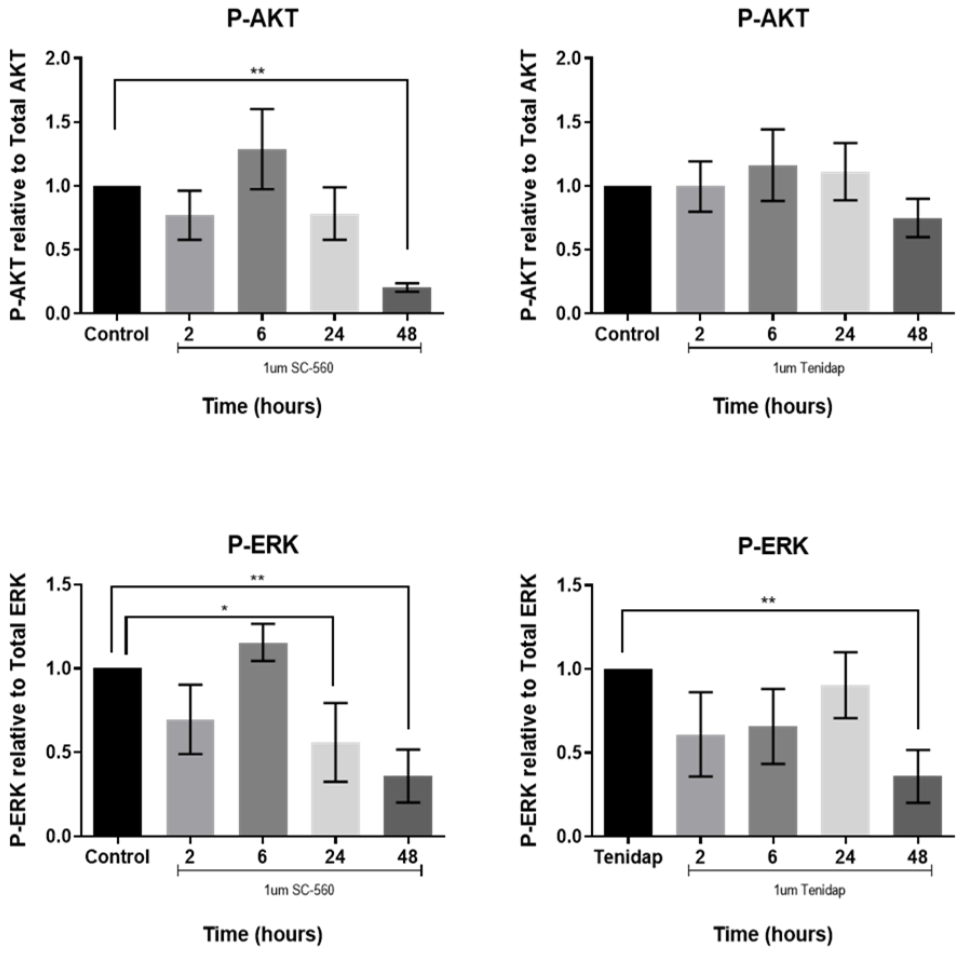

Figure 3. 17 The effects of PTGS1 inhibitors on U937 cell lines.

(A) *U937 cells were treated with either SC-560 or tenidap (1μM) and incubated for 2, 6, 24 and 48 hours. Total proteins were extracted and separated using 10% SDS-PAGE. Then, the immunoblot analysis was conducted using antibodies, including phospho-AKT and phospho-ERK1/2, as well as their unphosphorylated forms. To ensure equal loading of protein, β-actin was included as a loading control.* ***(B)*** *The densitometric levels of total protein band intensity were normalized with β-actin protein levels, and each value was then calculated relative to the untreated cells.* ***(C)*** *The densitometric levels of phosphorylated protein band intensity were normalized with their respective total protein levels, and each value was then calculated relative to the untreated cells. Statistical analysis was conducted using one-way ANOVA with Dunnett's multiple comparison test (n=3), and significance was set at *P≤0.05, **P≤0.01, ***P≤0.001 and ****P≤0.0001. The results represent the mean +/- SEM for three independent experiments. The bar charts presented were generated using GraphPad Prism 8 software.*

A

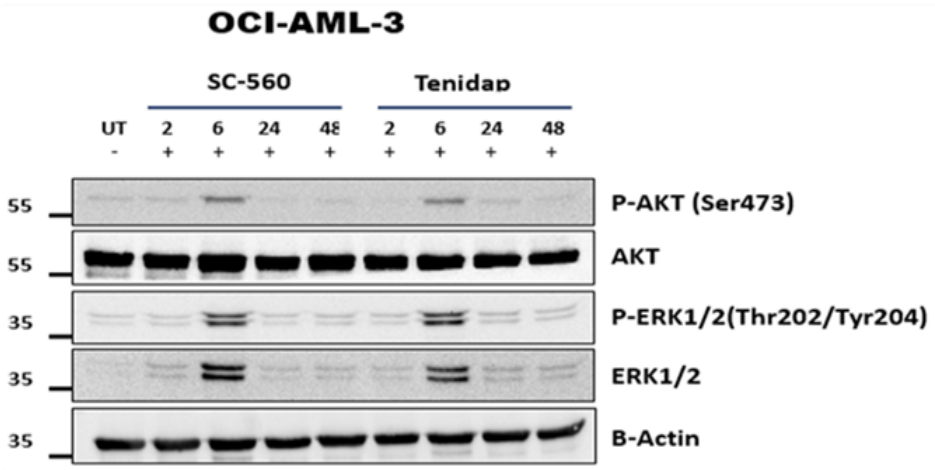
OCI-AML-3
SC-560
Tenidap
UT 2 6 24 48 2 6 24 48
- + + + + + + + +
55
55
35
35
35
P-AKT (Ser473)
AKT
P-ERK1/2(Thr202/Tyr204)
ERK1/2
B-Actin

B

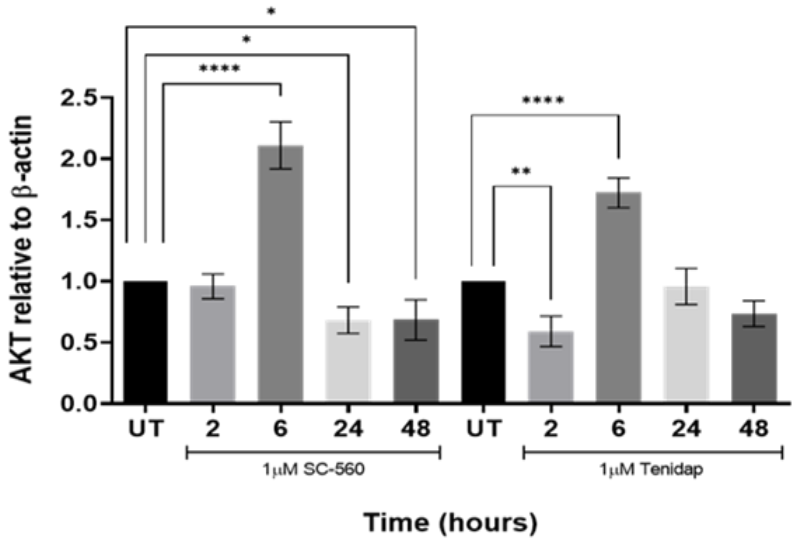
AKT relative to β-actin
0.0
0.5
1.0
1.5
2.0
2.5
*
*
****
****
**
UT 2 6 24 48 UT 2 6 24 48
1μM SC-560
1μM Tenidap
Time (hours)

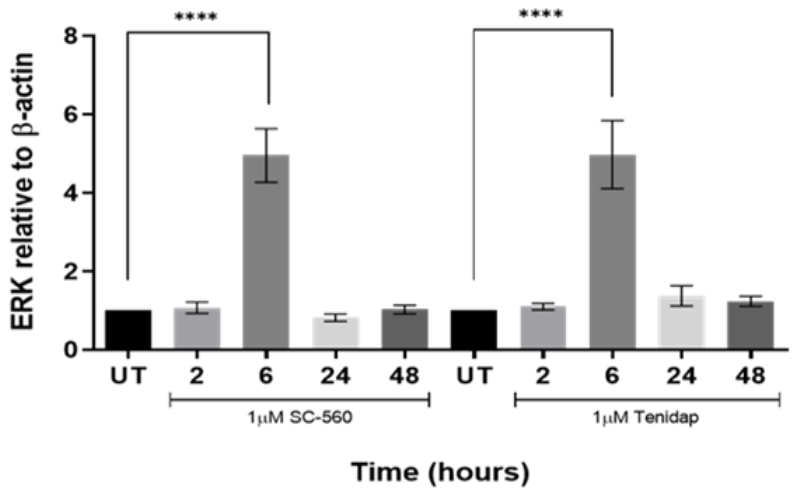
ERK relative to β-actin
0
2
4
6
8
****
****
UT 2 6 24 48 UT 2 6 24 48
1μM SC-560
1μM Tenidap
Time (hours)

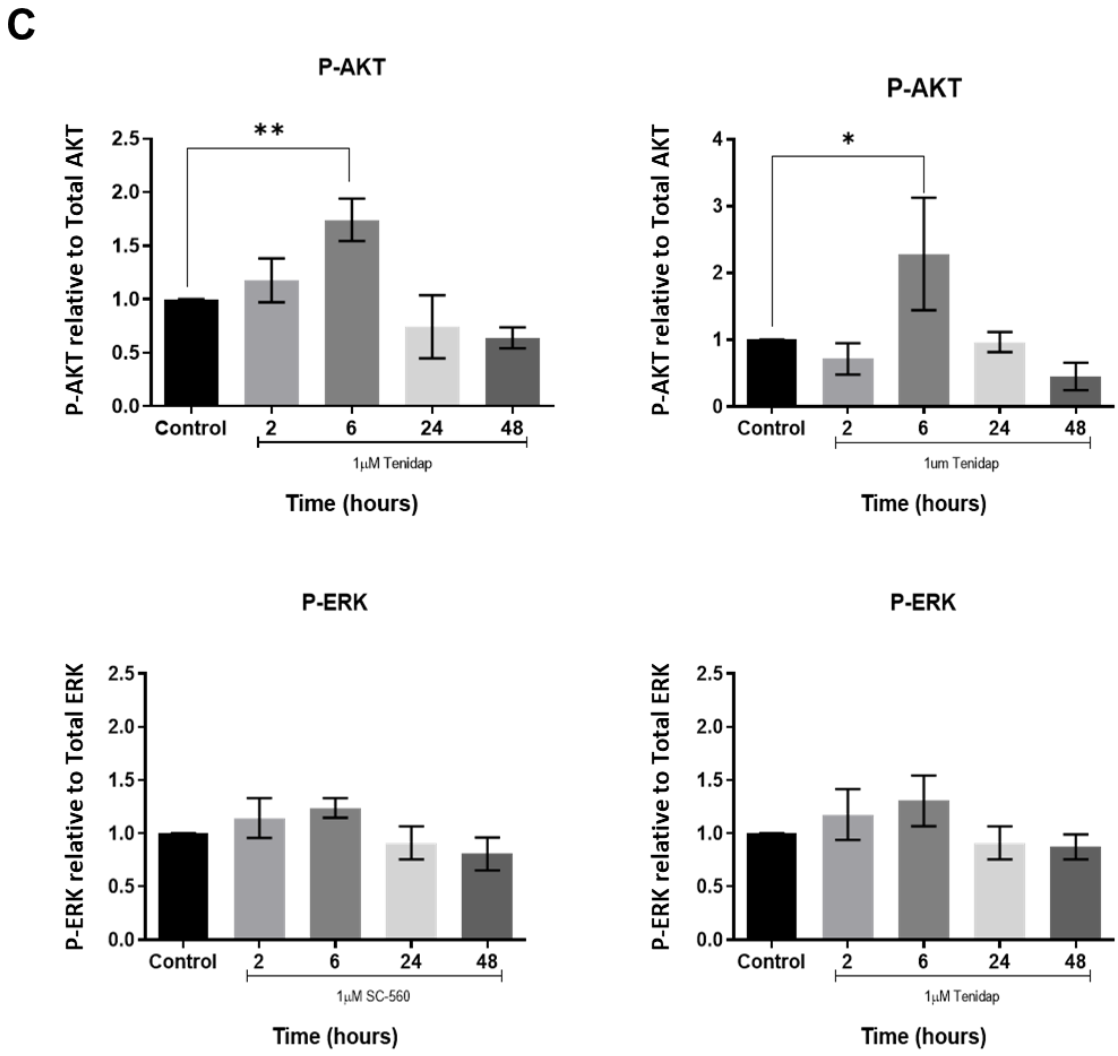

Figure 3. 18 The impact of PTGS1 inhibitors on OCI-AML-3 cell lines.

(A) *OCI-AML-3 cells were treated with SC-560 or tenidap (1μM) and then incubated for different time periods ranging from 2 to 48 hours. Total proteins were extracted and separated by 10% SDS-PAGE, followed by immunoblot analysis using antibodies against phospho-AKT and phospho-ERK1/2, as well as their unphosphorylated forms. β-actin was used as a loading control to ensure equal protein loading.* ***(B)*** *The densitometric levels of total protein band intensity were normalized with β-actin protein levels, and each value was then calculated relative to the control cells.* ***(C)*** *The densitometric levels of phosphorylated protein band intensity were normalized with their respective total protein levels, and each value was then calculated relative to the untreated cells. Statistical analysis was conducted using one-way ANOVA with Dunnett's multiple comparison test (n=3), and significance was set at *P≤0.05, **P≤0.01, ***P≤0.001 and ****P≤0.0001. The results represent the mean +/- SEM for three independent experiments. The GraphPad Prism 8 software was used to generate the bar charts presente.*

3.4 Discussion

Major Findings Summary:

The expression of *PTGS1* is higher in HSCs but not *PTGS2*, and it decreases with lineage commitment in myeloid progenitors, according to bioinformatic study of publicly accessible databases. Interestingly, in AML datasets (TCGA, Verhaak), increased *PTGS1* expression is linked to a lower overall survival rate, but no correlation is observed with *PTGS2*. Data obtained in vitro show that *PTGS1* inhibition (SC560, Tenidap) causes cell cycle arrest, promotes apoptosis, and decreases cell proliferation.

Discussion:

The findings of patient analysis carried out for this study reveal a significant impact of *PTGS1* on overall survival of patients, which is not found for *PTGS2*. This difference in effect points to the possibility that each gene has a different role in the AML cell. Various researchers have recently proposed biomarkers using genes which demonstrate differential expression when comparing AML patients and healthy subjects (Handschuh et al. 2018), or comparing AML patients with good outcomes against those with poor outcomes (Dzneladze et al. 2015). The research reveals significant variations in gene expression across different AML patients, and analysis of these helps to uncover novel targets for therapies. In summary, the complexity of AML is clear from these findings, demonstrating influences from a range of variables in genes and the environment, with genetic and mutational differences causing differing forms of AML, each with their own implications clinically.

The findings point to a linked between patterns in expression of genes such as *PTGS1* and “stemness” or self-renewing capacity of HSCs and the LSC-phenotype (Corces-Zimmerman et al. 2014; Yu et al. 2020). *PTGS1* is shown to be expressed most strongly in HSCs and myeloid progenitor cells, which have the strongest association with AML (Wesely et al. 2020). The most significant point from the study results is the distinctive patterns in which *PTGS1* is expressed at each stage of differentiation in HSCs. It is significant that *PTGS1* is expressed most strongly within the subgroup of HSCs that are most primitive, with self-renewing and quiescent characteristics. These findings point to the possibility that *PTGS1’s* contribution in AML cold involve maintain HSC stemness. When MEP generation is initiated, expression is also high, but then becomes downregulated in GMPs, in line with its role in commitment to lineages and mechanisms for myeloid lineage differentiation: this is frequently found for AML-associated genes, such as *MEIS1, GATA1, CEBPA, RUNX1, NPM1* and *KIT*. On the other hand, changes in AML blast *PTGS1* expression, in which it does not become downregulated in GMP-like cells, point to disrupted differentiation signalling. Significantly, HSC-linked genes frequently have associations with poor AML outcomes, and likelihood that *PTGS1* is associated with HSCs presents the possibility of evaluating the possible contribution of this gene to making AML prognoses. The high complexity of the findings, with numerous associations between variables and the presence of small samples, could limit the conclusions which can be drawn, although the general conclusions are valid.

During preliminary studies investigating *PTGS2* inhibitors, SC-560 was discovered, belonging to the class of diaryl heterocycles, and which has

significantly assisted with studies of the role of PTGS1-derived prostaglandin in inflammatory processes and pain (Smith, Zhang et al. 1998). SC-560 has been investigated pharmacologically in relation to a range of pathologies, and specifically, cancers. Significantly, it has been investigated in modelling studies of ovarian cancer, in the angiogenesis of which *PTGS1* concentration is raised within the epithelial zone of tumours (Smith et al. 1998; Gupta et al. 2003). In this modelling, SC-560 was shown to inhibit proliferation in a similar range to different inhibitor agents. However, those agents had greater potency and needed a higher dosage. Notably, PGE2 changed the way in which SC-560 caused VEGF suppression due to arachidonic acid when given in a comparatively low dosage (Pannunzio and Coluccia 2018). Immunohistochemical investigation of sampled tumours shows that, in SKOV-3 xenograft models, SKOV-3 cells mainly demonstrate *PTGS1* isoform expression. Treating SC-560 using doses tailored towards inhibiting *PTGS1* led to decreased growth of tumours ranging between minor and moderate. The findings included the unexpected result that SC-560 given in combination with taxol or cisplatin was frequently more effective compared to the drugs given singly when evaluated based on various end points, including angiogenic activity, proliferative activity and apoptosis (Pannunzio and Coluccia 2018).

Our findings demonstrate suppression of cell growth by SC-560 with Tenidap, pointing clearly to a role of *PTGS1's* in progressing the cell cycle, with notable inhibitory effects on cell growth but without cells dying completely suggesting the role of *PTGS1* not in direct mediation of survival but in regulating the cell cycle. The impacts of Tenidap and SC-560 in inhibiting cell growth found can form an initial step towards mapping the function of *PTGS1* in managing the

cell cycle, potentially leading to novel therapeutic strategies targeting the mechanisms which support cells to proliferate abnormally.

Observations reveal pharmacologically-induced cell accumulation within the cell cycle's G1 stage, decreasing accordingly during the G2 stage. There are also increases in both phosphorylated AKT (p-AKT) and phosphorylated ERK (p-ERK), and these drug-based impacts imply interesting possibilities in terms of their mechanisms. As shown by Torii et al. (2006), the effects suggest that the drugs act upon important checkpoints in regulation of the cell cycle. Accumulation in G1 may indicate that the cycle is blocked or delayed in transitioning to the S phase, which could be driven by the drugs interfering with factors which drive this progression from G1 to S, while the reduction in G2 suggests an effect on how the transition between G2 and M is regulated. Increased levels of p-AKT and p-ERK may point to responses to the stoppage of the cell cycle in which survival and proliferation are activated to compensate for this disruption, in a potential feedback mechanism. Taken as a whole, these results reflect the complexity of interactions between pharmacological changes to the cell cycle and cascading signal pathways, and offer a basis for building understandings of the mechanisms underpinning the impacts seen for the drugs.

Our research work highlights a significant difference between *PTGS1* and *PTGS2*: as earlier discussed, *PTGS1* showed a close association with outcome in acute myeloid leukaemia, and when suppressed, this affected how the AML cell developed, while this was not seen for *PTGS2*. This notable difference in contribution to AML pathogenesis increases understandings of how exactly

PTGS1 and *PTGS2* function. The next chapter aims therefore to model *PTGS1/PTGS2* in AML to examine their specific functions.

Chapter IV

4.1 Introduction

Dysregulated gene expression is a crucial factor in the progression of cancers (Sager 1997; Garnis et al. 2004; Yu et al. 2020). An example of this is the tumour suppressor gene *PTEN*, which often shows alteration in cancer, and where loss-of-function mutation occurs, leads to uncontrolled growth of cells (Milella et al. 2015). Further, tumours, whether *MYC* or another oncogene is the driving factor, rely on *MYC* to be over-expressed in order to grow, with over-expression of *MYC* forming a vital contributor to malignant transformation (Gabay et al. 2014). In cancer, *MYC* expression is demonstrated to be driven by PGE2 (Xia et al. 2014). To investigate this association in acute myeloid leukaemia, 2 cell lines were selected: HL60, with over-expression of *MYC*; and cell line U937, in which *MYC* is normally expressed.

Various experimentally approaches are available to evaluate *PTGS1* and *2* function within AML. First, the impacts of downregulating each gene can be assessed through selective reduction of *PTGS1* and *PTGS2* expression via small interfering RNA (siRNA) or short hairpin RNA (shRNA) techniques. Moreover, complete inhibition of the functions of *PTGS1/PTGS2* is achievable through knockout of the gene, based on introducing a specific mutation or using CRISPR-Cas9 techniques, to demonstrate the significance of these genes in progression of AML. For this study, over-expression was selected for investigation, as a typical characteristic of AML. Genes which are over-expressed are important to investigate in order to understand different cell processes at a molecular level, as well as being useful in assessing the function of genes and in determining novel phenotypic forms (Prelich 2012; Robinson et al. 2021; Rai et al. 2022).

Molecular biology approaches include DNA cloning, in which pieces of DNA, including genes, are copied identically (Davis 2012). In this procedure, a targeted piece of DNA is transferred from an organism into a self-replicating genetic component: e.g., a plasmid taken from bacteria (Brown 2020). These recombinant gene / regulatory component-carrying plasmid is then introduced into specific cell lines with the aim that the gene of interest will be over-expressed in them (McLenachan et al. 2007).

If the aim however is to introduce a regulatory effect stably and in a lasting manner, it is more effective to use lentiviral transfection to build a stable cell line (Tomás et al. 2018). This technique allows genes to be efficiently knocked down or upregulated for longer term regulation (Tomás et al. 2018, Chen et al. 2020).

4.2 Aims

1. To determine the contribution of *PTGS1* and *PTGS2* genes to survival, proliferation and drug resistance.

2. To examine the influence of *PTGS1* and *PTGS2* over-expression on prostaglandin E2 (PGE2) production in AML cells.

3. To evaluate the role of *PTGS1* and *PTGS2* over-expression in regulating reactive oxygen species (ROS) levels in AML.

4.3 Results

4.3.1 Characterization of pLenti-C-Myc-DDK-P2A-Puro Vector for PTGS1 and PTGS2 Gene Insertion

The *PTGS1* gene was inserted into the third-generation lentiviral vector pLenti-C-Myc-DDK-P2A-Puro using standard molecular cloning techniques (**Figure 4. 1**). *PTGS1* and *PTGS2* cDNA was a kind gift from Darryl C.Zeldin (National Institute of Environmental Health Sciences (NIEHS), Durham, North Carolina) supplied in the pBluescript packaging vector, from which subcloning was performed (**Figure 4. 1A, D**). The pLenti-C-Myc-DDK-P2A-Puro vector contains specific restriction sites, namely SgfI and MluI, which facilitate the insertion of the *PTGS1* gene at a precise location within the vector. The pLenti-C-Myc-DDK-P2A-Puro vector provides additional elements, such as the C-Myc and DDK (FLAG) tags, which allow for the detection and purification of the PTGS1 protein product in the modified target cell lines, downstream of transduction. To confirm the generation of the PTGS1 vector construct, a digestion assay was performed using the SgfI and MluI restriction enzymes, which target the specific restriction sites present in the plasmid construct (**Figure 4. 1B**). The *PTGS1* gene, with a size of 1797 base pairs (bp), was expected to be released from the plasmid backbone, which has a size of 7100 base pairs (bp), upon digestion. The resulting fragments were separated and visualised using agarose gel electrophoresis after subjecting the cloned plasmid to the SgfI and MluI digestion. The anticipated outcome of the digestion was the generation of two distinct DNA bands: one representing the *PTGS1* gene fragment (1797 bp) and the other representing the plasmid backbone fragment (7100 bp) (**Figure 4.**

1C). By comparing the observed fragment sizes to the expected sizes, the successful digestion of the cloned plasmid could be confirmed. The presence of the *PTGS1* gene fragment would indicate that the PTGS1 cDNA was correctly inserted into the plasmid construct. In contrast, the plasmid backbone fragment's presence would confirm the plasmid's overall integrity.

Similarly, pLenti-C-Myc-DDK-P2A-Puro was employed for the precise insertion of the *PTGS2* gene using SgfI and MluI restriction sites (**Figure 4. 1E**). These restriction sites enable the accurate placement of the *PTGS1* gene at a defined genomic locus within the vector, ensuring proper alignment and orientation. By utilising the specific restriction enzymes SgfI and MluI, which target the unique restriction sites within the plasmid construct, a digestion assay was performed to confirm the integrity of the cloned plasmid. This assay aimed to liberate the 1812 bp long *PTGS2* gene from the 7100 bp long plasmid backbone through enzymatic digestion. The cloned plasmid was subjected to digestion using the SgfI and MluI enzymes, and the resulting fragments were separated and visualised using agarose gel electrophoresis. During this process, it was anticipated that two distinct DNA bands would appear: one corresponding to the *PTGS2* gene fragment (1797 bp) and the other representing the plasmid backbone fragment (7100 bp)

A

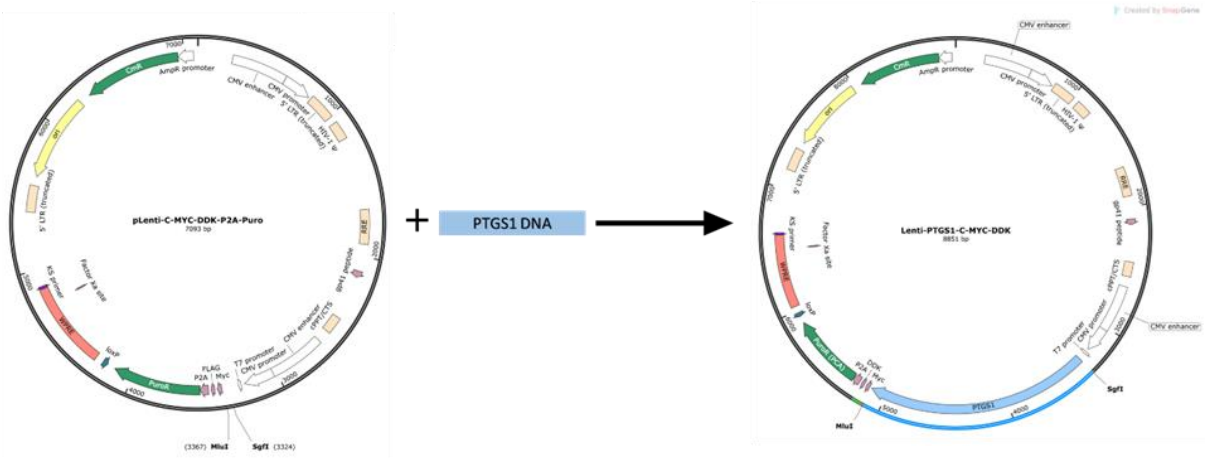
pLenti-C-MYC-DDK-P2A-Puro
7093 bp
PTGS1 DNA
Lenti-PTGS1-C-MYC-DDK
8851 bp

B

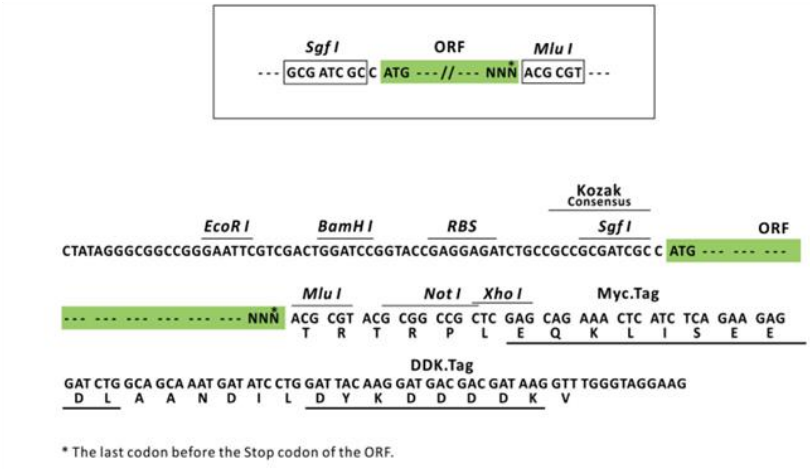
Sgf I
ORF
Mlu I
--- GCG ATC GCC ATG --- // --- NNN ACG CGT ---
Kozak Consensus
EcoR I
BamH I
RBS
Sgf I
ORF
CTATAGGGCGGCCGGGAATTCGTCGACTGGATCCGGTACCGAGGAGATCTGCCGCCGCGATCGC C ATG --- --- ---
Mlu I
Not I
Xho I
Myc.Tag
--- --- --- --- --- --- NNN ACG CGT ACG CGG CCG CTC GAG CAG AAA CTC ATC TCA GAA GAG
T R T R P L E Q K L I S E E
DDK.Tag
GAT CTG GCA GCA AAT GAT ATC CTG GAT TAC AAG GAT GAC GAC GAT AAG GTT TGGGTAGGAAG
D L A A N D I L D Y K D D D D K V
* The last codon before the Stop codon of the ORF.

C

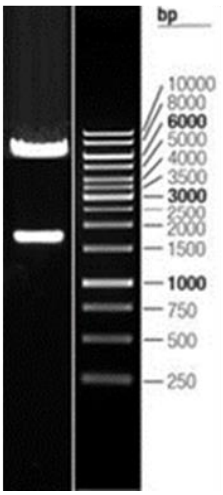
bp
10000
8000
6000
5000
4000
3500
3000
2500
2000
1500
1000
750
500
250

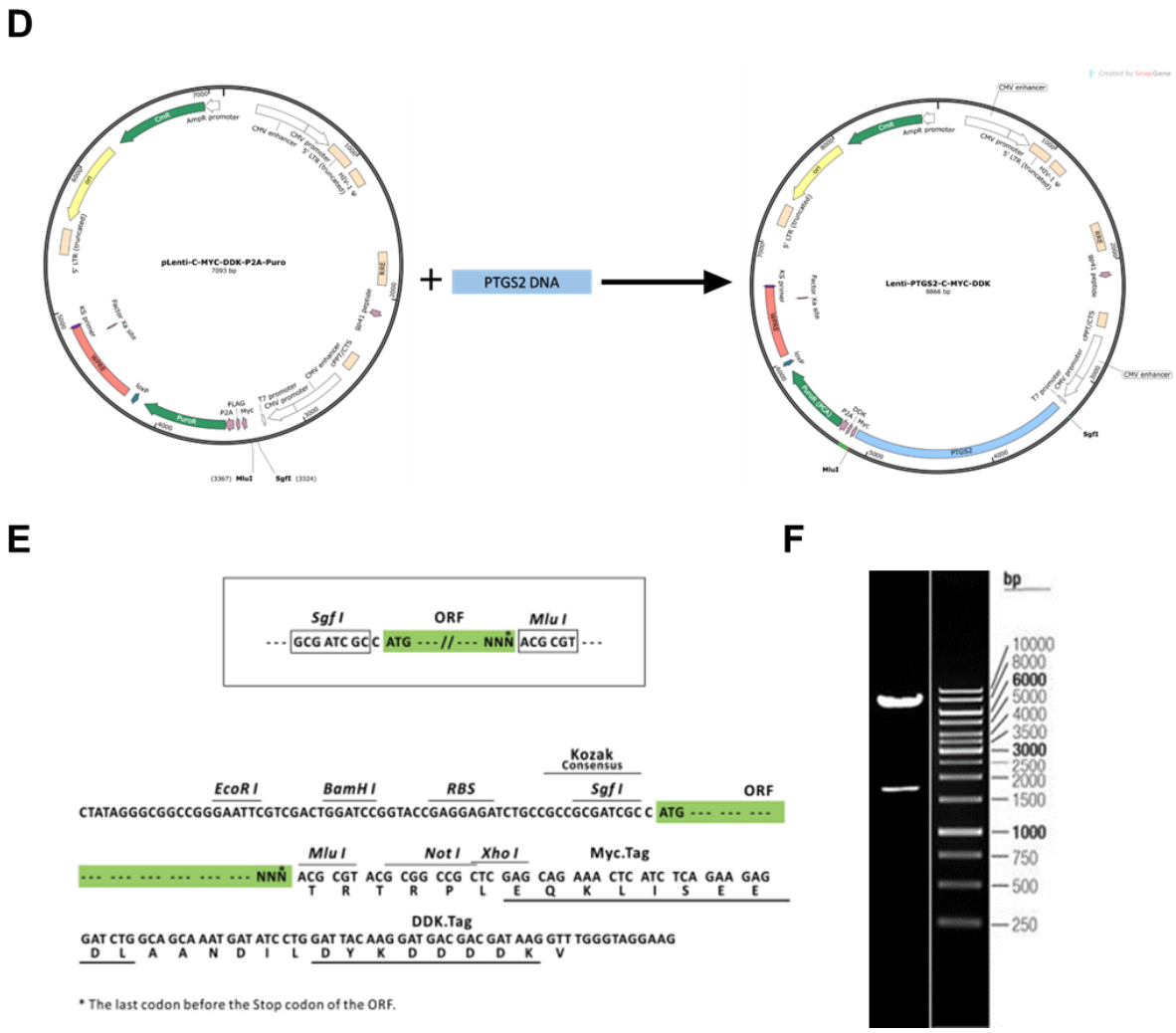

Figure 4. 1 Cloning PTGS1 and PTGS2 into pLenti-C-Myc-DDK-P2A-Puro plasmid.

(A, D) *Schematic plasmid map of modified pLenti-C-Myc-DDK-P2A-Puro plasmid used for cloning. (**B, E**) Cloning scheme involved the utilisation of the SgfI and MluI restriction enzymes. (**C, F**) Digestion with SgfI and MluI results in two band. SnapGene 7.1 software was used to generate the schematic plasmid map.*

4.3.2 Optimizing Lentiviral transfection of *PTGS1/2* into HEK293t cells for efficient over-expression

In this chapter, we aimed to investigate the function of *PTGS1/2* by creating stable AML cell lines over-expressing both genes separately. Given the extreme difficulty of gene transfer to myeloid lineage cells, we must employ the lentiviral gene-delivery strategies in AML cell lines. The first step is to generate *PTGS1* and *PTGS2* lentiviral particles by overexpressing the 3 vector lentivirus system (Transfer vector, packaging vector and envelope vector) first in 293T cell lines. The HEK293T cell line is a widely used model for studying molecular and cellular biology due to its high transfection efficiency and ease of handling. The *PTGS1* or *PTGS2* was cloned into a plasmid vector with the puromycin selection gene to allow the selection of transfection cells. The plasmid was then transfected into the HEK293T cell lines using the transfection reagent described in the materials and method chapter.

The transfection efficiency was then assessed using GFP fluorescence, a reporter gene on the control pLenti-C-Myc-DDK-P2A-GFP vector. Both transfected and un-transfected (control) cells were visualized under a fluorescence microscope. We observed a high level of bright green fluorescence in the transfected cells, while un-transfected cells exhibited no green fluorescence (**Figure 4. 2A**). This indicates that the transfer vector was successfully transfected into the HEK293T cells.

Next, we performed a Western blot analysis to confirm the successful transfection of *PTGS1* or *PTGS2* into the HEK293T cells. Western blotting revealed a band corresponding to PTGS1 protein at the expected molecular

weight in the transfected cells, which was almost absent in the control (wild-type) cells. Moreover, a high level of PTGS2 protein was shown in the transfected cell compared to control cells. The figure also showed a loading control band (β-actin) to ensure equal protein loading in each sample (**Figure 4. 2B**).

The densitometric levels of PTGS1 and PTGS2 were used to measure the intensity of bands on western blot images. The cells transfected with 10µl or 20 µl of the *PTGS1* plasmid displayed a significant increase in PTGS1 protein level with 35-fold and 64-fold change compared to the control cells, respectively. Furthermore, overexpression of *PTGS2* showed a significant increase in PTGS2 protein expression levels with a fold change of 7-fold increase compared to control cells (**Figure 4. 2C**).

These findings confirm that our plasmid-based transfection approach was successful in inducing over-expression of *PTGS1* and *PTGS2* in HEK293T cells and that the GFP reporter gene and western blot analysis can be used as reliable tools to confirm successful transfection and over-expression of target genes successful transfection and over-expression of target genes. This HEK293T can be utilised further in *PTGS1*- and *PTGS2* over-expression lentiviral production for AML transduction.

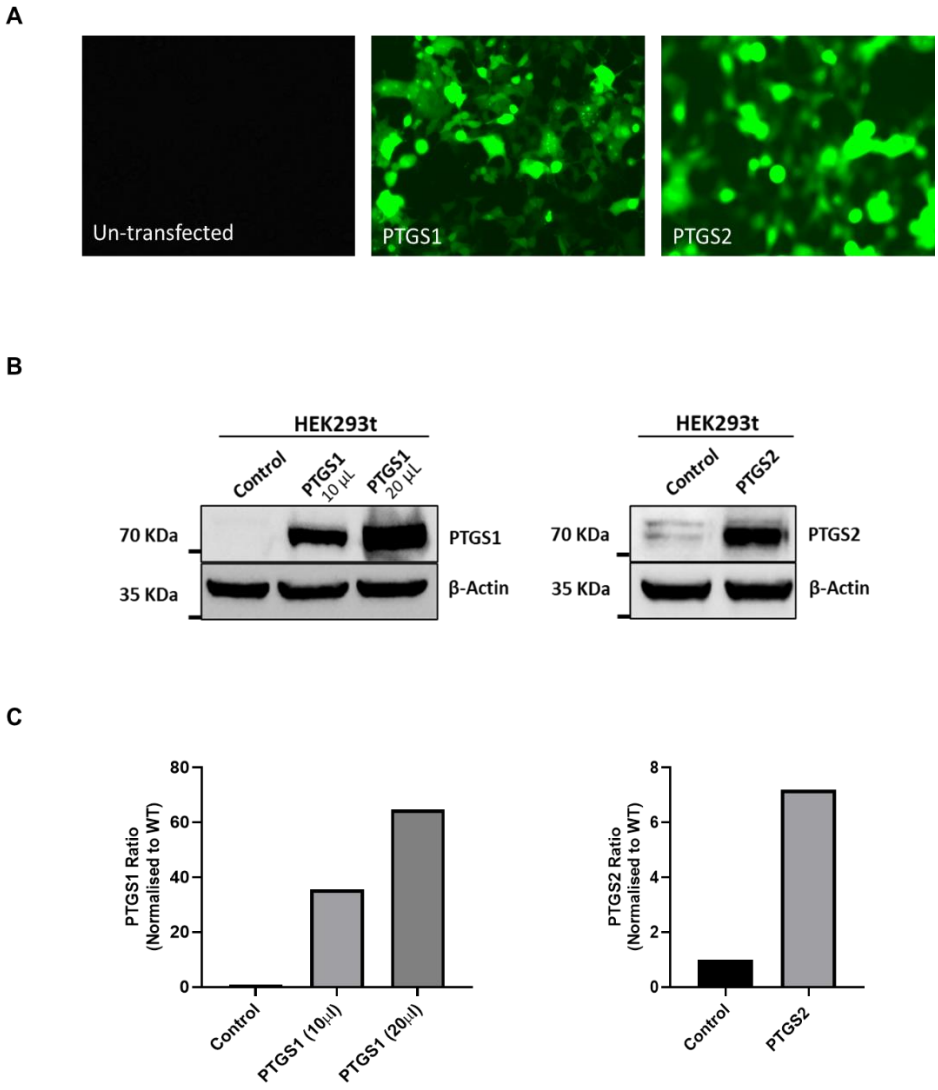

Figure 4. 2 Lentiviral-mediated over-expression of PTGS1/2 into 293t cell lines.

(A) *HEK293t cells were transfected with pLenti-C-Myc-DDK-P2A-GFP. Un-transfected cells were used as a negative control. 48 hours post-transfection, the cells were observed under a fluorescence microscope to detect GFP expression.* ***(B)*** *Western blot shows the PTGS1 and PTGS2 protein levels, after transfection with pLenti-C-Myc-DDK-P2A-Puro, in the HEK293T cell line. The protein samples (20 µg) were separated by SDS-PAGE and transferred onto a nitrocellulose or membrane, followed by incubation with a PTGS1 or PTGS2 antibody. β-actin was used as a loading control to ensure equal protein loading. The membrane was then visualised using chemiluminescent substrates by the ChemiDoc imaging system (Bio-Rad).* ***(C)*** *The densitometric levels of proteins band intensity were normalised with their β-actin protein levels, and each value was then calculated relative to the un-transfected cells (control cells).*

4.3.3 Detection of *PTGS1/2* over-expression in AML cells transduced with Lentiviral-mediated over-expression of *PTGS1/2*

To better characterise the function of *PTGS1* and *PTGS2*, both were overexpressed in the AML cell lines, including U937 and HL-60, by lentiviral transduction. The transduction efficiency was first evaluated using GFP fluorescence as a reporter gene. Next, puromycin selection was performed to select cells that had successfully integrated a plasmid containing a selectable marker (puromycin N-acetyltransferase). The puromycin N-acetyltransferase (PAC) allows the cells to become resistant to the antibiotic puromycin, which is toxic to cells that do not have it. By selecting only cells that have successfully integrated the plasmid and have become resistant to puromycin, we can produce a clonal population of *PTGS1/2* overexpressing AML cells.

To perform puromycin selection, U937 and HL-60 were plated with varying concentrations of puromycin and counted daily using a haemocytometer after diluting 1:1 in PBS with trypan blue. The cells were visualised and imaged using a microscope, as shown in **Figure 4. 3 A**. 72 hours post-selection, cells were counted, and puromycin dose-response curves were

generated. The results showed that U937 and HL-60 cells overexpressing the puromycin-resistance cassette (and thus, *PTGS1* or *PTGS2*) have become resistant to puromycin compared to control cells (**Figure 4. 3B**). These resistant cells were plated in fresh RPMI Medium for expansion, and further downstream experiments.

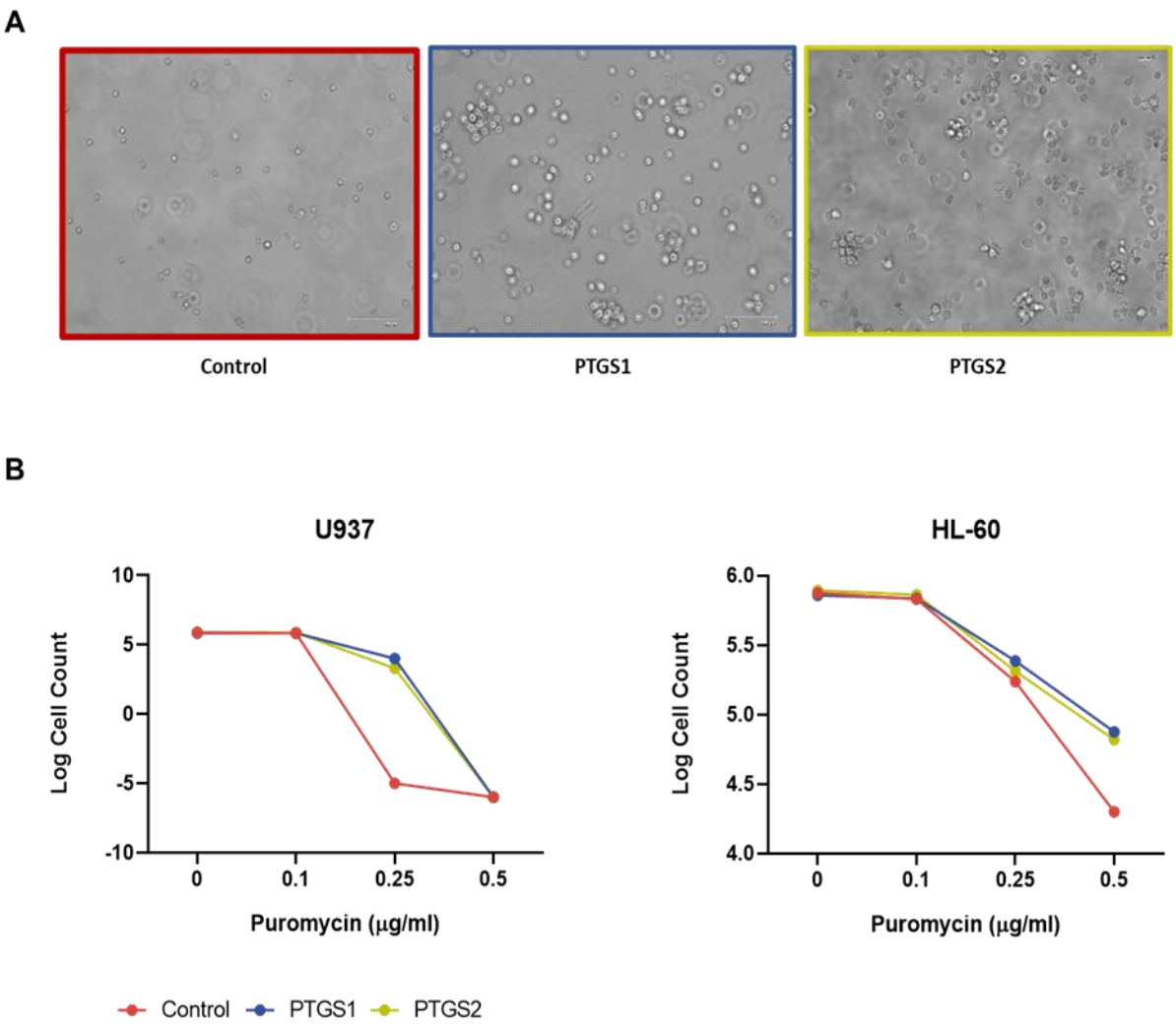

Figure 4. 3 Puro-selection curves for U937 and HL-60 cell lines.

*U937 and Hl-60 cells were treated with varying concentrations of puromycin (0, 0.1, 0.25 and 0.5 µg/ml). (**A**) U937 cells were imaged under a microscope 72 hours post-treatment with 0.25µg/ml. (**B**) The cells were counted after 72h using a haemocytometer after being diluted 1:1 in PBS with trypan blue. Puromycin was removed when there was approximately 80% death in the control cells. GraphPad Prism 8 software was used to generate puro-selection curves.*

To validate the over-expression of *PTGS1* and *PTGS2* in AML cell lines, mRNA levels were measured using qPCR. A significant increase in the mRNA expression levels of *PTGS1* was observed in both U937 and HL-60 cell lines upon transfection with Lenti-PTGS1 compared to control cells. Similarly, the mRNA levels expression of *PTGS2* was significantly higher in both cells following transducing with Lenti-PTGS2 and puro-selection compared to control cells (**Figure 4. 4**) These results confirm that the plasmid-based transfection and puro-selection methods were effective in inducing over-expression of *PTGS1* and *PTGS2* in AML cell lines.

To further validate our results, whole cell lysates were gained from untreated cells expressing *PTGS1* or *PTGS2*, as well as control U937 and HL-60 cells. The use of the Western blotting technique has revealed a conspicuous band of PTGS1 and PTGS2 protein at the expected molecular weight in the transduced cells, whereas such protein was barely detectable or detectable in the control (wild-type) cells (**Figure 4. 5A**). Upon conducting densitometry, it was found that the protein levels of PTGS1 and PTGS2 were markedly elevated in both U937 and HL-60 cells that were transduced with *PTGS1* or *PTGS2* vector compared to the U937 and HL-60 wild-type (control cells). The fold change in PTGS1 and PTGS2 protein were found to be 8.7 and 22.1 times, respectively greater in U937 cell line (**Figure 4. 5B**). Similarly, the expression of PTGS1 and PTGS2 protein were 27.2X and 19.4 higher in HL-60 cell lines (**Figure 4. 5C**).

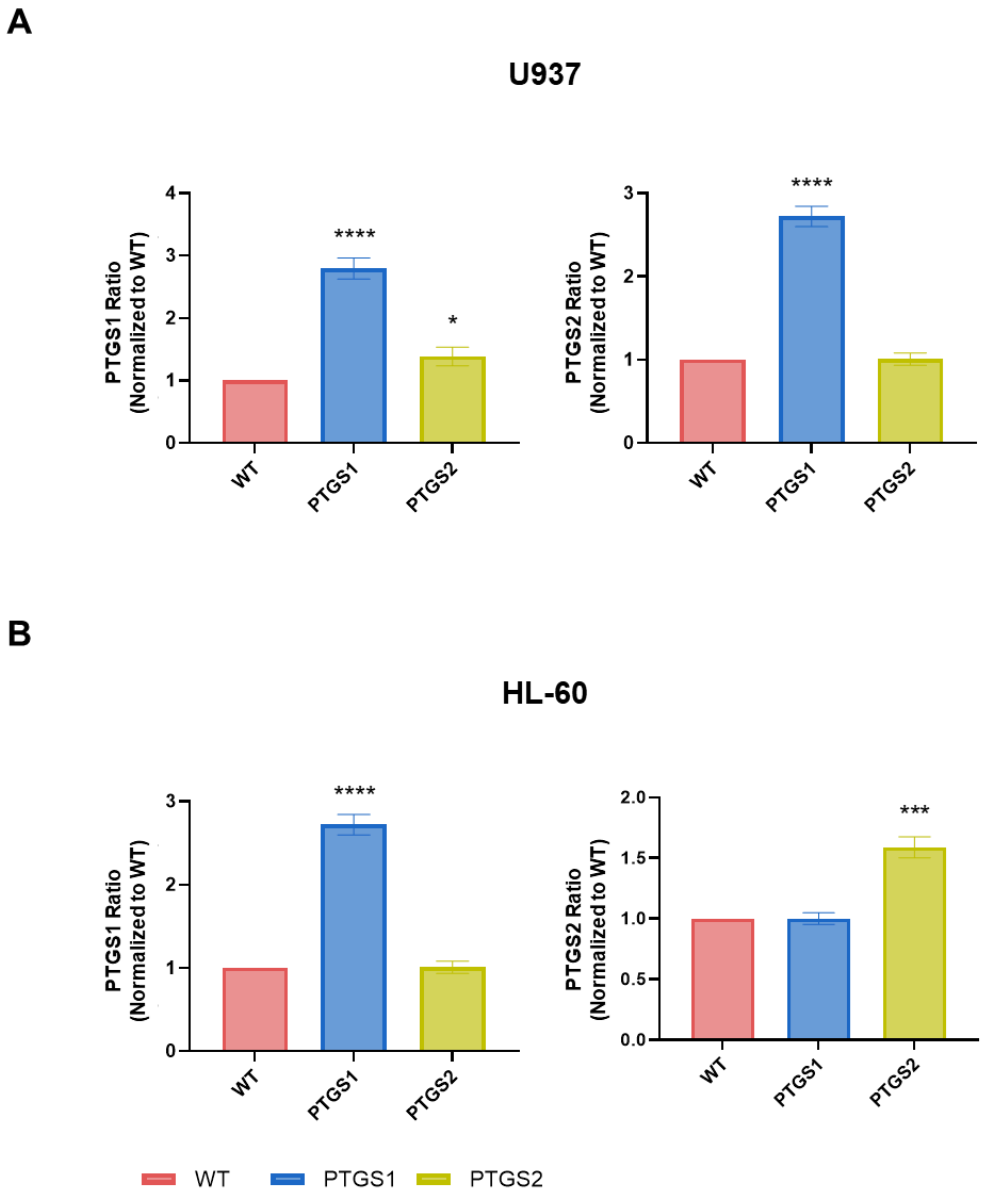

Figure 4. 4 The successful over-expression of PTGS1 and PTGS2 in U937 and HL-60 cell lines.

*Gene expression was evaluated through qPCR, with expression relative to U937 or HL-60 Wild-type cell lines. Normalisation was carried out using β-actin as housekeeping genes and the $^{\Delta\Delta}$Ct method. Subsequently, A and B refer to U937 or HL-60 cells. The statistical significance was assessed using one-way ANOVA coupled with Dunnett's multiple comparison test (n=3); ***P ≤0.001 and ****P ≤0.0001. The obtained results were indicative of the mean +/- SEM for three independent experiments. GraphPad Prism 8 software was used to generate and analyse the results presented*

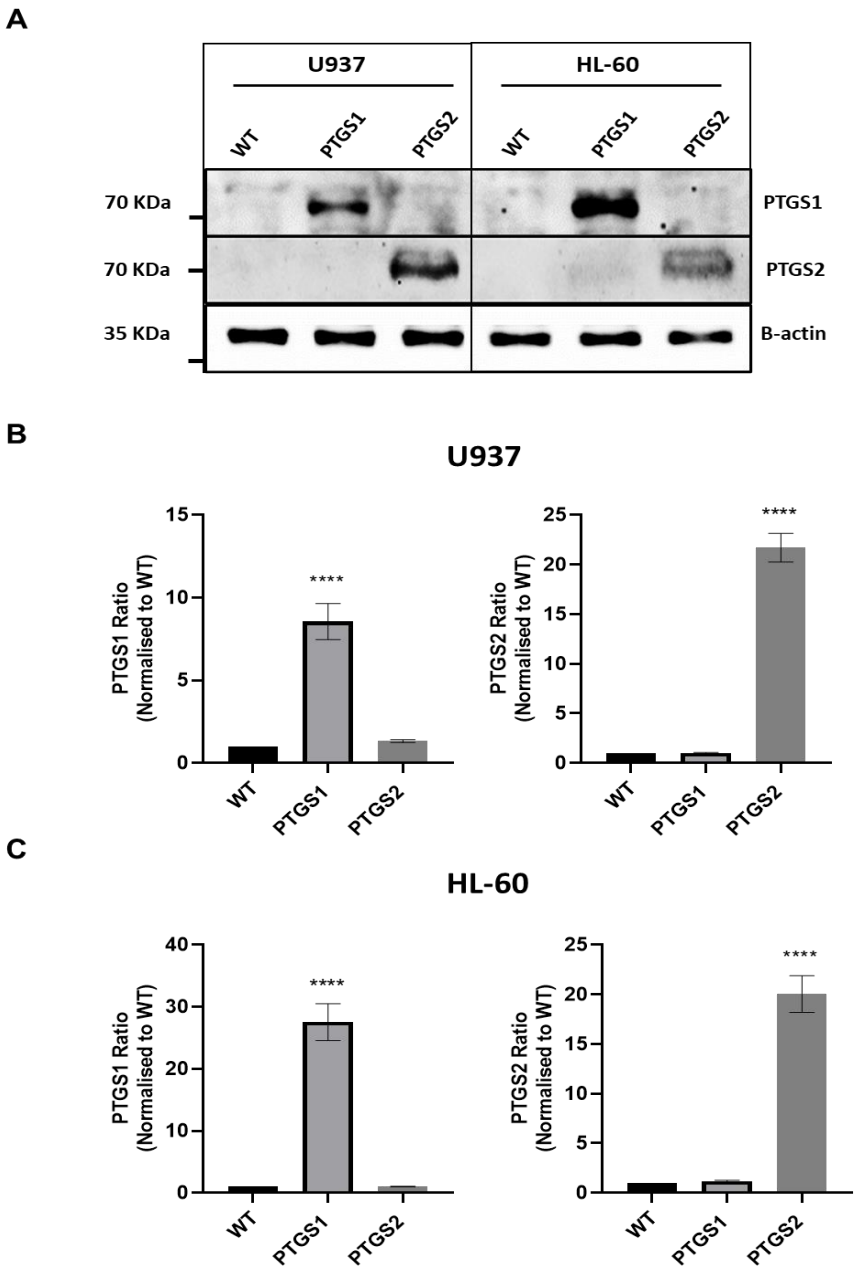

Figure 4. 5 PTGS1/2 over-expression in AML cell lines markedly increased PTGS1/2 protein.

(A) *Western blot analysis was performed on whole cell lysates from un-transduced or transduced cells (U937 and HL-60) with plasmid overexpress PTGS1/2. 30µg of protein was loaded per well and probed with either anti-PTGS1 or anti-PTGS2, with anti-β-actin used as a loading control.* ***(B)*** *The protein intensity was quantified using densitometry and normalised to β-actin, and each value was then calculated relative to the un-transduced cells. Significance testing was done by one-way ANOVA with Dunnett's multiple comparison test (n=3), ****P ≤0.0001. Results represent the mean +/- SEM for 3 independent experiments.*

4.3.4 The elevation of PGE2 production in AML cells overexpressing PGTS1 and -2

We next investigated the effect of *PTGS1* and *PTGS2* on the production of prostaglandin E2, as both isoforms of cyclooxygenase are known to increase PGE2 secretion. The assessment of the PGE2 levels in wild-type AML cell lines, including U937 and HL-60, and those overexpressing *PTGS1* and *PTGS2* in the current study demonstrated the higher level of PGE2 in U937 cells that overexpressing *PTGS1* and *PTGS2* compared with U937 wild-type group (p=0.0001 and 0.0006, respectively) (**Figure 4. 6A**). Similarly, in HL-60 cells, statistical analysis revealed a significant difference between the wild-type cells and *PTGS1* over-expression cells, with a p-value of less than 0.01. Notably, the PGE2 level was significantly increased in *PTGS2* over-expression compared to wild-type ($P \leq 0.001$) (**Figure 4. 6B**).

Next, to examine the specific role of *PTGS1* in PGE2 synthesis and secretion, the AML cells were treated with either SC-560 or Tenidap and untreated cells were used as control cells. The results revealed significant inhibition of PGE2 secretion in both wild-type cells and cells overexpressing *PTGS1* following treatment with either SC-560 or Tenidap. However, intriguingly, these treatments did not significantly impact PGE2 secretion in cells overexpressing *PTGS2*. This finding suggests that SC-560 and Tenidap effectively reduce PGE2 levels in AML cells, indicating the effectiveness of PTGS1 inhibitors (**Figure 4. 7**).

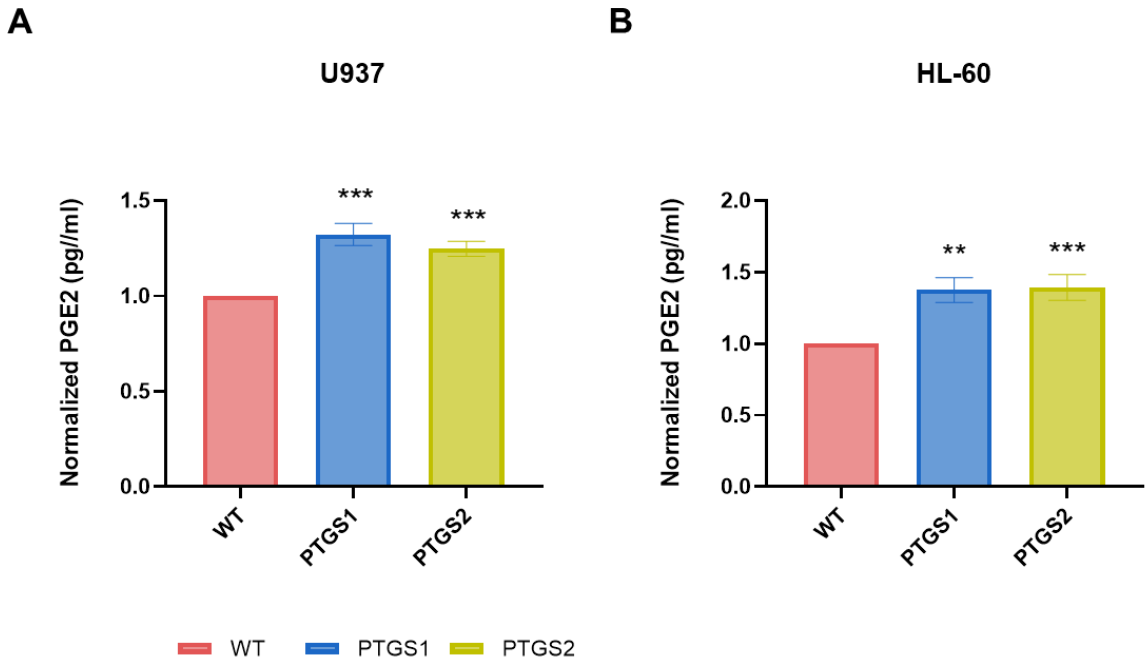

Figure 4. 6 Detection of PGE2 levels in AML cells and modelling PTGS1 and PTGS2 in AML cell-line models.

(A) *U937 and* ***(B)*** *HL-60 cells were plated and incubated for 96 hours prior to analysis using PGE2 ELISA kit. PGE2 levels in the cell supernatant were graphed as a bar chart, with the Y-axis representing the levels of the PGE2 normalised to wild-type group, and the X-axis indicating the different groups (wild-type, PTGS1 and PTGS2). The quantitative results were indicative of the mean +/- SEM for three technical replicates. one-way ANOVA using Dunnett's multiple comparison test was applied to evaluate the statistical significance (n=3, **P<0.01, ***P<0.001vs control group. GraphPad Prism 8 software was used to generate and analyse the results presented*

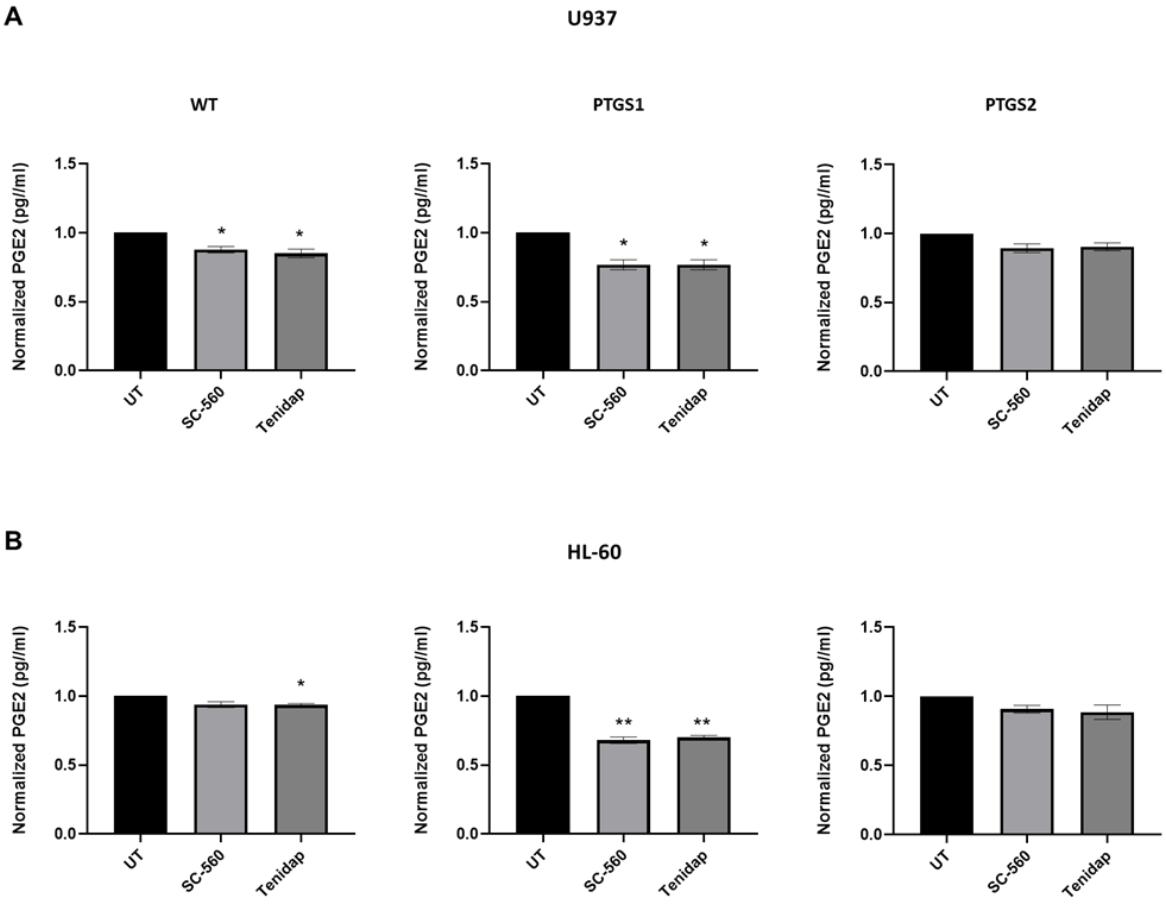

Figure 4. 7 Targeting PTGS1 efficiently modulated PGE2 production in AML cells.

(A) *U937 and* ***(B)*** *HL-60 cells were cultured and incubated with SC-560 or tenidap for 96 hours before analysis using a PGE2 ELISA kit to measure PGE2 levels in the cell supernatant. The obtained data was presented as a bar chart, where the Y-axis represented PGE2 levels normalized to the un-treated cells in each group, and the X-axis represented different groups (wild-type, PTGS1, and PTGS2). The results were presented as mean ± SEM from three technical replicates. Statistical analysis was performed using one-way ANOVA with Dunnett's multiple comparison test (n=3, **P<0.01, ***P<0.001 vs control group). This analysis allowed for the evaluation of statistical significance between the treated groups and the control group. GraphPad Prism 8 software was used to generate and analyse the results presented*

4.3.5 Exploring variations in cell signalling pathways between U937 and HL-60

In order to understand the fundamental mechanisms of cellular functions, it is critical to identify the signalling pathways that are differentially activated between U937 and HL-60 cells that may influence PTGS1/2 signalling. Our results revealed significant differences in the protein levels between these cell lines. Notably, we detected decreased protein levels of **phospho-NPM**, **total-NPM** and significantly **MYC** in U937 cells compared to HL-60 cells. The densitometric levels of these protein band intensities were significantly higher in HL-60 cells (****P≤0.0001), while the protein band intensity of **phosph-GSK3β** and **phospho-STAT-5** was significantly higher in U937 cells relative to HL-60 cells (P=0.023, ****P≤0.0001, respectively) (**Figure 4. 8**).

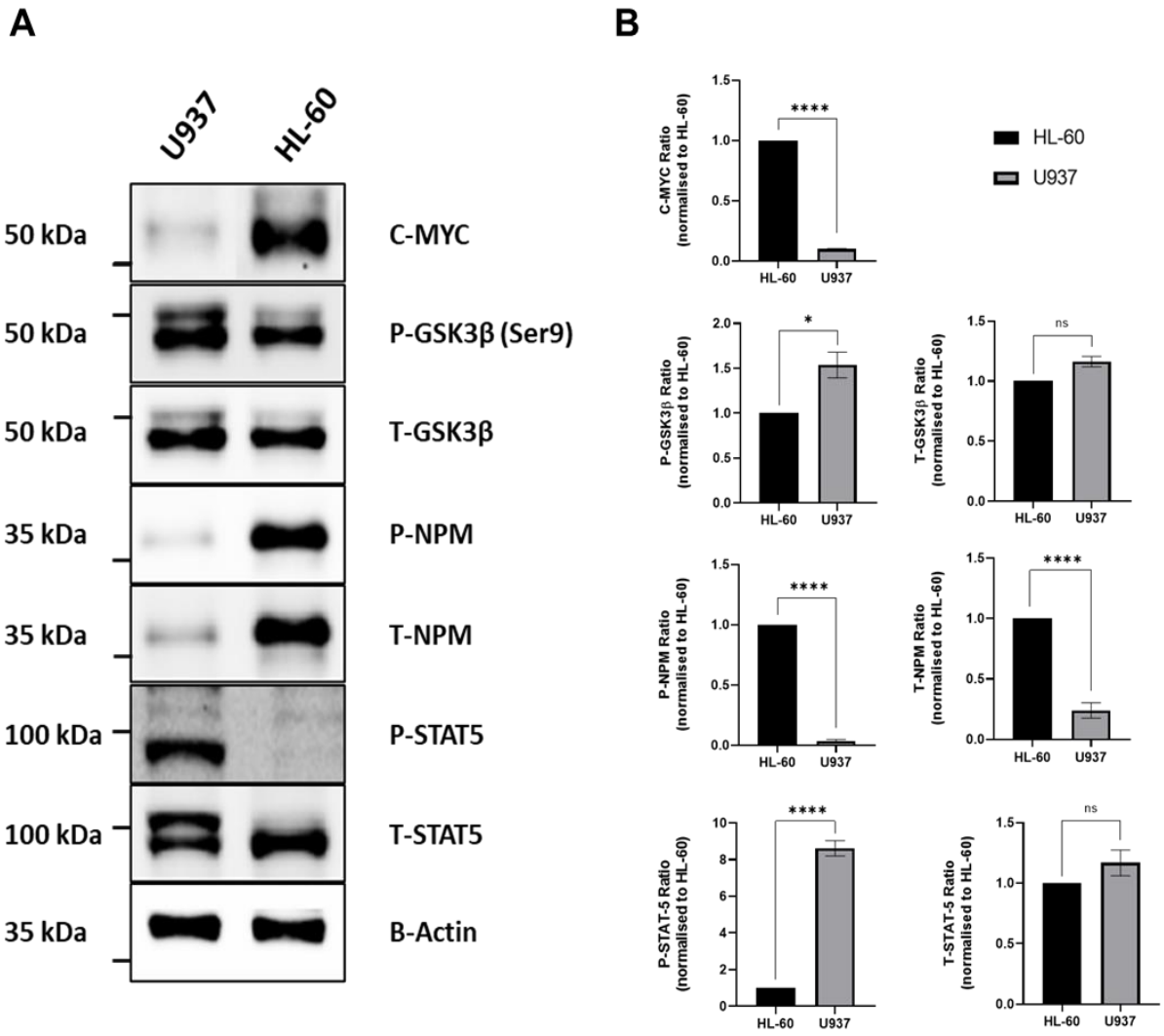

Figure 4. 8 Comparative analysis of cell signalling pathways in AML cells.

(A) *Total proteins were extracted from U937 and HL-60 cells and separated using 10% SDS-PAGE. Then, the immunoblot analysis was done using antibodies specific to phospho-GSK3β, phospho-NPM, phospho-STAT-5 and C-MYC, as well as their unphosphorylated forms. To ensure consistent loading of protein, β-actin was contained as a loading control.* ***(B)*** *The densitometric levels of total protein band intensity were normalized with β-actin protein levels, and each value was then calculated relative to the HL-60 cells. A two-tailed unpaired t-test was conducted to determine statistical significance, and significance was set at *P≤0.05, and ****P≤0.0001. The results represent the mean +/- SEM for three independent experiments. GraphPad Prism 8 software was used to generate and analyse the results presented*

4.3.6 The influence of *PTGS1* or *PTGS2* over-expression on cytarabine efficacy

We next aimed to assess the effect of *PTGS1* and *PTGS2* over-expression on the response of cells to the AML standard-of-care chemotherapeutic agent cytarabine (cytosine arabinoside; ara-C). U937 and HL-60 wild-type cells, as well as U937 and HL-60, which overexpress either *PTGS1* or *PTGS2*, were subjected in vitro to increasing concentrations of ara-C (0.01-10 µM) for 72 hours, and cell viability was evaluated using Trypan blue.

Dose-response curves over 96h demonstrated that HL-60 cell line is less sensitive to ara-C (EC_{50} 0.053 µM, **Figure 4. 9B**) compared to U937 cells (EC_{50} 0.0425 µM, **Figure 4. 9A**). In U937 cells, the wild-type cells exhibited the lowest EC_{50} value of 0.042, suggesting the highest sensitivity to the cytarabine. This indicates that these cells require a lower concentration of cytarabine to achieve a significant response compared to the *PTGS1* and *PTGS2* groups. In contrast, the cells characterized by *PTGS1* over-expression displayed a higher EC_{50} value of 0.092, which revealed a decreased sensitivity to the cytarabine compared to the control cells. Remarkably, the *PTGS2* cells demonstrated an intermediate EC_{50} value of 0.049, implying a moderate sensitivity between the control and *PTGS1* cells (**Figure 4. 9A**).

Additionally, HL-60 wild-type cells showed the lowest EC_{50} value of 0.053, representing the highest sensitivity to cytarabine. On the other hand, the *PTGS1* cells had a slightly higher EC_{50} value of 0.079, indicating reduced sensitivity compared to the wild-type cells. Similarly, the *PTGS2* cells displayed

an EC_{50} value of 0.061, demonstrating intermediate sensitivity between the wild-type and *PTGS1* cells (**Figure 4. 9B**).

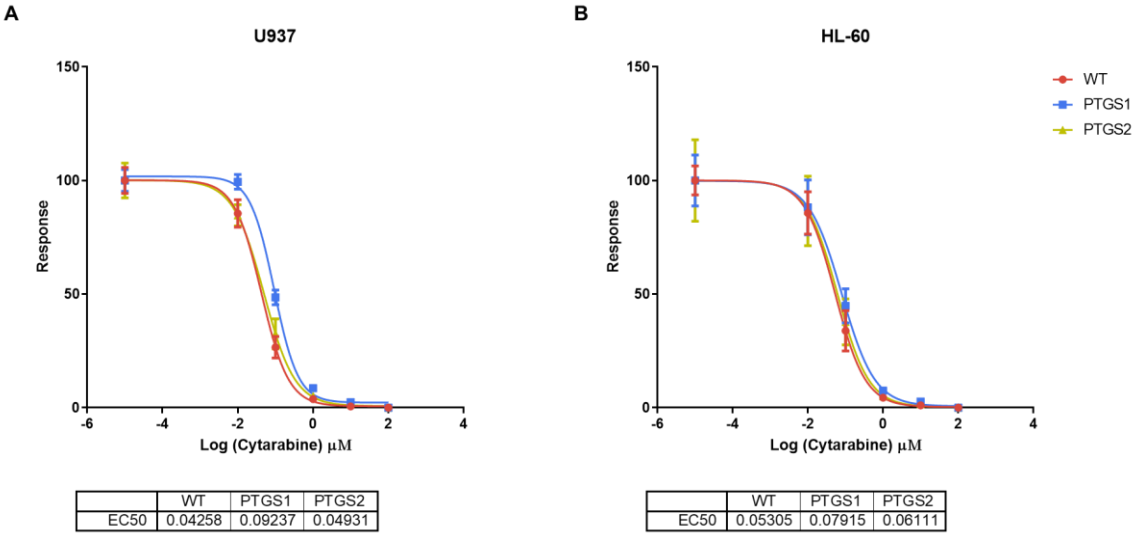

	WT	PTGS1	PTGS2
EC50	0.04258	0.09237	0.04931

	WT	PTGS1	PTGS2
EC50	0.05305	0.07915	0.06111

Figure 4. 9 Wild-type cells were more sensitive to cytarabine than PTGS1.

(A) *U937 and* ***(B)*** *HL-60 cells were treated with various concentrations of ara-C. Viability estimation was performed at 72 hours post-treatment by mixing trypan blue with a cell suspension and then counting the cells under a microscope. The graphs show the number of cells measured in each sample concentration as a % of that measured in the vehicle control sample. The dose-response curves were fitted by nonlinear regression using the GraphPad Prism 8 program (n = 3).*

Next, U937 and HL-60 were exposed to different cytarabine concentrations (0.1, 0.2, and 0.3) for 96 hours. After the treatment period, we evaluated the level of apoptosis using flow cytometry (**Figure 4. 10A**). Specifically, we compared the apoptosis levels between the wild-type cells and those overexpressing either *PTGS1* or *PTGS2*. Interestingly, our results demonstrated that the wild-type U937 cells exhibited the highest level of apoptosis compared to cells with *PTGS1* or *PTGS2* over-expression. At the lower concentrations of 0.1 and 0.2μM, significant differences emerged between U937 wild-type and both *PTGS1* and *PTGS2* ($p<0.001$). Wild-type cells demonstrated higher responses compared to *PTGS1* and *PTGS2*. Interestingly, at the highest concentration of 0.03μM, *PTGS2* over-expression did not demonstrate a significant difference compared to wild-type cells ($P=0.1218$), while *PTGS1* over-expression still exhibited significantly lower responses ($P<0.001$) (**Figure 4. 10B**). This suggests that *PTGS2* over-expression may confer some level of protection against the higher concentration of cytarabine.

Likewise, no significant differences were observed in the untreated HL-60 cells comparison analysis between wild-type and *PTGS1* ($p=0.7426$) or *PTGS2* ($p=0.9651$). However, at the 0.1μM concentration, a significant difference was found between wild-type and *PTGS1* ($p=0.006$), indicating a notable variation in response to cytarabine. In contrast, no significant difference was detected between wild-type and *PTGS2* ($p=0.0754$). Moving on to the 0. 2μM concentration, a highly significant difference was found between wild-type and *PTGS1* ($p<0.0001$). Additionally, a significant difference was observed between wild-type and *PTGS2* ($p=0.0067$), although the effect size was smaller than

PTGS1. At the 0.3μM concentration, a significant difference was perceived between wild-type and *PTGS1* cells (p=0.0008), indicating a considerable variation in response. However, no significant difference was detected between wild-type and *PTGS2* (p=0.9372) (**Figure 4. 10B**).

We also treated those cells with cytarabine (0.3μM) at varying time points. We then conducted a comparison analysis between U937 wild-type and either *PTGS1* or *PTGS2* overexpressed cells. No significant changes were observed when comparing wild-type (wild-type) and either *PTGS1* or *PTGS2* under the untreated condition (p=0.7717 or 0.8956, respectively). Similarly, no changes were seen between wild-type and *PTGS1* or *PTGS2* 48 hours post-treatment (p= 0.8016, 0.8331, and 0.8036, respectively). Nevertheless, a considerable difference was found between wild-type and *PTGS1* (p=0.0002) and also between wild-type and *PTGS2* (p=0.0013) at the 72-hour time point. Notably, the most substantial differences were observed at the 96-hour time interval, where both wild-type vs *PTGS1* and wild-type vs *PTGS2* exhibited highly significant differences (p≤0.0001) (**Figure 4. 10C**). These results suggest that *PTGS1* and *PTGS2* exert a protective mechanism against the cytotoxicity induced by cytarabine in cells.

Also, during our investigation, HL-60 cells were subjected to treatment with cytarabine (0.3μM) for various time points. No significant differences were observed between the control cells (untreated cells) for wild-type and PTGS1 or *PTGS2* regarding their response to cytarabine (p=0.34 and 0.91, respectively). 48 post-treatment, the comparison between wild-type and *PTGS1* or *PTGS2* remained non-significant (*PTGS1*: p=0.9147, PTGS2: p=0.6025). However, at 72 and 96 hours, intriguing findings emerged. At these time points,

wild-type cells exhibited a significantly distinct response compared to *PTGS1* and *PTGS2*. The comparison between wild-type and *PTGS1* yielded a highly significant p-value of p=0.0033 at 72 hours and p=0.0017 at 96 hours. Similarly, wild-type cells exhibited a statistically significant response difference compared to *PTGS2* as p-value p=0.0461 at 72 hours and p=0.0425 at 96 hours (**Figure 4. 10C**). These findings suggest that both *PTGS1* and *PTGS2* play a role in the cellular response to cytarabine, but the impact of that *PTGS1*, and to a lesser extent, *PTGS2* protects AML from cytarabine treatment.

To provide insights into the activation or inhibition of key signalling pathways involved in apoptosis, we measured apoptosis protein levels by examining specific proteins such as Bcl-2 family members or markers of DNA fragmentation (**Figure 4. 11**). We aimed to determine their potential involvement in the regulation of apoptosis in AML wild-type cells or *PTGS1/2* over-expression models. U937 and HL-60 cells were treated with 0.3μM for 24 or 48 hours, followed by immunoblotting with indicated antibodies. The western blot analysis revealed that cells cytarabine caused a significant increase in PARP cleavage (a common marker for apoptosis induction) after 48 hours in U937 wild-type cells, while in both *PTGS1* and *PTGS2* over-expression models, the level of change was greatly reduced compared to wild-type cells. In contrast, there was a significant increase in PARP cleavage 48 hours post-treatment in either HL-60 wild-type cells or both over-expression models, but the level of change was the smallest in *PTGS1* over-expression cells. Also, we observed that Bim protein level was very low in untreated cells. Although Bim protein level was significantly increased 48h post cytarabine treatment in all cell lines, it was much lower in *PTGS1* over-expression models compared to control cells in both

cell lines. Interestingly, in HL60 cells, the over-expression of *PTGS1*, and to a lesser extent *PTGS2*, resulted in a dramatic increase in basal BCL-XL protein levels compared to controls.

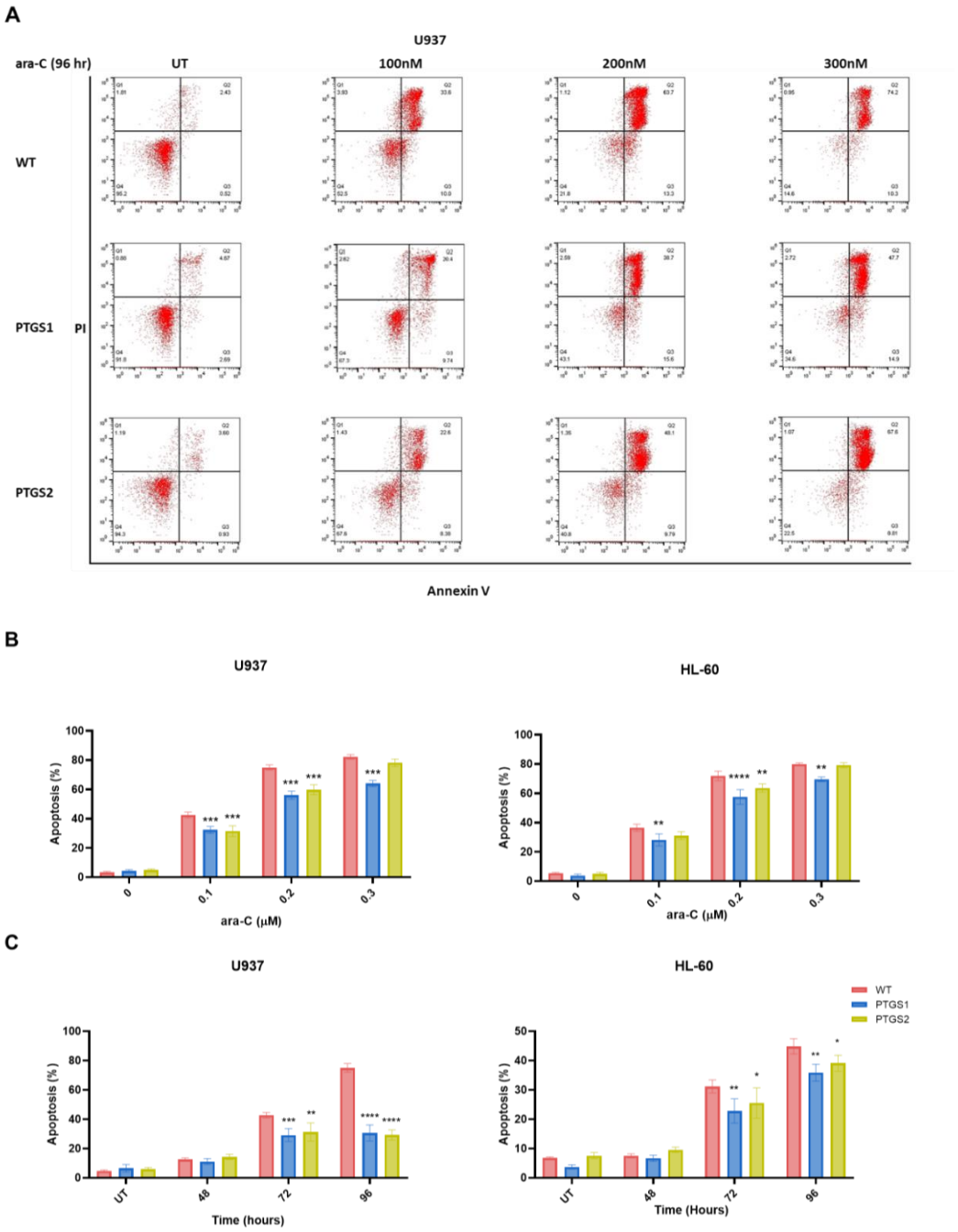

Figure 4. 10 Differential effects of PTGS1 and PTGS2 on cellular response to cytarabine in AML cells

(A) *Flow cytometry was utilised to assess apoptosis using Annexin V/PI staining.* ***(B)*** *U937 and HL-60 cells were incubated for indicated times with increasing concentrations of cytarabine.* ***(C)*** *Also, U937 and HL-60 cells were incubated for various time points (0, 48, 72 and 96h) with 0.3μM cytarabine. Following which apoptosis was measured using Annexin V/PI staining. Significance testing was done by one-way ANOVA using Dunnett's multiple comparison test (n=3), *P ≤ 0.05, **P ≤ 0.01 ***p ≤ 0.001 and 01 ****p ≤ 0.0001. Results represent the mean +/- SEM for 3*

independent experiments. GraphPad Prism 8 software was used to generate and analyse the results presented

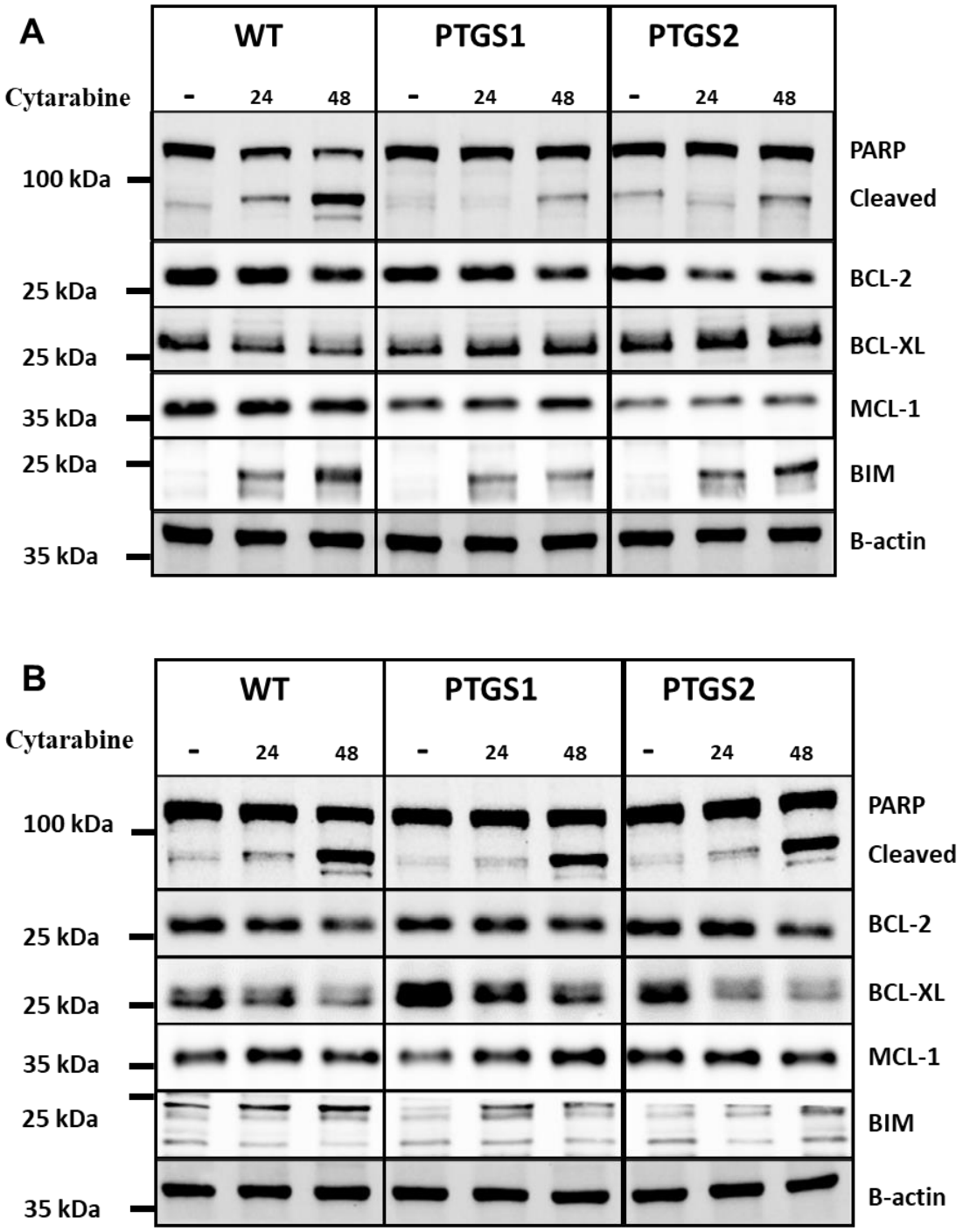

Figure 4. 11 Apoptosis signalling pathways in AML wild-type cells or PTGS1/2 over-expression models

(A) *U937 and* ***(B)*** *HL-60 were treated with 0.3μM for 24 or 48 h. 10% SDS-PAGE was used to separate 30μg of cellular total proteins, blotted onto nitrocellulose membrane*

followed by immunoblotting with indicated antibodies. β-actin was used as a loading control. ChemiDoc imaging system was used to detect the proteins band.

4.3.7 Synergistic effects of *PTGS1* Inhibitors and cytarabine on apoptosis induction

We next aimed to investigate the effects of combining *PTGS1* inhibitors (SC-560 or Tenidap) and the chemotherapeutic agent cytarabine on apoptosis induction. The U937 and HL-60 were used, and the wild-type cells were compared to cells overexpressing either the *PTGS1* or *PTGS2* genes. In untreated conditions, no significant differences were noted between wild-type and *PTGS1* or *PTGS2* regarding their apoptotic response (p=0.9417 and 0.7174). However, upon treatment with cytarabine (0.3μM) alone, the comparison between wild-type and *PTGS1* showed a substantial increase in apoptosis (p ≤0.0001). Similarly, Wild-type cells exhibited a significant increase in apoptosis compared to *PTGS2*, albeit to a lesser extent (p=0.0311). When cells were treated with 0.3μM cytarabine, the mean percentage of U937 wild-type apoptotic cells was determined to be 84%, while *PTGS1* overexpressed cells had a lower mean value of 47%. *PTGS2* overexpressed cells exhibited an intermediate proportion value of 67% in terms of apoptotic cell population. These results indicate that *PTGS1* over-expression may lead to a reduced cellular response to cytarabine compared to U937 wild-type and *PTGS2* overexpressed cells (**Figure 4. 12A**).

Furthermore, when wild-type cells were co-treated with both SC-560 (1μM) and cytarabine (0.3μM), a synergistic effect in the induction of apoptosis was observed. In wild-type cells, the apoptotic rates showed an increase of 6%, suggesting a heightened cellular response compared to the cytarabine treatment alone. *PTGS1* overexpressed cells also exhibited a notable elevation of 23% apoptosis, indicating an improvement in the cellular response upon co-

treatment. Similarly, in the co-treatment condition of Tenidap (1μM) and cytarabine (0.3μM), U937 wild-type cells displayed a further increase in the cell death rates to 90.5%, indicating a continued enhancement of the cellular response. *PTGS1* overexpressed cells exhibited a mean value of 73%, suggesting a significant improvement in the cellular response compared to the cytarabine treatment alone (**Figure 4. 12A**). These findings suggest that *PTGS1* inhibition can contribute to increasing the cytarabine efficacy when SC-560 or Tenidap is combined with cytarabine.

In contrast to U937 cells, HL-60 cells demonstrated higher resistance to cytarabine treatment. Firstly, when treated with 0.3μM of cytarabine, HL-60 wild-type cells exhibited a mean apoptotic percentage of 78.4%. In comparison, *PTGS1* overexpressed cells showed a slightly lower mean apoptotic percentage of 64.2%, suggesting a potential inhibitory effect of *PTGS1* over-expression on cytarabine-induced apoptosis. Conversely, *PTGS2* overexpressed cells showed a mean apoptotic percentage of 75.4%, which is more comparable to wild-type cells. Furthermore, the combined treatment of SC-560 (1μM) with cytarabine (0.3μM) resulted in a mean apoptotic percentage of 79% in HL-60 wild-type cells. Notably, *PTGS1* overexpressed cells exhibited a higher mean apoptotic percentage of 77 % under the same treatment condition, suggesting an enhanced apoptotic response. *PTGS2* overexpressed cells displayed comparable mean apoptotic rats of 78% when treated with the combination of SC-560 and cytarabine (**Figure 4. 12B**).

Similarly, in the case of the combination of 1μM Tenidap with 0.3μM cytarabine, HL-60 wild-type cells exhibited a slightly lower mean apoptotic percentage of 76% compared to cytarabine treatment alone. Interestingly, *PTGS1*

overexpressed cells showed a comparable mean apoptotic percentage of 72.5% to HL-60 wild-type cells (**Figure 4. 12B**). Together, these findings suggest that the combination of the *PTGS1* inhibitors (SC-560 or Tenidap) with cytarabine synergistically enhances apoptosis induction in AML cells, highlighting the potential therapeutic benefits of targeting the *PTGS1* pathway in combination with chemotherapeutic agents.

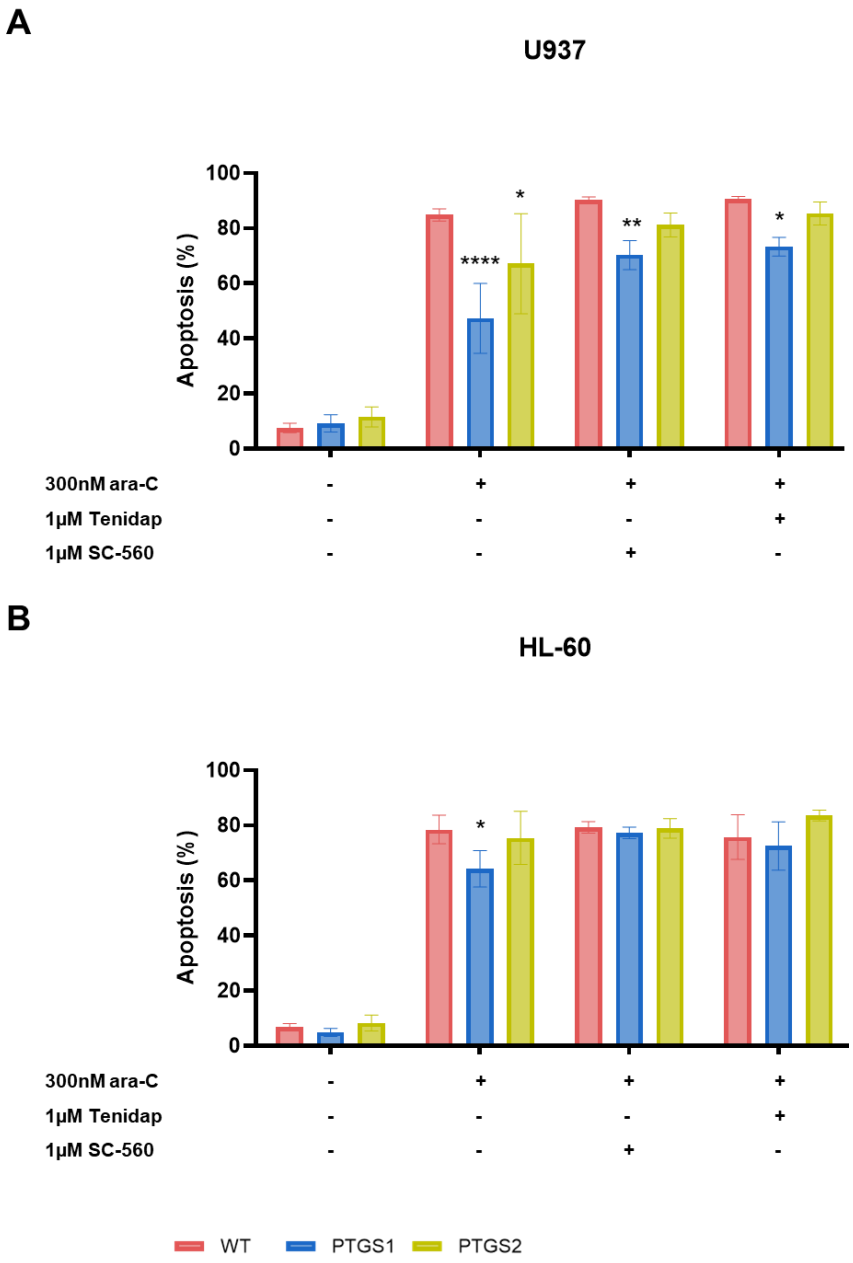

Figure 4. 12 Improving cytarabine efficacy through PTGS1 modulation.

(A) *U937 and* ***(B)*** *HL-60 cells were incubated for indicated times (72h) with three treatment conditions: 0.3μM ara-C (cytarabine), 1μM SC-560 + 0.3μM ara-C, and 1μM Tenidap + 0.3μM ara-C. Following which apoptosis was measured using Annexin V/PI staining. Significance testing was done by one-way ANOVA using Dunnett's multiple comparison test (n=3), *P ≤ 0.05, **P ≤ 0.01 ***p ≤ 0.001 and 01 ****p ≤ 0.0001. Results represent the mean +/- SEM for 3 independent experiments. GraphPad Prism 8 software was used to generate and analyse the results presented*

4.3.8 Modulation of ROS production in AML cells by *PTGS1* and *PTGS2*

Prostaglandins and reactive oxygen species (ROS) signalling in cancer cells are known to be linked. To provide insight into oxidative stress induced by cytarabine treatment and the role *PTGS1*/*2* may play in this signalling, we measured ROS levels using the CellROX Green dye. The CellROX Green dye is a fluorogenic probe that detects and quantifies cellular ROS levels.

In both U937 and HL-60 cells in un-treated condition, we observed that there was no statistically significant difference in terms of ROS levels between the wild-type and *PTGS1* (U937: p=0.6303 and HL-60: p=0.9806. **Figure 4. 13B**). Similarly, the comparison between wild-type and *PTGS2* resulted in a p-value of 0.8853 (U937) and 0.09387 (HL-60), suggesting no significant difference in ROS levels between these groups. Thus, under untreated conditions, *PTGS1* and *PTGS2* did not exhibit notable variations in terms of cellular ROS levels compared to the wild-type.

However, we observed a distinct pattern when examining the cytarabine treatment condition. Comparing wild-type and *PTGS1*, we observed a substantial reduction in ROS levels in *PTGS1-overexpressing* cells after cytarabine exposure ($p<0.0001$). This suggests that the over-expression of *PTGS1* protects against oxidative stress in AML cells by reducing reactive oxygen species compared to the wild type. Furthermore, the comparison between wild-type and *PTGS2* in the cytarabine treatment condition resulted in a p-value of 0.0309 and 0.0045, respectively, indicating a significant difference in ROS levels between these groups. This suggests that cytarabine treatment

also influenced the cellular ROS levels associated with *PTGS2*, albeit to a lesser extent than *PTGS1*.

Additionally, the analysis showed similar trends in the cells treated with cytarabine combined with SC-560. The comparison between wild-type and *PTGS1* showed a significant difference in U937 cells and HL-60 cells ($p < 0.0001$ and $p=0.0016$, respectively. **Figure 4. 13B**). This suggests that the combined treatment with cytarabine and *PTGS1* inhibitor resulted in significant changes in the ROS levels between these groups. However, when directly comparing the cytarabine alone and the combined treatment conditions in U937 *PTGS1* over-expression cells, we also obtained a highly significant p-value of less than 0.0001. In HL60 cells, there was no statistically significant difference in ROS levels between *PTGS1* cells treated with cytarabine alone and *PTGS1* cells treated with the combination ($p= 0.9311$). This suggests a notable difference in ROS levels associated with *PTGS1* between these two treatment groups in U937 but not HL-60 cells and points to differential downstream signalling. The *PTGS1* inhibition resulted in a further modulation of cellular ROS levels.

On the other hand, the comparison between wild-type and *PTGS2* in the combined treatment condition showed a significant difference ($p=0.0033$). However, the comparison between the cytarabine alone and the combined treatment conditions resulted in no statistically significant difference in ROS levels associated with *PTGS2* between these two treatment groups ($p=0.2648$). These results indicate that the *PTGS1* inhibitor combined with cytarabine

treatment did not significantly affect the modulation of ROS levels specifically related to *PTGS2-overexpression*.

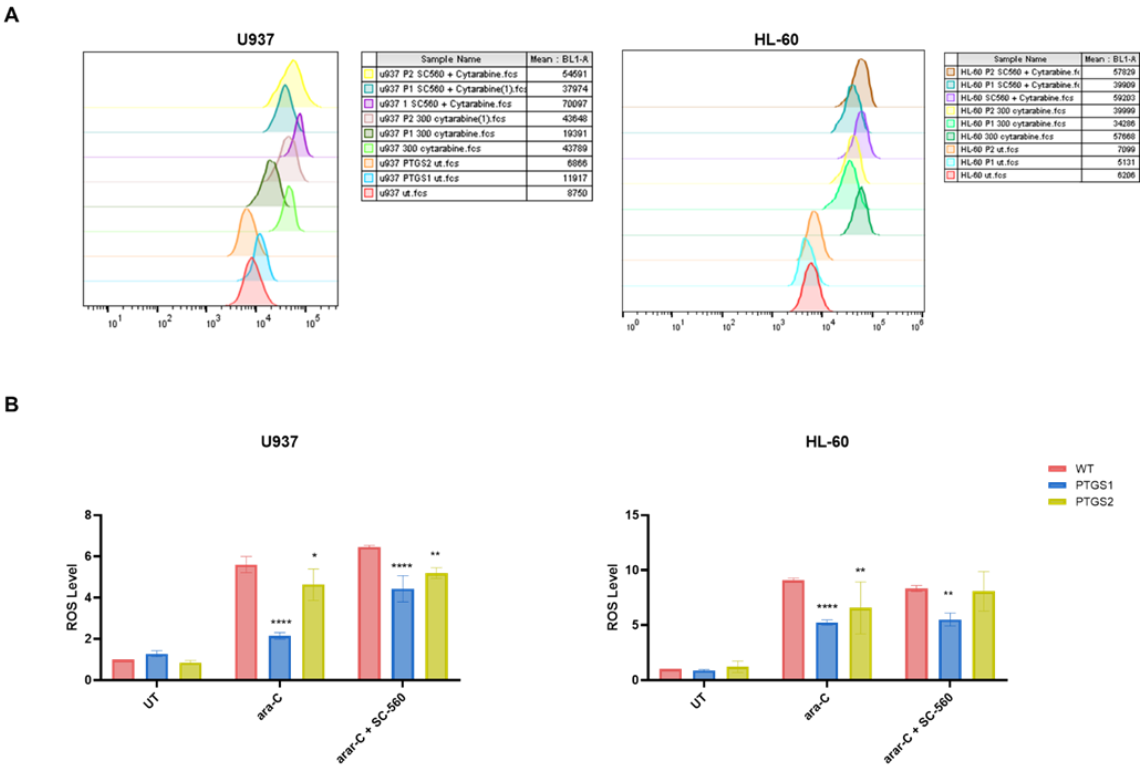

Figure 4. 13 Impact of the PTGS1 and PTGS2 on the cellular ROS levels

U937 and HL-60 cells were treated with a concentration of 0. 3µM cytarabine (ara-C) or/and 1µM SC-560, and incubated for 24 hours. Following the recommended treatment duration, the cells were stained with CellROX Green, a fluorescent probe specific for detecting ROS. The CellROX Green dye was added to the cell culture medium at a final concentration of 5µM and incubated for 30 minutes at 37°C. To quantify the cellular ROS levels, flow cytometry was employed. ***(A)*** *The stained cells were analysed using a flow cytometer, which allowed for the measurement of mean fluorescence intensity (MFI) emitted by the CellROX Green dye. The fluorescence intensity served as an indicator of the cellular ROS levels, providing quantitative information regarding the oxidative stress within the treated cells.* ***(B)*** *Significance testing was done by one-way ANOVA using Dunnett's multiple comparison test (n=3), *P ≤ 0.05, **P ≤ 0.01 ***p ≤ 0.001 and 01 ****p ≤ 0.0001. Results represent the mean +/- SEM for 3 independent experiments. GraphPad Prism 8 software was used to generate and analyse the results presented*

Next, we evaluated the mitochondrial superoxide in both cell lines in different experimental conditions utilising the fluorescent dye MitoSOX by flow cytometry (**Figure 4. 14A**).

In U937 cell lines, no significant difference was observed when comparing *PTGS1* to wild-type in untreated conditions (p=0.0799). Also, no significant difference was found when comparing *PTGS2* to wild-type in the untreated condition (p=0.1696). In U937 cells treated with cytarabine (0.3μM), both *PTGS1* and *PTGS2* showed a highly significant difference compared to the control group (wild-type). When comparing *PTGS1* to wild-type, the result was indicated by a p-value of less than 0.0001, indicating a difference in mitochondrial superoxide levels. Similarly, when comparing *PTGS2* to wild-type, the result was also indicated by a p-value of 0.0013, suggesting a significant alteration in mitochondrial superoxide levels in the presence of *PTGS2*. We also measured the effect of cytarabine combined with *PTGS1* inhibitor (SC-560) on the mitochondrial superoxide level of the AML cells. In the cytarabine combined with SC-560 condition, no significant difference was observed when comparing *PTGS1* to wild-type (p= 0.7689). However, when we compared the *PTGS1* cells treated with cytarabine combined with SC-560 to *PTGS1* cells treated with cytarabine alone, there was a significant increase in mitochondrial superoxide production (p=0.0133).

Additionally, when comparing *PTGS2* to wild-type, no significant difference was found, indicated by a (p= 0.6931) (**Figure 4. 14B**). Also, there was no significant in mitochondrial superoxide production when *PTGS2* cells treated with

cytarabine combined with SC-560 were compared to *PTGS2* cells treated with cytarabine alone (P=0.7547). These findings suggest that both enzymes, *PTGS1* and *PTGS2*, play a role in modifying mitochondrial superoxide production and may affect cellular responses and oxidative stress. Furthermore, the combination of cytarabine with SC-560 significantly increases mitochondrial superoxide production, suggesting a potential interaction between *PTGS1* inhibition and cytarabine-induced oxidative stress in U937 cells.

In HL-60 cells, no significant differences were observed when comparing wild-type to PTGS1 (p = 0.8337) or *PTGS2* (p = 0.9345) in untreated conditions. Similarly, no significant differences were found in the cytarabine treatment condition when comparing wild-type to *PTGS1* (p = 0.9702) or *PTGS2* (p = 0.8789). This indicates that the presence of *PTGS1* or *PTGS2* does not significantly affect mitochondrial superoxide levels in the presence of cytarabine treatment. Furthermore, when comparing the wild-type to *PTGS1*, the p-value was 0.2376, suggesting no significant difference in mitochondrial superoxide levels between these groups. On the other hand, when comparing the wild-type to *PTGS2*, the p-value was 0.0461, indicating a significant alteration in mitochondrial superoxide levels in the presence of *PTGS2* when cytarabine combined with SC-560. Nonetheless, there was no significant mitochondrial superoxide level when *PTGS2* cells treated with cytarabine combined with SC-560 were compared to *PTGS2* cells treated with cytarabine alone (p=0.9855) (**Figure 4. 14B**).

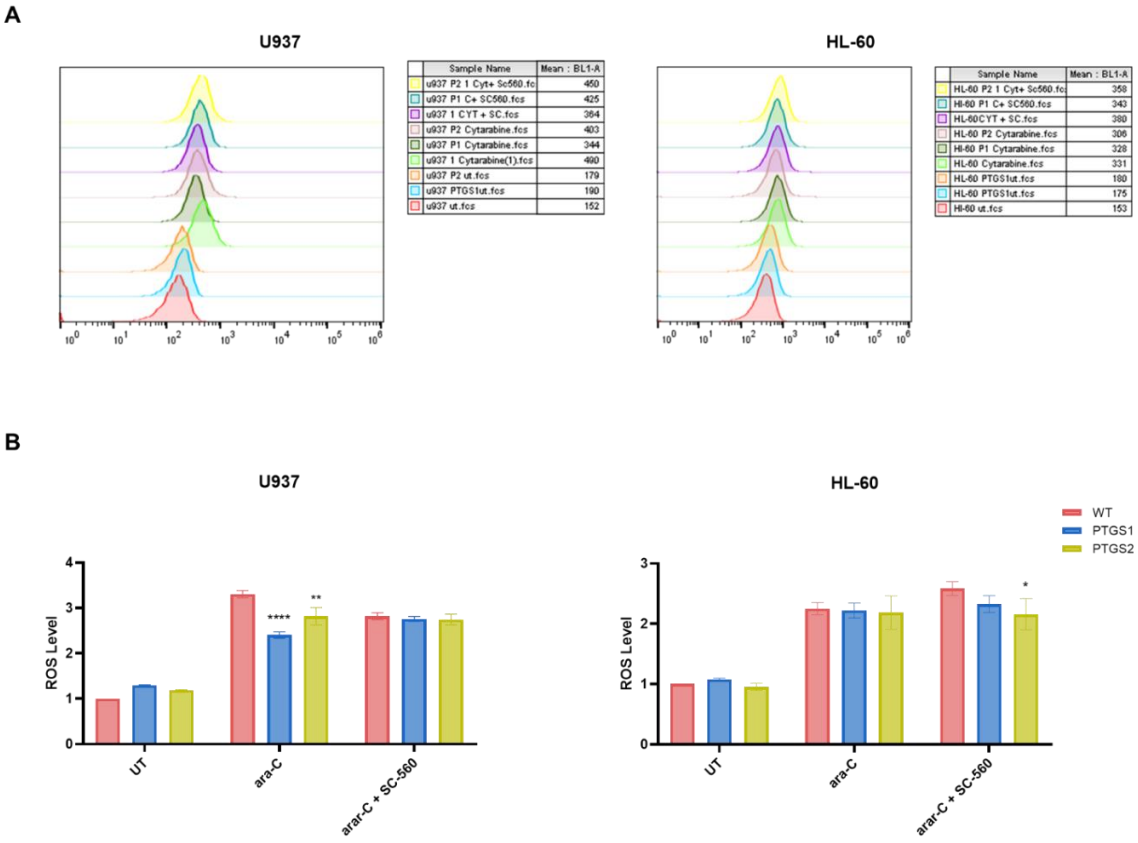

Figure 4. 14 Impact of PTGS1 and PTGS2 on mitochondrial superoxide levels.

U937 and HL-60 cells were cultured in a 6-well plate at a density of 5x10^5 cells per ml in 2 ml of RPMI medium. The cells were incubated overnight at 37°C in a 5% CO_2 environment to promote cell growth. Subsequently, the cells were treated with cytarabine (0.3 µM) or/and SC-560(1µM), and incubated for a duration of 24 hours. After the recommended treatment period, the cells were stained with the MitoSOX™ working solution at a final concentration of 5µM. The staining procedure involved incubating the cells in the dark for 10 minutes at 37°C. ***(A)*** *The cells were then subjected to flow cytometry analysis using appropriate machine settings. (B) Statistical analysis was performed using one-way analysis of variance (ANOVA) with Dunnett's multiple comparison test (n=3) to determine the significance of the observed results. Significance levels were designated as follows: *P ≤ 0.05, **P ≤ 0.01, ***P ≤ 0.001, and ****P ≤ 0.0001. The reported results represent the mean values with the standard error of the mean (SEM) calculated from three independent experiments. GraphPad Prism 8 software was used to generate and analyse the results presented*

4.3.9 The effect of *PTGS1/2* over-expression on signalling pathways in AML cells

To study the effect of either *PTGS1* or *2 over-expression* on signalling pathways, Western blot was used to detect the protein levels of MPO, MYC, AKT, ERK1/2, STAT5, CREB, GSK3β and β-catenin in U937 cells, and the results were shown **Figure 4. 15**. While a weak MPO band was detected in U937 control cells, the protein level of **MPO** was detected with strong band in both *PTGS1* and *PTGS2* overexpressed cells (**Figure 4. 15A**). The densitometry values obtained from the western blot bands were used to calculate the fold change in MPO protein levels. Compared to the control cells, the *PTGS1* cells exhibited a fold change of 21, indicating a significant increase in **MPO** protein levels ($p<0.0001$). Similarly, the *PTGS2* cells showed a fold change of 20, indicating a significant elevation in **MPO** protein levels compared to the control cells (**Figure 4. 15B**). Also, a very weak MYC band was seen in U937 control cells. At the same time, **MYC** had a strong band in both *PTGS1* and *PTGS2* overexpressed cells. Both *PTGS1* and *PTGS2* cells showed a fold change of approximately 5, indicating a substantial increase in **MYC** protein levels compared to the control cells ($P<0.0001$). Moreover, the **phospho-CREB** band was detected in both U937 control and *PTGS2* cells, whereas no band was in *PTGS1* overexpressed cells. The relative levels of **p-CREB** were significantly reduced in both *PTGS1* and *PTGS2* overexpressed cells compared to control cells ($p < 0.0001$).

The **phospho-AKT** band could also be seen in U937 control and *PTGS1* cells but not in *PTGS2* overexpressed cells. The control cells had a strong band,

while a weak band was seen in *PTGS1* overexpressed cells. The level of **p-AKT** was reduced significantly by 88% and 99% in *PTGS1* and *PTGS2* overexpressed cells, respectively ($p < 0.0001$). Additionally, in the control cells, the protein level of ERK1/2 was considered as a baseline, with a fold change of 1. However, in the *PTGS1* overexpressed cells, the relative protein level increased with a fold change of 1.8, indicating an upregulation of **ERK1/2** protein level. On the other hand, in the *PTGS2* overexpressed cells, the protein level exhibited a slight increase with a fold change of 1.1, suggesting a weaker effect on **ERK1/2** expression compared to the *PTGS1*.

Furthermore, the relative protein levels of **phospho-STAT5** and **phospho-GSK3β** were analysed in control cells and compared to cells overexpressing *PTGS1* and *PTGS2*. The results revealed that the protein levels of **Phospho-STAT5** and **phospho-GSK3β** were much lower in both *PTGS1* and *PTGS2* overexpressing cells compared to the control cells ($p < 0.0001$). The **Phospho-β catenin** protein levels were also investigated in control, *PTGS1*, and *PTGS2* cells. The results demonstrated that the protein levels of **Phospho-β catenin** were significantly higher in both *PTGS1* and *PTGS2* cells compared to the control cells ($p= 0.001$ and $p< 0.0001$, respectively). This suggests that the over-expression of *PTGS1* and *PTGS2* may have a stimulatory effect on activating the beta-catenin signalling pathway. Generally, *PTGS1/PTGS2* over-expression in AML cell models upregulates **MYC** and **MPO** while downregulating numerous signalling pathways such as **p-CREB**, **p-AKT**, **p-STAT5**, and **p-GSK3β**.

A

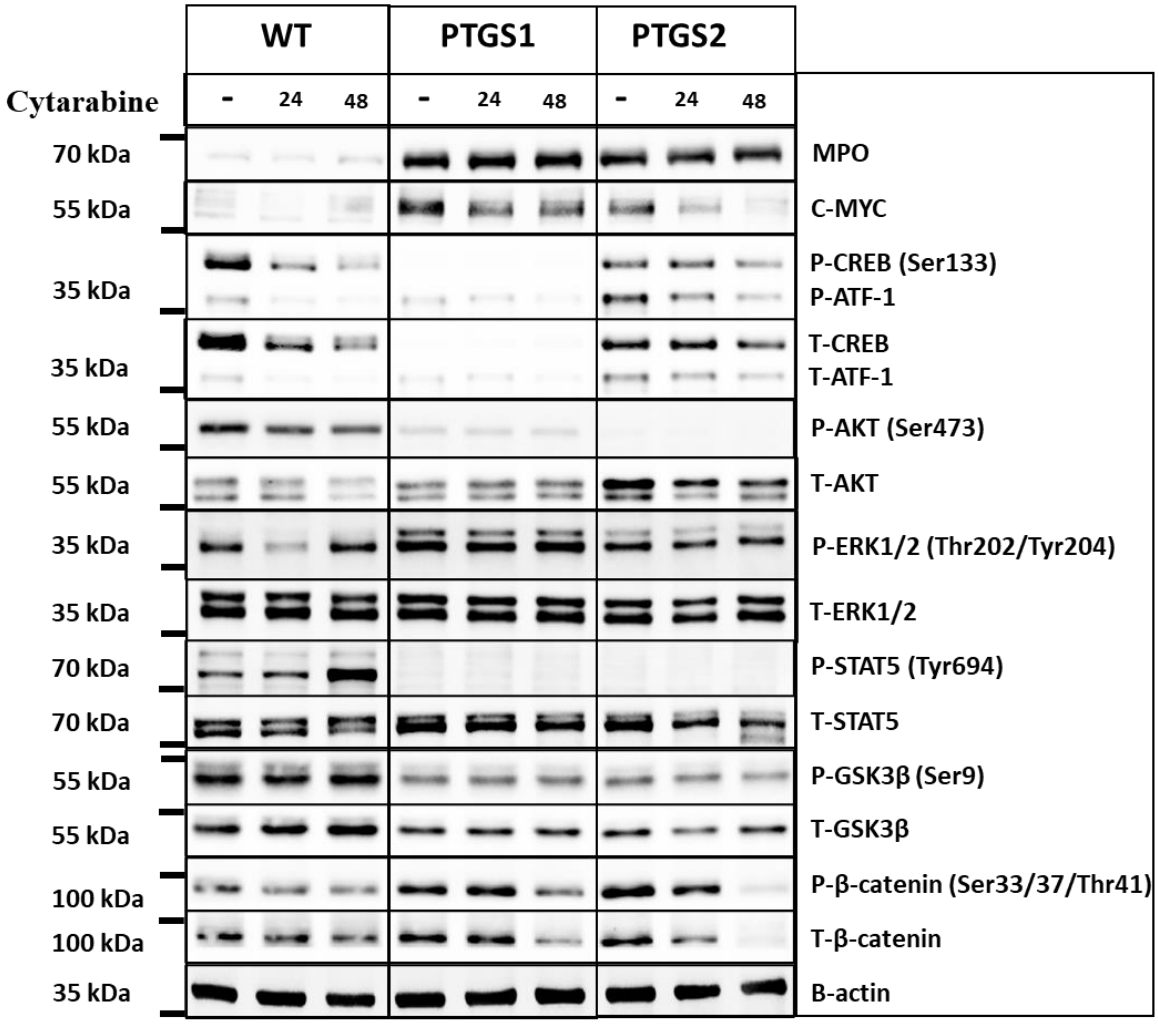
WT
PTGS1
PTGS2
Cytarabine
-
24
48
-
24
48
-
24
48
70 kDa
MPO
55 kDa
C-MYC
35 kDa
P-CREB (Ser133)
P-ATF-1
35 kDa
T-CREB
T-ATF-1
55 kDa
P-AKT (Ser473)
55 kDa
T-AKT
35 kDa
P-ERK1/2 (Thr202/Tyr204)
35 kDa
T-ERK1/2
70 kDa
P-STAT5 (Tyr694)
70 kDa
T-STAT5
55 kDa
P-GSK3β (Ser9)
55 kDa
T-GSK3β
100 kDa
P-β-catenin (Ser33/37/Thr41)
100 kDa
T-β-catenin
35 kDa
B-actin

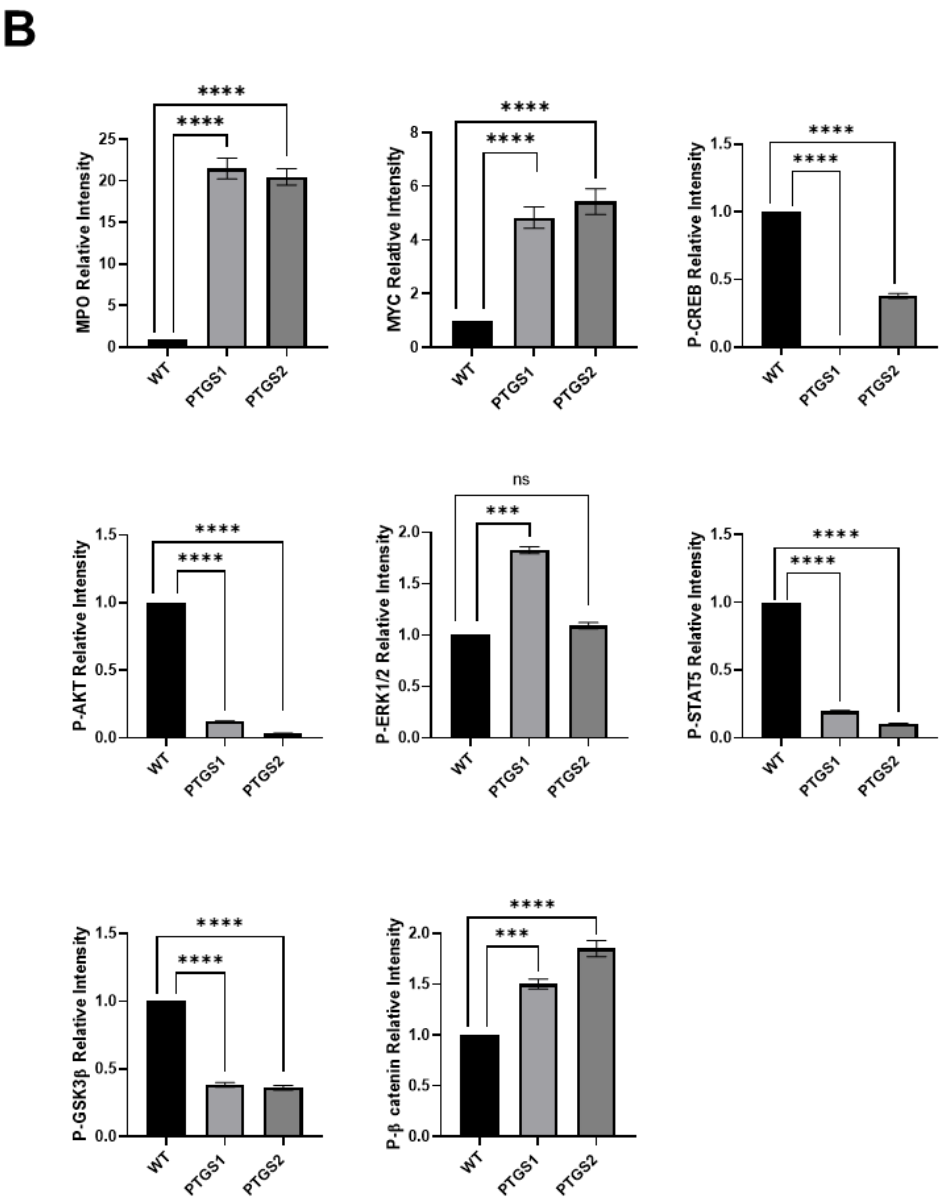

Figure 4. 15 PTGS1/2 promotes survival signalling in U937 AML over-expression models.

Protein expression of selected known signalling partners of PTGS1/2 in cells treated with cytarabine (0.3μM) for 24 and 48 hours. Cellular total proteins (30μg) were separated using 10% SDS-PAGE and transferred onto a nitrocellulose membrane. Immunoblotting was performed using specific antibodies as indicated for protein detection. To ensure equal loading of proteins, β-actin was used as a loading control. ***(A)*** *The proteins on the membrane were visualized using a ChemiDoc imaging system, allowing for the detection and analysis of protein bands.* ***(B)*** *The relative levels of proteins were determined by densitometric analysis of the band intensities on the blot using Image J software. MPO was included in this analysis due to its relevance to the*

*findings discussed in the subsequent chapter. The statistical analysis was conducted using one-way analysis of variance (ANOVA) with Dunnett's multiple comparison test (n=3). A significance level of P<0.05 was considered statistically significant. Notably, the symbol "****" (four stars) indicated an extremely high level of significance, with P<0.0001. GraphPad Prism 8 software was used to generate and analyse the results presented*

4.4 Discussion

Major Findings Summary:

In AML cell lines overexpression of *PTGS1* boosted WNT signalling, increased levels of PGE2 secretion and reversed the effects of *PTGS1* inhibitors. Cytarabine resistance is another effect of *PTGS1* over-expression, associated with reduced levels of reactive oxygen species production (ROS).

Discussion:

Clinically, cytarabine resistance is a significant issue in treating AML, and suppressing *PTGS* has potential to address this problem. The results of this study contribute to knowledge of *PTGS1* and *PTGS2* functions in the responses of AML cells to therapies. Specifically, cells in which *PTGS1* was over-expressed were observed to have decreased apoptosis compared with wild-type cells, which suggests that *PTGS1* contributes to AML cell survival and might allow the cells to resist cytarabine. Interestingly, the findings show that *PTGS2* also contributes to protection, in contrast to typical observations in individuals with AML. The differences in effects observed in AML cells lead to the question of the specific individual roles of *PTGS1* and *2* and how far suppressing these genes impacts outcomes for patients. It is possible that *PTGS2* will not show the experimentally observed protective effect for AML in the clinical context, where a complex range of variables are in play, such as the microenvironment, characteristics of individual patients and genetic heterogeneity. Thus, there may be considerable complexity and specificity of context in the association of *PTGS2* expression with outcomes in AML.

The results linking *PTGS1* to reduced apoptosis potentially suggests that if *PTSG1* were blocked, this could increase AML cells' vulnerability to cytarabine and other drugs. This points to the potential for therapies targeting *PTGS1* inhibition to support established therapies for AML by tackling drug resistance. Additional research should be undertaken to examine patterns of expression for *PTGS1* and *PTGS2* for AML patients and their association with response to therapeutic interventions and patient outcome. This would build on the findings from experiment presented here, to produce data which are therapeutically relevant. This type of translational may provide more detailed understanding of the possibilities for PTGS inhibitor therapies for AML and how this could improve AML treatment.

Changes in ROS level were determined for each of the 2 cell lines by applying CellROX Green dye, but the lack of change in HL60 cells with MitoSOX staining leads to questions about mechanisms. CellROX functions to allow general determination of ROS level intracellularly using multiple cell sources, including mitochondria. In contrast, MitoSOX functions by specifically targeting mitochondrial ROS generation. Thus, these discrepancies in findings might point to raised aggregated ROS levels in the HL60 cell line intracellularly, but perhaps coming from a non-mitochondrial source: e.g. organelles and cytoplasm. Thus, the higher level of overall ROS in this cell line could complicate the task of comparing treatment group and control, by masking difference in ROS levels in the mitochondria.

Protein expression profile alterations as presented in **Figure 4.15** are informative in terms of possible actions of the protein of interest within AML, as well as its role downstream from PTGS signalling. An association is reported

between increased expression of β-catenin worsened event-free survival rate in AML (Gruszka et al. 2019). Wnt/β-catenin signalling forms a high-complexity protein network controlling proliferation and self-renewal in the AML cell (Simon et al. 2005). FLT3 mutations are observed often in AML and play a role in Wnt/β-catenin signalling in this context. Where FLTG3 signalling is abnormal in AML, there is increased transcriptional activity and nuclear localisation of β-catenin, which induces MYC generation downstream (Yu et al. 2022). GSK3β has a controlling role for β-catenin, such that when GSK3β is inhibited, β-catenin is then activated (Shahid et al. 2022). Significantly, based on observation for this study, PTGS1/2 could play a role in regulating β-catenin through upregulation of Wnt/β-catenin signalling. It is clear from examining the interactions of significant signalling molecules that AML pathogenesis is highly complex, pointing to varied possibilities for therapies.

The MYC protein forms a vital factor in AML, with its expression significantly influencing therapeutic response and outlook. Increased MYC expression in AML is associated with worse outcomes in terms of survival, as well as greater resistance to chemotherapy (Ohanian et al. 2019). The findings of this study show the ability of *PTGS1* and *PTGS2* to increase expression of *MYC* within the AML cell. In the same manner, this could point to a possible influence of PTGS inhibition on the way MYC is expressed in AML. On the other hand, the HL60 cell line of AML shows a high underlying expression of MYC. MYC plays a vital role in the development and proliferative activity in cells, as well as in downstream gene transcription for genes important to a range of biological activities (Zhou et al. 2021). Knowledge of the specific mechanisms involved in

dysregulated MYC in AML is not currently complete, however. A clearer picture of MYC regulation in AML might support novel therapeutic approaches.

The *PTGS1* overexpression not only resulted in a noticeable increase in WNT signalling but also led to elevated secretion of PGE2 highlighting the complex effects of this protein on many cellular pathways. Markedly, this chapter showed a reversal of *PTGS1* inhibitor effects, demonstrating a potential role in overcoming pharmacological therapies that aim to inhibit this enzyme. Moreover, the observed association between overexpression of *PTGS1* and cytarabine resistance was explored, revealing an association with reduced ROS production levels. These results illustrate the complexity of the roles played by PTGS1 and PTGS2. Therefore, in the next chapter, we use the Next Generation Sequencing (NGS) technique to comprehensively exploration of gene expression patterns in cell models through NGS transcriptomics.

Chapter V

5.1 Introduction

The effects of Next Generation Sequencing (NGS) for genomic analysis have been revolutionary, and this technique is a powerful approach to investigations of cancers such as AML (Kim et al. 2019; Leisch et al. 2019; El Achi and Kanagal-Shamanna 2021). Using NGS multiple RNA or DNA pieces can be sequenced at the same time, leading to high throughput to give a comparatively huge amount of genomic data (Ilyas et al. 2015; Leisch et al. 2019; El Achi and Kanagal-Shamanna 2021). By efforts to sequence whole exomes and at times whole genomes, NGS can help in identification of AML-related genetic changes, whether occurring frequently or rarely, including point mutation, small insertions and deletions (indels), copy number variations (CNVs), and differences in structure (Ilyas et al. 2015; Kim et al. 2019; Leisch et al. 2019).

Use of NGS has underpinned discoveries of new and recurring fusion genes and mutations in AML, and has revealed various molecular mechanisms in leukemogenesis for the first time (Ilyas et al. 2015; Leisch et al. 2019). Moreover, the technique has led rapid progression of knowledge around the molecular genetics of AML, creating new possibilities in developing molecules with strong therapeutic efficacy as well as processes for individually-tailored therapies and monitoring which are proving revolutionary in this area of medicine (El Achi and Kanagal-Shamanna 2021).

The contribution of NGS to understandings of AML pathogenesis as well as the cancer's clonal evolution, which has strengthened practice in both pathology and oncology. The creation of more complete genetic profiling for AML through NGS allows for targeted therapeutic interventions based upon molecular

features of the disease, allowing it to be more effectively controlled and decreasing recurrence. To summarise, NGS has been central to a more advanced understanding of the complexity of AML and to the development of new therapeutic approaches and management strategies (El Achi and Kanagal-Shamanna 2021).

5.2 Aims

1. To identify and validate novel signalling pathways downstream of *PTGS1* and *PTGS2* expression in cell models through NGS transcriptomics.

2. To identify the contribution of the *PTGS1/PTGS2* transcriptome to chemoresistance in AML models

5.3 Results

5.3.1 Gene expression clustering analysis reveals consistency and reproducibility in RNA-seq Data

First, hierarchical clustering was performed on all samples, and the resultant heatmap of the RNA-seq data revealed that the technical replicates of each sample exhibit a strong clustering pattern, indicating good reproducibility and consistency within the experimental conditions. This clustering pattern suggests that the gene expression profiles of the replicates within each sample are highly similar (**Figure 5. 1A**). The observed clustering of the replicates within each sample provides confidence in the experimental design and suggests that any variations observed in gene expression are more likely to be attributable to biological factors rather than technical artefacts. This clustering pattern strengthens the reliability of the RNA-seq data and supports the subsequent analyses and interpretations based on the gene expression profiles.

The correlation matrix analysis using the top 75% most abundant genes expressed in the RNA-seq data reveals a clustering pattern where the three replicates within each sample exhibit a strong positive correlation and group together (**Figure 5. 1B**). This clustering pattern signifies the high similarity in gene expression profiles among the replicates, again confirming that most variance is biological and occurs between cell-lines and treatments rather than technical (i.e. between technical replicates).

Principal Component Analysis (PCA) of the gene expression data reveals a clear difference between the *PTGS1* or *PTGS2* and the control samples in U937 cells. This indicates that the gene expression profiles of the U937 control

replicates exhibit a distinct pattern, differing from both the *PTGS1* and the *PTGS2 overexpression* samples. The PCA analysis also demonstrates that the gene expression profiles of the HL-60 cells exhibit little variation. This highlights that overall transcriptome variation in U937 driven by overexpression of *PTGS1/2* is far greater than in HL-60 cells, in which the HL60-control, HL60^{PTGS1} and HL60^{PTGS2} overexpression cells all group together (**Figure 5. 1C**). This is in contrast to the U937 cells where the U937-control cells group together separately from the U937^{PTGS1} and U937^{PTGS2} overexpressing cells. Notably, the PCA analysis suggests that cytarabine treatment does not affect the transcriptome in either U937 or HL60 cell line enough to separate from the control cells, which is not to say there are no significant changes but that the overall transcriptome is more similar to the control than any other condition.

A

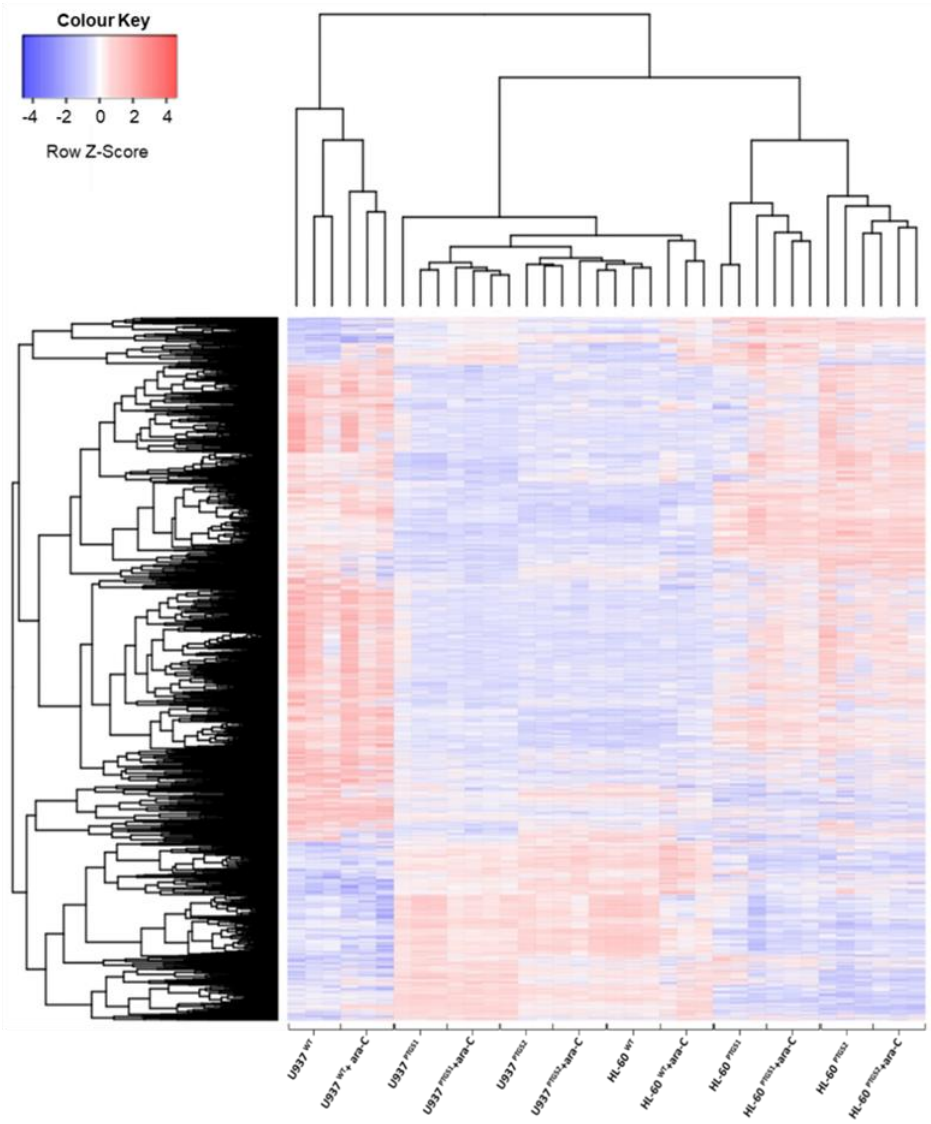
Colour Key
-4 -2 0 2 4
Row Z-Score
U937 WT
U937 WT + ara-C
U937 P53S1
U937 P53S1 + ara-C
U937 P53S2
U937 P53S2 + ara-C
HL-60 WT
HL-60 WT + ara-C
HL-60 P53S1
HL-60 P53S1 + ara-C
HL-60 P53S2
HL-60 P53S2 + ara-C

B

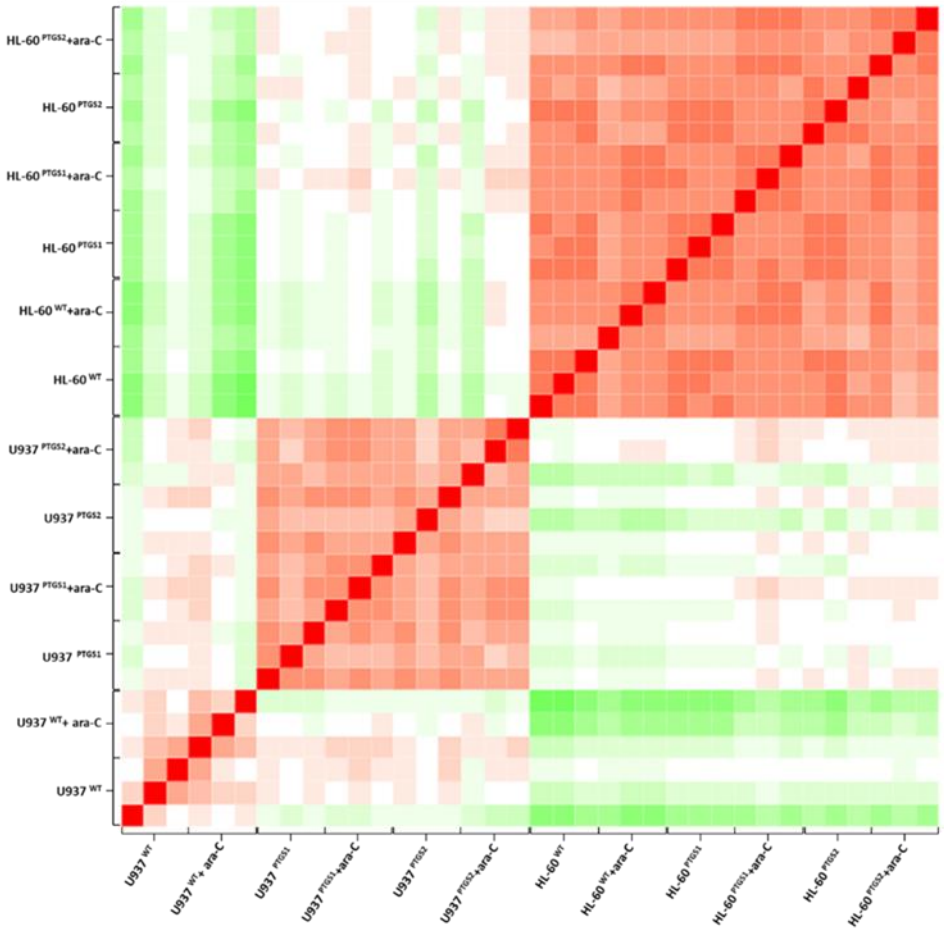
HL-60 PTGS2+ara-C
HL-60 PTGS2
HL-60 PTGS1+ara-C
HL-60 PTGS1
HL-60 WT+ara-C
HL-60 WT
U937 PTGS2+ara-C
U937 PTGS2
U937 PTGS1+ara-C
U937 PTGS1
U937 WT+ ara-C
U937 WT
U937 WT
U937 WT+ ara-C
U937 PTGS1
U937 PTGS1+ara-C
U937 PTGS2
U937 PTGS2+ara-C
HL-60 WT
HL-60 WT+ara-C
HL-60 PTGS1
HL-60 PTGS1+ara-C
HL-60 PTGS2
HL-60 PTGS2+ara-C

C

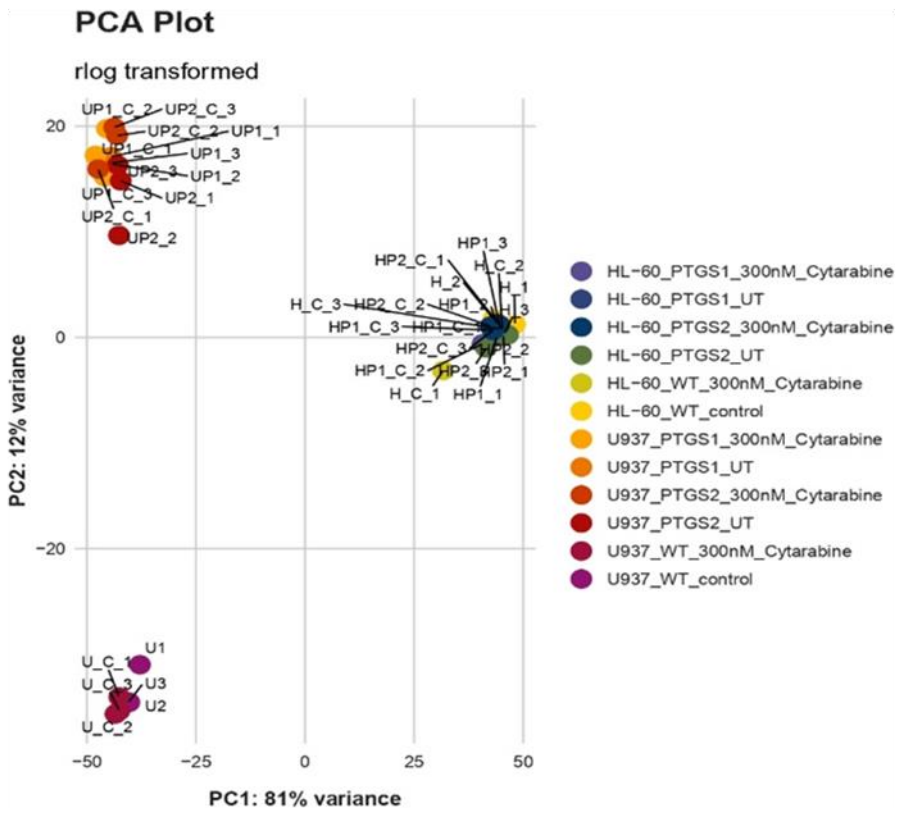
PCA Plot
rlog transformed
PC2: 12% variance
PC1: 81% variance
20
0
−20
−50
−25
0
25
50
HL−60_PTGS1_300nM_Cytarabine
HL−60_PTGS1_UT
HL−60_PTGS2_300nM_Cytarabine
HL−60_PTGS2_UT
HL−60_WT_300nM_Cytarabine
HL−60_WT_control
U937_PTGS1_300nM_Cytarabine
U937_PTGS1_UT
U937_PTGS2_300nM_Cytarabine
U937_PTGS2_UT
U937_WT_300nM_Cytarabine
U937_WT_control

Figure 5. 1 Reproducibility and consistency of gene expression profiles

(A) *The heat map visually represents the most variable gene expression levels across the samples, where each row represents a gene and each column represents a sample. The colour intensity in the heat map indicates the expression level of each gene, with deep red colour indicating higher expression and deep blue colour indicating lower expression. By grouping the replicates together in distinct clusters, the heat map demonstrates that the gene expression patterns among the replicates within each sample are more similar to each other than to the replicates from other samples.* ***(B)*** *In the correlation matrix, each row and column represent a sample, and the matrix elements represent the correlation coefficients between the gene expression profiles of the samples. A higher correlation coefficient signifies a stronger positive correlation, indicating similar gene expression patterns, while a lower correlation coefficient suggests weaker or negative correlations, implying divergent gene expression patterns. Both the heat map and the correlation matrix were generated using iDEP.96 platform.* ***(C)*** *PCA analyses indicate the substantial difference in thousands of genes induced by PTGS1 and PTGS2 over-expression in U937 cells. There is little variation among replicates.*

5.3.2 Summary of basic comparison between U937 control and *PTGS1* or *PTGS2* over-expression models

A Pearson Correlation analysis was performed across all conditions to bring more clarity into the similarities and differences between the U937 control, *PTGS1*, and *PTGS2* models. The purpose of this analysis was to determine how closely these models are related to one another and to evaluate those connections. **Figure 5. 2J** displayed a strong correlation between *PTGS1* and *PTGS2* (R = 0.95), which is expected considering the common pathways they both use. However, less correlation was seen between control cells and *PTGS1* cells (Figure 5. 2B, R = 0.91). Moreover, the correlation between control cells and *PTGS2* cells seemed to be the lowest of all the comparisons (**Figure 5. 2C**, R = 0.90).

A full summary of NGS analysis for U937 cells so far is demonstrated in Figure 5. 3. The Venn diagram analysis was performed to investigate the similarity and difference in the gene expression patterns between U937 control, $U937^{PTGS1}$ overexpressed, $U937^{PTGS2}$ overexpressed cells under either untreated or cytarabine treated conditions. The 12571 overlapping genes represented a subset of genes that were commonly expressed in all un-treated cell lines **Figure 5. 3A**. In addition, the Venn diagram revealed 12660 overlapping genes that showed commonly expressed genes in all cell lines under the cytarabine treatment condition **Figure 5. 3B**. These Venn diagrams specifically show the extensive similarity of the signalling pathways as well as the areas of specificity. I examine the routes in more detail to shed light on their similarities and differences in the following sections.

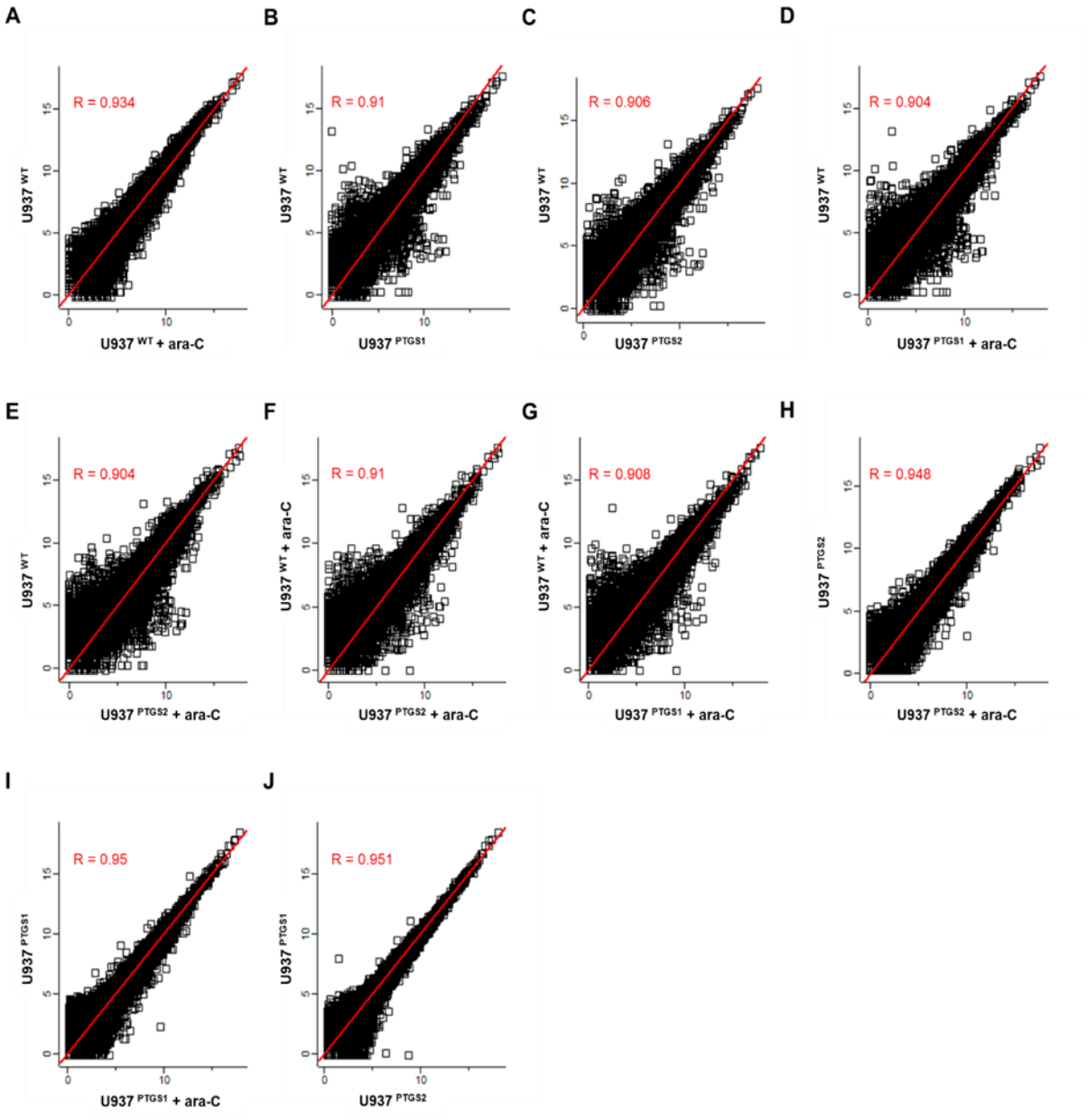

Figure 5. 2 Correlation study between control, PTGS1 and PTGS2 cells in U937.

*The values of X and Y axes in the scatterplot are the averaged normalised values of three sample replicates (log_2 scaled). The dispersion of points across the plot provides a visual representation of the strength and direction of the correlation between the two variables. (**J**) The plot reveals a strong positive correlation between PTGS1 and PTGS2. Perseus 1.6.8.0 software was used to generate scatterplots.*

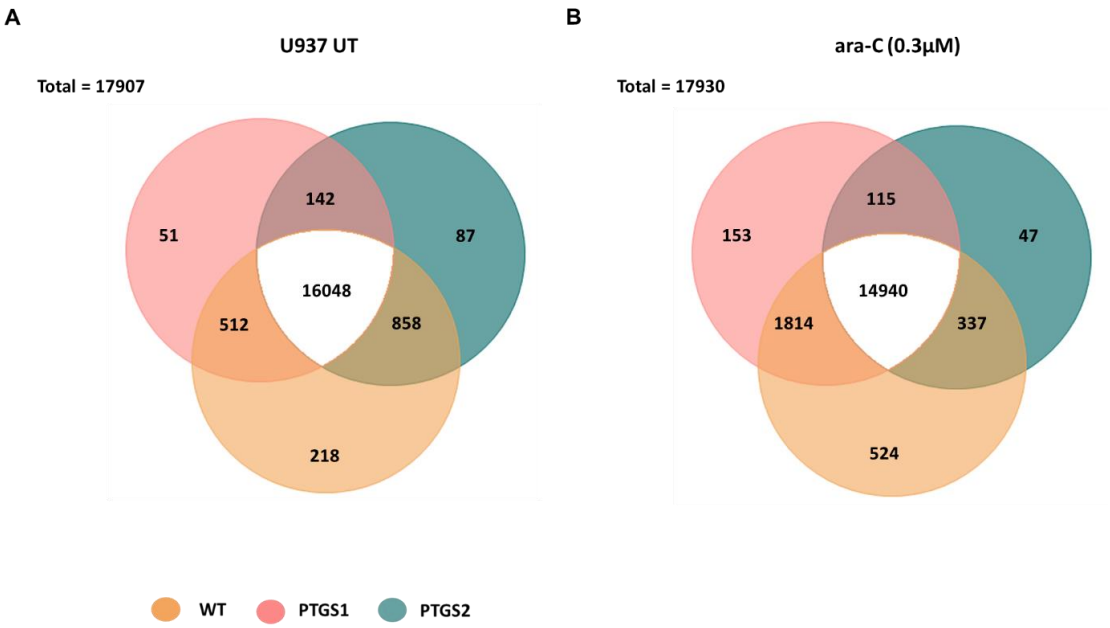

Figure 5. 3 Venn Diagram insights into overlapping genes across U937 control cells and PTGS1/2 cells

The Venn diagram displays the gene expression overlaps across three distinct cell lines, including U937 wild-type, U937 ^{PTGS1}, and U937 ^{PTGS2}. These graphic shed light on the similarities and differences in gene expression patterns between the ***(A)*** *untreated and* ***(B)*** *cytarabine-treated conditions. Perseus 1.6.8.0 software was used for data filtering, enabling the exclusion of irrelevant or low-quality data points from the dataset. Then, the iDEP.96 platform was employed to visualise the relationships between these cells through Venn diagrams.*

5.3.3 Identification of the *PTGS1-overexpression* associated transcriptome.

We next investigated the variation in the gene expression patterns between U937 control, U937 *PTGS1* overexpressed, U937 *PTGS2* overexpressed, HL-60 control, HL-60 *PTGS1* overexpressed and HL-60 *PTGS2* overexpressed cells under either un-treated **Figure 5. 4A** or cytarabine treated conditions **Figure 5. 4B**. The 12571 overlapping genes represented a subset of commonly expressed genes in all untreated cell lines. In addition, the Venn diagram revealed 12660 overlapping genes that showed commonly expressed genes in all cell lines under the cytarabine treatment condition.

We then performed a gene expression profile comparison to identify the differentially expressed genes (DEGs) between the control cells and *PTGS1* overexpressed cells, aiming to assess the genes regulated by *PTGS1*. DEGs were defined as genes with significantly different expression levels between the two cells in both U937 and HL-60 cell lines, with at least a one-fold change (False Discovery Rate correction (FDR), $p < 0.05$). Altogether, in both cell lines, 26 upregulated and 11 downregulated genes were identified in *PTGS1* overexpressed cells (**Figure 5. 4A**), which compares to 54 unique DEGS in *PTGS2 overexpressing* cells.

These gene sets were then analysed with gene ontology (GO) network analysis tools, and Biological Process-enrichment terms were identified using the g:profiler tool and the top 10 pathways were selected as shown in **Figure 5. 5B** and **C**. Notably, overexpression of *PTGS1* leads to widespread transcriptomic

changes in AML cells, including immune gene networks and myeloid cell activation.

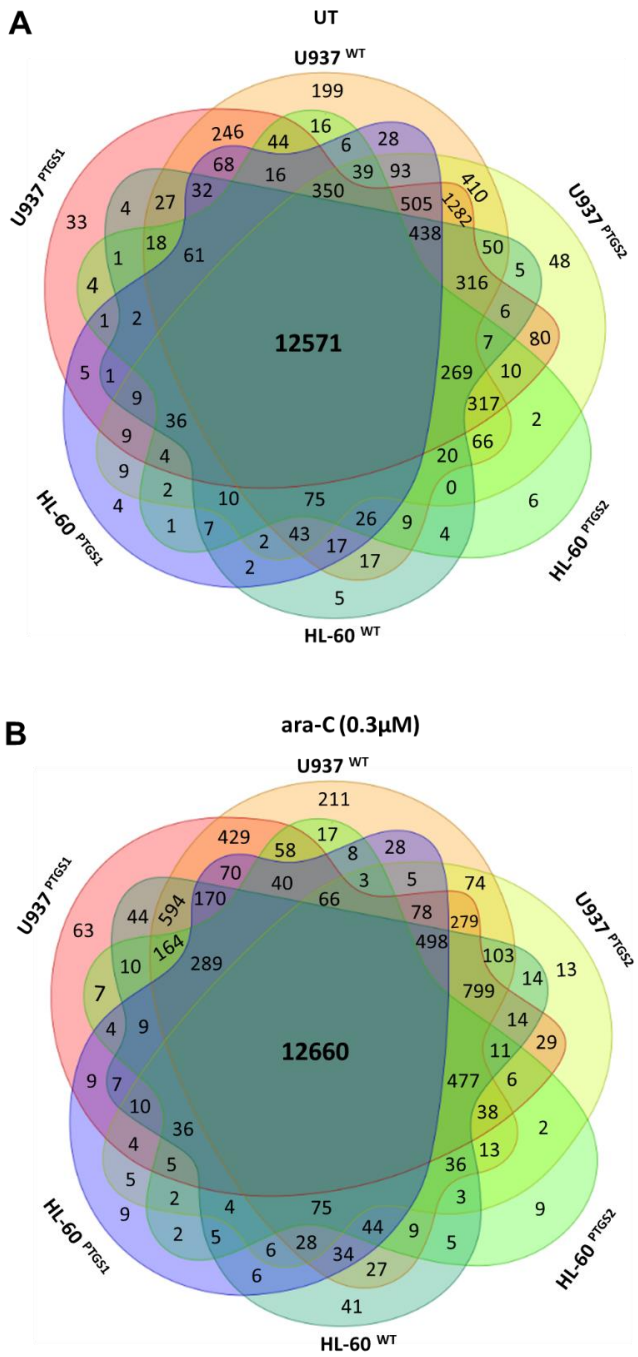

Figure 5. 4 The comparative Venn diagram analysis of gene expression in AML cell lines.

The Venn diagram shows the gene expression overlaps among six different cell lines, including U937 wild-type, U937 PTGS1, U937 PTGS2, HL-60 wild-type, HL-60 PTGS1, and HL-60 PTGS2. This diagram provides insights into the common and different gene expression patterns among ***(A)*** *untreated and* ***(B)*** *cytarabine treatment conditions. Perseus 1.6.8.0 software was used for data filtering, enabling the exclusion of irrelevant or low-quality data points from the dataset. Then, the iDEP.96 platform was employed to visualise the relationships between these cells through Venn diagrams.*

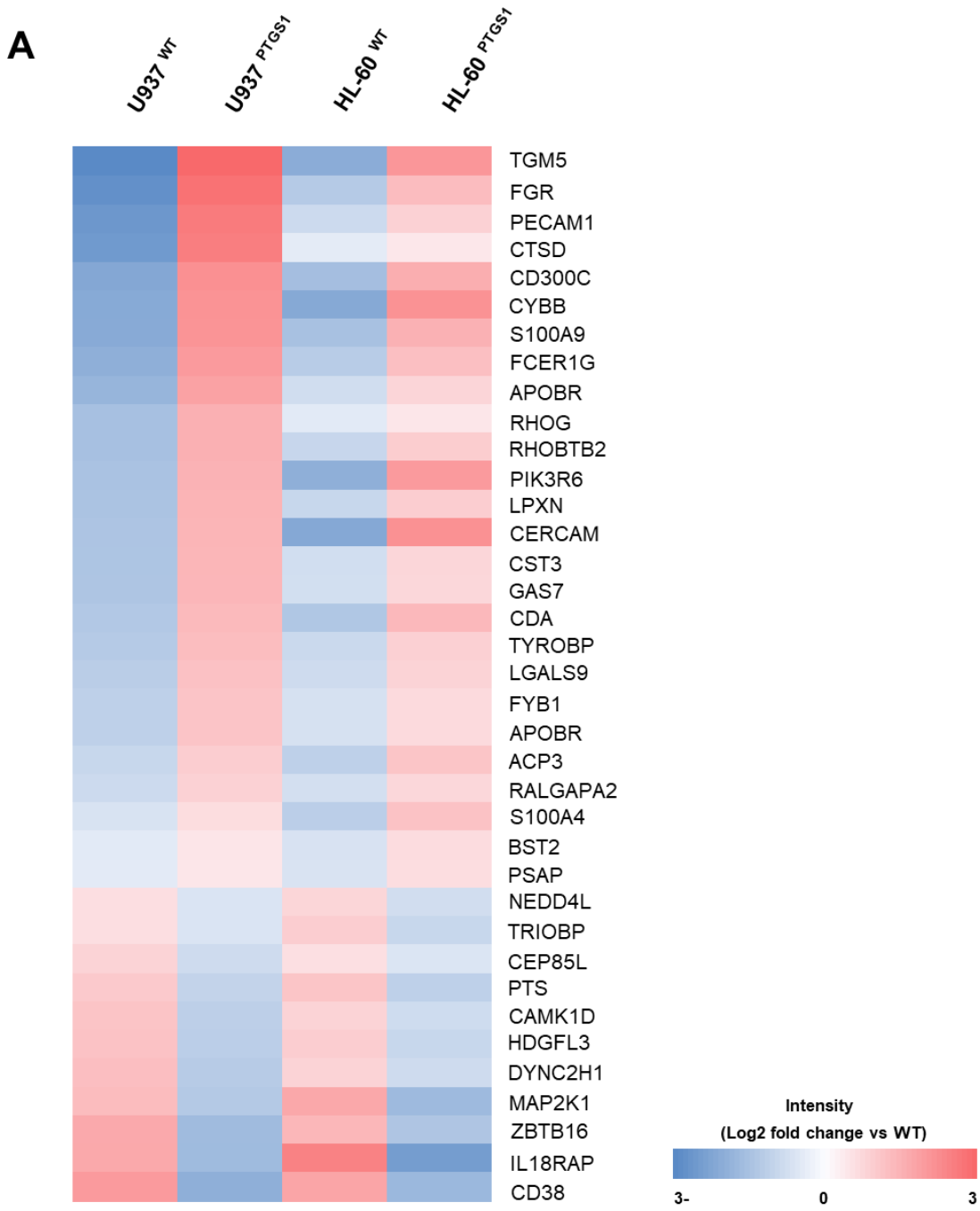
A
U937 WT
U937 PTGS1
HL-60 WT
HL-60 PTGS1
TGM5
FGR
PECAM1
CTSD
CD300C
CYBB
S100A9
FCER1G
APOBR
RHOG
RHOBTB2
PIK3R6
LPXN
CERCAM
CST3
GAS7
CDA
TYROBP
LGALS9
FYB1
APOBR
ACP3
RALGAPA2
S100A4
BST2
PSAP
NEDD4L
TRIOBP
CEP85L
PTS
CAMK1D
HDGFL3
DYNC2H1
MAP2K1
ZBTB16
IL18RAP
CD38
Intensity
(Log2 fold change vs WT)
3-
0
3

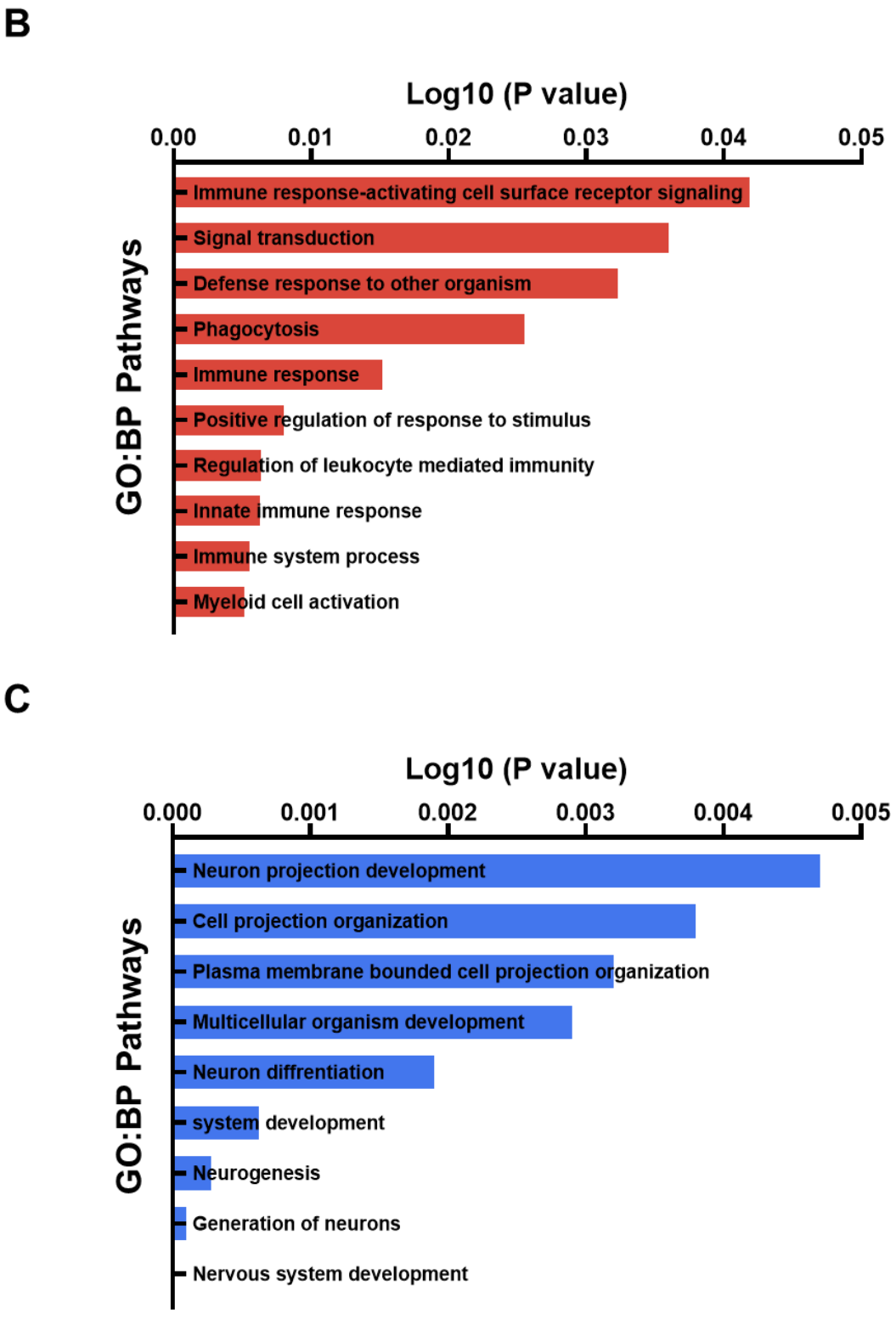

Figure 5. 5 PTGS1 drives immune transcriptome signatures.

(A) *Heatmap shows the common 37 DEGs between wild-type and PTGS1 overexpressed cells in U937 and HL-60 cells. This data was extracted using the iDEP.96 platform. Subsequently, these common 37 DEGs were further graphically*

represented using the Microsoft Excel. The blue denotes downregulation, whereas red denotes upregulation. Colour intensities showed levels of change, as shown in the colour key. The iDEP.96 platform was applied to obtain the networks associated with ***(B)*** *the top 10 upregulated and* ***(C)*** *the top 10 downregulated gene networks in U937 and HL-60 PTGS1 over-expression models (PTGS1 vs wild-type). Subsequently, these networks were further graphically represented using the GraphPad Prism 8 software.*

5.3.4 Identification of the *PTGS1- regulated* transcriptome in U937 cells.

To evaluate the *PTGS1-regulated* genes in U937 cells, the gene expression profiles between the U937 control cells and U937 *PTGS1* cells was compared to find the DEGs. Altogether, 1029 upregulated and 906 downregulated genes were identified (**Figure 5. 6**). The heat map showed that the expression levels of many genes in control cells were significantly different from those in *PTGS1*. The top 17 upregulated genes and 17 downregulated genes ranked by their levels of differences were listed in **Table 5. 1**.

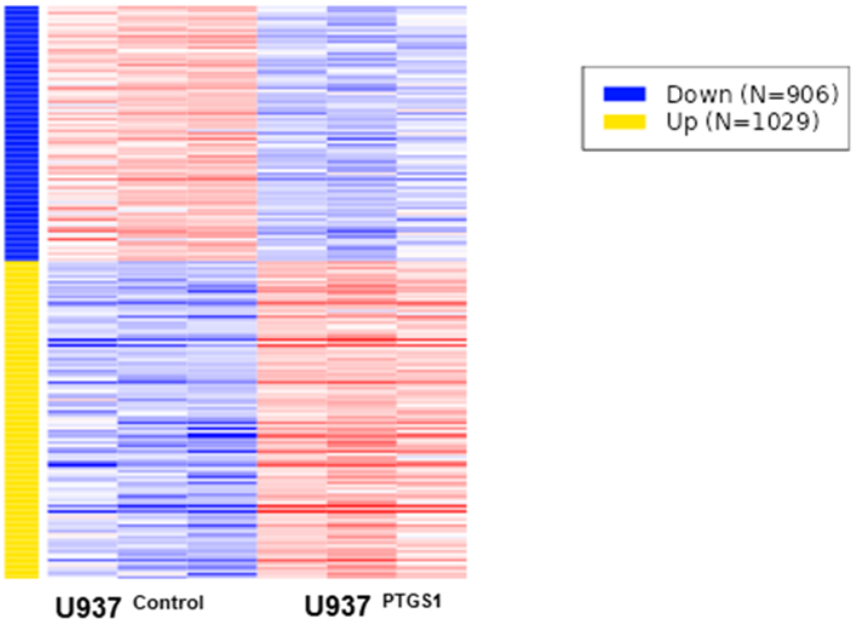

Figure 5. 6 Investigation of PTGS1-regulated genes by comparing expression profiles between the PTGS1 over-expression and U937 control cells.

Perseus 1.6.8.0 software was used for data filtering using 2 of 3 biological replicates in at least one group. Subsequently, the top DEGs were gained and graphically represented using the iDEP.96 platform. These top DEGs between PTGS1 over-expression and U937 control cells are displayed as a heat map. Red indicates upregulation and green indicates downregulation.

Table 5. 1 The top DEGs genes for comparison between U937 control and *PTGS1* cells

Symbol	log_2 Fold Change	P value	Symbol	log_2 Fold Change	P value
MPO	-12.93	1.71E-08	***CBR1***	6.19	2.09E-03
ANKRDA	-8.92	1.50E-05	***PSTPIP2***	6.23	3.20E-04
S100Z	-8.92	8.56E-08	***CTBP2***	6.32	2.46E-06
INHBA	-8.6	4.59E-05	***CD52***	6.56	2.96E-07
LIN28B	-7.92	8.38E-05	***IFT57***	6.56	4.51E-07
SNRPN	-7.69	2.41E-05	***FCN1***	6.66	8.23E-08
TCEAL8	-7.36	1.98E-04	***F2RL3***	6.81	8.62E-06
SPANXB1	-7.35	3.51E-05	***PITX1***	6.89	8.61E-05
ANGPT1	-7.15	6.75E-05	***IL32***	7.16	7.71E-06
ULBP3	-6.83	5.55E-06	***NRIP3***	7.36	5.70E-05
KRT9	-6.67	6.69E-04	***TPSAB1***	7.53	4.73E-08
DACH1	-6.65	9.69E-05	***SOD3***	7.61	5.55E-06
SPAG6	-6.6	2.53E-05	***RAB31***	7.64	8.07E-08
PKIB	-6.53	1.00E-05	***TPSB2***	7.95	8.07E-08
NTS	-6.5	1.58E-07	***HS3ST2***	7.96	8.46E-07
SNX19	-6.43	3.51E-03	***S100P***	8.18	7.36E-11
TRIM58	-6.42	2.04E-04	***CST7***	8.63	1.94E-11

Similarly, a comparative analysis of gene expression profiles was conducted between U937 cells with *PTGS1* overexpression and U937 control cells after cytarabine exposure. This comparison aimed to detect differentially expressed genes between these two cell types under treatment condition. Remarkably, a total of 982 genes were found to be upregulated, while 833 genes were downregulated in the U937 *PTGS1* cells (as illustrated in **Figure 5. 7**). A visual representation of the gene expression differences was presented in a heat map, revealing significant variations in expression levels between the control and *PTGS1* model. These findings underscore the influence of *PTGS1* on the expression of numerous genes in the U937 cell line.

To further investigate the most prominent DEGs, the top 34 upregulated genes and downregulated genes were selected based on their respective levels of difference. **Table 5. 2** provides detailed information about these genes, including their names, $\log_2$ fold change (a measure of the magnitude of expression change), and p-value (indicating the statistical significance of the changes).

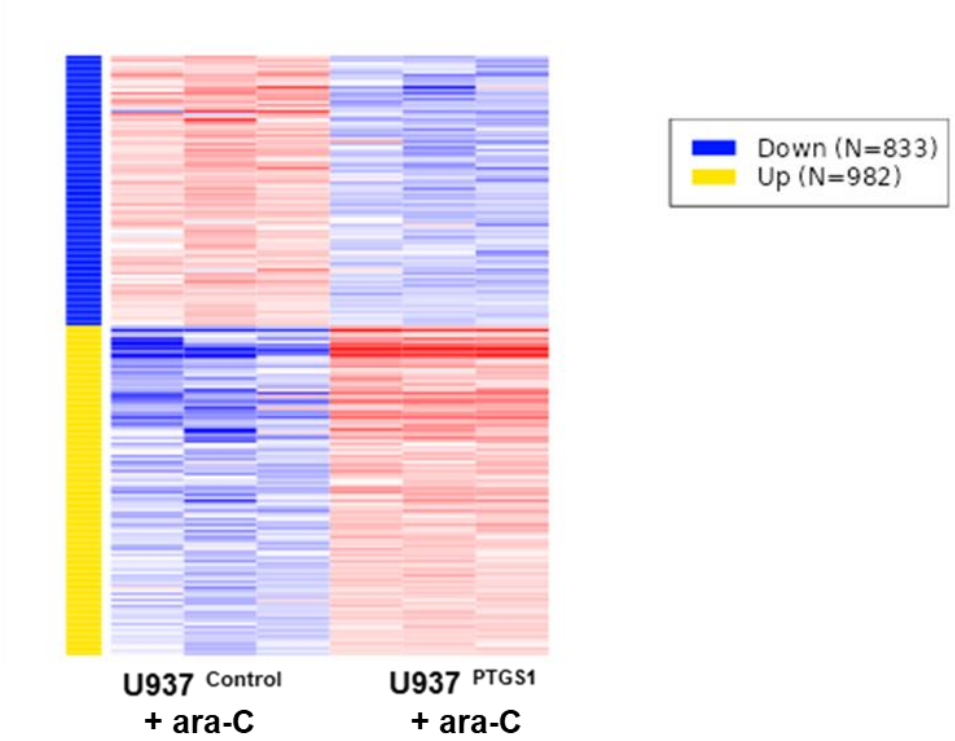

Figure 5. 7 Comprehensive analysis of PTGS1-dependent genetic responses to cytarabine in U937 Cells.

Perseus 1.6.8.0 software was used for data filtering using 2 of 3 biological replicates in at least one group. Subsequently, the top DEGs were gained and graphically represented using the iDEP.96 platform. Under cytarabine treatment condition, the top DEGs between PTGS1 over-expression and U937 control cells were identified, and their expression profiles were visualised using a heatmap. In the heatmap, red indicates genes that are elevated, while green indicates genes that are downregulated.

Table 5. 2 The top DEGs genes for comparison between U937 control and *PTGS1* cells under cytarabine treatment.

Symbol	log_2 Fold Change	P value	Symbol	log_2 Fold Change	P value
MPO	-10.92	1.15E-115	***FCN1***	5.95	1.08E-91
GALM	-6.15	2.38E-13	***CTBP2***	6.08	1.90E-96
C13orf46	-5.78	3.18E-02	***IFT57***	6.22	3.39E-111
SEPTIN11	-5.72	2.83E-100	***TPSB2***	6.24	1.51E-35
MUC20	-5.32	5.33E-05	***AK5***	6.26	7.00E-10
CYP46A1	-4.97	6.25E-14	***SERPINB2***	6.31	2.78E-14
CEMIP	-4.83	3.99E-03	***TPSAB1***	6.34	6.59E-28
S100P	5.18	0.00E+00	***IL32***	6.36	1.44E-86
KRT2	5.22	5.06E-06	***VENTX***	6.74	6.60E-07
HS3ST2	5.23	3.98E-23	***CBS***	6.91	2.53E-27
AP3M2	5.28	1.25E-28	***RAB31***	6.94	8.83E-195
TNFRSF10A	5.32	6.54E-16	***PRRG4***	7.61	8.74E-25
CEACAM6	5.35	2.44E-43	***SOD3***	7.66	1.85E-15
GALNT14	5.38	1.32E-32	***NRIP3***	7.74	5.14E-12
ANPEP	5.43	2.32E-23	***CST7***	7.84	6.03E-244
VWA5A	5.46	3.49E-25	***SRPX***	7.85	1.52E-07
ENDOD1	5.7	1.94E-29	***PITX1***	10.64	7.95E-17

5.3.5 The Influence of *PTGS1* over-expression on Biological Processes Enriched in DEGs between U937 control and U937 *PTGS1* overexpressed cells.

In this section, we conducted a thorough analysis of gene expression changes induced by *PTGS1* overexpression. Specifically, we investigated 1029 upregulated genes and 906 downregulated genes (see **Section 5.3.4**) using GO analysis with Biological Process-enrichment terms. The top 30 pathways are shown in **Figure 5. 8A**.

Our enrichment analysis gave important insights into the pathways and cellular processes that *PTGS1* directly affected. The significant relationships between the DEGs and important functions, such as the up-regulation of leukocyte activation, neutrophil degranulation, granulocyte activation and immune response, were among the most noteworthy findings (**Figure 5. 8B**). Also, there were a number of associations between DEGs downregulated upon *PTGS1* overexpression such as cell division, cell cycle and metabolic process (**Figure 5. 8C**). The majority of the DEGs were shown to have a significant role in the immune response pathway, which is a somewhat surprising finding from the study. This shows that *PTGS1* overexpression potentially impacts the immune system and may help to control immunological-related activities and reactions in the cellular environment.

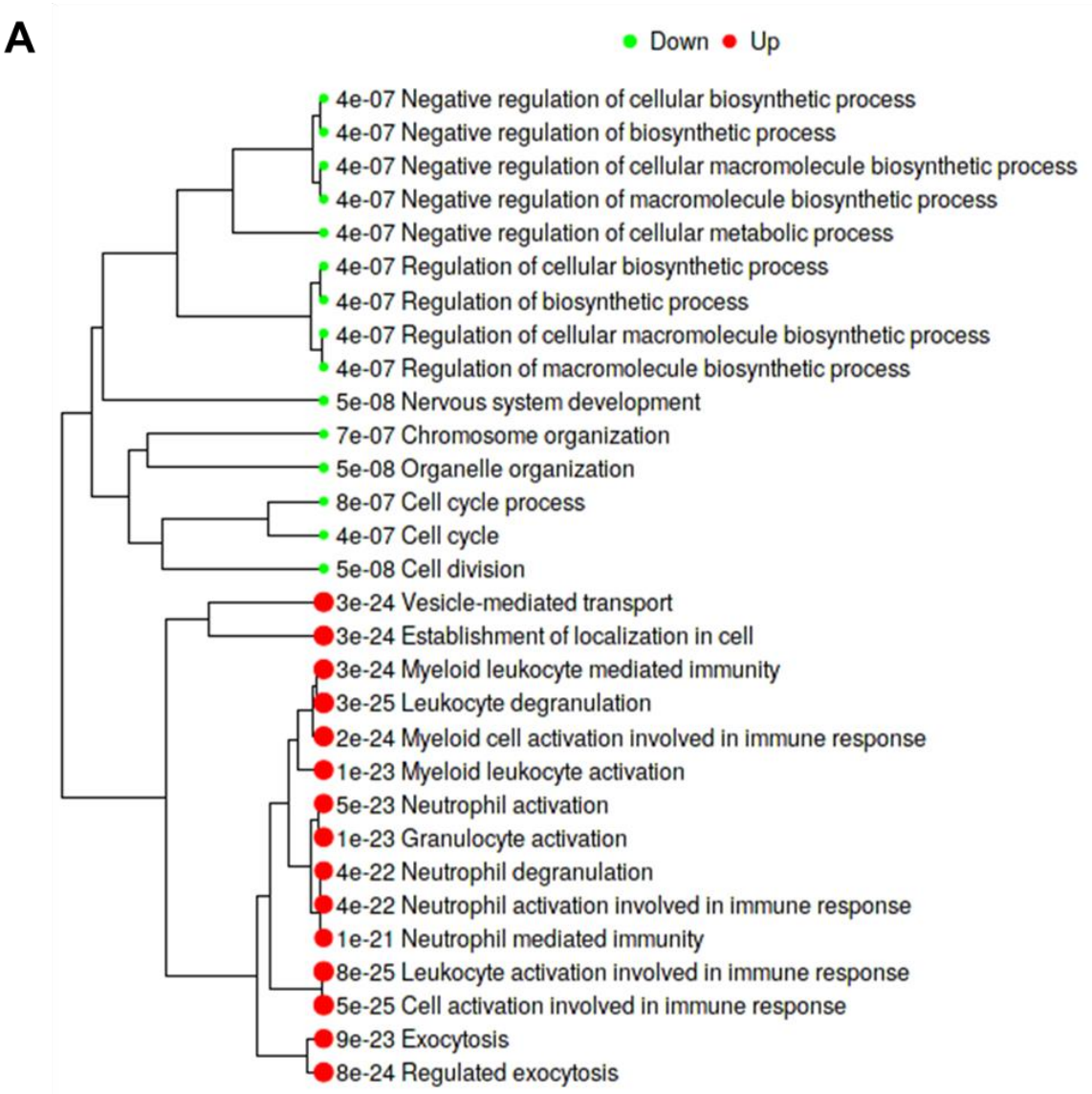
A
Down
Up
4e-07 Negative regulation of cellular biosynthetic process
4e-07 Negative regulation of biosynthetic process
4e-07 Negative regulation of cellular macromolecule biosynthetic process
4e-07 Negative regulation of macromolecule biosynthetic process
4e-07 Negative regulation of cellular metabolic process
4e-07 Regulation of cellular biosynthetic process
4e-07 Regulation of biosynthetic process
4e-07 Regulation of cellular macromolecule biosynthetic process
4e-07 Regulation of macromolecule biosynthetic process
5e-08 Nervous system development
7e-07 Chromosome organization
5e-08 Organelle organization
8e-07 Cell cycle process
4e-07 Cell cycle
5e-08 Cell division
3e-24 Vesicle-mediated transport
3e-24 Establishment of localization in cell
3e-24 Myeloid leukocyte mediated immunity
3e-25 Leukocyte degranulation
2e-24 Myeloid cell activation involved in immune response
1e-23 Myeloid leukocyte activation
5e-23 Neutrophil activation
1e-23 Granulocyte activation
4e-22 Neutrophil degranulation
4e-22 Neutrophil activation involved in immune response
1e-21 Neutrophil mediated immunity
8e-25 Leukocyte activation involved in immune response
5e-25 Cell activation involved in immune response
9e-23 Exocytosis
8e-24 Regulated exocytosis

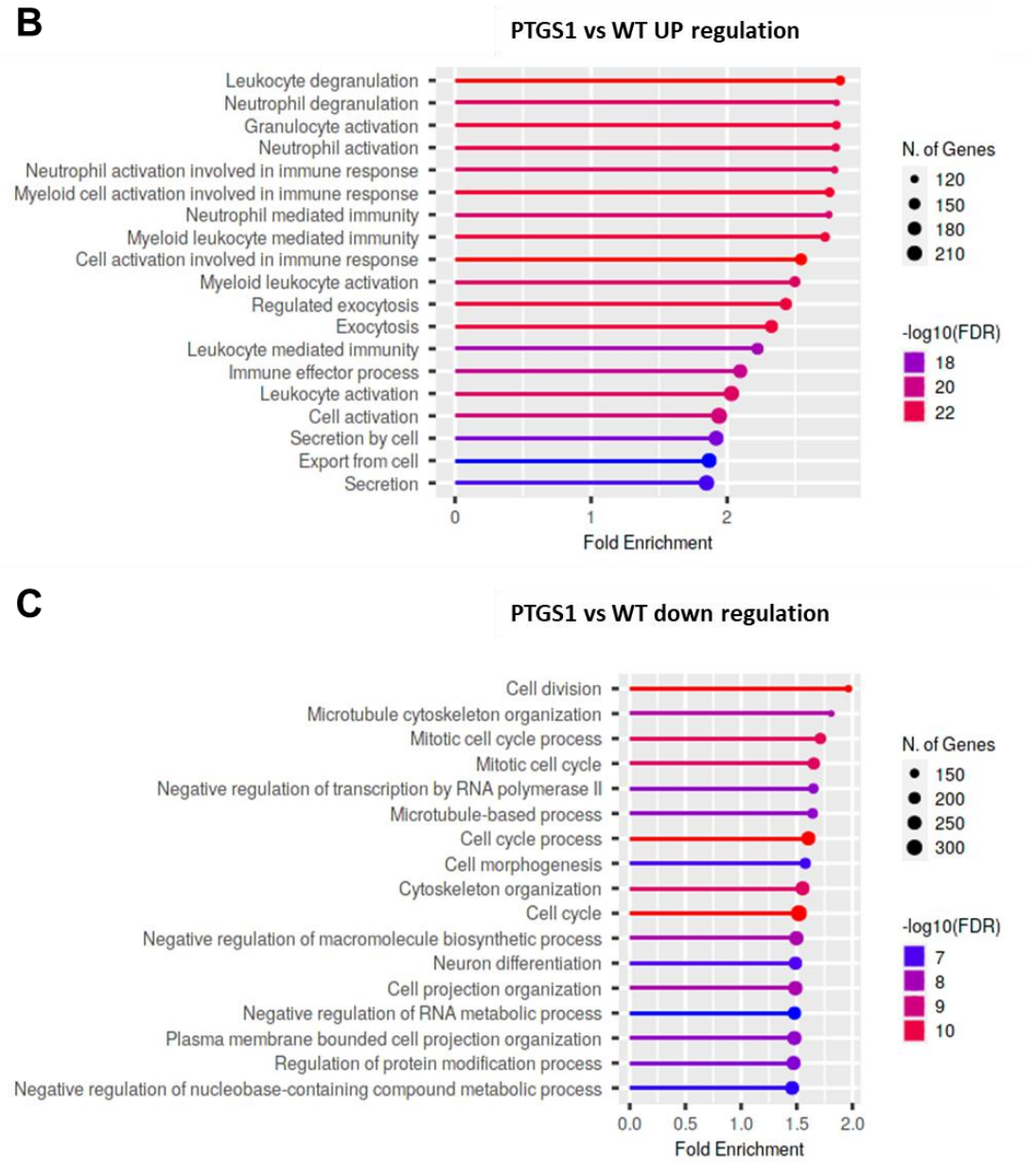

Figure 5. 8 Gene Ontology (GO) analysis of Biological Process networks enriched with PTGS1-overexpression associated DEGs.

ShinyGO 0.80 platform was used to generate the hierarchical clustering trees and the bar charts, representing enriched GO terms or pathways. ***(A)*** *Phylogenetic neighbourhood analysis of biological process networks. Nearby gene sets on the tree share stronger gene relationships (i.e. more significantly enriched DEGs). The size of the dot reflects P values.* ***(B)*** *The top 18 up-regulation pathways and* ***(C)*** *top 18 down-regulation pathways associated to DEGs between PTGS1 vs control cells. The length of the bar charts was inversely correlated with the folds of pathway enrichment. The route change levels were represented by -log$_{10}$(FDR). The dot size reflects the number of genes.*

Similarly, we aimed to understand the effects of cytarabine on gene expression changes induced by *PTGS1* over-expression. To achieve our aim, we focused on 982 upregulated genes and 833 downregulated genes in the context of *PTGS1* over-expression treated with cytarabine compared to control cells (wild-type treated with cytarabine). We systematically discovered the functional effects of the gene expression changes induced by *PTGS1* and cytarabine treatment by applying the GO Biological Process-enrichment analysis. Then, we identified the most significant pathways through our analysis, and the top 30 up and down pathways are visually represented in **Figure 5. 9A**. This allowed us to obtain valuable insights into molecular pathways and the cellular processes that were specifically changed by *PTGS1*.

Among the intriguing results were the notable connections between the differentially expressed genes (DEGs) and pivotal processes, particularly the up-regulation of crucial immunological responses, neutrophil degranulation, leukocyte degranulation, and granulocyte activation (as depicted in **Figure 5. 9B**). These findings suggest that *PTGS1* over-expression could modulate the immune response, potentially influencing immune cell functions and inflammatory processes.

However, it is equally important to note that *PTGS1* over-expression exhibited a negative correlation with critical cellular processes such as protein localization and intraciliary transport and dendritic spine development (as demonstrated in **Figure 5. 9C**). These findings suggest that *PTGS1* over-expression may potentially interfere with the proper regulation of these crucial cellular functions, which are vital for cellular organization, transport, and synaptic plasticity.

A

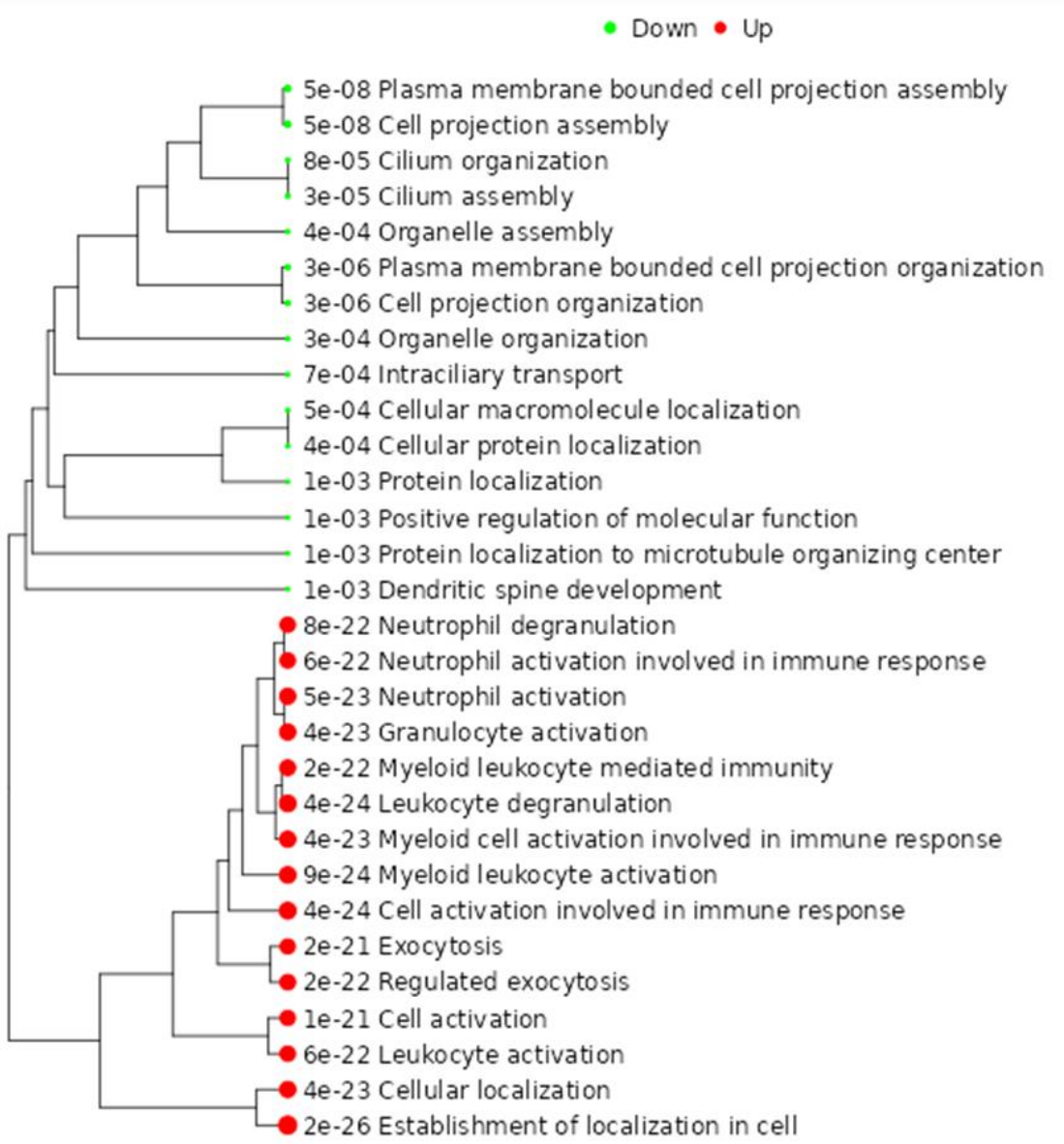
Down
Up
5e-08 Plasma membrane bounded cell projection assembly
5e-08 Cell projection assembly
8e-05 Cilium organization
3e-05 Cilium assembly
4e-04 Organelle assembly
3e-06 Plasma membrane bounded cell projection organization
3e-06 Cell projection organization
3e-04 Organelle organization
7e-04 Intraciliary transport
5e-04 Cellular macromolecule localization
4e-04 Cellular protein localization
1e-03 Protein localization
1e-03 Positive regulation of molecular function
1e-03 Protein localization to microtubule organizing center
1e-03 Dendritic spine development
8e-22 Neutrophil degranulation
6e-22 Neutrophil activation involved in immune response
5e-23 Neutrophil activation
4e-23 Granulocyte activation
2e-22 Myeloid leukocyte mediated immunity
4e-24 Leukocyte degranulation
4e-23 Myeloid cell activation involved in immune response
9e-24 Myeloid leukocyte activation
4e-24 Cell activation involved in immune response
2e-21 Exocytosis
2e-22 Regulated exocytosis
1e-21 Cell activation
6e-22 Leukocyte activation
4e-23 Cellular localization
2e-26 Establishment of localization in cell

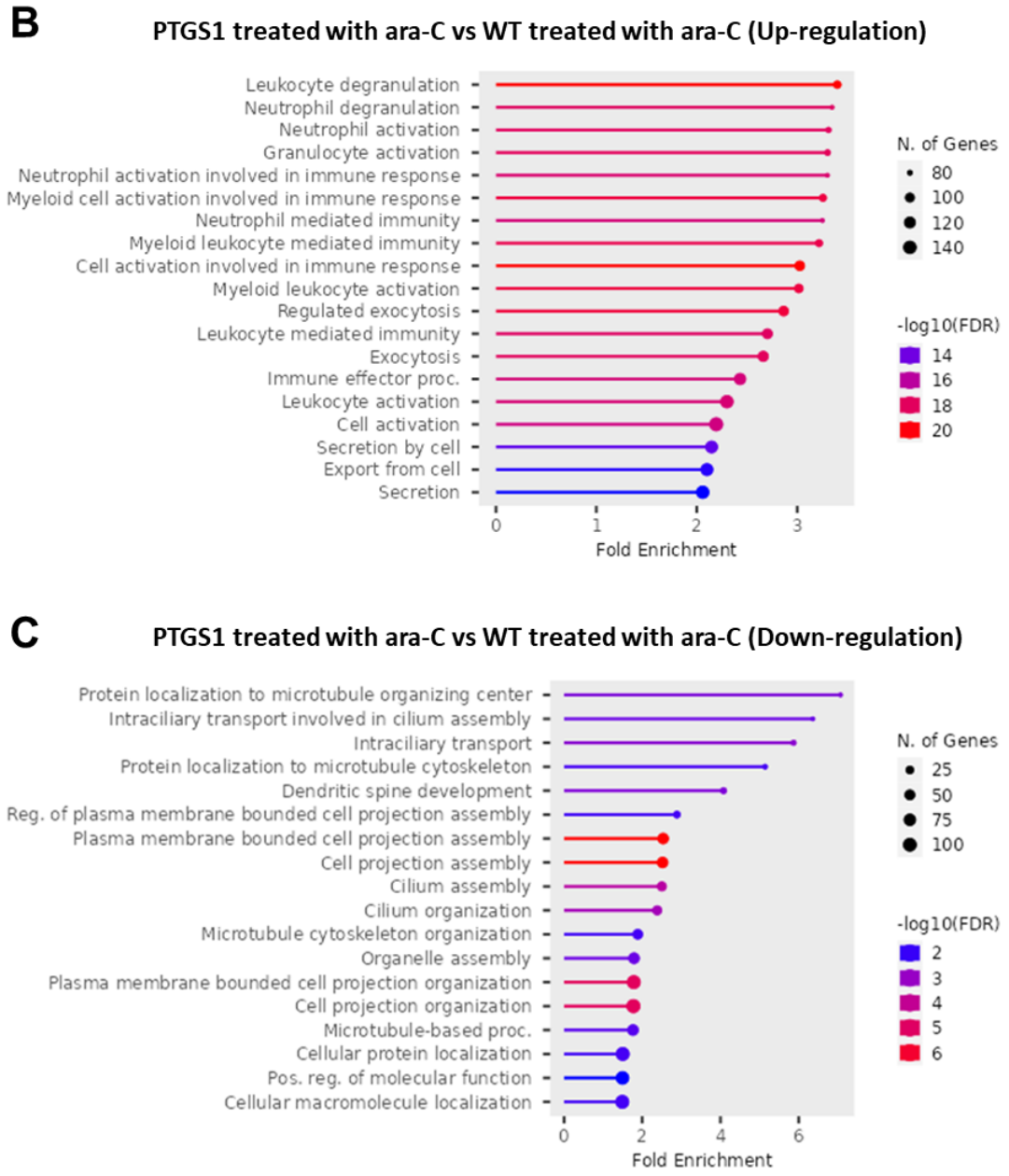

Figure 5. 9 Using the gene ontology biological process enrichment, the top 30 pathways connected to DEGs between PTGS1 and control cells under cytarabine treatment are displayed in a bar graph.

The hierarchical clustering trees and the bar charts, representing enriched GO terms or pathways were generated using ShinyGO 0.80 platform. ***(A)*** *On the tree, adjacent gene sets share more genes. The Dot size reflects P values. The top 18 pathways for up- and down-regulation linked with DEGs in PTGS1 vs. control cells are shown in* ***(B)*** *and* ***(C)****, respectively. The folds of pathway enrichment had an inverse relationship with the bar chart length. The -log$_{10}$(FDR) scale was used to depict the route change levels. The number of genes is reflected in the dot size.*

5.3.6 Identification of the *PTGS2-regulated* genes in U937 cells by comparing the expression profiles between *PTGS2* model and control cells.

Finding the DEGs required comparing the gene expression profiles of U937 ^{PTGS2} with U937 control cells in order to assess the *PTGS2*-regulated genes in U937 cells. In total, 1015 genes were found to be elevated and 913 to be downregulated (**Figure 5. 10**). The heat map revealed that numerous genes' expression levels in control cells and *PTGS1* differed noticeably. **Table 5.3.3** includes information on the gene names, $\log_2$ fold change, and p-value for the top 34 genes that were either up-regulated or down-regulated, ranked by the magnitude of the differences.

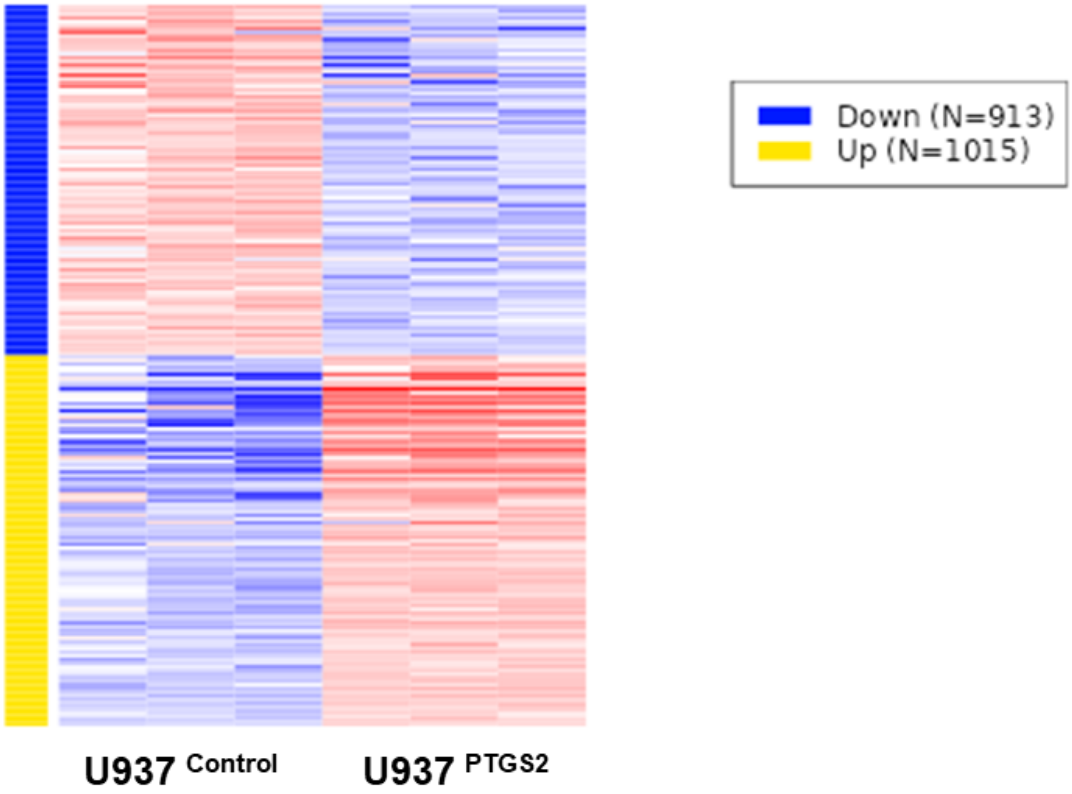

Figure 5. 10 Investigation of *PTGS2-regulated* genes by comparing expression profiles between the *PTGS2* over-expression and U937 control cells.

Perseus 1.6.8.0 software was used for data filtering using 2 of 3 biological replicates in at least one group. Subsequently, the top DEGs were graphically represented using the iDEP.96 platform. The top DEGs between PTGS2 over-expression and U937 control cells are displayed as a heat map. Red indicates upregulation, and green indicates downregulation.

Table 5. 3 The top DEGs genes for comparison between *PTGS2* model and U937 control.

Symbol	log_2 Fold Change	P value	Symbol	log_2 Fold Change	P value
GALM	-5.4	1.33E-10	***FCER2***	5.89	2.31E-46
EMP1	-5.21	2.18E-20	***CTBP2***	5.97	1.14E-97
MPO	-4.52	7.99E-128	***ANPEP***	6.1	1.33E-27
DHRS3	-4.35	2.00E-34	***IFT57***	6.11	2.70E-124
LY75	4.69	5.09E-07	***CNTNAP4***	6.31	2.41E-16
ITGAL	4.73	6.60E-90	***IL32***	6.49	2.40E-90
ZEB1	4.77	6.28E-37	***FCN1***	6.64	3.93E-82
NPDC1	4.84	6.21E-24	***NRIP3***	6.74	1.36E-09
SERPIN2	5.12	3.00E-12	***F2RL3***	7	1.39E-21
CCDC186	5.15	8.80E-23	***KRT2***	7.47	2.50E-07
MMP25	5.23	1.88E-21	***RAB31***	7.71	2.16E-143
PRRG4	5.26	7.91E-26	***TPSAB1***	7.89	2.95E-41
NXPH4	5.41	7.14E-14	***S100P***	7.97	2.10E-198
TGM5	5.64	1.41E-100	***TPSB2***	8.32	3.40E-55
CBR1	5.68	1.27E-14	***CST7***	8.52	1.86E-211
PITX1	5.74	7.77E-46	***VENTX***	8.78	3.20E-11
BARX1	5.85	4.07E-07	***HS3ST2***	9.55	4.09E-13

In a similar manner, a comparison of the gene expression profiles between U937^{PTGS2} cells and U937$^{\text{wild-type}}$ cells treated with cytarabine was carried out. With regard to these two cell types under treatment, this comparison sought to find genes that were differentially expressed. Intriguingly, it was discovered that 971 genes were upregulated and 950 genes were downregulated in the U937 ^{PTGS2} cells (as shown in **Figure 5. 11**). Significant variations in expression levels between the control and *PTGS1* model were seen when the differences in gene expression were shown graphically in a heat map. These results highlight the role of *PTGS2* in regulating multiple gene expression in the U937 cell line.

The top 34 upregulated genes and downregulated genes were chosen based on their respective levels of difference in order to study the most notable DEGs further. These genes are described in full in **Table 5.3.4**, which also includes their names, the $\log_2$ fold change and the p-value (which denotes the statistical significance of the changes).

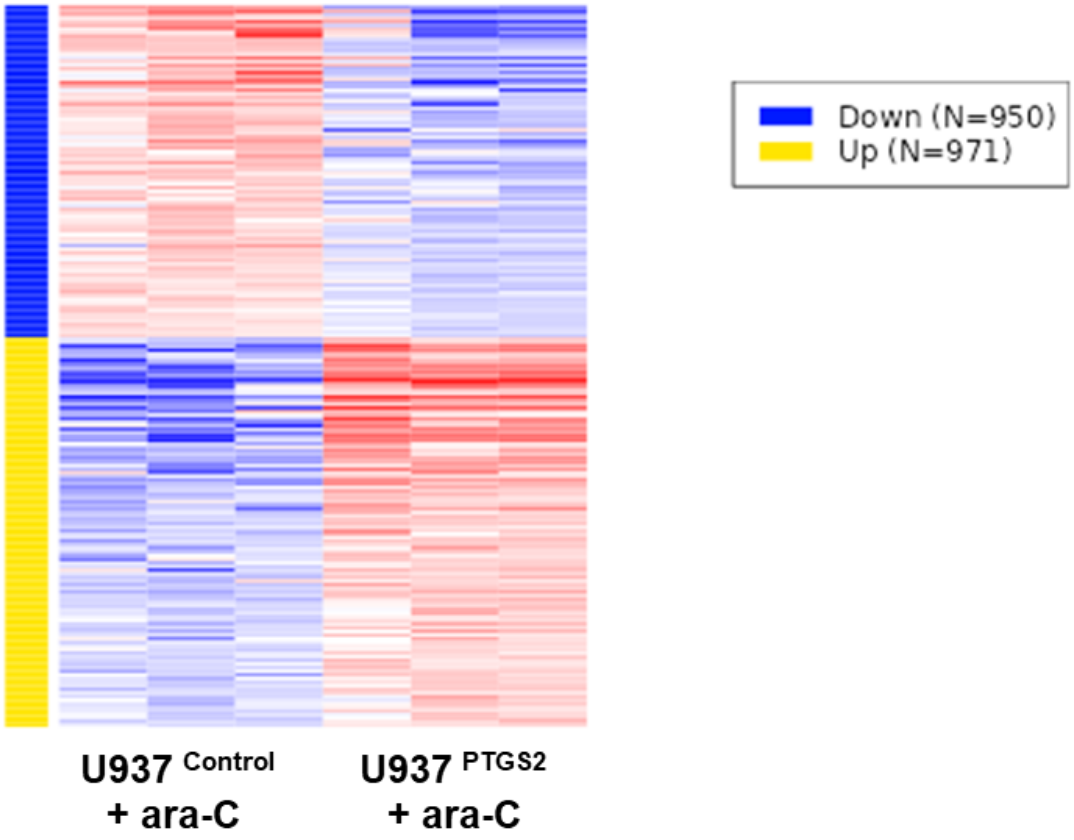

Figure 5. 11 Comprehensive analysis of PTGS1-dependent genetic responses to cytarabine in U937 Cells.

Data filtering was performed using 2 of every 3 biological replicates in at least one group using Perseus 1.6.8.0 software. The top DEGs were then obtained and visualized using the iDEP.96 platform. Following cytarabine treatment, the top DEGs between PTGS1 over-expression and U937 control cells were identified, and their expression profiles were visualised using a heatmap. In the heatmap, red indicates genes that are elevated, while green indicates genes that are downregulated.

Table 5. 4 The top DEGs genes for comparison between *PTGS2* model and U937 control under cytarabine treatment.

Symbol	log_2 Fold Change	P value	Symbol	log_2 Fold Change	P value
DKK1	-5.17	2.63E-03	***VWA5A***	6.02	1.36E-09
SCN4A	-5.14	1.02E-04	***ANPEP***	6.02	7.26E-08
SEPTIN11	-4.75	2.03E-14	***IFT57***	6.07	2.83E-14
MARCKSL1	-4.71	3.04E-09	***RAB13***	6.09	1.18E-08
KRT18	-4.67	1.28E-02	***CBR1***	6.13	1.30E-06
LMO1	4.59	1.56E-08	***CTBP2***	6.2	2.00E-13
CNTNAP4	4.59	3.04E-07	***AP3M2***	6.24	1.58E-09
PDK1	4.6	6.65E-11	***TPSB2***	6.76	1.16E-10
NXPH4	4.61	4.85E-09	***SERPINB2***	6.81	3.21E-07
KRT2	4.62	2.96E-07	***TPSAB1***	6.87	2.26E-09
C21orf62	4.66	2.76E-14	***RAB31***	7.12	3.01E-16
KIF21A	4.66	7.75E-09	***CBS***	7.14	1.19E-08
GSPT2	4.66	6.36E-07	***PRRG4***	7.43	8.32E-11
F2RL3	4.69	1.80E-07	***IL32***	7.48	1.15E-12
NKG7	4.7	5.54E-12	***CST7***	7.51	2.55E-24
ARNTL	4.75	1.86E-07	***NRIP3***	8.01	1.48E-08
PSTPIP2	4.86	7.93E-07	***PITX1***	8.22	2.63E-11

5.3.7 The Influence of *PTGS2* over-expression on GO of Biological Processes Enriched in DEGs between U937 control and U937 *PTGS2* overexpressed cells.

In this section, we thoroughly examined the alterations in gene expression brought on by *PTGS2* over-expression. Specifically, utilising the GO Biological Process-enrichment keywords, we looked into 1015 upregulated genes and 913 downregulated genes. The top 30 paths are then shown in **Figure 5. 12A**.

Surprisingly, our enrichment analysis provided crucial insights into the cellular processes and pathways that *PTGS2* specifically impacted. Among the interesting results were the connections between the differentially expressed genes (DEGs) and critical processes, including the up-regulation of immunological response, neutrophil degranulation, leukocyte degranulation, and granulocyte activation (**Figure 5. 12B**). However, there were negative relationships between the over-expression of *PTGS2* and critical processes such cell division, the cell cycle, and metabolic process. Excitingly, the analysis revealed that most DEGs play a key role in the immune response pathway. This demonstrates that *PTGS2* over-expression significantly affects the immune system and might aid in regulating immunologically-related activities and reactions in the cellular environment.

A

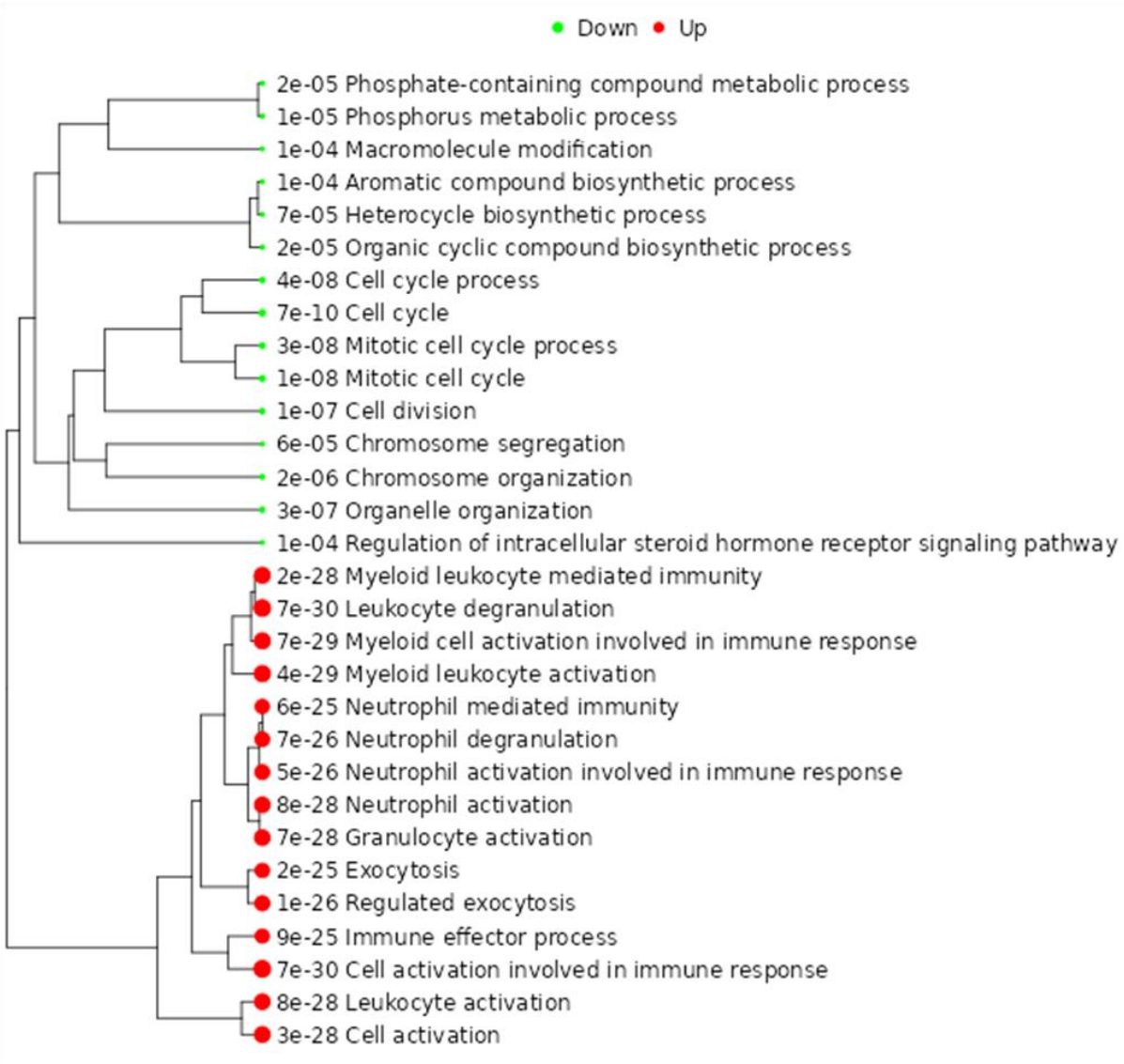
Down
Up
2e-05 Phosphate-containing compound metabolic process
1e-05 Phosphorus metabolic process
1e-04 Macromolecule modification
1e-04 Aromatic compound biosynthetic process
7e-05 Heterocycle biosynthetic process
2e-05 Organic cyclic compound biosynthetic process
4e-08 Cell cycle process
7e-10 Cell cycle
3e-08 Mitotic cell cycle process
1e-08 Mitotic cell cycle
1e-07 Cell division
6e-05 Chromosome segregation
2e-06 Chromosome organization
3e-07 Organelle organization
1e-04 Regulation of intracellular steroid hormone receptor signaling pathway
2e-28 Myeloid leukocyte mediated immunity
7e-30 Leukocyte degranulation
7e-29 Myeloid cell activation involved in immune response
4e-29 Myeloid leukocyte activation
6e-25 Neutrophil mediated immunity
7e-26 Neutrophil degranulation
5e-26 Neutrophil activation involved in immune response
8e-28 Neutrophil activation
7e-28 Granulocyte activation
2e-25 Exocytosis
1e-26 Regulated exocytosis
9e-25 Immune effector process
7e-30 Cell activation involved in immune response
8e-28 Leukocyte activation
3e-28 Cell activation

Figure 5. 12 A bar graph using the Gene Ontology Biological Process Enrichment shows the top 30 pathways connected to DEGs between PTGS1 and control cells.

ShinyGO 0.80 platform was used to generate the hierarchical clustering trees and the bar charts, representing enriched GO terms or pathways. ***(A)*** *On the tree, gene sets close by sharing more genes. The dot size reflects P values. The top 18 up-regulation pathways and the top 18 down-regulation pathways linked to DEGs in PTGS1 vs. control cells are shown in* ***(B)*** *and* ***(C)****, respectively. The folds of pathway enrichment were inversely linked with the length of the bar charts. -log$_{10}$(FDR) was used to show the levels of route alteration. The number of genes is indicated by the size of the dot.*

Determining how cytarabine affects the changes in gene expression brought on by *PTGS2* over-expression was another aspect of our goal. In the setting of *PTGS2* over-expression under the influence of cytarabine treatment, compared to control cells (wild-type cells treated with cytarabine), we focused on 950 downregulated genes and 971 up-regulated genes as a result of this investigation.

We carefully identified the functional implications of the changes in gene expression brought on by the combined effects of *PTGS2* over-expression and cytarabine treatment using the exacting GO Biological Process-enrichment analysis. The results were visually represented in **Figure 5. 13A**, which artfully shows the top 30 upregulated and downregulated pathways. Next, using the results of our study, we determined which pathways were the most significant. This made it possible to learn important things about the cellular processes and molecular pathways that *PTGS1* specifically altered.

The remarkable relationships between the differentially expressed genes (DEGs) and important processes, particularly the up-regulation of critical immunological responses, neutrophil degranulation, leukocyte degranulation, and granulocyte activation (as shown in **Figure 5. 13B**), were among the intriguing findings. These results imply that *PTGS2* over-expression may regulate the immunological response, possibly affecting inflammatory and immune cell activities.

PTGS2 over-expression, however, showed down-regulation of crucial cellular processes such as regulation of phospholipid efflux, protein phosphorylation,

and regulation of transferase activity (as shown in **Figure 5. 13C**), which is equally significant to highlight.

A

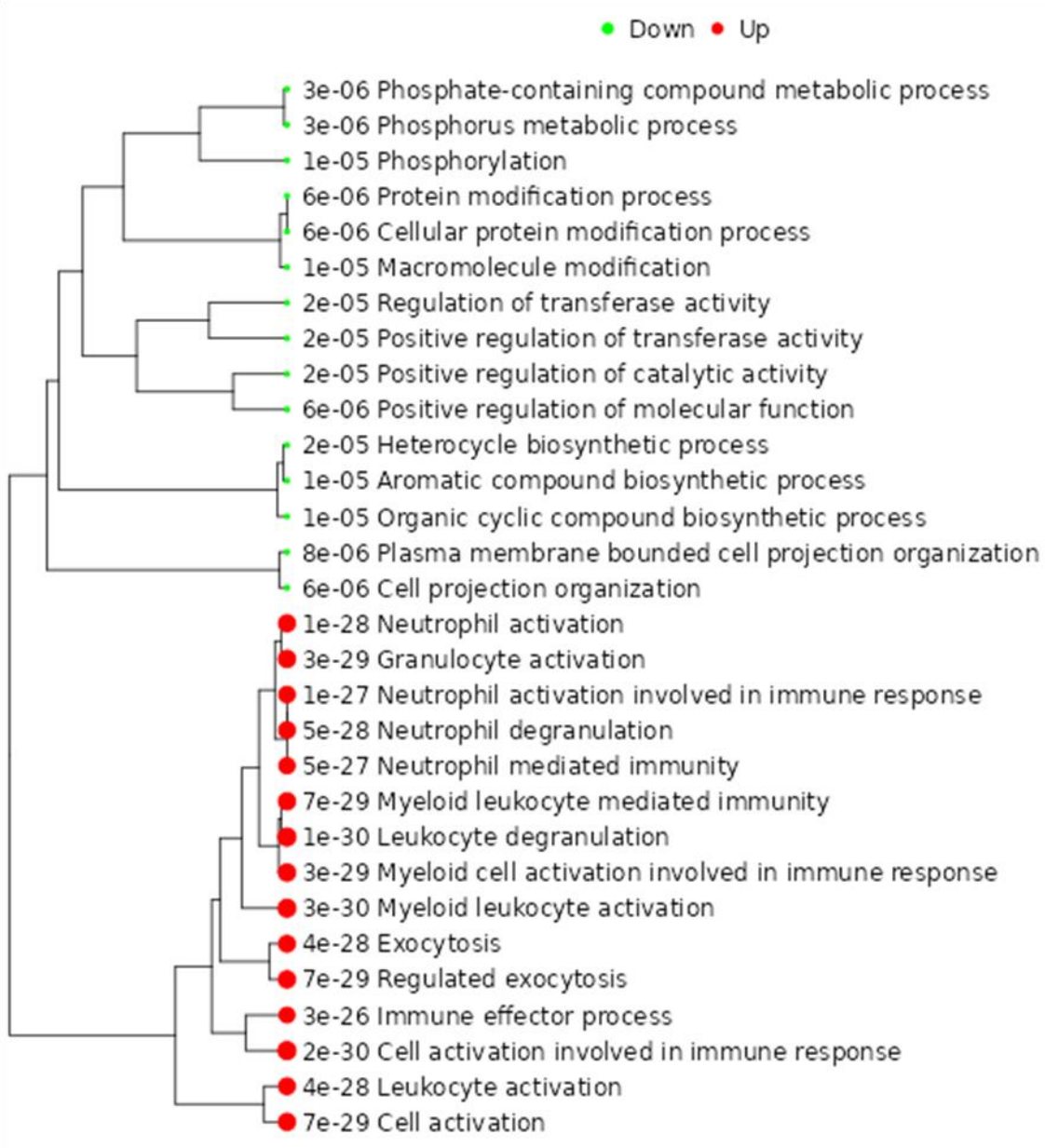
Down
Up
3e-06 Phosphate-containing compound metabolic process
3e-06 Phosphorus metabolic process
1e-05 Phosphorylation
6e-06 Protein modification process
6e-06 Cellular protein modification process
1e-05 Macromolecule modification
2e-05 Regulation of transferase activity
2e-05 Positive regulation of transferase activity
2e-05 Positive regulation of catalytic activity
6e-06 Positive regulation of molecular function
2e-05 Heterocycle biosynthetic process
1e-05 Aromatic compound biosynthetic process
1e-05 Organic cyclic compound biosynthetic process
8e-06 Plasma membrane bounded cell projection organization
6e-06 Cell projection organization
1e-28 Neutrophil activation
3e-29 Granulocyte activation
1e-27 Neutrophil activation involved in immune response
5e-28 Neutrophil degranulation
5e-27 Neutrophil mediated immunity
7e-29 Myeloid leukocyte mediated immunity
1e-30 Leukocyte degranulation
3e-29 Myeloid cell activation involved in immune response
3e-30 Myeloid leukocyte activation
4e-28 Exocytosis
7e-29 Regulated exocytosis
3e-26 Immune effector process
2e-30 Cell activation involved in immune response
4e-28 Leukocyte activation
7e-29 Cell activation

Figure 5. 13 The top 30 pathways associated to DEGs between PTGS2 and control cells treated with cytarabine are shown in a bar graph using the gene ontology biological process enrichment.

*The hierarchical clustering trees and the bar charts, representing enriched GO terms or pathways were obtained by ShinyGO 0.80 platform**. (A)** Adjacent gene sets on the tree share more genes. P values are reflected in dot size. In PTGS1 vs. control cells, the top 18 pathways for up- and down-regulation associated with DEGs are depicted in **(B)** and **(C)**, respectively. The length of the bar chart was inversely related to the folds of route enrichment. The -log10(FDR) scale represented the route change levels. The size of the dots corresponds to the number of genes.*

5.3.8 Cell surface antigen profiles in response to *PTGS1/2* expression modulation

In an effort to confirm the findings from our NGS data, we study the expression of specific cell surface antigens that may be involved in altered immune signalling in AML upon *PTGS*1/2 expression. Our analysis showed that CD86 and CD33, both essential in immune interactions and cellular signalling, exhibited no significant changes between *PTGS*1 or *PTGS2* modulated conditions and the wild-type (wild-type) cells in U937 cell lines. This outcome provided additional evidence that *PTGS1* or *PTGS2* modulation might not substantially impact the expression of these antigens. Conversely, our investigation into the human leukocyte antigen (HLA) complex, encompassing HLA-A, HLA-B, and HLA-C subtypes, revealed a significant decrease in expression upon the over-expression of *PTGS*1 or *PTGS*2. This result concurred with the trends from our NGS data and suggested a potential downregulatory role of increased either *PTGS*1 or *PTGS*2 levels on the HLA-mediated immune recognition pathway. Furthermore, our study displayed a significant increase in CD52 expression upon over-expression of either *PTGS*1 or *PTGS*2 (**Figure 5. 14A**).

Similarly, in HL-60 cells, we observed no changes in CD33 and CD86 expression between *PTGS*1 or *PTGS*2 modulation and the wild-type condition. Notably, there was a minor decrease in the HLA-A, HLA-B, and HLA-C antigens upon over-expression of *PTGS*1 or *PTGS*2. This slight decrease maintained the trend seen in U937 cells, reinforcing the potential impact of *PTGS*1/2 on the HLA-mediated immune recognition pathway. Similarly, we noted a small increase in CD52 expression upon *PTGS*1 or *PTGS*2 over-expression,

mirroring the pattern observed in AML-3 cells (**Figure 5. 14B**). This finding supported our NSG findings and hinted at an intricate association between *PTGS* enzyme expression and CD52, likely impacting immune modulation and intercellular communication pathways.

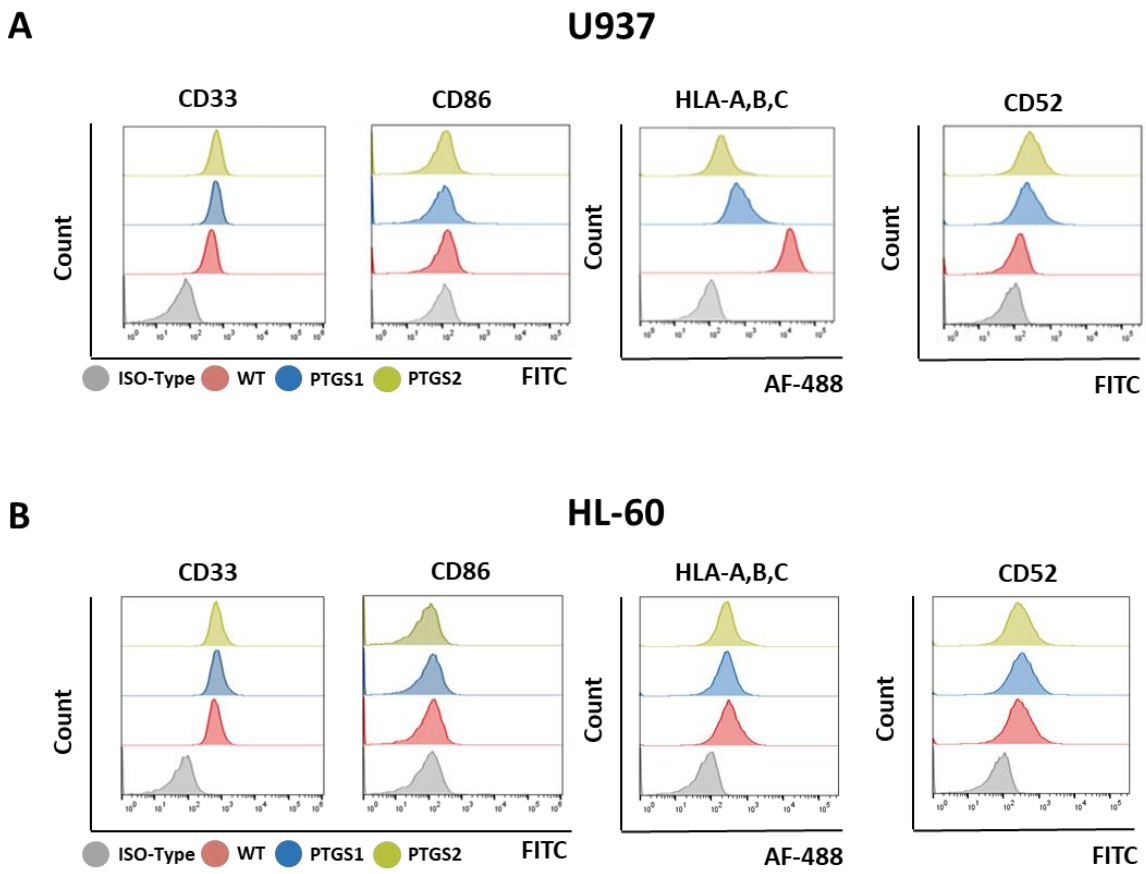

Figure 5. 14 Cell Surface Antigens expression changes upon PTGS1/2 expression changes.

*AML cell lines (**A**) U937and (**B**) HL60, with PTGS1 and PTGS2 overexpression, were stained with fluorophore-conjugated antibodies against the CD33, CD86, HLA-A, B, C or CD52. The cells were stained with 1 µg of CD marker antibody or 2.5 µg of an isotype control antibody for 20 min before being washed once with PBS. Pellets were re-suspended in PBS, and cells were analysed by flow cytometry using FlowJo™ v10 Software. Plots show FITC, or Alexa flour-488 signal corresponding to surface antigen expression.*

5.3.9 Suppression of CD8 T-Cell proliferation in AML cell lines upon *PTGS1/2* overexpression

To further substantiate the validity of our NGS findings, we investigated the impact of *PTGS1/2* overexpression on AML cell interaction with the immune system, beginning with *in vitro* T-cell proliferation. Our study showed that the over-expression of *PTGS*1 or *PTGS2* led to a pronounced inhibition of T-cell proliferation (**Figure 5. 15**). Specifically, in U937 cell line, our results indicated that control cells exhibited a proliferation rate of 62.6%, while cells with *PTGS*1 over-expression displayed a markedly reduced proliferation rate of 50.1%. We also examined the effects of *PTGS*2 over-expression on T-cell proliferation, revealing a further reduced proliferation rate of 31.9% (**Figure 5. 15C**).

Similarly, in HL-60 cell line, our results showed that control cells exhibited a proliferation rate of 33%, while cells with *PTGS*1 over-expression demonstrated a markedly reduced proliferation rate of 28%. We also examined the effects of *PTGS*2 modulation on T-cell proliferation, revealing a further reduced proliferation rate of 27.4% (**Figure 5. 15D**). This aligned seamlessly with the trends we initially observed in our NGS data, effectively reinforcing the robustness of our initial findings.

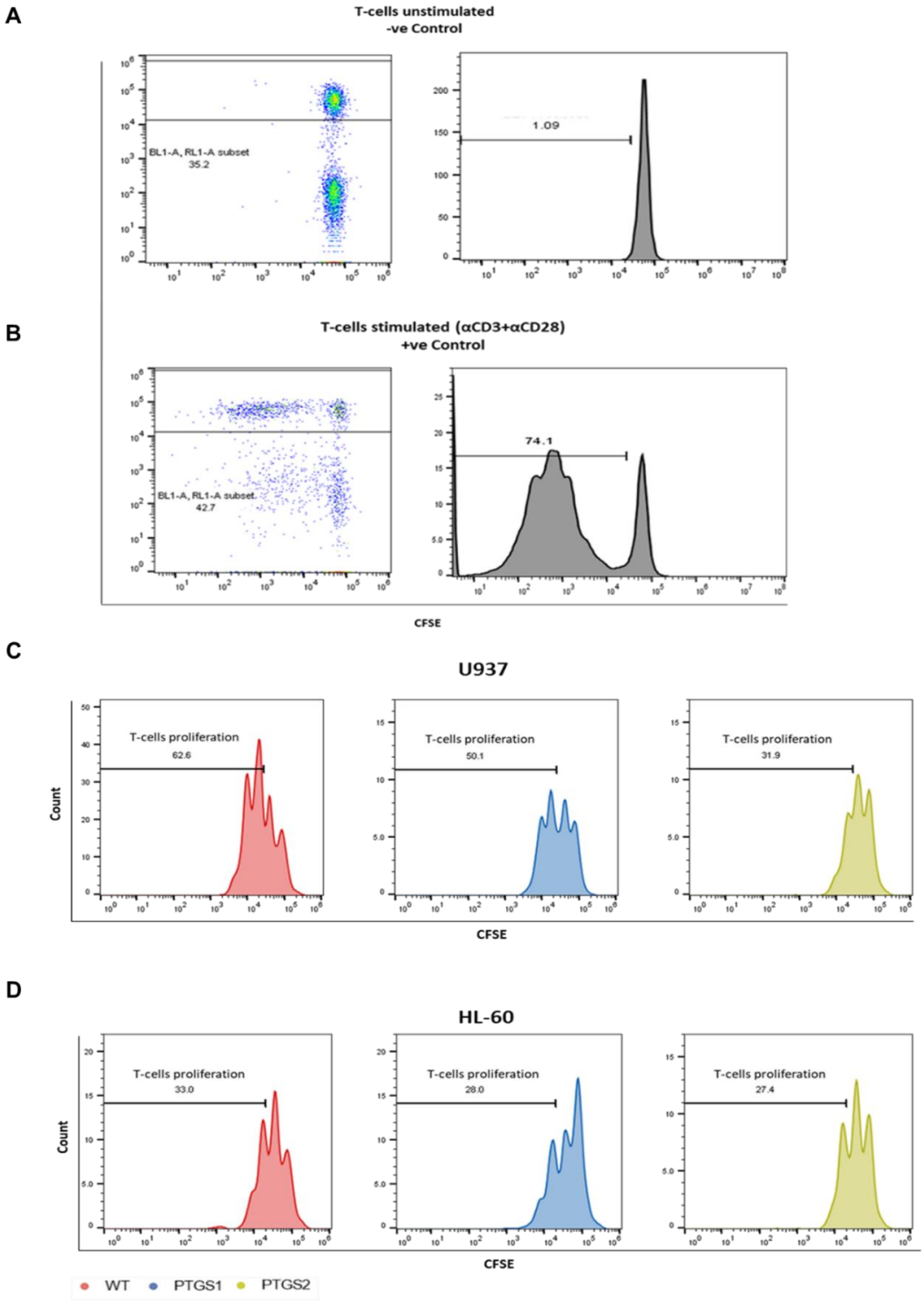

Figure 5. 15 PTGS1/2 over-expression supress CD8 T-cell proliferation in AML cell lines.

*PBMCs Purified T-cells cultured **(A)** unstimulated (negative control) or **(B)** stimulated with αCD3+αCD28 (positive control). Either **(C)** PTGS1 or **(D)** PTGS2 inhibit the proliferation of the CD8+ve T-cell in both U937 and HL-60 cell lines. The results were analysed by flow cytometry using FlowJo™ v10 Software.*

5.4 Discussion

Major Findings Summary:

This chapter investigated the effects of overexpressing PTGS1 and PTGS2 on RNA expression in cell models. It found that immunological activation and degranulation processes were upregulated, whereas biosynthetic pathways were downregulated. Disparities with earlier results may be explained by timing variances, even though the top protein MPO was unexpectedly shown to be downregulated. Cytarabine treatment essentially had no influence on these outcomes. The investigation did not allow for in-depth comparisons, but it did offer a general summary of the affected processes. By assessing the expression of pertinent surface molecules, the validity of some expression changes was verified. Lastly, the effects on T cell contacts were evaluated, establishing a connection between modifications in immune activation and particular mechanistic changes in a subset of molecules that control immune cell signalling.

Discussion:

Transcriptomics refers to the field of study centring on the transcriptome, as the entire RNA transcript set which the genome of a cell or larger organism generates: i.e., what is expressed by the total set of genes. The development of NGS has been transformative for transcriptomics, enabling multi-dimensional analysis of the RNA contents within cells with high throughput and lowered cost (Morozova et al. 2009). RNA-seq forms a highly effective technique in identification of differential transcript expression across specific biological mechanisms, capable of uncovering novel biomarkers which can support

researchers in discovering and developing new pharmaceutical agents (Yang et al. 2020). RNA-seq allows the transcriptome to be analysed in detail, and novel variations in transcripts to be detected (Byron et al. 2016). As part of this, comprehensive data on the genome for AML, among other cancers, has been generated through the Cancer Genome Atlas (TCGA) project. The data offers insight into the processes which underpin AM at molecular level, leading to the identification of possible targets for therapies as well as biomarkers to inform diagnostic and prognostic work (Anaparthy et al. 2019). Other applications of A-seq have uncovered likely targets in individually-tailored therapeutic interventions for AML: for example, protein kinase FLT3, showing mutations across a percentage of individuals with AML (Morozova et al. 2009), in addition to various novel AML prognostic biomarkers (Dzneladze et al. 2015).

The current study utilised two cell lines of AML: U937 and HL60, which differ in their genetic and molecular profile in ways which may have a significant impact on response when *PTGS1* is inhibited. HL60's NPM1 mutation for example might contribute significantly to this cell line's different response. The differential expression of MYC as a classic proto-oncogen across the two lines is interesting. Upregulation of MYC by PGE2 has previously been established (Krysan et al. 2014), leading to the investigation in this study of whether AML phenotypes driven by PGE2 depend on MYC. The modelling suggests pre0existing over-expression of MYC by HL60 cells, with the possibility that regulation of this expression follows different mechanisms in the two cell lines. A comparison of signalling was therefore conducted, investigating the HL60 cells as an MYC-dependent AML cell line as opposed to the U937 cell line in which upregulation of MYC signalling could occur through PGE2.

An unexpected alteration noted in U937 cells was a significant shift in transcription networks linked to immunological activities. A number of different cells, such as neutrophils, leukocytes and granulocytes, form the basis for innate immune responses, as they co-operatively contribute to immune function, removing pathogenic materials and maintaining homeostasis. They are capable of rapid migration to infection sites, and show a number of types of effector function, including degranulation in neutrophils and leukocytes, activation of granulocytes and exocytosis, as well as immune responses subject to regulation via *PTGS1*. Such mechanisms can lead granular content to be released, including antimicrobial peptides, ROS and proteases into phagosomes or the spaces between cells, and their cause degradation or destruction of the pathogen. These mechanisms are also capable of modifying inflammatory responses through the release of mediators such as cytokines and chemokines, then activating and recruiting further immune cells (Capucetti et al. 2020; Gierlikowska et al. 2021; Margraf et al. 2022). The significant control of immune response attributed to such pathways implies their prime importance in the clinical setting. Resistance to cancer therapies is due at times to the inadequate function of immune cells in identifying and destroying cancer cells. Moreover, in cancer cells, the immunological pathways utilised have complex relations to progression of the cell cycle, which they are capable of influencing. When these mechanisms become dysregulated, frequently under the influence of PGE2 and other molecules, poorer therapeutic outcomes are seen. PGE2-caused activation of EP2 and EP4 as G protein-coupled receptors alter the functioning of myeloid immune cells, including dendritic cells and macrophages. EP2 and EP4 signalling increases cyclic adenosine monophosphate (cAMP)

level within the cell because Gs protein is stimulated. In addition, EP4 links with the inhibitory Gi protein, reducing synthesis of cAMP.

The results presented point to the potential impacts of over-expressed *PTGS1* upon immune system function, and possible contribution to regulating functions related to this, as well as response within the cellular environment. The implications of such advances are highly significant to future understandings of the complex ways that *PTGS1* interacts with immunological functions. AA is converted to form the established immunomodulatory lipid mediator PEG2 by both PTGS1 and 2 enzymes. It is known that PGE2 blocks NK and T-cells and other immune effector cells, as well as promoting suppressor immune cell development, which thus suppresses anti-tumour immune function (Kalinski 2012; Bödder et al. 2023). Further knowledge of the functions of *PTGS1* in relation to the immune system is needed in order to uncover further mechanisms underpinning oncogenesis and development of cancers. A clear picture of the ways in which *PTGS1* influences immunological activity might open up further directions in cancer research and lead to new therapeutic approaches, based on the immune system's centrality for monitoring and combatting tumours. This chapter is an exploratory investigation of altered processes and their potential immune implications, even though these findings offer fascinating insights into immune cell implications. However, a clear connection to earlier findings regarding cell maturation or chemotherapy sensitivity is still lacking.

Chapter VI

General Discussion

Building on our significant findings, it is clear that *PTGS1* is essential for the control of haematological processes and the advancement of AML. As noted in Chapter 1, the association between increased *PTGS1* expression and lower overall survival in AML patients provides context for comprehending its functional implications. Mechanistic insights are presented in Chapter 2, where it is demonstrated that *PTGS1* overexpression enhances WNT signalling, PGE2 secretion, and resistance to cytarabine. This could account for some of the reported clinical outcomes in patients with elevated *PTGS1* expression. Furthermore, as discussed in Chapter 3, the unique transcriptome alterations induced by *PTGS1* and *PTGS2* emphasize the importance of developing a comprehensive knowledge of the functions these genes perform in AML.

Our research has involved bioinformatics work to analyse published datasets, yielding important insights into *PTGS1's* function in HSCs, along with what this implies in AML. Importantly, greater expression of *PTGS1,* but not *PTGS2*, is seen in connection with HSCs but this is slowly reduced as myeloid progenitor cells progress towards committing to a lineage. It is notable that although increased expression of *PTGS2* is not associated with poorer survival rates for AML as observed in datasets including TCGA and Verhaak, greater expression of *PTGS1* is strongly associated with reduction in survival. Moreover, research in vitro also points to the central importance of *PTGS1,* the inhibition of which by Tenidap or SC-560 significantly influenced suppression of cell growth, as well as stimulating apoptosis and inducing cell cycle arrest. These findings support the possibility of targeting PTGS1 therapeutically, and suggest the need for more research to establish *PTGS1's* functions. In AML cells, greater expression of *PTGS1* is associated with higher WNT signalling levels and

increased generation of PGE2, as well as partial reversal of *PTGS1* inhibitor activity. In addition, lower ROS generation is associated with *PTGS1* resistance mediated by Cytarabine. Notably, specific transcriptome alterations occurring when *PTGS1* and *PTGS2* are over-expressed in AML give an avenue to understanding the variable outcomes found clinically for cases of AML in which this over-expression is present. The findings in this area are unexpected in suggesting that *PTGS1* and *PTGS2* have differential transcriptome regulation. While the findings might imply that *PTGS1* and *PTGS2* have other functions than producing PGE2, caution in interpretation is needed, as PGE2 was produced in subcellular *PTGS1/2* localisation. Taken overall, the findings emphasise the complexity of *PTGS1's* roles within AML, as well as the potential for targeting in novel therapies, and further studies are required to address these points.

The study findings are significant for AML patients, and particularly in the areas of addressing resistance to chemotherapies and in survival. This research offers intriguing new findings related to the role of *PTGS1* in AML, in which over-expression has a strong association with reduced overall survival, despite the fact that these are not directly correlated. The implication of this is that *PTGS1* could prove to be an effective marker for prognosis. This study also focuses attention on the important association linking *PTGS1* to AML chemotherapy resistance. A reduced ROS generation level is also linked to higher *PTGS1* expression, and especially when considering cytarabine resistance. Reduced chemosensitivity in AML cells is explainable through this mechanism, and so *PTGS1* could be targeted in order to sensitise cells to chemotherapy. We therefore conclude that *PTGS1* has the potential to be clinically significant for

AML, and strategies to target it might improve survival and reduce chemotherapeutic resistance, broadening the range of treatment options and bringing hope to patients. However, for the findings here to be validated and translated into effective therapies, further clinical research is needed.

NGS has transformed genomics and contributed significantly to biomedical knowledge, as a reliable, high-throughput technique used to elucidate highly complex systems such as the genome and transcriptome. NGS allows for rapid, comparatively inexpensive sequencing of DNA and RNA, pushing analysis further than previously feasible. In investigating cancer, these attributes have facilitated broad explorations across the whole range of changes to genes in cancer, including variation in number of copies, mutations, and structurally rearranged areas underpinning tumorigenesis and cancer progression. NGS facilitates identification of mutations associated with poorer outcomes, treatment resistance and phenotypic aggressiveness of disease through allowing close examination of the genomics of cancer cells. In addition, NGS has brought completely new understandings of the transcriptome, allowing for exact measurement of the level at which genes are expressed.

High levels of precision are needed to identify biomarkers for a poor prognosis. Analysis of patterns of gene expression over large samples of individuals with cancer can reveal genetic signatures or genes as biomarkers which correlate with severe disease, therapeutic resistance or likelihood that a tumour will metastasise. Such markers form a vital tool for evaluating risks and choosing interventions. Moreover, NGS has facilitated the discovery of biomarkers which are challenging to uncover via previous sequencing approaches, including epigenetic alterations, non-coding RNAs, and fusion genes. Such novel

discoveries open new areas for targeting through therapies and increase understandings of molecular mechanisms in cancer progression.

Future work

Advanced *in vitro* models:

For accurately simulating the complex tumour microenvironment, advanced *in vitro* models must be developed. Co-culture systems with stromal cells, immunological effectors such T cells, NK cells, and macrophages, or endothelial cells can offer priceless insights into the complex interactions between cancer cells and their environment. Such models can give light on the broader effects of *PTGS1/2* by clarifying the processes of immune evasion and angiogenesis regulation.

Multi-Omics methodologies:

Combining NGS data with other omics techniques like proteomics, metabolomics, and epigenomics can provide a comprehensive view of the molecular environment. Our understanding can become more nuanced as a result of this method's ability to reveal post-transcriptional and post-translational alterations that affect *PTGS1/2* activity and downstream pathways.

***In vivo* models:**

Moving from cell lines to *in vivo* models, particularly AML mice models like MLL-AF9, has the potential to provide a more thorough knowledge of the involvement of PTGS1/2 in disease progression. With the aid of these models, it is possible to assess how PTGS inhibitors affect vital aspects such tumour growth, the spread of metastatic lesions, and interactions with the immune system.

Appendix

Table A. 1 Table of abbreviations are used.

Abbreviation	Cell type
HSC	Haematopoietic stem cell
MPP	Multipotential progenitors
CMP	Common myeloid progenitor cell
GMP	Granulocyte monocyte progenitors
MEP	Megakaryocyte-erthyroid progenitor cell
Early PM	Early Promyelocyte
Late PM	Late Promyelocyte
MY	Myelocyte
MM	Metamyelocytes
BC	Band cell
PMN	Polymorphonuclear cells
Mono	Monocytes

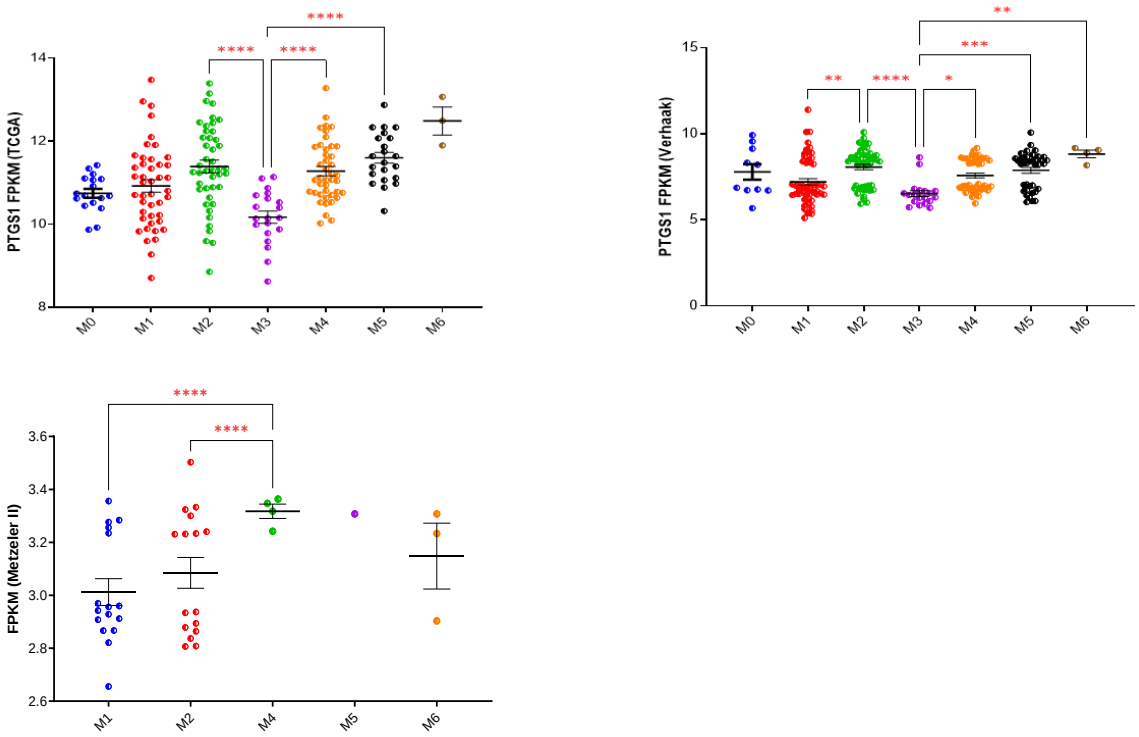

Figure A. 1 PTGS expression across AML FAB classification.

*Two-way ANOVA significance testing was conducted using Sidak's multiple comparisons test. Values are displayed as the log_2 transformed mean value. Legend is as following: ^{ns} p: non-significant, * p < 0.05, ** p < 0.01, ***p < 0.001 and ****p < 0.0001.*

Table A. 2 Statistical test for an overall difference between FAB classification

Dunnett's multiple comparisons test	95.00% CI of diff.	P Value
M1 vs. M2	-1.520 to -0.2082	0.0023
M2 vs. M3	0.6384 to 2.445	<0.0001
M3 vs. M4	-1.971 to -0.1262	0.0147
M3 vs. M5	-2.297 to -0.4090	0.0006
M3 vs. M6	-4.148 to -0.4513	0.005
M0 vs. M5	-1.666 to -0.04888	0.0298
M0 vs. M6	-3.310 to -0.1742	0.0188
M1 vs. M3	0.07628 to 1.427	0.0185
M1 vs. M5	-1.334 to -0.02668	0.0354
M1 vs. M6	-3.059 to -0.07113	0.0334
M2 vs. M3	0.5456 to 1.896	<0.0001
M3 vs. M4	-1.790 to -0.4295	<0.0001
M3 vs. M5	-2.205 to -0.6584	<0.0001
M3 vs. M6	-3.867 to -0.7664	0.0003

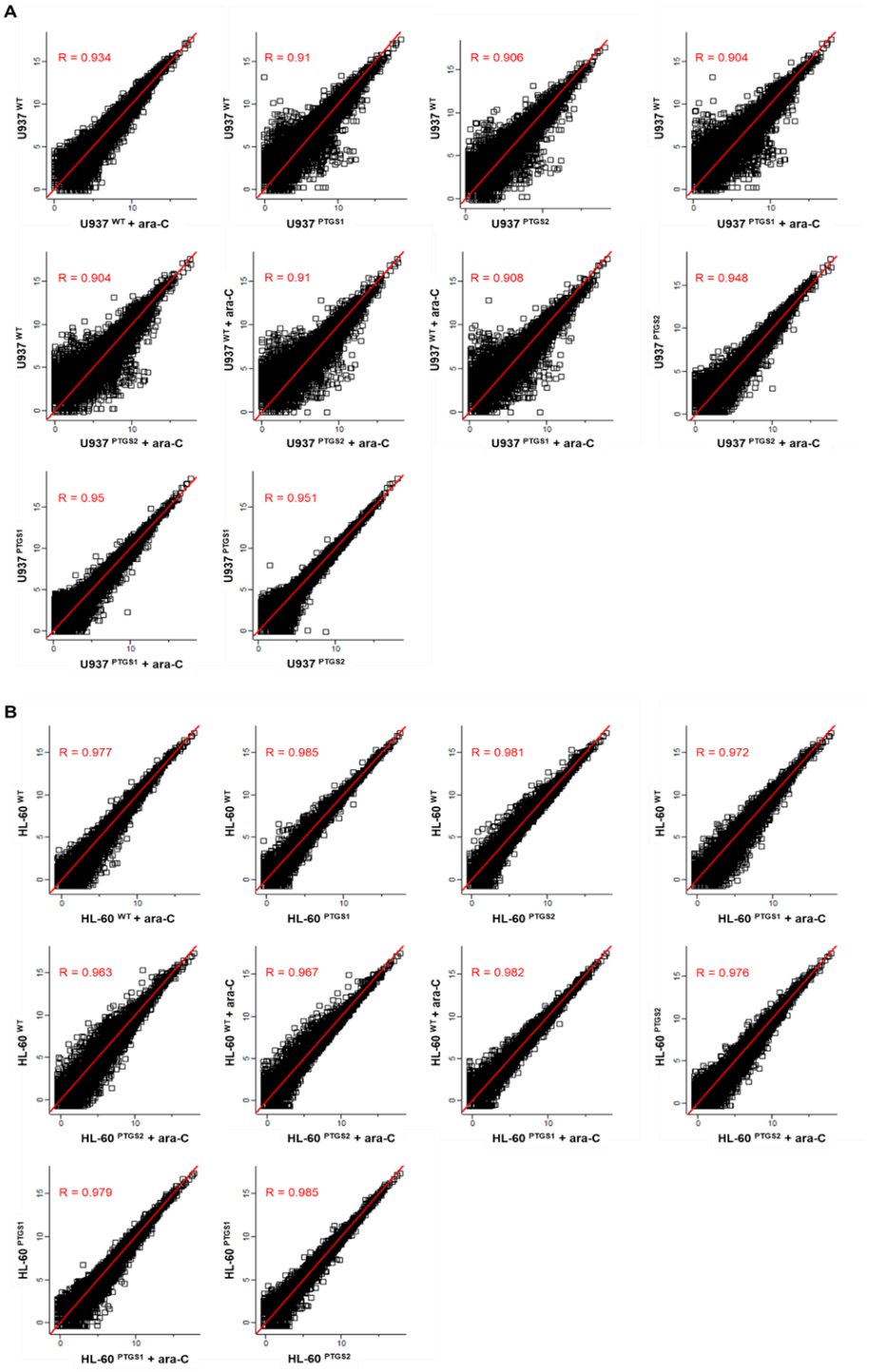

Figure A. 2 Pearson Correlation analysis reveals relationships between control cells and PTGS1/2 over-expression models.

Scatter plots exhibit Pearson Correlation (R) between these three cell lines in both ***(A)*** *U937 and* ***(B)*** *HL-60. The values of X and Y axes in the scatterplot are the averaged normalized values of three replicate (log_2 scaled). The plot reveals a strong positive correlation between PTGS1 and PTGS2. Perseus 1.6.8.0 software was used to generate scatterplots.*

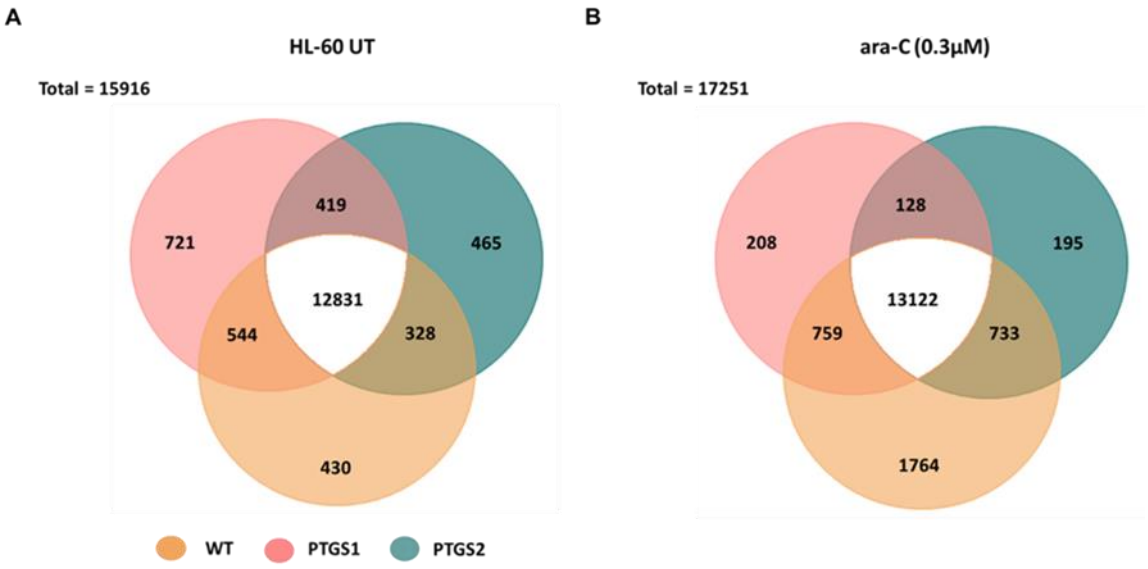

Figure A. 3 Venn Diagram insights into overlapping genes across Hl-60 control cells and PTGS1/2 cells

*The Venn diagram displays the gene expression overlaps across three distinct cell lines, including U937 wild-type, U937 PTGS1, and U937 PTGS2. This graphic shaded light on the similarities and differences in gene expression patterns between the **(A)** untreated and **(B)** cytarabine-treated conditions. Perseus 1.6.8.0 software was used for data filtering, enabling the exclusion of irrelevant or low-quality data points from the dataset. Then, the iDEP.96 platform was employed to visualise the relationships between these cells through Venn diagrams.*

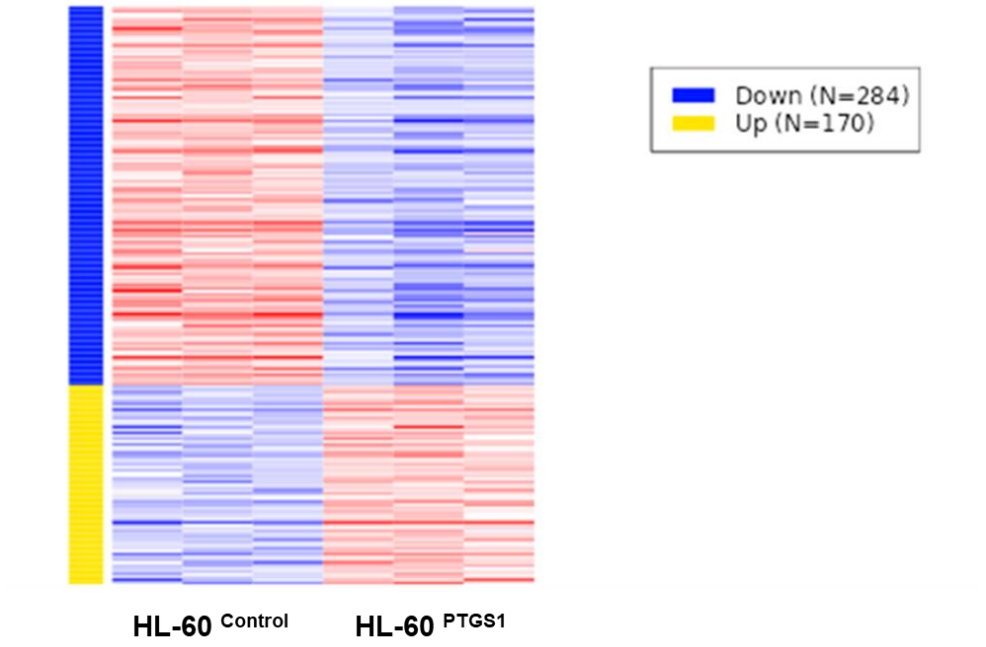

Figure A. 4 Investigation of PTGS1-regulated genes by comparing expression profiles between the PTGS1 over-expression and HL-60 control cells.

To evaluate the PTGS1-regulated genes in HL-60 cells, a comparison of the gene expression profiles between the HL-60 control cells and HL-60 PTGS1 cells was performed in order to find the DEGs. The top DEGs between PTGS1 over-expression and HL-60 control cells are displayed as a heat map. Red indicates upregulation and green indicates downregulation. 170 upregulated and 284 downregulated genes were identified. The heat map showed that the expression levels of many genes in control cells were significantly different from those in PTGS1.

Table A. 3 The top DEGs genes for comparison between HL-60 control and *PTGS1* cells

Symbol	log2 Fold Change	P value	Symbol	log2 Fold Change	P value
MTLN	-3.59	8.91E-04	***EMILIN2***	-1.79	1.16E-05
GNB2	-2.65	5.79E-03	***CD38***	-1.77	7.11E-03
PRC1	-2.54	2.90E-02	***FH***	-1.76	6.35E-03
CDK14	-2.39	3.39E-09	***NECTIN1***	-1.7	2.19E-03
PLAUR	-2.27	6.38E-03	***MYD88***	-1.68	9.39E-02
FGFR1	-2.2	2.12E-04	***C16orf74***	-1.65	5.45E-02
DUSP7	-2.1	2.57E-03	***CMC2***	-1.65	1.56E-02
LAX1	-2.1	8.64E-05	***MAP2K1***	-1.62	2.62E-02
NDUFB3	-2.08	1.66E-04	***PARP12***	-1.58	2.62E-02
KDM7A	-2.07	7.02E-07	***CD96***	-1.55	6.58E-05
TAP2	-2.06	4.18E-03	***EBPL***	-1.54	5.11E-04
EIF2D	-1.96	9.48E-03	***ITGAM***	1.48	4.31E-03
TSC22D4	-1.91	1.03E-02	***S100A9***	1.54	2.50E-03
PSMA5	-1.9	2.16E-02	***CD84***	1.63	7.98E-05
SRP9	-1.89	3.08E-02	***PLCB1***	1.92	3.36E-04
DERA	-1.87	5.86E-02	***TGM5***	2.34	4.08E-09
COMT	-1.85	8.64E-05	***CYBB***	2.52	6.99E-11

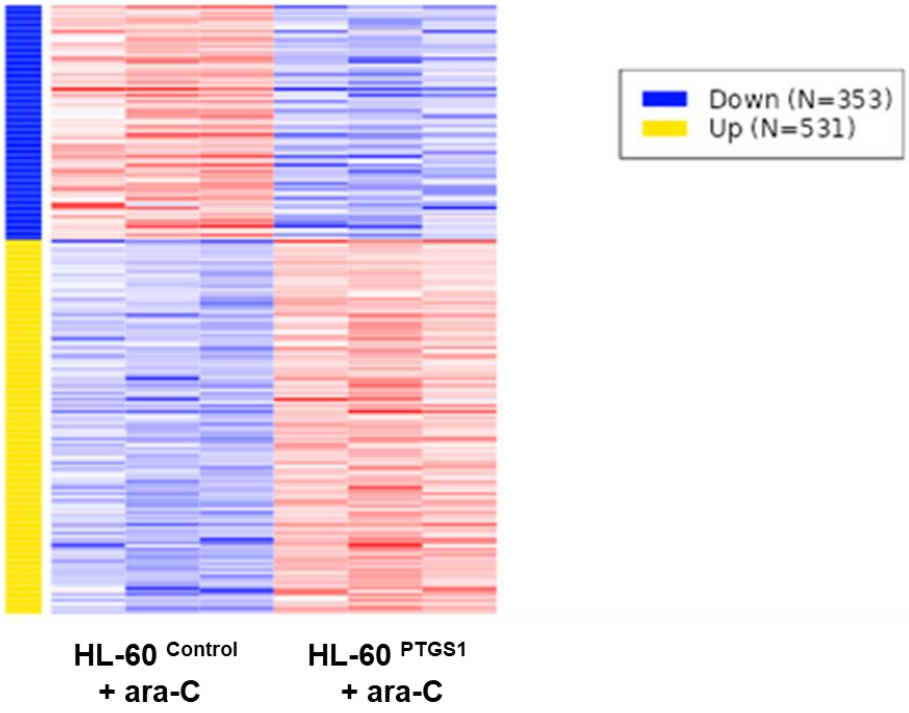

Figure A. 5 Comprehensive analysis of PTGS1-dependent genetic responses to cytarabine in U937 Cells.

Following cytarabine treatment, the top DEGs between PTGS1 over-expression and HL-60 control cells were identified, and their expression profiles were visualised using a heatmap. This comparison aimed to detect differentially expressed genes between these two cell types in cytarabine condition. Remarkably, a total of 531 genes were found to be upregulated, while 353 genes were downregulated in the HL-60 PTGS1 cells in the heatmap, red indicates genes that are elevated while green indicates genes that are downregulated.

Table A. 4 The top DEGs genes for comparison between U937 control and *PTGS1* cells in cytarabine treatment.

Symbol	log_2 Fold Change	P value	Symbol	log*2* Fold Change	P value
ANXA2	-2.69	6.22E-02	***MELTF***	-1.74	3.73E-02
RAB13	-2.46	3.96E-02	***NDUFB3***	-1.73	7.03E-03
PALLD	-2.33	3.18E-02	***NPAS1***	1.38	8.92E-02
LGALS3	-2.33	2.26E-02	***ADGRE1***	1.41	5.55E-02
CDK14	-2.26	1.01E-07	***NCF1***	1.42	5.03E-02
LAX1	-2.24	3.67E-04	***BCOR***	1.52	3.03E-05
GNB2	-2.17	8.36E-02	***S100A9***	1.55	1.24E-02
NRP2	-2.17	1.64E-02	***PLCB1***	1.66	2.40E-02
TTC7B	-2.08	1.45E-03	***AOAH***	1.69	2.44E-02
KRBA1	-2.01	3.66E-02	***CD37***	1.71	4.18E-03
PCSK5	-1.94	2.40E-02	***FGR***	1.71	1.25E-03
TSC22D4	-1.92	3.20E-02	***CDA***	1.74	5.77E-04
EPHB4	-1.88	4.64E-02	***HSPA1L***	1.82	7.78E-03
WRAP73	-1.88	8.31E-02	***TGM5***	1.83	1.91E-05
SERPINB10	-1.86	3.45E-02	***ANKRD50***	1.85	6.22E-02
CD96	-1.76	5.28E-05	***IGFBP2***	2.09	2.78E-02
SEMA3A	-1.76	7.19E-02	***CYBB***	2.28	2.51E-08

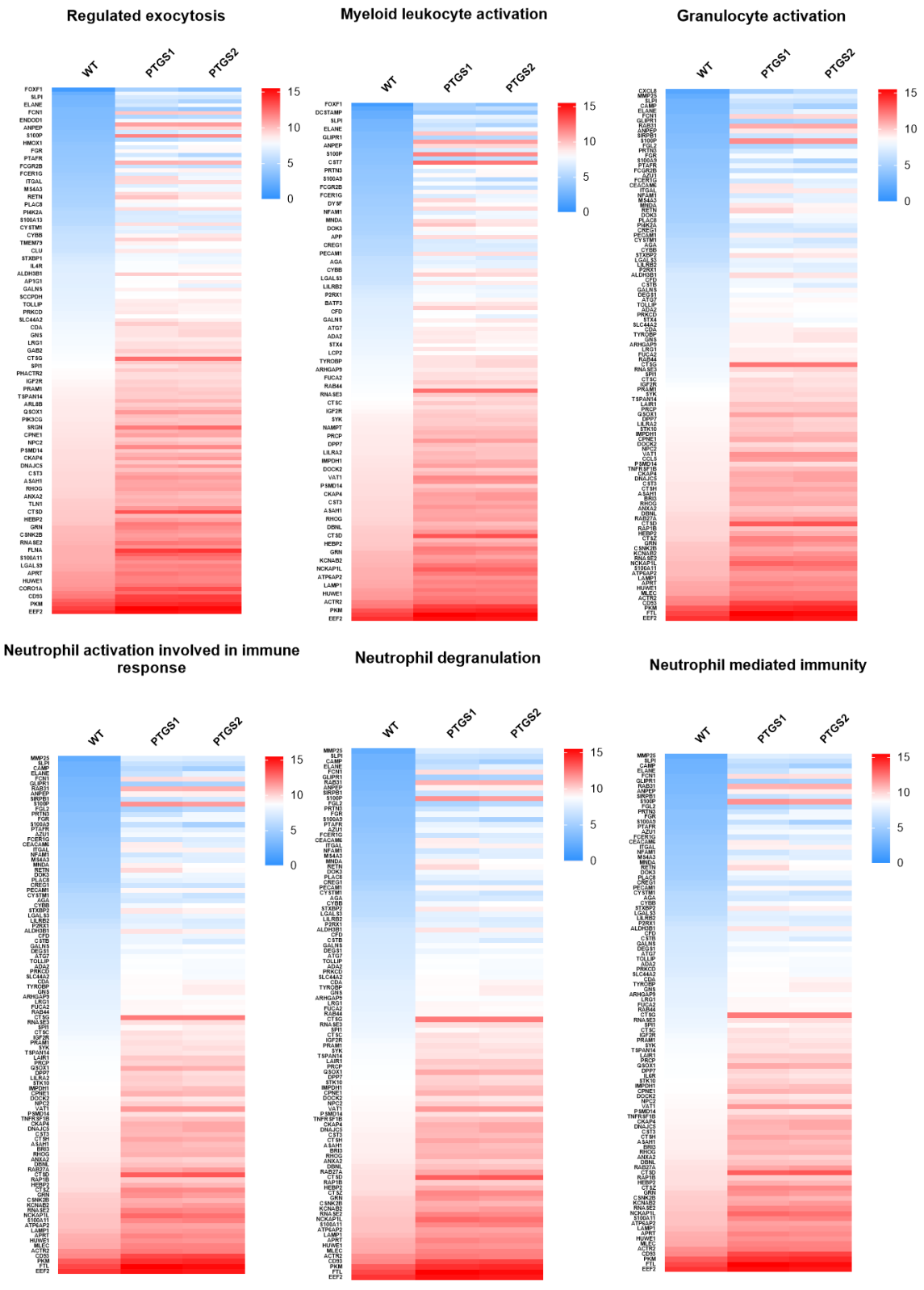
Regulated exocytosis
Myeloid leukocyte activation
Granulocyte activation
Neutrophil activation involved in immune response
Neutrophil degranulation
Neutrophil mediated immunity
WT
PTGS1
PTGS2
15
10
5
0

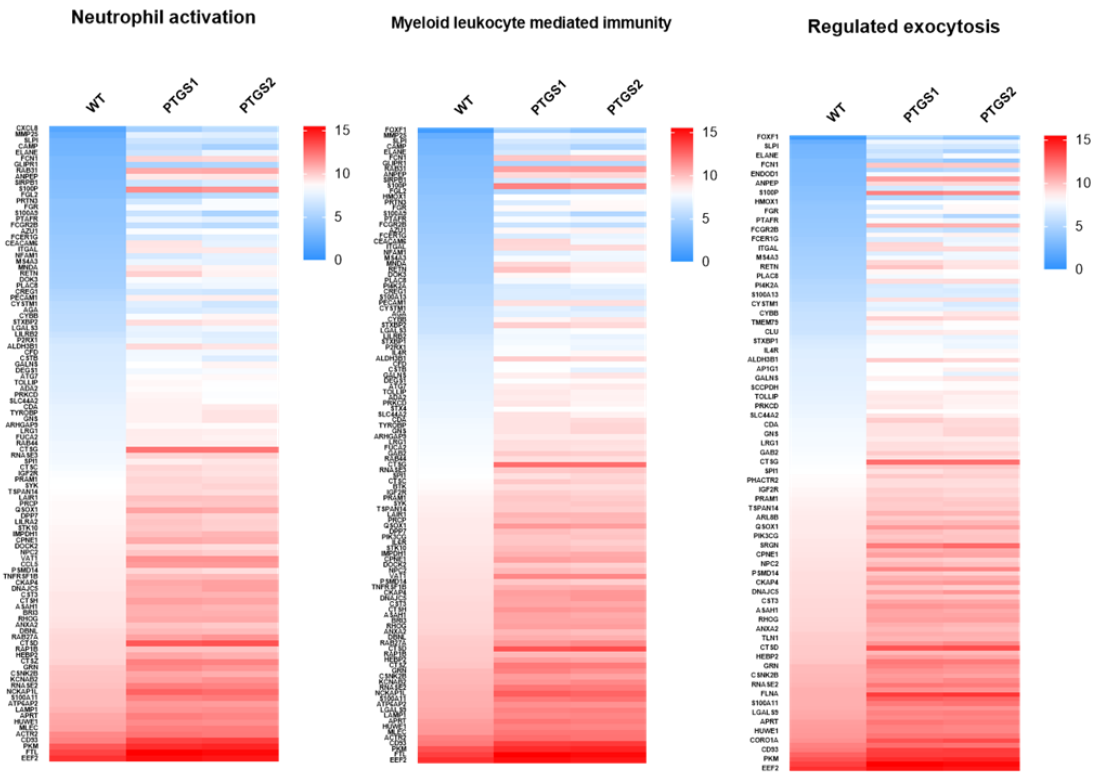

Figure A. 6 Further analysis identified the most pronounced DEGs in each pathway.

Using two of every three biological replicates in at least one group, Perseus 1.6.8.0 software was used to filter data. Following that, the iDEP.96 platform was utilized to extract the top DEGs in each pathway. Subsequently, these DEGs were further graphically represented using the Microsoft Excel.

References

Anaparthy, N., Y.-J. Ho, L. Martelotto, M. Hammell and J. Hicks (2019). "Single-cell applications of next-generation sequencing." Cold Spring Harbor Perspectives in Medicine **9**(10).

Appelbaum, F. R. (2003). "The current status of hematopoietic cell transplantation." Annual review of medicine **54**(1): 491-512.

Arai, H., S. Hori, I. Aramori, H. Ohkubo and S. Nakanishi (1990). "Cloning and expression of a cDNA encoding an endothelin receptor." Nature **348**(6303): 730-732.

Arber, D. A., A. Orazi, R. Hasserjian, J. Thiele, M. J. Borowitz, M. M. Le Beau, C. D. Bloomfield, M. Cazzola and J. W. Vardiman (2016). "The 2016 revision to the World Health Organization classification of myeloid neoplasms and acute leukemia." Blood, The Journal of the American Society of Hematology **127**(20): 2391-2405.

Balaban, R. S., S. Nemoto and T. Finkel (2005). "Mitochondria, oxidants, and aging." cell **120**(4): 483-495.

Beinortas, T., I. Tavorienė, T. Žvirblis, R. Gerbutavičius, M. Jurgutis and L. Griškevičius (2016). "Chronic myeloid leukemia incidence, survival and accessibility of tyrosine kinase inhibitors: a report from population-based Lithuanian haematological disease registry 2000–2013." BMC cancer **16**: 1-10.

Ben Nasr, M., F. D'Addio, A. M. Malvandi, S. Faravelli, E. Castillo-Leon, V. Usuelli, F. Rocchio, T. Letizia, A. B. El Essawy and E. Assi (2018). "Prostaglandin E2 stimulates the expansion of regulatory hematopoietic stem and progenitor cells in type 1 diabetes." Frontiers in immunology **9**: 1387.

Bennett, J. M., D. Catovsky, M. T. Daniel, G. Flandrin, D. A. Galton, H. R. Gralnick and C. Sultan (1976). "Proposals for the classification of the acute leukaemias French-American-British (FAB) co-operative group." British journal of haematology **33**(4): 451-458.

Bhattacharya, P., M. Thiruppathi, H. A. Elshabrawy, K. Alharshawi, P. Kumar and B. S. Prabhakar (2015). "GM-CSF: An immune modulatory cytokine that can suppress autoimmunity." Cytokine **75**(2): 261-271.

Bigarella, C. L., R. Liang and S. Ghaffari (2014). "Stem cells and the impact of ROS signaling." Development **141**(22): 4206-4218.

Bödder, J., L. M. Kok, J. A. Fauerbach, G. Flórez-Grau and I. J. M. de Vries (2023). "Tailored PGE2 Immunomodulation of moDCs by Nano-Encapsulated EP2/EP4 Antagonists." International Journal of Molecular Sciences **24**(2): 1392.

Botha, J. H., K. M. Robinson, N. Ramchurren, K. Reddi and R. J. Norman (1986). "Human esophageal carcinoma cell lines: prostaglandin production, biological properties, and behavior in nude mice." Journal of the National Cancer Institute **76**(6): 1053-1056.

Broudy, V. C., N. L. Lin and K. Kaushansky (1995). "Thrombopoietin (c-mpl ligand) acts synergistically with erythropoietin, stem cell factor, and interleukin-11 to enhance murine megakaryocyte colony growth and increases megakaryocyte ploidy *in vitro*."

Brown, T. A. (2020). Gene cloning and DNA analysis: an introduction, John Wiley & Sons.

Brunner, A. M., F. Campigotto, H. Sadrzadeh, B. J. Drapkin, Y. B. Chen, D. S. Neuberg and A. T. Fathi (2013). "Trends in all-cause mortality among patients with chronic myeloid leukemia: a Surveillance, Epidemiology, and End Results database analysis." Cancer **119**(14): 2620-2629.

Burnett, A. K., N. H. Russell, R. K. Hills, A. E. Hunter, L. Kjeldsen, J. Yin, B. E. Gibson, K. Wheatley and D. Milligan (2013). "Optimization of chemotherapy for younger patients with acute myeloid leukemia: results of the medical research council AML15 trial." Journal of clinical oncology **31**(27): 3360-3368.

Burnett, A. K., N. H. Russell, R. K. Hills, J. Kell, J. Cavenagh, L. Kjeldsen, M.-F. McMullin, P. Cahalin, M. Dennis and L. Friis (2015). "A randomized

comparison of daunorubicin 90 mg/m2 vs 60 mg/m2 in AML induction: results from the UK NCRI AML17 trial in 1206 patients." Blood, The Journal of the American Society of Hematology **125**(25): 3878-3885.

Byrd, J. C., K. Mrózek, R. K. Dodge, A. J. Carroll, C. G. Edwards, D. C. Arthur, M. J. Pettenati, S. R. Patil, K. W. Rao and M. S. Watson (2002). "Pretreatment cytogenetic abnormalities are predictive of induction success, cumulative incidence of relapse, and overall survival in adult patients with de novo acute myeloid leukemia: results from Cancer and Leukemia Group B (CALGB 8461) Presented in part at the 43rd annual meeting of the American Society of Hematology, Orlando, FL, December 10, 2001, and published in abstract form. 59." Blood, The Journal of the American Society of Hematology **100**(13): 4325-4336.

Byron, S. A., K. R. Van Keuren-Jensen, D. M. Engelthaler, J. D. Carpten and D. W. Craig (2016). "Translating RNA sequencing into clinical diagnostics: opportunities and challenges." Nature Reviews Genetics **17**(5): 257-271.

Canaani, J., E. Beohou, M. Labopin, G. Socie, A. Huynh, L. Volin, J. Cornelissen, N. Milpied, T. Gedde-Dahl and E. Deconinck (2017). "Impact of FAB classification on predicting outcome in acute myeloid leukemia, not otherwise specified, patients undergoing allogeneic stem cell transplantation in CR 1: An analysis of 1690 patients from the acute leukemia working party of EBMT." American journal of hematology **92**(4): 344-350.

Capelli, D., D. Menotti, A. Fiorentini, F. Saraceni and A. Olivieri (2022). "Overcoming Resistance: FLT3 Inhibitors Past, Present, Future and the Challenge of Cure." Cancers **14**(17): 4315.

Capucetti, A., F. Albano and R. Bonecchi (2020). "Multiple roles for chemokines in neutrophil biology." Frontiers in immunology **11**: 1259.

Castaigne, S., C. Pautas, C. Terré, E. Raffoux, D. Bordessoule, J.-N. Bastie, O. Legrand, X. Thomas, P. Turlure and O. Reman (2012). "Effect of gemtuzumab ozogamicin on survival of adult patients with de-novo acute

myeloid leukaemia (ALFA-0701): a randomised, open-label, phase 3 study." The Lancet **379**(9825): 1508-1516.

Cerchione, C., A. Romano, N. Daver, C. DiNardo, E. J. Jabbour, M. Konopleva, F. Ravandi-Kashani, M. P. Martelli, A. Isidori and G. Martinelli (2021). "IDH1/IDH2 inhibition in acute myeloid leukemia." Frontiers in Oncology **11**: 639387.

Chagastelles, P. C. and N. B. Nardi (2011). "Biology of stem cells: an overview." Kidney international supplements **1**(3): 63-67.

Chen, J., J. Yang, Q. Wei, L. Weng, F. Wu, Y. Shi, X. Cheng, X. Cai, C. Hu and P. Cao (2020). "Identification of a selective inhibitor of IDH2/R140Q enzyme that induces cellular differentiation in leukemia cells." Cell Communication and Signaling **18**(1): 1-12.

Chen, Y. H., C. Pallant, C. J. Sampson, A. Boiti, S. Johnson, P. Brazauskas, P. Hardwicke, M. Marongiu, V. M. Marinova and M. Carmo (2020). "Rapid lentiviral vector producer cell line generation using a single DNA construct." Molecular Therapy-Methods & Clinical Development **19**: 47-57.

Cheng, K., P. Sportoletti, K. Ito, J. G. Clohessy, J. Teruya-Feldstein, J. L. Kutok and P. P. Pandolfi (2010). "The cytoplasmic NPM mutant induces myeloproliferation in a transgenic mouse model." Blood, The Journal of the American Society of Hematology **115**(16): 3341-3345.

Cheson, B. D., J. M. Bennett, K. J. Kopecky, T. Büchner, C. L. Willman, E. H. Estey, C. A. Schiffer, H. Doehner, M. S. Tallman and T. A. Lister (2003). "Revised recommendations of the international working group for diagnosis, standardization of response criteria, treatment outcomes, and reporting standards for therapeutic trials in acute myeloid leukemia." Journal of clinical oncology **21**(24): 4642-4649.

Chou, W.-C., S.-C. Chou, C.-Y. Liu, C.-Y. Chen, H.-A. Hou, Y.-Y. Kuo, M.-C. Lee, B.-S. Ko, J.-L. Tang and M. Yao (2011). "TET2 mutation is an unfavorable prognostic factor in acute myeloid leukemia patients with intermediate-risk

cytogenetics." Blood, The Journal of the American Society of Hematology **118**(14): 3803-3810.

Cieślar-Pobuda, A., J. Yue, H.-C. Lee, M. Skonieczna and Y.-H. Wei (2017). ROS and oxidative stress in stem cells, Hindawi. **2017**.

Corces-Zimmerman, M. R., W.-J. Hong, I. L. Weissman, B. C. Medeiros and R. Majeti (2014). "Preleukemic mutations in human acute myeloid leukemia affect epigenetic regulators and persist in remission." Proceedings of the National Academy of Sciences **111**(7): 2548-2553.

Däbritz, J. (2014). "Granulocyte macrophage colony-stimulating factor and the intestinal innate immune cell homeostasis in Crohn's disease." American Journal of Physiology-Gastrointestinal and Liver Physiology **306**(6): G455-G465.

Daver, N., R. F. Schlenk, N. H. Russell and M. J. Levis (2019). "Targeting FLT3 mutations in AML: review of current knowledge and evidence." Leukemia **33**(2): 299-312.

Davis, L. (2012). Basic methods in molecular biology, Elsevier.

De Kouchkovsky, I. and M. Abdul-Hay (2016). "Acute myeloid leukemia: a comprehensive review and 2016 update." Blood cancer journal **6**(7): e441-e441.

Desitter, I., B. S. Guerrouahen, N. Benali-Furet, J. Wechsler, P. A. Jänne, Y. Kuang, M. Yanagita, L. Wang, J. A. Berkowitz and R. J. Distel (2011). "A new device for rapid isolation by size and characterization of rare circulating tumor cells." Anticancer research **31**(2): 427-441.

Ding, L., H. Gu, Z. Lan, Q. Lei, W. Wang, J. Ruan, M. Yu, J. Lin and Q. Cui (2019). "Downregulation of cyclooxygenase-1 stimulates mitochondrial apoptosis through the NF-κB signaling pathway in colorectal cancer cells." Oncology reports **41**(1): 559-569.

Döhner, H., E. H. Estey, S. Amadori, F. R. Appelbaum, T. Büchner, A. K. Burnett, H. Dombret, P. Fenaux, D. Grimwade and R. A. Larson (2010). "Diagnosis and management of acute myeloid leukemia in adults: recommendations from an international expert panel, on behalf of the European LeukemiaNet." Blood, The Journal of the American Society of Hematology **115**(3): 453-474.

Dohner, H., D. Weisdorf and C. Bloomfield (2015). "Acute myeloid leukemia." N Engl J Med **373**(12): 1136-1152.

Döhner, K., R. F. Schlenk, M. Habdank, C. Scholl, F. G. Rücker, A. Corbacioglu, L. Bullinger, S. Fröhling, H. Döhner and A. S. Group (2005). "Mutant nucleophosmin (NPM1) predicts favorable prognosis in younger adults with acute myeloid leukemia and normal cytogenetics: interaction with other gene mutations." Blood **106**(12): 3740-3746.

Dumas, P.-Y., C. Naudin, S. Martin-Lannerée, B. Izac, L. Casetti, O. Mansier, B. Rousseau, A. Artus, M. Dufossée and A. Giese (2019). "Hematopoietic niche drives FLT3-ITD acute myeloid leukemia resistance to quizartinib via STAT5-and hypoxia-dependent upregulation of AXL." Haematologica **104**(10): 2017.

Duncker, P. (2018). Granulocyte-Macrophage Colony-Stimulating Factor: Linking the Adaptive and Innate Immune Systems in Autoimmune Demyelinating Disease.

Dzneladze, I., R. He, J. Woolley, M. H. Son, M. Sharobim, S. Greenberg, M. Gabra, C. Langlois, A. Rashid and A. Hakem (2015). "INPP4B overexpression is associated with poor clinical outcome and therapy resistance in acute myeloid leukemia." Leukemia **29**(7): 1485-1495.

El Achi, H. and R. Kanagal-Shamanna (2021). "Biomarkers in acute myeloid leukemia: leveraging next generation sequencing data for optimal therapeutic strategies." Frontiers in Oncology **11**: 748250.

Estey, E. and H. Döhner (2006). "Acute myeloid leukaemia." The Lancet **368**(9550): 1894-1907.

Falini, B., I. Nicoletti, M. F. Martelli and C. Mecucci (2007). "Acute myeloid leukemia carrying cytoplasmic/mutated nucleophosmin (NPMc+ AML): biologic and clinical features." Blood **109**(3): 874-885.

Fathi, A. T., S. A. Wander, R. Faramand and A. Emadi (2015). Biochemical, epigenetic, and metabolic approaches to target IDH mutations in acute myeloid leukemia. Seminars in hematology, Elsevier.

Fenaux, P., G. J. Mufti, E. Hellstrom-Lindberg, V. Santini, C. Finelli, A. Giagounidis, R. Schoch, N. Gattermann, G. Sanz and A. List (2009). "Efficacy of azacitidine compared with that of conventional care regimens in the treatment of higher-risk myelodysplastic syndromes: a randomised, open-label, phase III study." The lancet oncology **10**(3): 223-232.

Fernandez, H. F., Z. Sun, X. Yao, M. R. Litzow, S. M. Luger, E. M. Paietta, J. Racevskis, G. W. Dewald, R. P. Ketterling and J. M. Bennett (2009). "Anthracycline dose intensification in acute myeloid leukemia." New England Journal of Medicine **361**(13): 1249-1259.

Gabay, M., Y. Li and D. W. Felsher (2014). "MYC activation is a hallmark of cancer initiation and maintenance." Cold Spring Harbor perspectives in medicine **4**(6).

Gaidzik, V. and K. Döhner (2008). Prognostic implications of gene mutations in acute myeloid leukemia with normal cytogenetics. Seminars in oncology, Elsevier.

Gale, R. E., C. Green, C. Allen, A. J. Mead, A. K. Burnett, R. K. Hills and D. C. Linch (2008). "The impact of FLT3 internal tandem duplication mutant level, number, size, and interaction with NPM1 mutations in a large cohort of young adult patients with acute myeloid leukemia." Blood, The Journal of the American Society of Hematology **111**(5): 2776-2784.

Galloway, J. L. and L. I. Zon (2003). "3 ontogeny of hematopoiesis: examining the emergence of hematopoietic cells in the vertebrate embryo."

Garnis, C., T. P. Buys and W. L. Lam (2004). "Genetic alteration and gene expression modulation during cancer progression." Molecular Cancer **3**(1): 1-23.

Gierlikowska, B., A. Stachura, W. Gierlikowski and U. Demkow (2021). "Phagocytosis, degranulation and extracellular traps release by neutrophils—the current knowledge, pharmacological modulation and future prospects." Frontiers in Pharmacology **12**: 666732.

Gill, S., S. K. Tasian, M. Ruella, O. Shestova, Y. Li, D. L. Porter, M. Carroll, G. Danet-Desnoyers, J. Scholler and S. A. Grupp (2014). "Preclinical targeting of human acute myeloid leukemia and myeloablation using chimeric antigen receptor–modified T cells." Blood, The Journal of the American Society of Hematology **123**(15): 2343-2354.

Greenhough, A., H. J. Smartt, A. E. Moore, H. R. Roberts, A. C. Williams, C. Paraskeva and A. Kaidi (2009). "The COX-2/PGE 2 pathway: key roles in the hallmarks of cancer and adaptation to the tumour microenvironment." Carcinogenesis **30**(3): 377-386.

Grimwade, D. and S. D. Freeman (2014). "Defining minimal residual disease in acute myeloid leukemia: which platforms are ready for “prime time”?" Blood, The Journal of the American Society of Hematology **124**(23): 3345-3355.

Grundler, R., L. Brault, C. Gasser, A. N. Bullock, T. Dechow, S. Woetzel, V. Pogacic, A. Villa, S. Ehret and G. Berridge (2009). "Dissection of PIM serine/threonine kinases in FLT3-ITD–induced leukemogenesis reveals PIM1 as regulator of CXCL12–CXCR4-mediated homing and migration." Journal of experimental medicine **206**(9): 1957-1970.

Gruszka, A. M., D. Valli and M. Alcalay (2019). "Wnt signalling in acute myeloid leukaemia." Cells **8**(11): 1403.

Guan, Y., B. Gerhard and D. E. Hogge (2003). "Detection, isolation, and stimulation of quiescent primitive leukemic progenitor cells from patients with

acute myeloid leukemia (AML)." Blood, The Journal of the American Society of Hematology **101**(8): 3142-3149.

Gupta, R. A., L. V. Tejada, B. J. Tong, S. K. Das, J. D. Morrow, S. K. Dey and R. N. DuBois (2003). "Cyclooxygenase-1 is overexpressed and promotes angiogenic growth factor production in ovarian cancer." Cancer research **63**(5): 906-911.

Handschuh, L., M. Kaźmierczak, M. C. Milewski, M. Góralski, M. Łuczak, M. Wojtaszewska, B. Uszczyńska-Ratajczak, K. Lewandowski, M. Komarnicki and M. Figlerowicz (2018). "Gene expression profiling of acute myeloid leukemia samples from adult patients with AML-M1 and-M2 through boutique microarrays, real-time PCR and droplet digital PCR." International journal of oncology **52**(3): 656-678.

Hara, T. and A. Miyajima (1996). Function of the IL-3 receptor system in hematopoiesis. Gene Technology: Stem Cell and Leukemia Research, Springer.

Harris, R. E. (2007). "Cyclooxygenase-2 (cox-2) and the inflammogenesis of cancer." Inflammation in the Pathogenesis of Chronic Diseases: 93-126.

He, X., Y. Zhu, Y.-C. Lin, M. Li, J. Du, H. Dong, J. Sun, L. Zhu, H. Wang and Z. Ding (2019). "PRMT1-mediated FLT3 arginine methylation promotes maintenance of FLT3-ITD+ acute myeloid leukemia." Blood, The Journal of the American Society of Hematology **134**(6): 548-560.

Heimbruch, K. E., J. B. Fisher, C. T. Stelloh, E. Phillips, M. H. Reimer, A. J. Wargolet, A. E. Meyer, K. Pulakanti, A. D. Viny and J. J. Loppnow (2021). "DOT1L inhibitors block abnormal self-renewal induced by cohesin loss." Scientific Reports **11**(1): 1-12.

Hernández-García, D., C. D. Wood, S. Castro-Obregón and L. Covarrubias (2010). "Reactive oxygen species: a radical role in development?" Free Radical Biology and Medicine **49**(2): 130-143.

Heuser, M., F. Thol and A. Ganser (2016). "Clonal hematopoiesis of indeterminate potential: a risk factor for hematologic neoplasms." Deutsches Ärzteblatt International **113**(18): 317.

Ihle, J. N. (1992). "Interleukin-3 and hematopoiesis." Chemical immunology **51**: 65-106.

Ilyas, A. M., S. Ahmad, M. Faheem, M. I. Naseer, T. A. Kumosani, M. H. Al-Qahtani, M. Gari and F. Ahmed (2015). "Next generation sequencing of acute myeloid leukemia: influencing prognosis." BMC genomics **16**(1): 1-12.

Ishikawa, F., S. Yoshida, Y. Saito, A. Hijikata, H. Kitamura, S. Tanaka, R. Nakamura, T. Tanaka, H. Tomiyama and N. Saito (2007). "Chemotherapy-resistant human AML stem cells home to and engraft within the bone-marrow endosteal region." Nature biotechnology **25**(11): 1315-1321.

Jagannathan-Bogdan, M. and L. I. Zon (2013). "Hematopoiesis." Development **140**(12): 2463-2467.

Jaiswal, S., P. Fontanillas, J. Flannick, A. Manning, P. V. Grauman, B. G. Mar, R. C. Lindsley, C. H. Mermel, N. Burtt and A. Chavez (2014). "Age-related clonal hematopoiesis associated with adverse outcomes." New England Journal of Medicine **371**(26): 2488-2498.

Jan, M., T. M. Snyder, M. R. Corces-Zimmerman, P. Vyas, I. L. Weissman, S. R. Quake and R. Majeti (2012). "Clonal evolution of preleukemic hematopoietic stem cells precedes human acute myeloid leukemia." Science translational medicine **4**(149): 149ra118-149ra118.

Jordan, C. T. (2007). "The leukemic stem cell." Best practice & research Clinical haematology **20**(1): 13-18.

Juliusson, G., P. Antunovic, Å. Derolf, S. Lehmann, L. Möllgård, D. Stockelberg, U. Tidefelt, A. Wahlin and M. Höglund (2009). "Age and acute myeloid leukemia: real world data on decision to treat and outcomes from the Swedish Acute Leukemia Registry." Blood, The Journal of the American Society of Hematology **113**(18): 4179-4187.

Kalinski, P. (2012). "Regulation of immune responses by prostaglandin E2." The Journal of Immunology **188**(1): 21-28.

Kang, Y.-J., U. R. Mbonye, C. J. DeLong, M. Wada and W. L. Smith (2007). "Regulation of intracellular cyclooxygenase levels by gene transcription and protein degradation." Progress in lipid research **46**(2): 108-125.

Kaushansky, K. (1995). "Thrombopoietin: the primary regulator of megakaryocyte and platelet production." Thrombosis and haemostasis **74**(07): 521-525.

Kayser, S., R. F. Schlenk, M. C. Londono, F. Breitenbuecher, K. Wittke, J. Du, S. Groner, D. Spaeth, J. Krauter and A. Ganser (2009). "Insertion of FLT3 internal tandem duplication in the tyrosine kinase domain-1 is associated with resistance to chemotherapy and inferior outcome." Blood, The Journal of the American Society of Hematology **114**(12): 2386-2392.

Keating, S., S. Suciu, T. de Witte, F. Mandelli, R. Willemze, L. Resegotti, G. Broccia, J. Thaler, B. Labar and E. Damasio (1996). "Prognostic factors of patients with acute myeloid leukemia (AML) allografted in first complete remission: an analysis of the EORTC-GIMEMA AML 8A trial."

Keller, U. (1993). "Pathophysiology of cancer cachexia." Supportive care in cancer **1**: 290-294.

Kelly, L. M., Q. Liu, J. L. Kutok, I. R. Williams, C. L. Boulton and D. G. Gilliland (2002). "FLT3 internal tandem duplication mutations associated with human acute myeloid leukemias induce myeloproliferative disease in a murine bone marrow transplant model." Blood, The Journal of the American Society of Hematology **99**(1): 310-318.

Kennedy, V. E. and C. C. Smith (2020). "FLT3 mutations in acute myeloid leukemia: key concepts and emerging controversies." Frontiers in Oncology **10**: 612880.

Khwaja, A., M. Bjorkholm, R. E. Gale, R. L. Levine, C. T. Jordan, G. Ehninger, C. D. Bloomfield, E. Estey, A. Burnett and J. J. Cornelissen (2016). "Acute myeloid leukaemia." Nature reviews Disease primers **2**(1): 1-22.

Kim, B., H. Lee, J. Jang, S.-J. Kim, S.-T. Lee, J.-W. Cheong, C. J. Lyu, Y. H. Min and J. R. Choi (2019). "Targeted next generation sequencing can serve as an alternative to conventional tests in myeloid neoplasms." PLoS One **14**(3): e0212228.

Kohlmann, A., N. Nadarajah, T. Alpermann, V. Grossmann, S. Schindela, F. Dicker, A. Roller, W. Kern, C. Haferlach and S. Schnittger (2014). "Monitoring of residual disease by next-generation deep-sequencing of RUNX1 mutations can identify acute myeloid leukemia patients with resistant disease." Leukemia **28**(1): 129-137.

Kondo, M., A. J. Wagers, M. G. Manz, S. S. Prohaska, D. C. Scherer, G. F. Beilhack, J. A. Shizuru and I. L. Weissman (2003). "Biology of hematopoietic stem cells and progenitors: implications for clinical application." Annual review of immunology **21**(1): 759-806.

Konopleva, M. Y. and C. T. Jordan (2011). "Leukemia stem cells and microenvironment: biology and therapeutic targeting." Journal of clinical oncology **29**(5): 591.

Koranteng, F., B. Cho and J. Shim (2022). "Intrinsic and extrinsic regulation of hematopoiesis in Drosophila." Molecules and Cells **45**(3): 101.

Kremer, K. N., A. Dudakovic, M. E. McGee-Lawrence, R. L. Philips, A. D. Hess, B. D. Smith, A. J. Van Wijnen, J. E. Karp, S. H. Kaufmann and J. J. Westendorf (2014). "Osteoblasts protect AML cells from SDF-1-induced apoptosis." Journal of cellular biochemistry **115**(6): 1128-1137.

Krysan, K., R. Kusko, T. Grogan, J. O'Hearn, K. L. Reckamp, T. C. Walser, E. B. Garon, M. E. Lenburg, S. Sharma and A. E. Spira (2014). "PGE2-driven expression of c-Myc and oncomiR-17-92 contributes to apoptosis resistance in NSCLC." Molecular Cancer Research **12**(5): 765-774.

Kumar, C. C. (2011). "Genetic abnormalities and challenges in the treatment of acute myeloid leukemia." Genes & cancer **2**(2): 95-107.

Kumar, H., A. Dhir, A. J. Paterson, N. R. Anderson, S. Qiu, X. Zhao, R. Lu and R. Bhatia (2022). "PRMT5 Inhibition Enhances Elimination of FLT3-ITD AML Stem Cells in Combination with TKI Treatment." Blood **140**(Supplement 1): 3073-3074.

Leisch, M., B. Jansko, N. Zaborsky, R. Greil and L. Pleyer (2019). "Next generation sequencing in AML—on the way to becoming a new standard for treatment initiation and/or modulation?" Cancers **11**(2): 252.

Ley, T. J., L. Ding, M. J. Walter, M. D. McLellan, T. Lamprecht, D. E. Larson, C. Kandoth, J. E. Payton, J. Baty and J. Welch (2010). "DNMT3A mutations in acute myeloid leukemia." New England Journal of Medicine **363**(25): 2424-2433.

Li, H., F. Zhu, H. Chen, K. W. Cheng, T. Zykova, N. Oi, R. A. Lubet, A. M. Bode, M. Wang and Z. Dong (2014). "6-C-(E-phenylethenyl)-Naringenin Suppresses Colorectal Cancer Growth by Inhibiting Cyclooxygenase-16CEPN Suppresses Colon Cancer by Inhibiting COX-1." Cancer research **74**(1): 243-252.

Liersch, R., C. Müller-Tidow, W. E. Berdel and U. Krug (2014). "Prognostic factors for acute myeloid leukaemia in adults–biological significance and clinical use." British journal of haematology **165**(1): 17-38.

Lindsley, R. C., B. G. Mar, E. Mazzola, P. V. Grauman, S. Shareef, S. L. Allen, A. Pigneux, M. Wetzler, R. K. Stuart and H. P. Erba (2015). "Acute myeloid leukemia ontogeny is defined by distinct somatic mutations." Blood, The Journal of the American Society of Hematology **125**(9): 1367-1376.

Liu, Y.-C., J. Kwon, E. Fabiani, Z. Xiao, Y. V. Liu, M. Y. Follo, J. Liu, H. Huang, C. Gao and J. Liu (2022). "Demethylation and up-regulation of an oncogene after hypomethylating therapy." New England Journal of Medicine **386**(21): 1998-2010.

Löwenberg, B., G. J. Ossenkoppele, W. van Putten, H. C. Schouten, C. Graux, A. Ferrant, P. Sonneveld, J. Maertens, M. Jongen-Lavrencic and M. von Lilienfeld-Toal (2009). "High-dose daunorubicin in older patients with acute myeloid leukemia." New England Journal of Medicine **361**(13): 1235-1248.

Lu, L., L. Pelus and H. Broxmeyer (1984). "Modulation of the expression of HLA-DR (Ia) antigens and the proliferation of human erythroid (BFU-E) and multipotential (CFU-GEMM) progenitor cells by prostaglandin E." Experimental hematology **12**(9): 741-748.

Lu, L., L. Pelus, W. Piacibello, M. Moore, W. Hu and H. Broxmeyer (1987). "Prostaglandin E acts at two levels to enhance colony formation *in vitro* by erythroid (BFU-E) progenitor cells." Experimental hematology **15**(7): 765-771.

Ludin, A., S. Gur-Cohen, K. Golan, K. B. Kaufmann, T. Itkin, C. Medaglia, X.-J. Lu, G. Ledergor, O. Kollet and T. Lapidot (2014). "Reactive oxygen species regulate hematopoietic stem cell self-renewal, migration and development, as well as their bone marrow microenvironment." Antioxidants & redox signaling **21**(11): 1605-1619.

Luo, H., H.-H. Chiang, M. Louw, A. Susanto and D. Chen (2017). "Nutrient sensing and the oxidative stress response." Trends in Endocrinology & Metabolism **28**(6): 449-460.

Lutz, C. S. and A. L. Cornett (2013). "Regulation of genes in the arachidonic acid metabolic pathway by RNA processing and RNA-mediated mechanisms." Wiley Interdisciplinary Reviews: RNA **4**(5): 593-605.

Mann, Z., M. Sengar, Y. K. Verma, R. Rajalingam and P. K. Raghav (2022). "Hematopoietic stem cell factors: Their functional role in self-renewal and clinical aspects." Frontiers in Cell and Developmental Biology **10**: 453.

Marcucci, G., T. Haferlach and H. Döhner (2011). "Molecular genetics of adult acute myeloid leukemia: prognostic and therapeutic implications." Journal of Clinical Oncology **29**(5): 475-486.

Marcucci, G., K. Maharry, Y.-Z. Wu, M. D. Radmacher, K. Mrózek, D. Margeson, K. B. Holland, S. P. Whitman, H. Becker and S. Schwind (2010). "IDH1 and IDH2 gene mutations identify novel molecular subsets within de novo cytogenetically normal acute myeloid leukemia: a Cancer and Leukemia Group B study." Journal of clinical oncology **28**(14): 2348.

Marcucci, G., K. H. Metzeler, S. Schwind, H. Becker, K. Maharry, K. Mrózek, M. D. Radmacher, J. Kohlschmidt, D. Nicolet and S. P. Whitman (2012). "Age-related prognostic impact of different types of DNMT3A mutations in adults with primary cytogenetically normal acute myeloid leukemia." Journal of clinical oncology **30**(7): 742.

Mardiros, A., C. Dos Santos, T. McDonald, C. E. Brown, X. Wang, L. E. Budde, L. Hoffman, B. Aguilar, W.-C. Chang and W. Bretzlaff (2013). "T cells expressing CD123-specific chimeric antigen receptors exhibit specific cytolytic effector functions and antitumor effects against human acute myeloid leukemia." Blood, The Journal of the American Society of Hematology **122**(18): 3138-3148.

Margraf, A., C. A. Lowell and A. Zarbock (2022). "Neutrophils in acute inflammation: current concepts and translational implications." Blood, The Journal of the American Society of Hematology **139**(14): 2130-2144.

McCulloch, E. (1983). "Stem cells in normal and leukemic hemopoiesis (Henry Stratton Lecture, 1982)."

McLenachan, S., J. P. Sarsero and P. A. Ioannou (2007). "Flow-cytometric analysis of mouse embryonic stem cell lipofection using small and large DNA constructs." Genomics **89**(6): 708-720.

Mead, A. J., W. H. Neo, N. Barkas, S. Matsuoka, A. Giustacchini, R. Facchini, S. Thongjuea, L. Jamieson, C. A. Booth and N. Fordham (2017). "Niche-mediated depletion of the normal hematopoietic stem cell reservoir by Flt3-ITD–induced myeloproliferation." Journal of Experimental Medicine **214**(7): 2005-2021.

Metzeler, K. H., H. Becker, K. Maharry, M. D. Radmacher, J. Kohlschmidt, K. Mrózek, D. Nicolet, S. P. Whitman, Y.-Z. Wu and S. Schwind (2011). "ASXL1 mutations identify a high-risk subgroup of older patients with primary cytogenetically normal AML within the ELN Favorable genetic category." Blood, The Journal of the American Society of Hematology **118**(26): 6920-6929.

Meyers, S., J. Downing and S. Hiebert (1993). "Identification of AML-1 and the (8; 21) translocation protein (AML-1/ETO) as sequence-specific DNA-binding proteins: the runt homology domain is required for DNA binding and protein-protein interactions." Molecular and cellular biology **13**(10): 6336-6345.

Milella, M., I. Falcone, F. Conciatori, U. Cesta Incani, A. Del Curatolo, N. Inzerilli, C. Nuzzo, V. Vaccaro, S. Vari and F. Cognetti (2015). "PTEN: multiple functions in human malignant tumors." Frontiers in oncology **5**: 125824.

Mistry, J. J., C. Hellmich, J. A. Moore, A. Jibril, I. Macaulay, M. Moreno-Gonzalez, F. Di Palma, N. Beraza, K. M. Bowles and S. A. Rushworth (2021). "Free fatty-acid transport via CD36 drives β-oxidation-mediated hematopoietic stem cell response to infection." Nature Communications **12**(1): 7130.

Mohyeldin, A., T. Garzón-Muvdi and A. Quiñones-Hinojosa (2010). "Oxygen in stem cell biology: a critical component of the stem cell niche." Cell stem cell **7**(2): 150-161.

Morita, K., F. Wang, K. Jahn, T. Hu, T. Tanaka, Y. Sasaki, J. Kuipers, S. Loghavi, S. A. Wang and Y. Yan (2020). "Clonal evolution of acute myeloid leukemia revealed by high-throughput single-cell genomics." Nature communications **11**(1): 1-17.

Morozova, O., M. Hirst and M. A. Marra (2009). "Applications of new sequencing technologies for transcriptome analysis." Annual review of genomics and human genetics **10**: 135-151.

Mrózek, K., G. Marcucci, D. Nicolet, K. S. Maharry, H. Becker, S. P. Whitman, K. H. Metzeler, S. Schwind, Y.-Z. Wu and J. Kohlschmidt (2012). "Prognostic significance of the European LeukemiaNet standardized system for reporting

cytogenetic and molecular alterations in adults with acute myeloid leukemia." Journal of clinical oncology **30**(36): 4515.

Mrózek, K., G. Marcucci, P. Paschka, S. P. Whitman and C. D. Bloomfield (2007). "Clinical relevance of mutations and gene-expression changes in adult acute myeloid leukemia with normal cytogenetics: are we ready for a prognostically prioritized molecular classification?" Blood **109**(2): 431-448.

Nakanishi, M. and D. W. Rosenberg (2013). Multifaceted roles of PGE2 in inflammation and cancer. Seminars in immunopathology, Springer.

Network, C. G. A. R. (2013). "Genomic and epigenomic landscapes of adult de novo acute myeloid leukemia." New England Journal of Medicine **368**(22): 2059-2074.

Nowell, P. C. (1976). "The Clonal Evolution of Tumor Cell Populations: Acquired genetic lability permits stepwise selection of variant sublines and underlies tumor progression." Science **194**(4260): 23-28.

O'Donnell, M. R., C. N. Abboud, J. Altman, F. R. Appelbaum, D. A. Arber, E. Attar, U. Borate, S. E. Coutre, L. E. Damon and S. Goorha (2012). "Acute myeloid leukemia." Journal of the National Comprehensive Cancer Network **10**(8): 984-1021.

O'Donnell, M. R., M. S. Tallman, C. N. Abboud, J. K. Altman, F. R. Appelbaum, D. A. Arber, V. Bhatt, D. Bixby, W. Blum and S. E. Coutre (2017). "Acute myeloid leukemia, version 3.2017, NCCN clinical practice guidelines in oncology." Journal of the National Comprehensive Cancer Network **15**(7): 926-957.

Ohanian, M., U. Rozovski, R. Kanagal-Shamanna, L. V. Abruzzo, S. Loghavi, T. Kadia, A. Futreal, K. Bhalla, Z. Zuo and Y. O. Huh (2019). "MYC protein expression is an important prognostic factor in acute myeloid leukemia." Leukemia & lymphoma **60**(1): 37-48.

Palis, J. (2014). "Primitive and definitive erythropoiesis in mammals." Frontiers in physiology **5**: 3.

Palis, J. and M. C. Yoder (2001). "Yolk-sac hematopoiesis: the first blood cells of mouse and man." Experimental hematology **29**(8): 927-936.

Pannunzio, A. and M. Coluccia (2018). "Cyclooxygenase-1 (COX-1) and COX-1 inhibitors in cancer: A review of oncology and medicinal chemistry literature." Pharmaceuticals **11**(4): 101.

Paschka, P., R. F. Schlenk, V. I. Gaidzik, M. Habdank, J. Krönke, L. Bullinger, D. Späth, S. Kayser, M. Zucknick and K. Götze (2010). "IDH1 and IDH2 mutations are frequent genetic alterations in acute myeloid leukemia and confer adverse prognosis in cytogenetically normal acute myeloid leukemia with NPM1 mutation without FLT3 internal tandem duplication." Journal of clinical oncology **28**(22): 3636-3643.

Patel, J. P., M. Gönen, M. E. Figueroa, H. Fernandez, Z. Sun, J. Racevskis, P. Van Vlierberghe, I. Dolgalev, S. Thomas and O. Aminova (2012). "Prognostic relevance of integrated genetic profiling in acute myeloid leukemia." New England Journal of Medicine **366**(12): 1079-1089.

Pollyea, D. A. and C. T. Jordan (2017). "Therapeutic targeting of acute myeloid leukemia stem cells." Blood, The Journal of the American Society of Hematology **129**(12): 1627-1635.

Popat, U., M. De Lima, R. Saliba, P. Anderlini, B. Andersson, A. Alousi, C. Hosing, Y. Nieto, S. Parmar and I. Khouri (2012). "Long-term outcome of reduced-intensity allogeneic hematopoietic SCT in patients with AML in CR." Bone marrow transplantation **47**(2): 212-216.

Porter, R. L., M. A. Georger, O. Bromberg, K. E. McGrath, B. J. Frisch, M. W. Becker and L. M. Calvi (2013). "Prostaglandin E2 increases hematopoietic stem cell survival and accelerates hematopoietic recovery after radiation injury." Stem cells **31**(2): 372-383.

Prelich, G. (2012). "Gene overexpression: uses, mechanisms, and interpretation." Genetics **190**(3): 841-854.

Qi, S., Z. Fang, D. Wang, P. Menendez, K. Yao and J. Ji (2015). "Concise review: induced pluripotency by defined factors: prey of oxidative stress." Stem Cells **33**(5): 1371-1376.

Radzisheuskaya, A., P. V. Shliaha, V. Grinev, E. Lorenzini, S. Kovalchuk, D. Shlyueva, V. Gorshkov, R. C. Hendrickson, O. N. Jensen and K. Helin (2019). "PRMT5 methylome profiling uncovers a direct link to splicing regulation in acute myeloid leukemia." Nature structural & molecular biology **26**(11): 999-1012.

Rai, L. S., L. van Wijlick, M. Chauvel, C. d'Enfert, M. Legrand and S. Bachellier-Bassi (2022). "Overexpression approaches to advance understanding of Candida albicans." Molecular Microbiology **117**(3): 589-599.

Ramon, S., C. F Woeller and R. P Phipps (2013). "The influence of Cox-2 and bioactive lipids on hematological cancers." Current angiogenesis **2**(2): 135-142.

Ray, P. D., B.-W. Huang and Y. Tsuji (2012). "Reactive oxygen species (ROS) homeostasis and redox regulation in cellular signaling." Cellular signalling **24**(5): 981-990.

Reczek, C. R. and N. S. Chandel (2015). "ROS-dependent signal transduction." Current opinion in cell biology **33**: 8-13.

RICCIOTTI, E. and G. A. FITZGERALD (2011). "Prostaglandins and Inflammation: Inflammation." Arteriosclerosis, thrombosis, and vascular biology **31**(5): 986-1000.

Robinson, D., M. Place, J. Hose, A. Jochem and A. P. Gasch (2021). "Natural variation in the consequences of gene overexpression and its implications for evolutionary trajectories." Elife **10**: e70564.

Rocca, B. and G. A. FitzGerald (2002). "Cyclooxygenases and prostaglandins: shaping up the immune response." International immunopharmacology **2**(5): 603-630.

Rocca, B., N. Maggiano, A. Habib, G. Petrucci, M. Gessi, A. Fattorossi, L. Lauriola, R. Landolfi and F. O. Ranelletti (2002). "Distinct expression of cyclooxygenase-1 and-2 in the human thymus." European journal of immunology **32**(5): 1482-1492.

Rocca, B., P. Secchiero, G. Ciabattoni, F. O. Ranelletti, L. Catani, L. Guidotti, E. Melloni, N. Maggiano, G. Zauli and C. Patrono (2002). "Cyclooxygenase-2 expression is induced during human megakaryopoiesis and characterizes newly formed platelets." Proceedings of the National Academy of Sciences **99**(11): 7634-7639.

Rossi, L., G. A. Challen, O. Sirin, K. K.-Y. Lin and M. A. Goodell (2011). "Hematopoietic stem cell characterization and isolation." Stem Cell Migration: 47-59.

Rouzer, C. A. and L. J. Marnett (2009). "Cyclooxygenases: structural and functional insights." Journal of lipid research **50**: S29-S34.

Sager, R. (1997). "Expression genetics in cancer: shifting the focus from DNA to RNA." Proceedings of the National Academy of Sciences **94**(3): 952-955.

Salman, M. Y., J. M. Rowe and N. Weigert (2021). "Inhibition of FLT3: A Prototype for Molecular Targeted Therapy in Acute Myeloid Leukemia." Engineering **7**(10): 1354-1368.

Sánchez-Aguilera, A. and S. Méndez-Ferrer (2017). "The hematopoietic stem-cell niche in health and leukemia." Cellular and Molecular Life Sciences **74**: 579-590.

Sattler, M. and R. Salgia (2004). "Targeting c-Kit mutations: basic science to novel therapies." Leukemia research **28**: 11-20.

Schieber, M. and N. S. Chandel (2014). "ROS function in redox signaling and oxidative stress." Curr Biol **24**(10): R453-462.

Schiffer, C. A. (2014). "Optimal dose and schedule of consolidation in AML: is there a standard?" Best Practice & Research Clinical Haematology **27**(3-4): 259-264.

Schnittger, S., C. Schoch, W. Kern, C. Mecucci, C. Tschulik, M. F. Martelli, T. Haferlach, W. Hiddemann and B. Falini (2005). "Nucleophosmin gene mutations are predictors of favorable prognosis in acute myelogenous leukemia with a normal karyotype." Blood **106**(12): 3733-3739.

Sha, W., B. Brüne and A. Weigert (2012). "The multi-faceted roles of prostaglandin E2 in cancer-infiltrating mononuclear phagocyte biology." Immunobiology **217**(12): 1225-1232.

Shahid, A. M., I. H. Um, M. Elshani, Y. Zhang and D. J. Harrison (2022). "NUC-7738 regulates β-catenin signalling resulting in reduced proliferation and self-renewal of AML cells." Plos one **17**(12): e0278209.

Shaposhnik, Z., X. Wang, M. Weinstein, B. J. Bennett and A. J. Lusis (2007). "Granulocyte macrophage colony-stimulating factor regulates dendritic cell content of atherosclerotic lesions." Arteriosclerosis, thrombosis, and vascular biology **27**(3): 621-627.

Shlush, L. I. (2018). "Age-related clonal hematopoiesis." Blood, The Journal of the American Society of Hematology **131**(5): 496-504.

Shlush, L. I., S. Zandi, A. Mitchell, W. C. Chen, J. M. Brandwein, V. Gupta, J. A. Kennedy, A. D. Schimmer, A. C. Schuh and K. W. Yee (2014). "Identification of pre-leukaemic haematopoietic stem cells in acute leukaemia." Nature **506**(7488): 328-333.

Simon, M., V. L. Grandage, D. C. Linch and A. Khwaja (2005). "Constitutive activation of the Wnt/β-catenin signalling pathway in acute myeloid leukaemia." Oncogene **24**(14): 2410-2420.

Smith, C. C. (2019). "The growing landscape of FLT3 inhibition in AML." Hematology 2014, the American Society of Hematology Education Program Book **2019**(1): 539-547.

Smith, C. J., Y. Zhang, C. M. Koboldt, J. Muhammad, B. S. Zweifel, A. Shaffer, J. J. Talley, J. L. Masferrer, K. Seibert and P. C. Isakson (1998). "Pharmacological analysis of cyclooxygenase-1 in inflammation." Proceedings of the National Academy of Sciences **95**(22): 13313-13318.

Smith, W. L., D. L. DeWitt and R. M. Garavito (2000). "Cyclooxygenases: structural, cellular, and molecular biology." Annual review of biochemistry **69**(1): 145-182.

Smith, W. L. and R. Langenbach (2001). "Why there are two cyclooxygenase isozymes." The Journal of clinical investigation **107**(12): 1491-1495.

Sorror, M. L., M. B. Maris, R. Storb, F. Baron, B. M. Sandmaier, D. G. Maloney and B. Storer (2005). "Hematopoietic cell transplantation (HCT)-specific comorbidity index: a new tool for risk assessment before allogeneic HCT." Blood **106**(8): 2912-2919.

Stein, E. M. (2015). "IDH2 inhibition in AML: finally progress?" Best practice & research Clinical haematology **28**(2-3): 112-115.

Stein, E. M. (2023). "IDH2 inhibition in AML." Blood, The Journal of the American Society of Hematology **141**(2): 124-125.

Stein, E. M., G. Garcia-Manero, D. A. Rizzieri, R. Tibes, J. G. Berdeja, M. Jongen-Lavrencic, J. K. Altman, H. Dohner, B. Thomson and S. J. Blakemore (2015). "A phase 1 study of the DOT1L inhibitor, pinometostat (EPZ-5676), in adults with relapsed or refractory leukemia: safety, clinical activity, exposure and target inhibition." Blood **126**(23): 2547.

Tallman, M. S., H. T. Kim, E. Paietta, J. M. Bennett, G. Dewald, P. A. Cassileth, P. H. Wiernik and J. M. Rowe (2004). "Acute monocytic leukemia (French-American-British classification M5) does not have a worse prognosis than other subtypes of acute myeloid leukemia: a report from the Eastern Cooperative Oncology Group." Journal of clinical oncology **22**(7): 1276-1286.

Tamma, R. and D. Ribatti (2017). "Bone niches, hematopoietic stem cells, and vessel formation." International journal of molecular sciences **18**(1): 151.

Thomas, D. and R. Majeti (2017). "Biology and relevance of human acute myeloid leukemia stem cells." Blood, The Journal of the American Society of Hematology **129**(12): 1577-1585.

Timothy J. Ley, J. F. D., Christopher A. Miller, Li Ding, Cyriac Kandoth, Charles Lu, Michael D. McLellan, Daniel C. Koboldt, David E. Larson, Ling Lin, John W. Wallis, Joshua McMichael, Ken Chen, Michael C. Wendl, Krishna-Latha Kanchi, Heather Schmidt, Joelle Kalicki-Veizer, Robert S. Fulton, Lucinda L. Fulton, Elaine R. Mardis, Richard K. Wilson. Broad Institute: Gaddy Getz, Stacy B. Gabriel, Carrie Sougnez, Lihua Zou and Peter Westervelt. (2013). "Genomic and epigenomic landscapes of adult de novo acute myeloid leukemia." New England Journal of Medicine **368**(22): 2059-2074

Tomás, H., A. Rodrigues, M. Carrondo and A. Coroadinha (2018). "LentiPro26: novel stable cell lines for constitutive lentiviral vector production." Scientific reports **8**(1): 5271.

Torii, S., T. Yamamoto, Y. Tsuchiya and E. Nishida (2006). "ERK MAP kinase in G1 cell cycle progression and cancer." Cancer science **97**(8): 697-702.

Toulmin, E., S. Sonderegger, L. Cerruti, A. Terzic, F. Yan, N. Wong, I. Street, P. Stupple, S. Jane and A. H. Wei (2018). "PRMT5 Inhibition Selectively Targets Acute Myeloid Leukemia Stem Cells Though a p53-Dependent Mechanism." Blood **132**: 4061.

Trowbridge, J. J. (2019). "Intrinsic and Extrinsic Factors Driving Hematopoietic Stem Cell Aging and Bone Marrow Failure." Blood **134**: SCI-35.

Vetrie, D., G. V. Helgason and M. Copland (2020). "The leukaemia stem cell: similarities, differences and clinical prospects in CML and AML." Nature Reviews Cancer **20**(3): 158-173.

Wang, C., L. Dong, Z. Zhao, Z. Zhang, Y. Sun, C. Li, G. Li, X. You, X. Yang and H. Wang (2022). "Design and Synthesis of Novel PRMT1 Inhibitors and Investigation of Their Effects on the Migration of Cancer Cell." Frontiers in Chemistry **10**.

Wang, D. and R. N. DuBois (2010). "Eicosanoids and cancer." Nature Reviews Cancer **10**(3): 181-193.

Wang, P., X. Xiao, Y. Zhang, B. Zhang, D. Li, M. Liu, X. Xie, C. Liu, P. Liu and R. Ren (2021). "A dual inhibitor overcomes drug-resistant FLT3-ITD acute myeloid leukemia." Journal of Hematology & Oncology **14**(1): 1-5.

Wei, Q. and P. S. Frenette (2018). "Niches for hematopoietic stem cells and their progeny." Immunity **48**(4): 632-648.

Weissman, I. L. (2000). "Stem cells: units of development, units of regeneration, and units in evolution." cell **100**(1): 157-168.

Welch, J. S., T. J. Ley, D. C. Link, C. A. Miller, D. E. Larson, D. C. Koboldt, L. D. Wartman, T. L. Lamprecht, F. Liu and J. Xia (2012). "The origin and evolution of mutations in acute myeloid leukemia." Cell **150**(2): 264-278.

Wesely, J., A. G. Kotini, F. Izzo, H. Luo, H. Yuan, J. Sun, M. Georgomanoli, A. Zviran, A. G. Deslauriers and N. Dusaj (2020). "Acute myeloid leukemia iPSCs reveal a role for RUNX1 in the maintenance of human leukemia stem cells." Cell reports **31**(9).

Wouters, B. J. (2021). "Targeting IDH1 and IDH2 mutations in acute myeloid leukemia: Emerging options and pending questions." Hemasphere **5**(6).

Xia, S., J. Ma, X. Bai, H. Zhang, S. Cheng, M. Zhang, L. Zhang, M. Du, Y. Wang and H. Li (2014). "Prostaglandin E2 promotes the cell growth and invasive ability of hepatocellular carcinoma cells by upregulating c-Myc expression via EP4 receptor and the PKA signaling pathway." Oncology reports **32**(4): 1521-1530.

Yang, X., L. Kui, M. Tang, D. Li, K. Wei, W. Chen, J. Miao and Y. Dong (2020). "High-throughput transcriptome profiling in drug and biomarker discovery." Frontiers in genetics **11**: 19.

Yu, J., Y. Li, D. Zhang, D. Wan and Z. Jiang (2020). "Clinical implications of recurrent gene mutations in acute myeloid leukemia." Experimental hematology & oncology **9**: 1-11.

Yu, S., R. Han and R. Gan (2022). "The Wnt/β-catenin signalling pathway in Haematological Neoplasms." Biomarker Research **10**(1): 74.

Zhou, H., W. Liu, Y. Zhou, Z. Hong, J. Ni, X. Zhang, Z. Li, M. Li, W. He and D. Zhang (2021). "Therapeutic inhibition of GAS6-AS1/YBX1/MYC axis suppresses cell propagation and disease progression of acute myeloid leukemia." Journal of Experimental & Clinical Cancer Research **40**: 1-17.

Zidar, N., K. Odar, D. Glavac, M. Jerse, T. Zupanc and D. Stajer (2009). "Cyclooxygenase in normal human tissues–is COX-1 really a constitutive isoform, and COX-2 an inducible isoform?" Journal of cellular and molecular medicine **13**(9b): 3753-3763.

Zon, L. I. (2008). "Intrinsic and extrinsic control of haematopoietic stem-cell self-renewal." Nature **453**(7193): 306-313.